UNIVERSITY OF SOUTHAMPTON

Understanding the role of Chlorophyll Fluorescence in Nutrient Stress

by

Thomas J. Ryan-Keogh

A thesis submitted in partial fulfillment for the
degree of Doctor of Philosophy

in the
Faculty of Natural and Environmental Sciences
Ocean and Earth Science

October 2013

Declaration of Authorship

I, Thomas James Ryan-Keogh,

declare that this thesis entitled,

'Understanding the role of Chlorophyll Fluorescence in Nutrient Stress'

and the work presented in the thesis are both my own, and have been generated by me as the result of my own original research. I confirm that:

- This work was done wholly or mainly while in candidature for a research degree at this University;
- Where any part of this thesis has previously been submitted for a degree or any other qualification at this University or any other institution, this has been clearly stated;
- Where I have consulted the published work of others, this is always clearly attributed;
- Where I have quoted from the work of others, the source is always given. With the exception of such quotations, this thesis is entirely my own work;
- I have acknowledged all main sources of help;
- Where the thesis is based on work done by myself jointly with others, I have made clear exactly what was done by others and what I have contributed myself;
- parts of this work have been published as:

- Ryan-Keogh, T. J., Macey, A. I., Cockshutt, A. M., Moore, C. M. and Bibby, T. S., (2012), "The cyanobacterial chlorophyll-binding-protein IsiA acts to increase the *in vivo* effective cross-section of photosystem I under iron limitation", *Journal of Phycology*, Volume 48, Issue 1, Pages 145-154, doi: 10.1111/j.1529-8817.2011.01092.x
- Ryan-Keogh, T. J., Macey, A. I., Nielsdóttir, M. C., Lucas, M. I., Steigenberger, S. S., Stinchcombe, M. C., Achterberg, E. P., Bibby, T. S. and Moore, C. M., (2013), "Spatial and temporal development of phytoplankton iron stress in relation to bloom dynamics in the high latitude North Atlantic Ocean", *Limnology and Oceanography* ,Volume 58, Issue 2, Pages 533-545, dpi:10.4319/lo.2013.58.2.0533

- Achterberg, E. P., Moore, C. M., Henson, S. A., Steigenberger, S., Stohl, A., Eckhardt, S., Cassidy, M., Hembury, D., Klar, J., Lucas, M. I., Macey, A. I., Marsay, C. M., Ryan-Keogh, T. J., (2013), "Natural iron fertilisation by the Eyjafjallajökull volcanic eruption", *Geophysical Research Letters*, Volume 40, Pages 1-6, doi:10.1002/grl.50221.

Signed:

Date:

"Give me half a tanker of iron, and I will give you an ice age"

John Martin, 1988

UNIVERSITY OF SOUTHAMPTON

Abstract

Faculty of Natural and Environmental Sciences
Ocean and Earth Science

Doctor of Philosophy

by Thomas J. Ryan-Keogh

Phytoplankton exert a dominant influence on the biogeochemical cycling of the oceans, but iron limitation in this dynamic environment can exert a control on photosynthesis. Phytoplankton evolved coping mechanisms to overcome and alleviate the effects of iron limitation. One mechanism is the alteration of the thylakoid membrane and the expression of chlorophyll-binding proteins, which can alter the variable chlorophyll fluorescence signal. Firstly, a study of the chlorophyll-binding iron-stress-induced protein, IsiA, in *Synechocystis* PCC 6803 revealed a 60% increase under iron limitation, in agreement with the theoretical increase. On progressive iron-stress IsiA continued to accumulate without a concomitant increase in σ_{PSI}, while F_v/F_m, a measure of photochemical efficiency, continued to decrease. Secondly an oceanographic study to the high latitude North Atlantic in which chlorophyll fluorescence kinetics were used to measure the response to iron addition of *in situ* phytoplankton populations. The difference in the F_v/F_m between nutrient amended and control treatments ($\Delta(F_v/F_m)$) was used as a measure of the relative degree of iron stress. The combined observations of both long-term ($>$ 24 h) and short-term (24 h) indicated variability in the seasonal cycle of iron stress, with phytoplankton iron stress developing during the transition from prebloom to peak bloom conditions. Thirdly, similar physiological characteristics were also observed in an oceanographic study in the Ross Sea. The results further confirmed the highly variable response across temporal and spatial scales, but also within different phytoplankton groups. Consistent across all three studies is the reduction in F_v/F_m as the result of an elevated F_o signal, representing potentially unbound chlorophyll-binding proteins. These unbound chorophyll-binding proteins can dominate the total cellular chlorophyll, at least in culture, and reflect a large resource investment. These proteins may provide a rapid source of chlorophyll upon iron resupply. Irrespective of the underlying causes of unbound chloropyll-binding proteins, the potential large scale expression of such complexes provides a powerful diagnostic tool with which to investigate iron stress *in situ*.

Acknowledgements

There are many people and organisations to thank for their help with this research and the production of this thesis. Firstly, thank you to my supervisors, Mark Moore and Tom Bibby, for their support and encouragement throughout my PhD, without their inspiration and help with improving my science writing this thesis would not have been possible. Secondly, I would like to thank Eric Achterberg and Richard Sanders for their stimulating discussions in panel meetings and their continued interest in this work. At NOCS there have been many people who have helped me with data, sample processing and good ideas: Anna Macey, Sophie Richier, Nicola Pratt and the rest of the phytoplankton ecophysiology group. Special thanks to all members of D350, D354 and PRISM, both at NOCS and elsewhere, for interesting discussions and making these cruises very memorable.

Special thanks and a lot of love to David, my best friend and loving partner, for giving me the courage to pursue my dreams. He has been there by my side through all the ups and downs of my PhD, giving me the encouragement and support when I needed it most. I would also like to thank him for listening to my ramblings (sometimes incoherently) when things would go wrong and for helping me to find solutions to the problems.

I would like to thank my mum and Darin, for their support both emotionally and financially throughout my undergraduate degree and PhD. I have no doubt that I would not be where I am today without their unwavering support throughout my university education. To my brother Rory, my sisters Elle and Grace, and my nan and granddad, Rita and Gerry, I thank you. Even when my family no longer understood my science ramblings, they always showed an interest.

Finally to the many good friends at NOCS, without whom the last three and a half years would have been far more stressful and a lot less fun. Thanks to my office mates of past and present for putting up with me; to Colette for our many 'fresh air' breaks and the cans of 'can't', also to Cristina, Grant, Becky, Gemma and Jen for the many cheese and wine nights and listening to me to ramble about phytoplankton. I would also like to thank Jo Ferris for proof-reading this thesis for me, and reminding me of the correct placement for commas. A final special thanks to all the other countless friends I have made over the years throughout my PhD.

It is a great pleasure to thank all of the above people and organisations for making this thesis possible.

Contents

List of Figures

List of Tables

Abbreviations

BCP	**B**iological **C**arbon **P**ump
CDW	**C**ircumpolar **D**eep **W**ater
Chl	**C**hlorophyll
DIN	**D**issolved **I**norganic **N**itrogen
ETC	**E**lectron **T**ransport **C**hain (through PSII)
ETR	**E**lectron **T**ransport **R**ate (through PSII)
FRRf	**F**ast **R**epetition **R**ate **f**luorometer
FIRe	**F**ast **I**nduction **Re**laxation fluorometer
HLNA	**H**igh **L**atitude **N**orth **A**tlantic
HNLC	**H**igh **N**utrient-**L**ow **C**hlorophyll
IsiA	**I**ron-**S**tress-**I**nducible protein **A**
MCDW	**M**odified **C**ircumpolar **D**eep **W**ater
NPQ	**N**on-**P**hotochemical **Q**uenching
PAM	**P**ulse **A**mplitude **M**odification
PQ	**P**lasto**q**uinone
PSI	**P**hotos**y**stem **I**
PSII	**P**hotos**y**stem **II**

Chapter 1

Introduction

1.1 Phytoplankton

Phytoplankton, derived from the Greek words, phyto (plant) and plankton (made to wander or drift), are a group of aquatic photoautotrophs which use light and the pigment chlorophyll to grow through a process known as photosynthesis. Marine phytoplankton are organised into at least 8 major divisions or phyla, which in turn is made up of thousands ($\sim$25, 000) of unicellular species (Falkowski et al., 2004). One of these divisions is composed of the earliest oxygenic photosynthetic organisms, the Cyanobacteria, while the rest are composed of the more recently evolved eukaryotes. The largest and most dominant phytoplankton are represented by three groups, the Bacillariophycae (Diatoms), Dinophyceae (Dinoflagellates) and the Prymnesiophycae (Coccolithophores). The smaller phytoplankton, or picoplankton (0.2-2.0 μm), are predominantly represented by the prokaryotic Cyanophycae (Cyanobacteria), Prochlorophycae (Prochlorophytes) and Picoeukaryotes. All of these groups are adapted to different light and nutrient environments, which in turn is determined by the global circulation of the marine environment.

Phytoplankton account for less than 1% of global photosynthetic biomass, yet they are responsible for $\sim$50% of global primary production (Field et al., 1998). Annually this primary production results in 45-50 Gt Carbon being fixed by phytoplankton (Longhurst et al., 1995); they are also the primary food source and form the base of the oceanic food chain. Gaining a better understanding of how phytoplankton have adapted to

the highly dynamic marine environment, including adaptations of phylogeny to nutrient limitation, is an important goal for understanding the marine environment as a whole. A better understanding of phytoplankton nutrient limitation has implications for estimates of primary productivity which in turn feed into climate models, for potential geoengineering projects that might aim to alleviate the effects of nutrient limitation and also for quantification of all components of the marine system (i.e. sources/sinks/fluxes of nutrients, biomass - loss/growth etc.).

1.2 Evolutionary Histories

Before phytoplankton in modern oceans can be understood, the evolution of phytoplankton and in turn photosynthesis is required. The process of oxygenic photosynthesis appears to only have evolved once within the cyanobacterial clade but it was spread through various eukaryotic clades through a process known as endosymbiosis (Delwiche, 1999; Palmer, 2003). Eukaryotic host cells engulfed a coccoid cyanobacterium that eventually became a membrane-bound organelle known as a "plastid" (Falkowski et al., 2004). This eukaryotic cell already possessed a mitochondrion; gene loss over time led to both symbionts being reduced to metabolic 'slaves' within the host cell. Phytoplankton, therefore, share common metabolic functions and some pigments, such as Chlorophyll a, which is the dominant pigment involved in photosynthesis. However they have different evolutionary histories as a major schism occurred in the evolution that gave rise to two major plastid superfamilies. The green superfamily appropriated Chlorophyll b as an accessory pigment and is dominated by the green algae and their descendants, terrestrial plants (Butterfield, 2002; German, 1990). The red superfamily appropriated Chlorophyll c, and it retains the most features of cyanobacterial pigmentations (Falkowski et al., 2004).

The reasons for acquiring a plastid are most likely to be due to some major geological event in Earth's history that dramatically altered the environmental conditions, forcing organisms to adapt and evolve. The End-Permian mass extinction marked a major transition in the ocean's ecosystem structure, including widespread extensive anaerobic conditions (Isozaki, 1997; Knoll et al., 1996; Wignall and Twitchett, 1996). These conditions would have potentially lead to denitrification (Anbar and Knoll, 2002; Falkowski, 1997; Fennel et al., 2005), having a cascade of effects upon photoautotrophic organisms and heterotrophs. Therefore, the acquisition of a plastid would allow a heterotrophic

organism to retain fixed nitrogen within the cell while producing organic carbon via photosynthesis (Zaslavskaia et al., 2001).

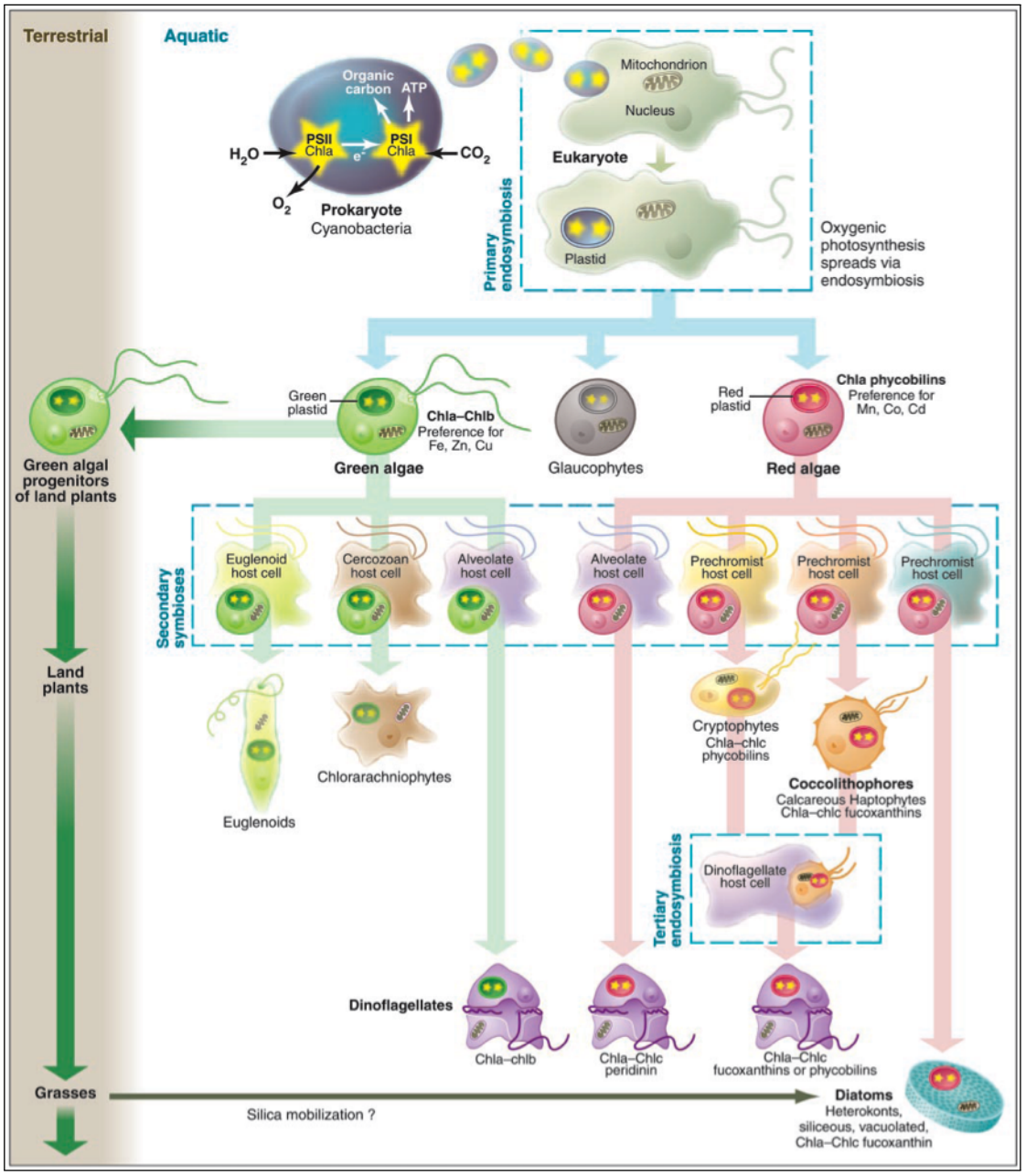

FIGURE 1.1: The basic pattern of the inheritance of plastids in eukaryotic phytoplankton. The original plastid, derived from an ancestral cyanobacterium, was incorporated into a eukaryotic host cell via an endosymbiotic event to form a primary symbiotic oxygenic eukaryote. Three major extant clades decended from the primary symbiont: a "green" clade, a "red" clade, and glaucocystophytes (Falkowski et al., 2004).

The acquisition of different plastids led to the preferential uptake of different trace elements; the red superfamily preferentially took up elements such as Cadmium (Cd), Cobalt (Co) and Manganese (Mn) while the green superfamily took up Copper (Cu),

Zinc (Zn) and Iron (Fe) (Quigg et al., 2003). Quigg et al. (2003) analysed the elemental composition of phytoplankton to test the 'plastid imprint' hypothesis, to determine whether the nutrient requirements of the phytoplankton where determined by either the original heteroptrophic host cells' genetic background or whether it is determined by the plastid inheritance. Their results confirmed that the original heterotrophic host cell determines the stoichiometry of major elements and the trace elemental quotas is determined by the plastid inheritance but not the contemporary plastid genome. This difference in elemental quotas will dictate the response of phytoplankton nutrient limitation within the dynamic ocean environment where nutrients are not distributed evenly.

Alongside the evolution of specific plastids for photosynthesis there was the evolution of light-harvesting complexes (LHCs), the phycobillisomes in *Synechococcus* and the Pcbs in *Prochlorococcus*. Phycobillisomes, stacks of chromophorylated protein complexes located externally to the thylakoid membrane, are encoded by the genes *cpc*, *cpe* and *apc* (Six et al., 2007). Pcbs, membrane-bound chlorophyll-binding proteins, are encoded by the *pcb* genes (Bibby et al., 2001d, 2003; Garczarek et al., 2000; Hess et al., 2001; Rocap et al., 2003). LHCs of eukaryotes function in the same capacity as the light-harvesting phycobilisomes of cyanobacteria, the collection of light energy to drive photochemistry of a reaction centre. All major groups of photosynthetic eukaryotes contain thylakoid membrane-intrinsic LHCs whose proteins are members of a superfamily of chlorophyll-carotenoid proteins (Green and Durnford, 1996). Yet the evolution of these proteins remains unclear, as no proteins homologous to the membrane-intrinsic LHCs have been found in any known cyanobacteria (Durnford et al., 1999); which provides a common link between the evolution of all eukaryotic plastids. It has been suggested that similar to the evolution of plastids, there is a common ancestor for both the red and green clade, yet the specific organisation of LHCs within these two lineages evolved independently (Durnford et al., 1999).

1.3 Photosynthesis

Phytoplankton are the primary photosynthetic organisms in the oceans which, through the process of oxygenic photosynthesis, convert sunlight into chemical energy through the production of oxygen and the assimilation of carbon dioxide into organic matter. This

is accomplished by a series of reactions associated with the thylakoid membranes,which are located in the chloroplast in eukaryotes and adjacent to the plasma membrane in prokaryotes (Behrenfeld and Milligan, 2013). The reactions are catalysed by two separate photosystems: photosystem I (PSI) and photosystem II (PSII). Equation 1.1 displays the light reaction and equation 1.2 displays the dark reaction; the specific details of this process will be outlined below (Nelson and Ben-Shem, 2004) (Figure 1.2).

Light reaction:

$$H_2O + NADP \xrightarrow[ADP+Pi \curvearrowright ATP]{\text{light energy + chlorophyll}} O_2 + NADPH + H^+ \tag{1.1}$$

Dark reaction:

$$CO_2 + NADPH + H^+ \xrightarrow[ATP \curvearrowright ADP+Pi]{\text{Rubisco}} [CH_2O]_n + H_2O + NADP \tag{1.2}$$

Light-harvesting complexes, containing photosynthetic pigments, capture and funnel the light energy to the reaction centre core. The LHCs may be embedded in the thylakoid membranes (e.g., in green algae and diatoms) or may be external structures on the stromal side (e.g., in phycobilisomes of cyanobacteria and red algae) (Behrenfeld and Milligan, 2013). Once light energy reaches the reaction centre core it initiates the translocation of an electron across the thylakoid membrane through a chain of cofactors (Figure 1.2). The energy captured induces the excitation of specialized reaction-centre chlorophylls (P700 in PSI and P680 in PSII), and in P680 it leads to electron transfer to a phaeophytin; referred to as "charge separation". Water, the electron donor for this process, is oxidized to O_2 and 4 protons (H^+) by PSII. This electron then transfers from the first quinone (Q_A) to the secondary quinone (Q_B), a loosely bound plastoquinone which is fully reduced after accepting two electrons. The reduced Q_B then binds two protons from the stroma and is released within the thylakoid membrane to become part of the plastoquinone (PQ) pool. The PQ diffuses within the membrane until it attaches to a binding site on the lumenal side of the cytochrome b6-f (cyt b_6/F) complex. The PQ then releases it protons into lumen, while transferring the electrons to cyt b_6/F. A plastocyanin transfers the electrons to the PSI reaction centre (P700), a special chlorophyll pair, but in order for this to happen P700 must be oxidized. This is achieved through a second light reaction whereby a photon is absorbed by PSI and leads to the transfer of

an electron to the primary electron acceptor of PSI; the electron from the plastocyanin then reduces P700. This electron is then transferred through four molecules to finally reduce ferredoxin, the reduced ferredoxin is subsequently used in numerous regulatory cycles and reactions. These include:

- Photorespiration
- Nitrogen reduction (only in Diazotrophs)
- Cyclic electron flow around PSI
- NADPH production - Carbon Fixation
- Mehler reaction

The charge separation combined with electron transfer and proton release into the lumen leads to the formation of an electrochemical and pH gradient across the thylakoid membrane (trans-ΔpH). This trans-ΔpH fuels ATP synthesis through the protein ATP-synthase (Junge, 1999). Furthermore, the ATP combined with NADPH is used to reduce CO_2 in the Calvin cycle (Herrmann, 1999), through the use of the catalysing enzyme Ribulose-1,5-bisphosphate carboylase/oxygenase (Rubisco) (Herrmann, 1999). The combination of light and dark reactions establishes the gross amount of production by phytoplankton and also places an upper bound on the overall biomass and productivity of ecosystems (Falkowski and Raven, 2007). There are other processes that can alter this net photosynthesis such as dark respiration, photorespiration and the Mehler Reaction.

1.4 Nutrient Limitation

The basis of our understanding of nutrient limitation in the oceans is formed from the work of Von Liebig (1840) and A.C. Blackman (1905). Liebig′s law of the minimum (Von Liebig, 1840) stated that the single nutrient at the lowest relative concentration will set an upper bound on the amount of new biomass that can be formed (the yield) (Cullen, 1991); this rule dictated the general approach to understanding phytoplankton nutrient stress in the oceans. Blackman (1905) expanded upon this idea when describing

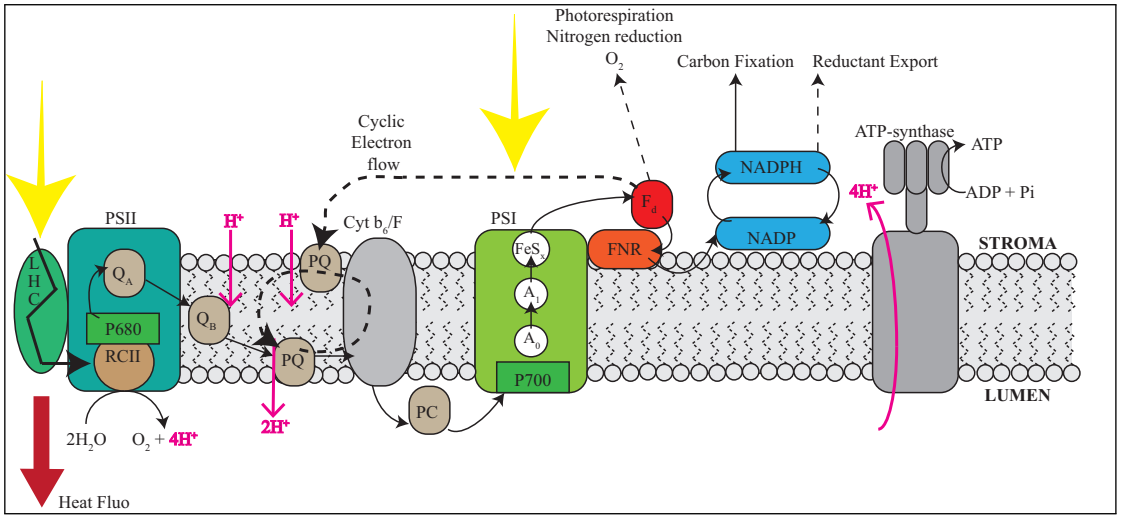

FIGURE 1.2: Schematic representation of the electron transport chain. The continuous black arrows indicate the linear electron flow while the dashed black arrows represent alternative paths. Also represented (in pink) are the sources of protons (H^+) to the lumen from the splitting of the water molecule and the transport by the plastoquinones; as well as the main sink of H^+ from the transport through the ATP-synthase protein complex. LHC - light-harvesting complex, RCII - reaction centre of PSII, P680 - special chlorophyll pair of PSII, Q_A - primary quinone, Q_B - secondary quinone, PQ - plastoquinone pool, Cyt b_6/f - cytochrome b_6/f complex, PC - plastocyanin, P700 - special chlorophyll pair of PSI, FNR - Ferredoxin-NADP reductase and F_d - Ferredoxin.

nutrient limitation; that low nutrient concentrations can also limit the specific growth rate of individual cells. These concepts are often referred to as Blackman and Liebig limitations and are used to explain nutrient limitation in the oceans.

The work of A.C. Redfield (1934) tied in with these respective limitations by examining the specific stoichiometry of the major macronutrients within phytoplankton, known as the Redfield ratio. This ratio of carbon, nitrogen, phosphorus and iron in phytoplankton (C_{106}:N_{16}:P_1:$Fe_{0.1\text{-}0.001}$) appeared to have a causal correlation with the NO_3^- and PO_4^{3-} (N:P) ratio in the ocean interior. Redfield (1958) concluded that the elemental composition of phytoplankton was 'uniform in a statistical sense' but the variations in inorganic Carbon, Nitrogen and Phosphate in seawater were the result of synthesis and decomposition of organic matter. As this ratio examines only the net effect of biological activity, it was conceived that there could be marked deviations from this ratio depending upon the individual types of organisms and their respective life histories.

1.4.1 Iron Limitation

The availability of major macronutrients (N, P & Si) was often considered to be the dominating influence on constraining phytoplankton biomass; but there are areas of the ocean that have high macronutrient concentrations and low chlorophyll concentrations, these are termed High-Nitrate Low-Chlorophyll (HNLC) regions. HNLC regions include the Southern Ocean and the sub-Arctic Pacific and can make up to ∼25% of the world's oceans (de Baar et al., 2005) in terms of the area. An alternative nutrient was preventing the phytoplankton from drawing down the residual macronutrients; one proposal was iron, the 4^{th} most abundant element in the Earth's crust, which can be found in low concentrations within aquatic ecosystems. Many previous studies had demonstrated the potential for limitation by iron (Brand, 1991; Brand et al., 1983; Gran, 1931, 1933; Hart, 1934; Harvey, 1938, 1966; Hendey, 1937; Menzel and Ryther, 1961; Ryther and Guillard, 1959; Ryther and Kramer, 1960; Subba Rao and Yeats, 1984; Sunda et al., 1991), but it was the work of Martin and Fitzwater (1988); Martin et al. (1989, 1990, 1994) and de Baar (1994); de Baar et al. (1990, 1995) that demonstrated that in HNLC regions, iron was the limiting nutrient for phytoplankton both in terms of Blackman and Liebig type limitations. From these results they proposed:

> 'that phytoplankton growth in major nutrient-rich waters is limited by iron deficiency' (Martin et al., 1991).

From this work it became apparent that iron was an important, if not the most important, micronutrient influencing plankton ecology, because of the role iron plays in regulating the photosynthetic apparatus.

1.4.1.1 Iron and the Photosynthetic Apparatus

Iron availability plays a central role in constraining photosynthesis and, therefore, phytoplankton productivity because the enzymes required for the photosynthetic reaction centres represent iron-enriched cellular systems containing a total of 23-24 atoms (Table 1.1) (Behrenfeld et al., 1996). Iron limitation can inhibit a number of components of this system, such as: the number of iron-containing photosynthetic proteins, the photochemistry of PSII, the amount of photooxidizable reaction centre pigment of PSI and the partial reaction rates associated with PSII and PSI (Ivanov et al., 2000).

TABLE 1.1: Iron components of the electron transport chains of the photosynthetic apparatus (Shi et al., 2007)

Complex	Fe-containing cofactor	Number of Fe atoms
Photosynthetic apparatus		23-24
PSII		3
	1 non-haem iron	1
	1 haem	1
	1 haem	1
Cytochrome b_6f complex		6
	3 haems	3
	1 haem	1
	1 [2Fe-2S]	2
PSI		12
	1 F_X ([4Fe-4S])	4
	1 F_A ([4Fe-4S])	4
	1 F_B ([4Fe-4S)]	4
Cytochrome c_{553}	1 haem	1
Ferredoxin	1 [2Fe-2S] centre	2

1.4.2 Multi-nutrient co-limitation

An alternative type of nutrient limitation has also been proposed, known as multi-nutrient co-limitation (Arrigo, 2005; Saito et al., 2005, 2008). Whereby the phytoplankton growth is not controlled by one specific nutrient, but growth is stimulated by the simultaneous addition of two or more different resources. This occurs when two or more nutrients are reduced to levels too low for cellular uptake, which can occur due to luxury uptake by phytoplankton thereby preferentially depleting the more abundant nutrient. This has been observed in nutrient-depleted waters of the Baltic Sea, where the addition of both N and P were required to stimulate phytoplankton growth (Seppala et al., 1999).

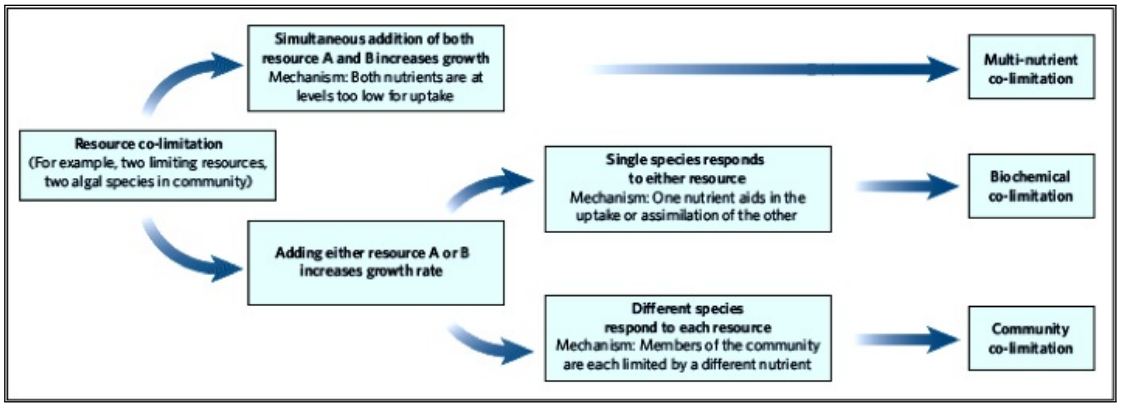

FIGURE 1.3: A breakdown of the three types of resource co-limitation (Arrigo, 2005).

When the addition of either one resource or another elicits a response in phytoplankton

growth, this maybe because of two different types of resource limitation, biochemical co-limitation and community co-limitation. Under biochemical co-limitation, the addition of one limiting resource may facilitate the uptake or assimilation of another (previously) limiting resource. For example the assimilation of resource A depends upon its abundance within the environment and the amount of cellular machinery for its assimilation and resource B (often a trace metal cofactor) is integral to the functioning of this cellular machinery (Figure 1.3). During culture (Sunda and Huntsman, 1997) and field (Maldonado et al., 1999) experiments, growth was enhanced either by increasing the light level or by adding Fe, an essential component of the photosynthetic apparatus.

Community co-limitation occurs when different niches of the phytoplankton community respond differently to addition of different resources. This can occur if individual members of the community are each limited by only a single nutrient. One example is the community co-limitation found in Fe-replete oligotrophic waters where N_2-fixing cyanobacteria are abundant and N and P are scarce. Addition of N stimulates the growth of phytoplankton that can assimilate DOP using alkaline phosphatase (Suzumura and Ingall, 2004), whereas the addition of P stimulates cyanobacterium such as *Trichodesmium* that can support their high N requirement through N_2 fixation (Karl et al., 1997; Wu et al., 2000).

Saito et al. (2008) attempts to explain the ambiguity associated with the above descriptions of co-limitation by proposing an alternative explanation:

1. Type I - Independent nutrient co-limiation
2. Type II - Biochemical substitution co-limitation
3. Type III - Biochemically dependent co-limitation

Type I concerns two elements that are biochemically exclusive, such as nitrogen and phosphorus, that are found in low enough concentrations to be limiting. Type II refers to two elements that can be substituted for the same biochemical role within the organism, such as zinc-cobalt. Whereas Type III is the limitation of one element that directly effects the uptake mechanism of another element, such as zinc-carbon. If we assume that primary productivity in the oceans is driven by bottom-up controls, then it is likely a combination of types I, II and III co-limitation exerting a specific influence

independently and/or simultaneously on the phytoplankton community (Saito et al., 2008). The role of co-limitation must be considered when examining iron limitation of phytoplankton as it may not be exclusively limiting.

1.5 Iron Biogeochemical Cycle

In order to understand how the iron concentrations of the ocean can be limiting, an understanding of the complex iron biogeochemical cycle is needed. This is roughly broken down into iron supply to the ocean and the chemical speciation of iron in the ocean. Iron supply to the oceans can be divided into three separate terms:

1. New supply - that which adds to the oceanic inventory, or
2. Recycled supply - the turnover of the oceanic inventory
3. Internal transport - exchange between ocean regions by currents

1.5.1 New Supply

One of the primary supplies of new iron the ocean, in areas such as the equatorial Atlantic, is atmospheric dust (Martin and Fitzwater, 1988) and early work on mapping the distribution of aerosol iron fluxes to the ocean demonstrated gradients (Duce and Tindale, 1991). These maps also revealed that the Southern Ocean, a remote HNLC region, is characterized by low aerosol-iron fluxes. This provided the first semi-quantitative causal link between low iron supply and low productivity (Duce and Tindale, 1991).

There are a multitude of new sources in the surface ocean which work on both temporal scales (seasonal and episodic) and spatial gradients (meridional to zonal). These new sources, with global flux estimates, include but are not limited to:

1. resuspension of coastal and shallow sediments (Moore and Braucher, 2008) - 50-250 Gg yr^{-1*}
2. glacial/iceberg melt (Smith et al., 2007) - 0.11-0.16 Gg yr^{-1}
3. seasonal sea-ice retreat (Lannuzel et al., 2008) - 0.5 Gg yr^{-1}

4. atmospheric dust (Duce and Tindale, 1991) - 560-1870 Gg yr^{-1}
5. hydrothermal activity (Klunder et al., 2011) - 50 Gg yr^{-1}
6. eddy shedding/sediment interactions (Bowie et al., 2009)
7. island wakes (Blain et al., 2007)
8. vertical diffusive flux (Boyd et al., 2005)
9. volcanism and volcanic ash (Gaiero et al., 2003)

All flux estimates (Gg yr^{-1}) are for aqueous iron, excepting resuspension of sediments and hydrothermal activity (*) which are filterable iron (Raiswell and Canfield, 2012).

There are other new iron sources evident in other oceanic regions, such as in coastal waters where both sedimentary (Elrod et al., 2004; Johnson et al., 1999) and riverine (Wetz et al., 2006) iron can cause pronounced nearshore to offshore gradients in dissolved iron concentrations (Nishioka et al., 2007). There are also other aerosol sources of iron such as extra-terrestial dust (Johnson, 2001), urban pollution (Sedwick et al., 2007a) and biomass burning (Luo et al., 2008). The combination of all these new sources of iron form a mosaic of supply mechanisms, which shows variation on regional, global and temporal scales.

1.5.2 Recycled Supply

The recycling of dissolved iron is biological mediated (Price and Morel, 1998) and, in the 1990s, studies demonstrated the capacity of bacteria and grazers in regenerating iron (Hutchins and Bruland, 1994; Lee and Fisher, 1993); this is important for understanding total production in the oceans. Total primary production is formed of 'new production' (that from new nutrients introduced to the system) and 'regenerated production' (that from nutrients that are recycled) (Banse, 1995). The 'regenerated production' is often greater, up to 6 times, than that of new production (Honjo et al., 2008). One potential source of iron recycling is grazing by mesozooplankton, zooplankton can act as 'iron shuttles' by grazing upon biomass below the nutricline and excreting faecal pellets into the surface waters. Giering et al. (2012) demonstrated that this form of iron transport can support between 6 - 59% of phytoplankton iron requirements in the North Atlantic.

Recycling of biogenic iron is not limited to that by mesozooplankton (Hutchins and Bruland, 1994; Sarthou et al., 2008), but can be recycled by microzooplankton (Barbeau et al., 1996; Maranger et al., 1998; Strzepek et al., 2005), viruses (Mioni et al., 2005) and heterotrophic bateria (Strzepek et al., 2005). The combination of these recycling pathways make up what is termed the microbial ferrous wheel (Kirchman, 1996) (Figure 1.4), which can rapidly mobilize the biogenic iron pool making it bioavailable.

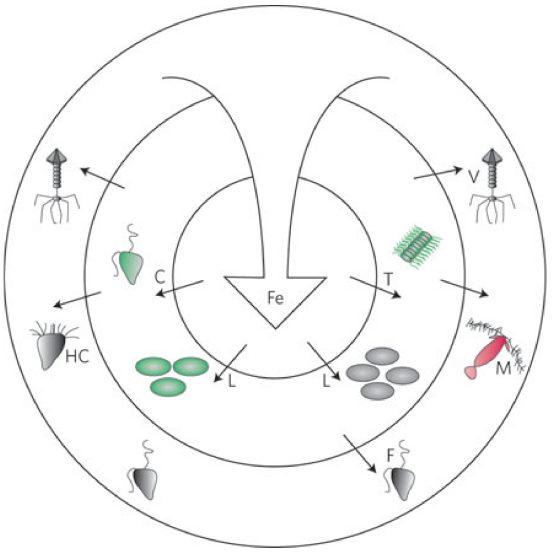

FIGURE 1.4: Schematic of the microbial ferrous wheel which drives iron recycling. Fe represents a generic pool of inorganic and organic, soluble, colloidal and particulate iron that is potentially available to phytoplankton. Iron acquisition strategies include: siderophore-mediated uptake (L), direct colloidal iron uptake (C) and dissolved iron uptake (T). After uptake, iron is rapidly cycled by heterotrophic flagellates (F), ciliates (HC), mesozooplankton (M) and viral lysis (V) (Boyd and Ellwood, 2010).

1.5.3 Internal Transport

Lateral velocities of mid-depth currents rarely exceed 10 cm s^{-1} in the ocean basins, yet undercurrents can be much faster, up to 100 cm s^{-1} (Mackey et al., 2002). During transport, nanoparticles of iron may dissolve to form aqueous Fe(III) or may become be scavenged by sediment grains or large aggregates. Another source of iron is the upwelling of deep water, however in model runs this is assumed to only supply ∼2.0% of the total input to the surface waters (Moore et al., 2001). This value is misleading, as large amounts of iron are entrained during deep winter mixing at high latitudes, particularly in the North Atlantic (Moore et al., 2001). Nielsdóttir et al. (2009) estimated that the input from winter mixing was 12-16 μmol Fe m^{-2} yr^{-1} in the North Atlantic, only

slightly less than the requirements to support potential annual new production in the North Atlantic.

1.5.4 Iron Speciation

Dissolved iron can exist in seawater in two forms (two different oxidation states), Fe(II) and Fe(III), which in turn can either be free or complexed with inorganic and organic ligands. Fe(III) is the thermodynamically stable form of iron and it dominates in surface seawater in the presence of oxygen (Byrne et al., 1988; Hudson and Morel, 1990; Turner et al., 1981; Zafiriou and True, 1980), whereas Fe(II) is stable under anoxic conditions. Both forms are more readily bioavailable in seawater than their organically complexed counterparts (Sunda, 2001).

1.5.5 Future Changes to Iron Availability

Continued emissions of anthropogenic CO_2 from the burning of fossil fuels, changing land use, and cement production, the partial pressure of CO_2 in the atmosphere is expected to reach 2000 μatm (Caldeira and Wickett, 2003) in $\sim$150 years. The equilibration of atmospheric CO_2 with the surface ocean will decrease the current pH value of seawater from 8.1 to 7.4 (Caldeira and Wickett, 2003). This decrease in pH will result in a reduction of both the concentrations of hydroxide and carbonate ions in most natural surface waters (Millero et al., 2009). While many studies have focused upon the result of climate change and ocean acidification upon carbonate chemistry, very few have considered the effects upon trace metal concentrations of the surface oceans. Millero et al. (2009) report upon the effect that pH will have upon iron, which suggests that this decrease in pH from 8.1 to 7.4 will increase the solubility of Fe(III) by about 40% thereby potentially decreasing the levels of iron limitation and increasing primary production.

1.6 Assessment of Iron Limitation

With the establishment of trace metal clean techniques in the 1970s (Bender and Gagner, 1976; Bender et al., 1977; Boyle and Edmond, 1975; Knauer and Martin, 1973), the potential for assessing iron limitation of phytoplankton in the oceans became a

possibility. The work of Martin and Fitzwater (1988) and de Baar et al. (1990) demonstrated through ship-board iron-addition bottle experiments that phytoplankton growth in HNLC regions could be stimulated (Figures 1.5 and 1.6). However as these shipboard experiments are prone to artefacts, a new approach was considered that focused upon mesoscale Fe addition experiments (FeAXs).

The main objective was to test whether Fe enrichment in certain areas, such as HNLC regions, would increase primary productivity but there was also a focus on whether Fe enrichment would have an effect on nutrient uptake and export (Boyd et al., 2007). There have been several FeAXs to date (Table 1.2), beginning in 1993 with IronEX I, where Fe was added to tropical HNLC surface waters of the eastern Pacific (Martin et al., 1994). All subsequent FeAXs followed a similar design in different HNLC regions and confirmed the capability for studying the biogeochemical cycling and phytoplankton responses in a discrete water parcel over temporal and spatial scales of weeks and kilometres (Boyd et al., 2007). While each one of these studies were testing the idea of iron limitation each yielded different results that are not highly consistent due to difference in methodologies and amounts of iron added. All studies demonstrated an increase in biomass with the addition of iron, despite the difference in dominant phytoplankton communities and bloom phase utilised. To complement these studies there have been ship-based observations of persistent blooms within HNLC waters, termed FeNXS (Fe natural enrichment experiments), which are driven by sustained and localized Fe enrichment such as CROZEX (Pollard et al., 2007), KEOPS (Blain et al., 2008) and South Georgia (Nielsdóttir et al., 2012).

Complementing the use of iron-addition shipboard experiments and mesoscale iron addition experiments was the introduction of fast repetition rate fluorometry (FRRf) which was used to examine the nutrient status of phytoplankton communities (Behrenfeld et al., 1996, 2006; Boyd and Abraham, 2001; Kolber et al., 1994; Moore et al., 2006a,b, 2008), which is described below.

TABLE 1.2: The main findings from 12 FeAXs (in chronological order from left to right) conducted between 1993 and 2005 (Boyd et al., 2007).

Property	IronEXI	IronEXII	SOIREE	EisenEX	SEEDS I	SOFEX-S	SOFEX-N	EIFEX	SERIES	SEEDS II	SAGE	FeeP
Fe added (kg)	450	450	1750	2350	350	1300	1700	2820	490	480	1100	1840
Temp. (°C)	23	25	2	3 to 4	11	-1	5	4 to 5	13	9 to 12	11.8	21
Season	Fall	Summer	Summer	Spring	Summer	Summer	Summer	Summer	Summer	Summer	Fall	Spring
Light (μmol quanta $m^{-2}s^{-1}$)	254 to 230	216 to 108	59 to 33	82 to 40	178 to 39	103 to 62	125 to 74		173 to 73		59 to 52	
Dilution rate (d^{-1})	0.27	0.18	0.07	0.04 to 0.43	0.05	0.08	0.1		0.07 to 0.16			0.4
Chloro., t = 0 (mg m^{-3})	0.2	0.2	0.2	0.5	0.9	0.2	0.3	0.6	0.4	0.8	0.6	0.04
Chloro. max (mg m^{-3})	0.6	3.3	2.3	2.8	23.0	2.5	2.4	3.0	5.5	2.4	1.3	0.07
MLD (m)	35	40	65	80	13	35	45	100	30	30	70	30
Bloom phase (duration, days)	evolving subducted	decline	evolving	evolving	evolving	evolving	evolving subducted	partial decline, evolving	decline	evolving	no bloom	no bloom
δDIC (mmol m^{-3})	6	26	17	14	58	21	13		36		nc	<1
δDMS (μmol m^{-3})	0.8	1.8	2.9	1.3, then to 0	nc	nc	increased		8.5, then to 5.7	nc	nc	nc
Dominant phyto-plankton	Mixed	Diatom	Diatom	Diatom	Diatom	Diatom	Mixed	Diatom	Diatom	Mixed	Mixed	*Cyanobact. Prochloro.*
Mesozoo-plankton stocks	increase	increase	nc	nc	nc	nc	nc	increase	increase	increase	nc	nc
Primary production (max/min ratio)	4	6	9	4	4	6	10	2	10		2	1.7

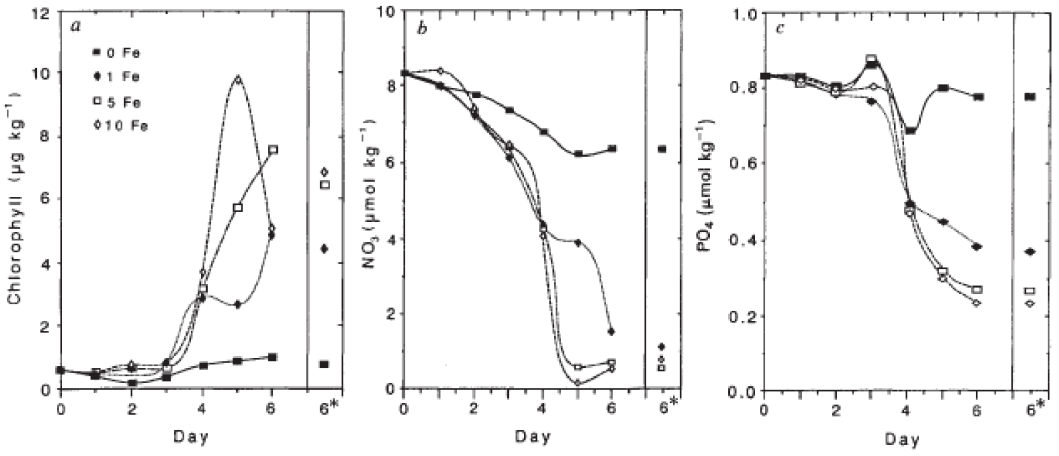

FIGURE 1.5: Results from the iron-addition experiments by Martin and Fitzwater (1988). a) Chlorophyll concentration (μg kg^{-1}, b) Nitrate concentrations (μM) and c) Phosphate concentrations (μM) versus experimental day in control and experimental bottles (1, 5 and 10 nmol Fe added per kg).

1.7 Fluorescence

Before explaining the theory of fast repetition rate fluorometry, fluorescence must first be defined. Fluorescence is the re-emission of energy in the form of a photon (light) as an electron returns to ground state from a singlet excited state (Figure 1.7). Chlorophyll-*a* absorbs light in the blue and red parts of the visible electromagnetic spectrum, where a chlorophyll molecule becomes excited and achieves a singlet state 1 (S_1) after absorbing a photon of less than 670 nm wavelength (Bolhàr-Nordenkampf and Öquist, 1993) (Equation 1.3). If this energy is not used in charge separation, heat dissipation or resonance energy transfer, fluorescence will occur as the energy drops out of the excited state (Equation 1.4). If the absorbed photon is of a shorter wavelength then the extra energy will excite the chlorophyll molecule to the singlet state 2 (S_2) and the heat is emitted as it rapidly decays to the S_1 state.

Excitation:

$$S_0 + h\nu_{ex} \rightarrow S_1 \tag{1.3}$$

Fluorescence (emission):

$$S_1 \rightarrow S_0 + h\nu_{em} + \text{heat} \tag{1.4}$$

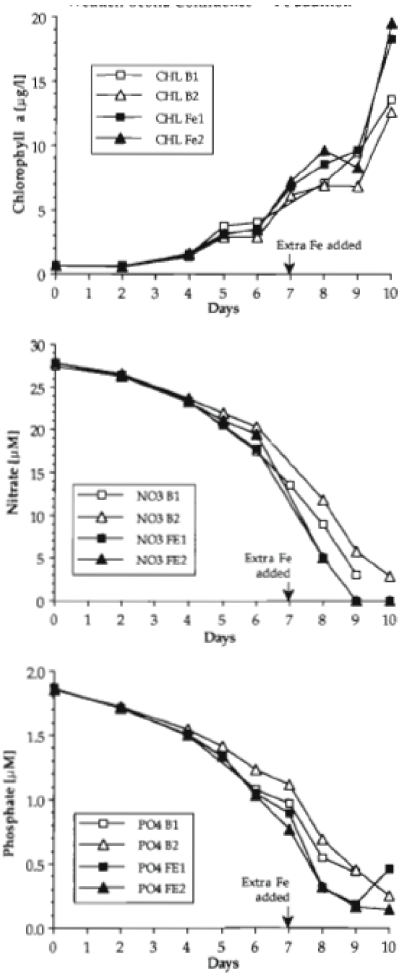

FIGURE 1.6: Results from the iron-addition experiments by de Baar et al. (1990). Chlorophyll concentration (μg L^{-1}, Nitrate concentrations (μM) and Phosphate concentrations (μM) versus experimental day in control and experimental bottles (Fe1 = 10 nM Fe and Fe2 = 20 nM Fe).

1.8 Fast Rate Repetition fluorometry Basic Theory

Fast repetition rate fluorometry (FRRf) is based upon the saturation of of the photosynthetic apparatus with light and the measurement of the fluorescence response (Fluorescence parameters are defined in Table 1.3). As previously described, during charge separation an electron (e^-) is donated from PSII to the first stable acceptor, the quinone Q_A, in the electron transfer chain, once the specialised chlorophyll *a*-protein complex RCII (P680) has received one photon. Prior to this, Q_A is oxidised, and the reaction centre is said to be open; when Q_A becomes reduced, the reaction centre is closed. The excitation energy that arrives at a closed RCII is 'excess' energy and can be transferred

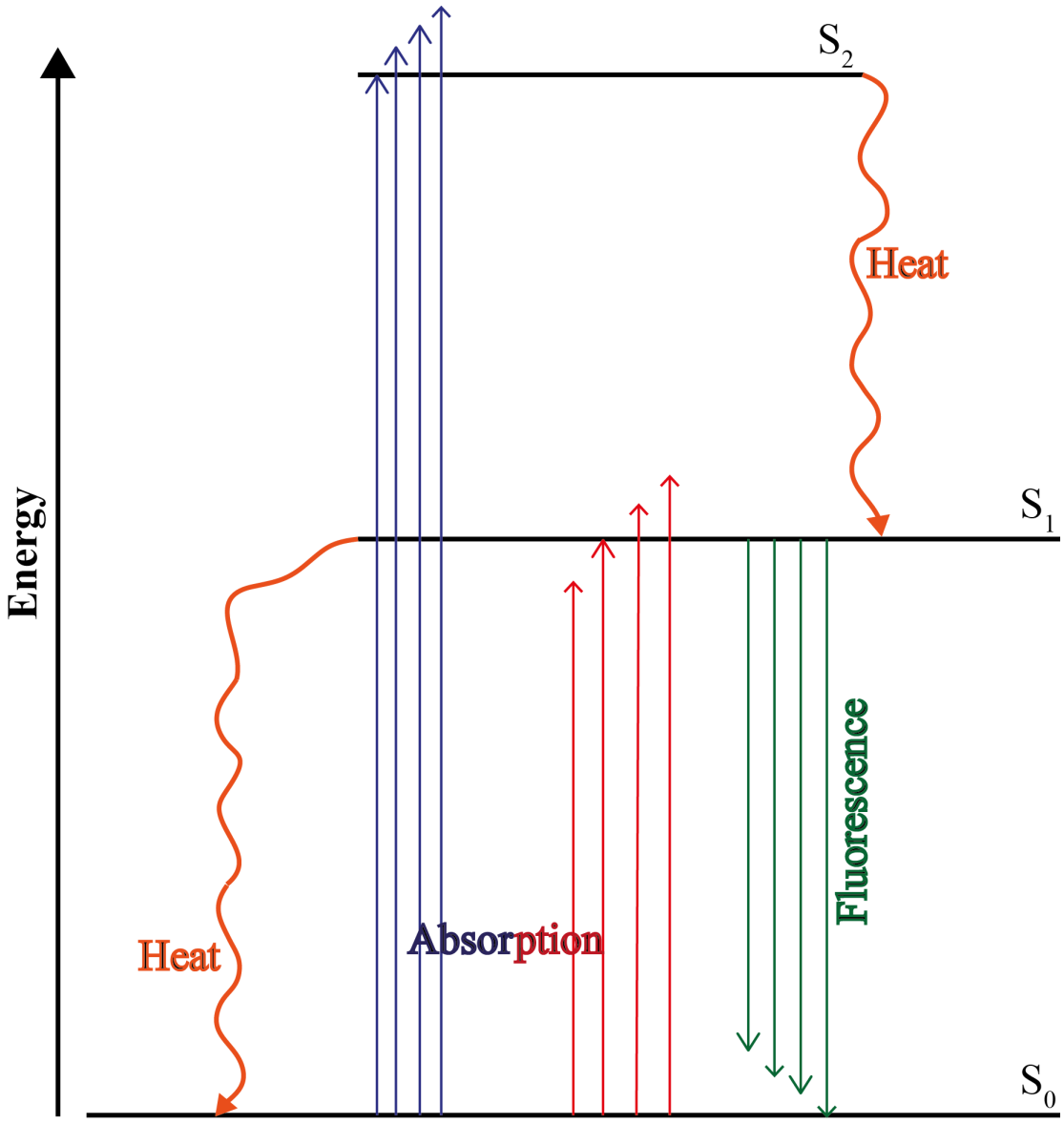

FIGURE 1.7: Energy levels and different types of transitions between electronic excited states when a photon is absorbed by chlorophyll *a*. If the photon absorbed is red light (<670 nm), the electron achieves a singlet state 1 (S_1), and the energy emitted is both heat and fluorescence to reach a ground state. If the photon absorbed is blue light (<420 nm), the electron achieves a singlet state 2 (S_2), before rapidly decaying as heat energy to S_1.

to another RCII or returned to the antenna where the energy may be emitted as fluorescence or lost through non-photochemical quenching (NPQ) as heat (Figure 1.8). The fluorescence yield (F) (Figure 1.9) is a quantitative measure of the excess energy fluorescing from PSII that is not involved in photochemistry and expelled as heat; it can be described as minimum yield (F_o) under zero irradiance conditions, or a maximum yield (F_m) under saturating irradiance when all RCIIs are closed.

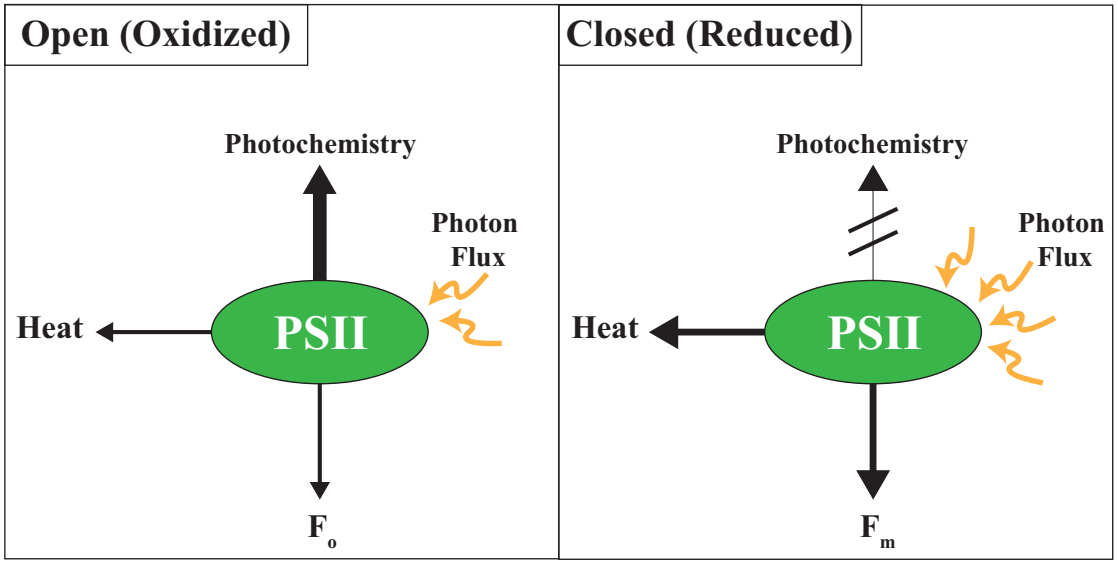

FIGURE 1.8: Schematic of fluorescence de-activation pathways for excitation energy. When excitation energy (irradiance) is low the RCII is oxidized (open), and fluorescence is low. An increase in excitation energy causes the RCII to become reduced (closed), and fluorescence increases.

The apparent quantum yield (ϕ) for photosynthesis is the ratio of energy received to that which is emitted and can be determined from the fluorescence properties of RCIIs that are fully open (F_o) and fully closed (F_m). The maximum change in the quantum yield of fluorescence (F_v/F_m, where F_v is F_m - F_o) reflects the proportion of energy received by RCIIs that are open to that which is emitted from closed RCIIs (Kolber et al., 1998). Based on laboratory studies of phytoplankton cultures, the maximum value for F_v/F_m is 0.65, and is <1.0 because of back reactions between donor chlorophyll molecules and the acceptor molecules (Schatz et al., 1988). Deviations in the observed value of F_v/F_m from the maximum value of 0.65 are seen under different environmental conditions (Falkowski and Kolber, 1995) and are considered to be indicative of variations in the fraction of RCIIs capable of converting absorbed light energy to photochemical energy (Geider et al., 1993a).

The rate at which the RCIIs are saturated from F_o to F_m (Figure 1.9) provides an indication of the area available for light interception relative to the number of reaction centres (σ_{PSII}) (Falkowski and Kolber, 1995; Vassiliev et al., 1994). As such, this term is not an actual size measurement but is a measure of the probability of photon absorption resulting in a photochemical event (Falkowski and Raven, 1997). For a given excitation energy, a larger σ_{PSII} indicates a high efficiency of light interception, and therefore a relatively fast rate of available RCII closure; a smaller σ_{PSII} would result in a longer time for light interception and hence RCII closure saturation. One such reason for different σ values is the expression of light-harvesting antenna proteins that are bound to either PSII or PSI; these proteins can be species specific. The reasons for the expression of these proteins relate to the different evolutionary histories of phytoplankton groups and for the acclimation to different oceanographic regimes (nutrients, light availability). More details regarding the application of this method, and protocols used are described in Chapter 2.

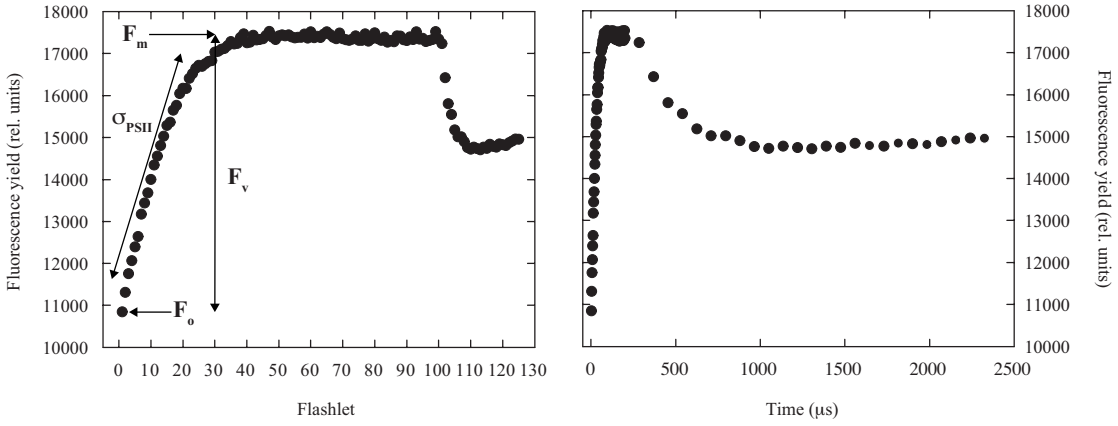

FIGURE 1.9: Schematic representation of the saturation of photosystem II (PSII) in terms of fluorescence yields detected by FRRf in response to excitation flashes. The same sequence is plotted against both flashlet number and time. The initial fluorescence yield (F_o) respresents background fluorescence whilst the maximum fluorescence yield (F_m) is induced once all the reaction centres (RCIIs) are closed, the difference between F_o and F_m provides the variable fluorescence F_v. The effective absorption cross section for PSII (σ_{PSII}) is given by the rate at which RCIIs are closed.

1.8.1 Uses of FRRf in Oceanography

FRRf was initially used *in situ* to assess the phytoplankton physiology in the oceans (Geider et al., 1993a; Greene et al., 1994; Kolber et al., 1990), with the knowledge that

TABLE 1.3: Fluorescence parameters and their definitions

Parameter	Definition	Units	Derivation
σ_{PSI}	Functional absorption cross-section for PSI	nm^{-2}	
σ_{PSII}	Functional absorption cross-section for PSII	nm^{-2}	
F_o	Minimum fluorescence yield (dark adapted, all RCIIs open)	I.U.	
F_m	Maximum fluorescence yield (dark adapted, all RCIIs closed with no NPQ)	I.U.	
F_v	Maximum variable fluorescence	Dimensionless	F_m - F_o
F_v/F_m	Maximum photochemical efficiency (quantum yield) of open RCIIs	Dimensionless	$(F_m - F_o)/F_m$

the maximal PSII photochemical efficiency (F_v/F_m) generally decreases under 'stressful' growth conditions (Geider et al., 1993b; Kolber et al., 1988, 1994). This concept led to FRRf measurements being applied across large temporal (Suggett et al., 2006a) and spatial (Behrenfeld et al., 1996; Moore et al., 2005, 2006a,b; Suggett et al., 2006b; Suzuki et al., 2002) (Figure 1.10) scales approaching those of entire oceanic ecosystems (Behrenfeld and Kolber, 1999; Behrenfeld et al., 2006; Suggett et al., 2006b) (Figure 1.11).

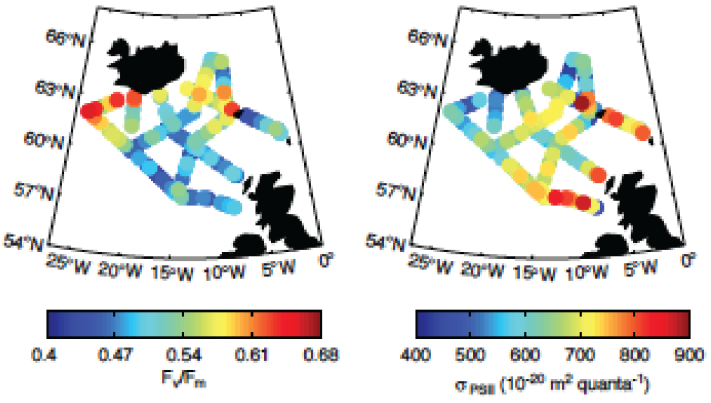

FIGURE 1.10: Maps of F_v/F_m and σ_{PSII} from Moore et al. (2005) in the Iceland Basin and Rockhall Trough of the North Atlantic.

FRRf measurements have also frequently been used in iron-addition experiments, both *in situ* (Figure 1.12) and in shipboard experiments (Figure 1.13). The results of such field measurements and experiments are not absolute measures of nutrient stress, as any FRRf measurement will contain both a physiological signal and a taxonomic signal (Campbell et al., 1998; Fishwick et al., 2006; Moore et al., 2005, 2006b; Prasil et al., 2008; Suggett et al., 2009, 2004). This is particularly important when working with

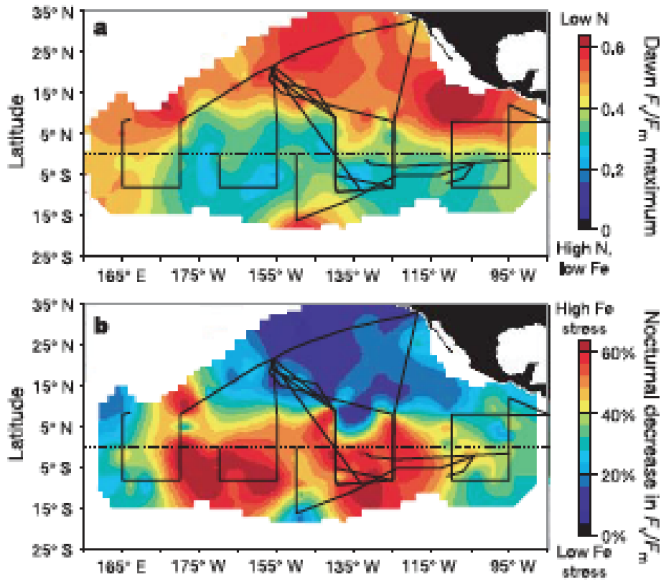

FIGURE 1.11: Maps of dawn maximum and nocturnal decrease in F_v/F_m from Behrenfeld et al. (2006) in the equatorial Pacific.

mixed communities in the oceans, as any physiological responses to iron addition may contain a taxonomic response as well.

Suggett et al. (2009) demonstrated that the magnitudes of variability in F_v/F_m and σ_{PSII} driven by changes in community structure exceed that induced by nutrient limitation, except in HNLC regions where strong phenotypic changes have been demonstrated upon relief of iron limitation. One such consistency with these nutrient addition experiments is that the timescale is greater than 24 hours, which allows for any changes in biomass to be measured. One such hypothesis for this change in biomass after 24 hours is a shift within the phytoplankton community. Therefore in order to differentiate between taxonomic signals and physiological signals experiment protocols must be utilised that do not allow for these subsequent changes in biomass and potential community structure.

1.9 P700 photo-oxidation kinetic Theory

Unlike PSII, which has a relatively high fluorescence yield at room temperature, PSI displays little fluorescence and no active fluorescence. Consequently, changes in absorption induced by charge separation of the core reaction centre chlorophyll P700 have been

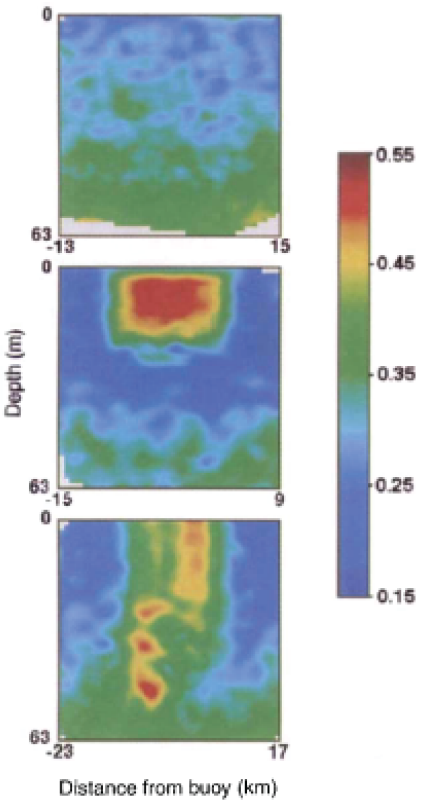

FIGURE 1.12: Changes in photochemical quantum efficiencies (F_v/F_m) in the upper 65 m of the water column resulting from the addition of nanomolar concentrations of iron in the equatorial Pacific Ocean, fromBehrenfeld et al. (1996).

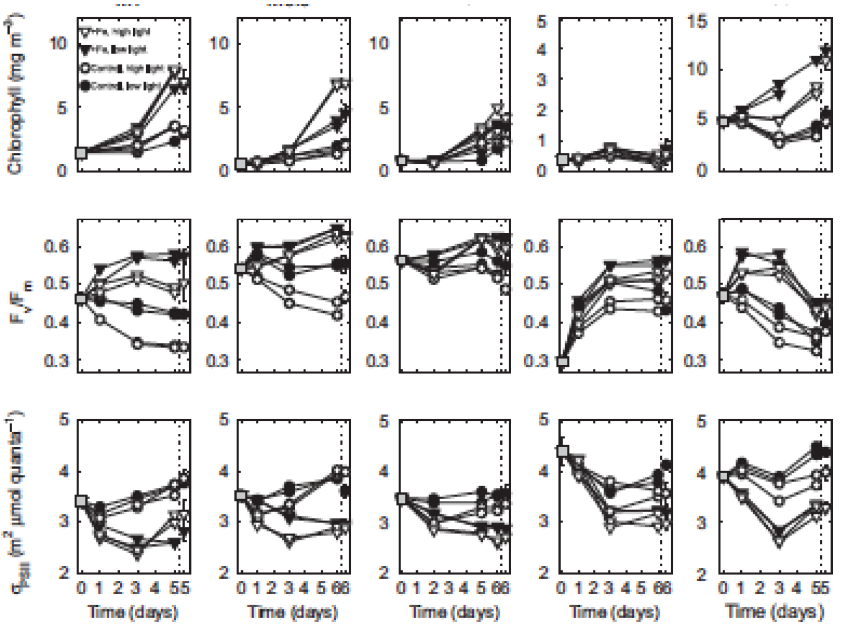

FIGURE 1.13: Results of iron addition bioassay experiments performed in the vicinity of the Crozet Plateau in the Southern Ocean from Moore et al. (2006b).

employed, which can be used to measure PSI characteristics such as the absolute cross-section. Several studies have attempted to measure the absolute cross-section of PSI (Boichenko and Litvin, 1986; Greenbaum and Mauzerall, 1986; Greenbaum et al., 1987; Melis, 1982; Melis and Anderson, 1983; Telfer et al., 1984), however the results of the experiments only provided a relative absorption cross-section. Zipfel and Owens (1991) demonstrated for the first time that P700 photo-oxidation kinetics can be used to determine the absolute PSI absorption cross-section. The basis of this was that the cross-section could be calculated from the effective rate constant for P700 photo-oxidation (K_{eff}) and unlike previous experiments that required whole cells; this technique could be applied to sub-cellular preparations. The data demonstrated that with a reasonable signal-to-noise ratio it was possible to measure a functional antenna size of PSI, however, the limitations of the method meant it was precluded from distinguishing small differences (10 - 20%) between samples. More details regarding this method and specific protocol can be found in Chapter 2.

1.10 Adaptations to Iron Limitation

Phytoplankton have evolved a wide range of mechanisms for coping with iron limitation, and these compensatory mechanisms were divided into three categories by Strauss (1994):

1. Retrenchment
2. Acquisition and storage
3. Compensation

Retrenchment refers to a reduction of physiological activities, the most notable is chlorosis; whereby the phytoplankton cell has reduced concentrations of chlorophyll or light-harvesting pigments (Greene et al., 1991, 1992). However, this response is not unique to iron limitation (Davey and Geider, 2001; Moseley et al., 2002). The second category, acquisition and storage, refers to excretion of siderophores and optimisation of iron storage systems respectively. Siderophores, high-affinity iron chelating compounds, are excreted by prokaryotic organisms, including cyanobacteria, (Haygood et al., 1993; Sunda, 2001) to chelate and solubilise aqueous iron species and iron minerals (Raiswell and Canfield,

2012). Eukaryotic organisms that are unable to produce siderophores may still be able to access this pool of iron (Granger and Price, 1999) via their membrane transporter systems (Amin et al., 2009; Maldonado and Price, 2001; Maldonado et al., 1999). The optimisation of iron storage systems includes the production of ferritin (Marchetti et al., 2009), an iron-storage protein, to safely concentrate and store iron while reducing the potential cell damage from reactive oxygen species and oxidative stress. Free iron is toxic to cells as it can act as catalyst in the formation of free radicals from reactive oxygen species. Ferritin binds to free ferrous irons and stores it in the ferric state, whereby its release can be safely controlled within the cell.

The third mechanism, compensation, can be further sub-divided into: alteration of thylakoid membrane, alteration of PSII:PSI ratio and overexpression of photosynthetic pigments. An example of alteration of the thylakoid membrane refers to the replacement of iron-containing proteins by an alternative protein without iron as a cofactor, the most notable is the replace of ferredoxin with flavodoxin (Ferreira and Straus, 1994; La Roche et al., 1996a). Changes in the PSII:PSI ratio arise due to the differential iron requirements for the separate photosystems (PSII = 3 iron atoms, PSI = 12 iron atoms), yet the function of an elevated PSII abundance of PSI is still not fully understood. Behrenfeld et al. (2008) proposed that the function of this elevated PSII:PSI ratio is to enhance ATP production though a PSII-MOX (midstream oxidase) pathway. The result of this alteration is a system in which PSI is focused on linear electron transfer (LET) for carbon fixation, whereas PSII activity is split between both LET and additional ATP production (Desquilbet et al., 2003). The PSII-MOX pathway results in a trans-thylakoid proton gradient, through PSII proton release in the lumen during water splitting and stromal consumption during MOX reduction of O_2 to H_2O (Behrenfeld and Milligan, 2013). Electrons flowing through PSI may also be redirected to the Mehler reactions to form H_2O rather than NADPH. All of the electron transport pathways described within this thesis are essential for cell functioning and the balancing of ATP/NADPH supply and demand (Behrenfeld et al., 2008).

The overexpression of photosynthetic pigments refers to the enigma of pigment synthesis increasing relative to growth rate during iron stress when macronutrient concentrations are high (Behrenfeld and Milligan, 2013). Several studies have found that the reductions in either chlorophyll concentrations or synthesis, under nutrient limitation, were less than that of the overall growth rate (Allen et al., 2008; Milligan, 1998; Moseley et al., 2002).

One of the most extensively studied pigment complexes that has been studied is the chlorophyll- and carotenoid-binding, iron-stress-induced protein IsiA of cyanobacteria, which is discussed in further detail in Chapter 3. The proposed function of IsiA and other pigment-protein complexes is to compensate for decreased PSI:PSII ratio by increasing PSI absorption cross-section (σ_{PSI}) (Bibby et al., 2001a,b,c; Boekema et al., 2001) by forming a PSI-IsiA complex. Yet in the study of IsiA it became apparent that the expression of IsiA associated with the increase in PSI cross-section could not account for the overall increase in bulk chlorophyll:reaction centre ratio (Riethman and Sherman, 1988). This excess of chlorophyll-binding proteins is not unique to cyanobacteria, it has been reported in several eukaryotic species as well (*Rhodella violacea* - (Desquilbet et al., 2003), *Dunaliella salina* - (Varsano et al., 2003, 2006), *Phaeodactylum tricornutum* - (Greene et al., 1991)).

The consequences of these excess chlorophyll-binding proteins is a reduction of F_v/F_m through an elevated F_o (Benesova et al., 2000; Berera et al., 2009; Davey and Geider, 2001; Desquilbet et al., 2003; Greene et al., 1992; Guikema and Sherman, 1983; Lin et al., 2001; Morales et al., 2001; Moseley et al., 2002; Price, 2005; Riethman and Sherman, 1988; Vassiliev et al., 1995), possibly due to being energetically disconnected from the photosynthetic electron transport chain (Behrenfeld et al., 2006). Understanding how these excess chlorophyll-binding proteins behave under iron limitation will provide a valuable insight into reconciling the response of iron-addition experiments with phytoplankton photophysiology. Their presence within eukaryotes has only recently been discovered (Varsano et al., 2003, 2006) and their role within the photosynthetic apparatus requires further clarification. The potential for these complexes to influence variable chlorophyll fluorescence will have wide ranging consequences for understanding photosynthetic physiology, iron addition responses and oceanographic measurements of primary productivity. The aim of this study is to quantify the abundance of these chlorophyll-binding proteins in culture, and to determine their potential influence within iron limited areas of the ocean.

1.11 Thesis Outline

The aim of this thesis is to gain a better understanding of the phenotypic response of phytoplankton to iron limitation, specifically the role of chlorophyll-binding proteins.

While their role has been greatly studied within cultural studies of cyanobacteria, their specific role has yet to be established. Moreover, these proteins have only recently been discovered within eukaryotes highlighting a potential physiological response that may be ubiquitous to all phytoplankton. These proteins have also yet to be investigated in the field, thus far these studies have been restricted to culture studies of model organisms. While there is not yet an absolute method to quantify these proteins in the field, there presence can be determined through the use of other methods. Such as the measurements of F_v/F_m upon the relief of iron addition, wherein excess chlorophyll-binding proteins are hypothesised to suppress F_v/Fm under iron limitation by increasing F_o.

In order to investigate the role and abundance of iron-stress induced chlorophyll-binding proteins the following objectives were set:

To quantify the abundance of the chlorophyll-binding protein IsiA within iron-limited cultures in Synechocystis *sp.* PCC 6803.

To measure the characteristics of variable chlorophyll fluorescence of an iron-limited culture (Synechocystis *sp.* PCC 6803) and iron limited oceanic regions (high latitude North Atlantic, Ross Sea).

To investigate the potential role of chlorophyll-binding proteins within phytoplankton and their effect upon variable chlorophyll fluorescence.

Iron limitation of Synechocystis *sp.* PCC 6803 is expected to induce the expression IsiA to a ratio of 6:1 with PSI, thereby increasing the relative effective cross-section of σ_{PSI}. Alongside this increase in IsiA, if the expression increases beyond the expected the ratio then the excess chlorophyll-binding protein will suppress the F_v/F_m of the iron limited cultures by increasing F_o. Iron limited field populations (the high latitude North Atlantic and the Ross Sea) will show the inverse when relieved from iron limitation, a decrease in F_o will result in an increase in F_v/F_m.

Data presented in this thesis were collected from one culture study and field studies in two oceanic regions (high latitude North Atlantic, Ross Sea). A description of methods used to collect, process and analyse the data, including sampling regimes and locations, is provided in **Chapter 2**. **Chapter 3** presents the abundance of the pigment-protein complex, IsiA, within an iron-limited *Synechosystis* sp. PCC 6803 culture and its potential role in affecting cellular physiology and variable chlorophyll fluorescence. **Chapter**

4 presents the results of nutrient addition incubation experiments in the high latitude North Atlantic, a highly productive region of global ocean. **Chapter 5** presents the results of nutrient addition incubation experiments in the Ross Sea, a globally important ecosystem, that is unique with its distinct seasonal succession between two phytoplankton taxa. A synthesis and summary of all the variable chlorophyll fluorescence data is given in **Chapter 6**, along with implications for further study on this topic.

Chapter 2

Materials and Methods

2.1 *Synechocystis* Growth Conditions

Synechocystis sp. PCC 6803 (Bricker et al., 1998) was grown photoheterotrophically in mineral medium in BG-11 (Williams, 1988) supplemented with glucose at 30°C and with illumination of 10 μmol photons nm^{-2} s^{-1}. These growth conditions were chosen to produce the maximum amount of available biomass for biophysical measurements, and are not to be considered as representative growth conditions for field populations. Iron-stressed cultures were obtained by inoculating into BG-11 medium without added iron. However this iron free media was not passed through a chelex to remove any residual iron. All cultures were grown under batch conditions for a period of 5 days, with inoculation of new experimental cultures carried out from cells grown under iron-replete conditions. Experiments were only carried out after the iron-replete starting stock were acclimated for 7 days. Cells were harvested every day over the course of 5 days with samples collected for protein quantification and chlorophyll content. Within each experiment all analyses were performed on triplicate independent cultures, results presented here are from a series of 3 independent experiments. For all experiment data please refer to Appendix A Tables A.1 and A.2.

2.2 High Latitude North Atlantic General

Data were obtained during two cruises of the *RRS* Discovery to the high latitude North Atlantic (HLNA), a spring cruise (D350) from 28th April to 10th May 2010 (Day of Year (DOY) 118-130) and a summer cruise (D354) from 4th July to 10th August 2010 (DOY 185-222). During the spring cruise 8 short-term (24 h) and 2 long-term (>24 h) incubation experiments were performed. A further 17 short-term and 7 long-term incubation experiments were undertaken during the summer cruise. Figure 2.1 displays the cruise track from both cruises and the set up locations of the incubation experiments. Long-term experiments were run between 48 h and 120 h dependent upon the residual nutrient stock of the initial water collected, i.e. low macronutrients equals a shorter experimental duration. The aim of the long-term experiments were to assess not only changes in the photophysiology following relief from iron addition but to also assess the changes in biomass and nutrient drawdown. Short-term experiments were run for 24 h as the aim was to only assess the changes in photophysiology without any of concomitant changes in biomass and nutrient drawdown.

2.3 The Ross Sea General

Data were obtained on a cruise of the R/V Nathaniel B. Palmer to the Ross Sea (NBP12-01), from 24th December 2011 to 10th February 2012 (DOY 358 - 041). During the cruise 29 short-term (24 h) and 3 long-term (>24 h) incubation experiments were performed. Figure 2.2 displays the set up locations of the incubation experiments. Short-term experiments followed the same objective as those set up in the HLNA. Long-term experiments were run for 168 h in the Ross Sea due to the decreased sea surface temperature, which is proposed to suppress the growth rate of the phytoplankton community.

2.4 Iron Enrichment Experiment Set Up

Incubation experiments were performed using a similar method to that employed previously in the HNLC Southern Ocean and Iceland basin (Moore et al., 2007; Nielsdóttir et al., 2009). Water for the experiments was collected using either a trace metal clean tow fish or CTD rosette system, and transferred unscreened into acid washed 1.0 L

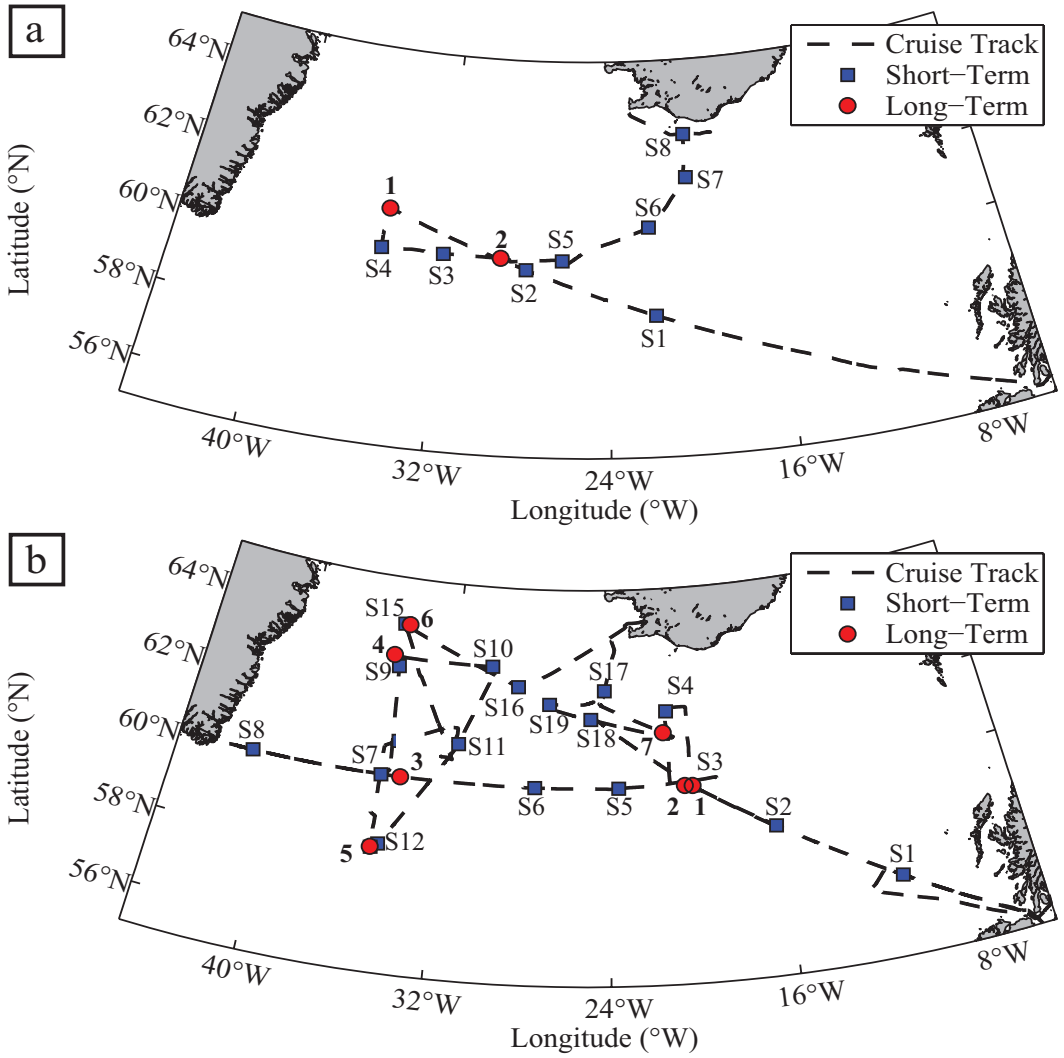

FIGURE 2.1: Maps of the High Latitude North Atlantic (HLNA) detailing the cruise track (dashed line) and experimental set-up locations (blue squares = short-term, red squares = long-term). a) Cruise track and experimental set-up locations during cruise D350 and b) Cruise track and experimental set-up locations during cruise D354. Long-term experiment numbers in bold, short-term experiments S1-S8, and S1-S19.

polycarbonate bottles (Nalgene) for the 24 h incubation experiments and 4.5 L polycarbonate bottles for the long-term incubation experiments. A smaller volume of water was used for the short-term experiments in order to allow for an increased sampling regime, thereby increasing the spatial and temporal range. All water was collected during the hours of darkness, except for PRISM where there was 24 h of sunlight. Incubation bottles were filled in a random order, with triplicate samples for initial measurements collected at the beginning, middle and end of the filling process. The water collected was unfiltered for grazers.

In addition to an unamended control, within the 24 h incubation experiments, different

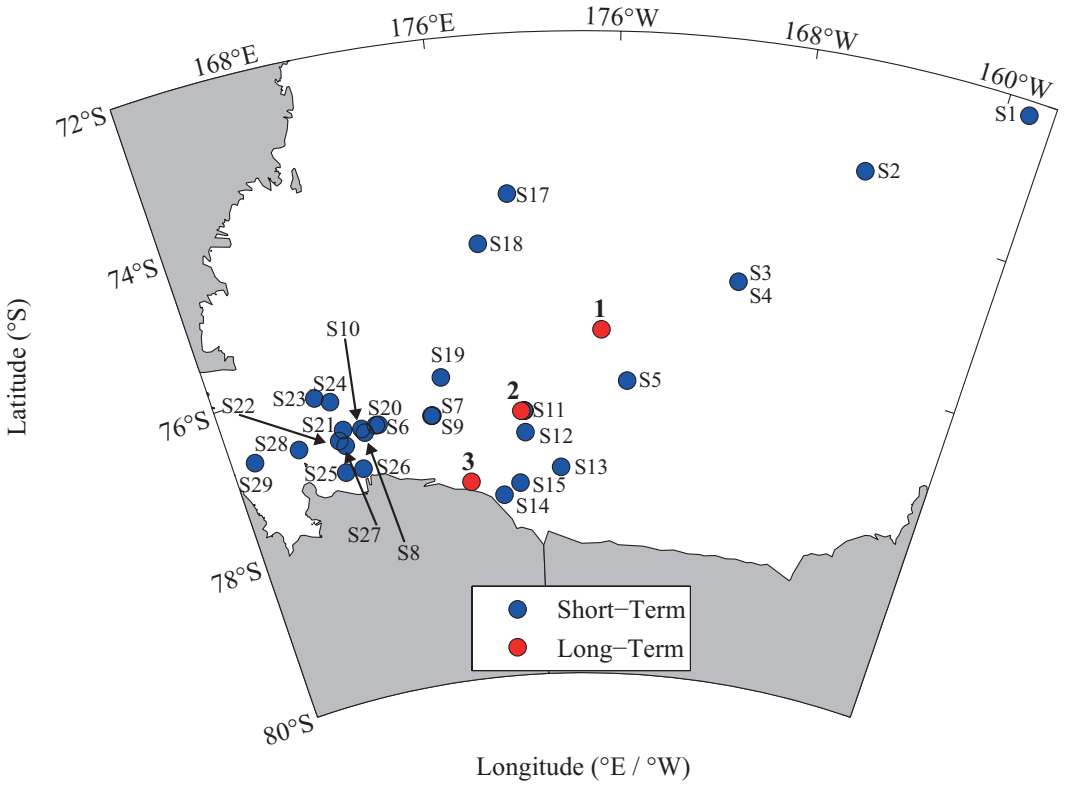

FIGURE 2.2: Map of the Ross Sea the experimental set-up locations during cruise NBP12-01. Red circles = long-term experiments, blue circles = short-term experiments. Long-term experiment numbers in bold.

treatments were amended with: 0.2 nmol L^{-1} $FeCl_3$, 2.0 nmol L^{-1} $FeCl_3$, 1.0 μmol L^{-1} NO_3^- or 2.0 nmol L^{-1} $FeCl_3$ and 1.0 μmol L^{-1} NO_3^- (hereafter, + 0.2 Fe, + 2.0 Fe, + 1.0 N and + FeN). During PRISM, experiments were run for 48 h and consisted of only a 2.0 nmol L^{-1} $FeCl_3$ and control treatment. All experimental conditions were conducted as biological duplicates or triplicates. Initial conditions and summaries for short-term experiments from D350 and D354 can be found in Appendix B Tables B.11, B.12, B.13 and B.14, and for PRISM in Appendix C Tables C.5 and C.6.

During D350 and D354, long-term experiments were run for 48 - 120 h and consisted of two treatments, a control and 2.0 nmol L^{-1} Fe addition only (hereafter, + Fe), or four treatments, a control, 2.0 nmol L^{-1} Fe, 2.0 μmol L^{-1} NO_3^- and 2.0 nmol L^{-1} Fe + 2.0 μmol L^{-1} NO_3^- (hereafter, + Fe, + N and + FeN). During PRISM, long-term experiments were run for 168 h and consisted of two treatments, a control and 2.0 nmol L^{-1} $FeCl_3$ addition only (hereafter, + Fe). Tables 2.1, 2.2 and 2.3 contain the treatment set up within each experiment and the duration of the experiment for D350, D354 and PRISM respectively. For D350 and D354 experiment locations and metadata can be

found in Appendix B Table B.1, experiment locations and metadata for PRISM can be found in Appendix C Table C.1. For all D350 and D354 experiment data please refer to Appendix B Tables B.2 to B.10. For all PRISM experiment data please refer to Appendix C Tables C.2 to C.4.

All bottles tops were sealed with film (Parafilm^{TM}) and bottles were double bagged with clear plastic bags to minimise contamination risks on deck. On-deck incubations were performed using 'blue lagoon' filters (LEE Filters) to provide light levels corresponding to 35% of above surface irradiance. As all sub-sampling was carried out during the hours of darkness, any potential fluctuations in irradiance should be negated during the dark acclimation. Excepting PRISM where there were 24 hours of irradiance, and measurements of mean irradiance were not shown to fluctuate greatly. Running surface seawater was used to control the temperature in the incubators. During D354 the average temperature fluctuation of surface seawater was less than 2 - 3 °C, excepting short-term experiment 8 which underwent a 12 °C temperature fluctuation. The average temperature fluctuation during PRISM ranged from 2 °C to -2 °C.

Table 2.1: Set up of the long-term nutrient addition experiments during D350

	Experiment	
Treatment	1	2
Control	✓	✓
2.0 nmol L^{-1} Fe	✓	✓
Duration (h)	120	120

Table 2.2: Set up of the long-term nutrient addition experiments during D354

	Experiment						
Treatment	1	2	3	4	5	6	7
Control	✓	✓	✓	✓	✓	✓	✓
2.0 nmol L^{-1} Fe	✓	✓	✓	✓	✓	✓	✓
2.0 μmol L^{-1} NO_3^-	✓	✓	✗	✗	✓	✗	✓
2.0 μmol L^{-1} NO_3^- + 2.0 nmol L^{-1} Fe	✓	✓	✗	✗	✓	✗	✓
Duration (h)	48	48	120	120	72	120	72

Table 2.3: Set up of the long-term nutrient addition experiments during PRISM

	Experiment		
Treatment	1	2	3
Control	✓	✓	✓
2.0 nmol L^{-1} Fe	✓	✓	✓
Duration (h)	168	168	168

2.5 Biomass and phytoplankton community structure

2.5.1 Chlorophyll *a*

Chlorophyll *a* (Chl *a*) was measured during culture studies and field studies to provide information on the relative abundance of this photosynthetic pigment, and as proxy for phytoplankton biomass. During culture studies, 0.5 - 2.0 mL water samples were filtered onto 25 mm glass fibre filters (GF/F) (Fisherbrand MF300 or Whatmann), and during D350, D354 and PRISM 50 - 250 mL, depending on the available biomass of the region, were filtered. The filters were extracted into 90% Acetone for 24 h in the dark at 4°C. Fluorimetric measurement of Chl *a* was performed using either a Turner Designs 10-AU or Turner Designs TD700 fluorometer following the methods of Welschmeyer (1994). On D350 and D354 size fractionated Chl *a* was also measured in <5 μm and >5 μm fractions. The >5 μm fraction was filtered onto a 5 μm polycarbonate filter (Whatman) and extracted as previously discussed. The <5 μm fraction was calculated by subtracting the >5 μm fraction from total Chl *a*. These size fractions were chosen to be representative of picoeukarotyes and larger phytoplankton (e.g. diatoms).

Growth rates based upon chlorophyll concentrations were calculated as follows.

$$\mu^{\mathrm{Chl}} = \frac{ln(Chl^{\mathrm{t=n}}/Chl^{\mathrm{t=0}})}{Time(t=n)} \tag{2.1}$$

2.5.2 Flow Cytometry

Flow cytometry samples were taken ($\sim$ 1.8 mL) for cell enumeration on culture samples. Samples were fixed in 1% paraformaldehyde and incubated at 4°C for 24 h before being flash frozen in liquid nitrogen and stored at -80°C. Enumeration was performed using a Becton Dickinson Facsort$^{\mathrm{TM}}$ flow cytometer (Becton Dickinson Biosciences, Oxford, UK), which allowed both cell enumeration of Synechocystis culture samples. A reference bead stock was added to all samples at a known concentration to enable enumeration using syringe pumped flow cytometry (Zubkov and Burkill, 2006).

2.6 FRRf Methodology

Measurements of PSII photosynthetic efficiency were achieved using fast repetition rate fluorometry. Two active chlorophyll fluorometers were employed throughout the course of my PhD project; the FastTracka^{TM} MKI (Chelsea technologies group, West Moseley, Surrey, U.K.) (D350, D354) and the FastTracka^{TM} MKII (Chelsea technologies group) (Culture Experiment, D350, D354, PRISM). On D350 and D354 FRRf data was collected underway using a FastTracka MKI system connected to the ship's non-toxic supply system, thereby removing any potential effects of biofouled water supplies.

The fast repetition rate technique employs a series of brief subsaturating excitation pulses or 'flashlets' where the intensity, duration and interval between them is independently controlled. The instrument uses a bank of blue light emitting diodes (LED) as an excitation source. Emitted fluorescence is collected through a pair of interface filters and a long pass filter. The fluorescence signal is detected using a photomultiplier and a small portion of the excitation light, detected by a photodiode, is used as a reference signal (Kolber et al., 1998).

A series of different single turnover (ST) excitation protocols were utilised throughout the course of this project. The protocols for the FRRf MKI are outlined in Table 2.4. The ST discrete settings consists of a series of 100 flashlets per sequence, each of 4.0 μs duration at 0.0 μs intervals. This protocol includes relaxation sequences to evaluate kinetics of reoxidation, which consists of 20 flashlets of 4.0 μs duration at 61.0 μs intervals. The number of acquisitions is set as required for this setting, and the PMT gain setting is decided upon the basis of the sample density, lower sample density equates to a higher PMT gain setting. The underway settings follows the same ST protocol, excepting the number of acquisitions and the PMT gain which is set to autoranging, with a 30 ms sleep time between acquisition. In both protocols the measurements are carried out within the dark chamber, with the data internally logged to a flashcard before downloading to desktop mode.

The ST protocols utilised with the FRRf MKII are outlined in Table 2.5, with the culture settings referring to the *Synechocystis* sp. PCC 6803 data and the discrete settings referring to the cruise data. The culture ST protocol consists of 300 flashlets per sequence at a 1.0 μs duration, with a series of 25 relaxation flashlets at 84.0 μ

duration. There was a total of 24 sequences per average, an interval of 100 ms between sequences. The LED set controls the intensity of the LEDs used to excite the sample. The discrete settings consisted of only 100 flashlets, with a lower LED set but with an increased number of sequences per average.

TABLE 2.4: FRRf settings employed for data collection with the FastTracka MKI system. *set as required.

Parameter	Discrete settings	Underway settings
Number of acquisitions	*	65535
Flash sequences per acquisition	16	16
Saturation flashes per sequence	100	100
Saturation flash duration	4	4
Saturation inter-flash delay	0	0
Relaxation flashes	enabled	enabled
Relaxation flashes per sequences	20	20
Relaxation flash duration	4	4
Relaxation inter-flash delay	61	61
Sleeptime between acquisitions	30	30000
PMT Gain	*	Autoranging
Analyse output	disabled	disabled
Desktop verbose mode	enabled	enabled
Light chamber	disabled	disabled
Dark chamber	enabled	enabled
Logging mode to internal flashcard	enabled	enabled

TABLE 2.5: FRRf settings employed for data collection with the FastTracka MKII system.

Parameter	Culture settings	Discrete settings
Sequences per average	24	64
Sequence interval (ms)	100	100
Acquisition pitch	35	1
No. of sat. flashlets	300	100
Flashlet duration (μs)	1	1
No. of rel. flashlets	25	25
Flashlet duration (μs)	84	84
LED set	128	48

During the first cruise (D350), a FastTracka MKI was also used to measure discrete samples as the MKII had thus far never been tested at sea by our research group. Figure 2.3 displays the comparison between the two different instruments for different bioassay experiments during D350. The curve fitting from the MKI measurements was performed using software run in MATLAB^{TM}, based on original codes provided by Laney

(2003). The comparison between the two instrument shows that there is a reasonably good agreement, for F_v/F_m ($R^2 = 0.87$) and σ_{PSII} ($R^2 = 0.79$). The wide range in both Fv/F_m and σ_{PSII} are indicative of the different physiological and taxonomic communities sampled. For the purpose of this thesis only values from the MKII machine will be used when discussing the FRRf results from the bioassay experiments. Corrections for instrument response and calibrations of fluorescence yields were performed using extracts of chlorophyll a.

All samples measured were dark acclimated for 30 min and FRRf measurements were corrected for the blank effect using carefully prepared 0.2-μm filtrates for all experiments and time-points (Cullen and Davis, 2003). Blanks were typically around 1% and always <10% of the maximal fluorescence signal. Size-fractionated FRRf measurements were performed by gentle filtration through a 5-μm polycarbonate filter, with the <5-μm fraction measured directly on the filtrate and the >5-μm fraction measured following gentle resuspension of retained cells in 0.2-μm filtered seawater.

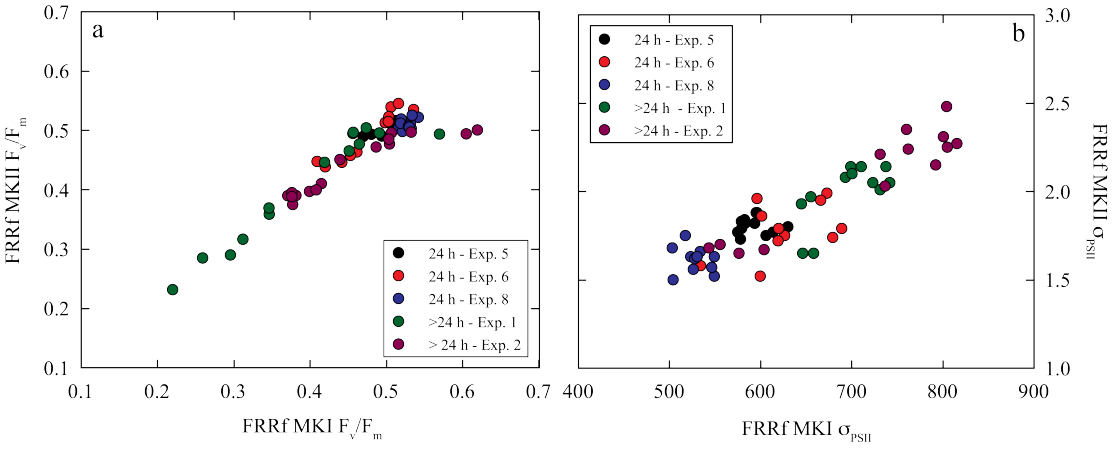

FIGURE 2.3: A comparison of the differential instrument response, a) F_v/F_m and b) σ_{PSII}, of the FastTracka MKI and FastTracka MKII from different incubation experiments measured during cruise D350.

2.7 PAM Methodology

The redox kinetics of P700 were measured following the absorption changes at 830 nm relative to 870 nm using the following custom protocol (Figure 2.4), these wavelengths were chosen in order to negate any potential interference from chlorophyll and plastocyanin. The custom protocol consisted of switching on the fluorescence measuring light

(FML) and switching the measuring light pulse frequency to max (MF-max) which is 400 kHz. After 10 ms a saturating multiple turnover flash (MT) was switched on for 3 ms. At the same time the MT was switched on and off, the sample and hold amplifier (S & H off) was also switched off due to the rapid changes in light. The intensity of the MT flash used for redox kinetics of P700 ranged from 5 mmol photons m^{-2} s^{-1} to 20 mmol photons m^{-2} s^{-1}.

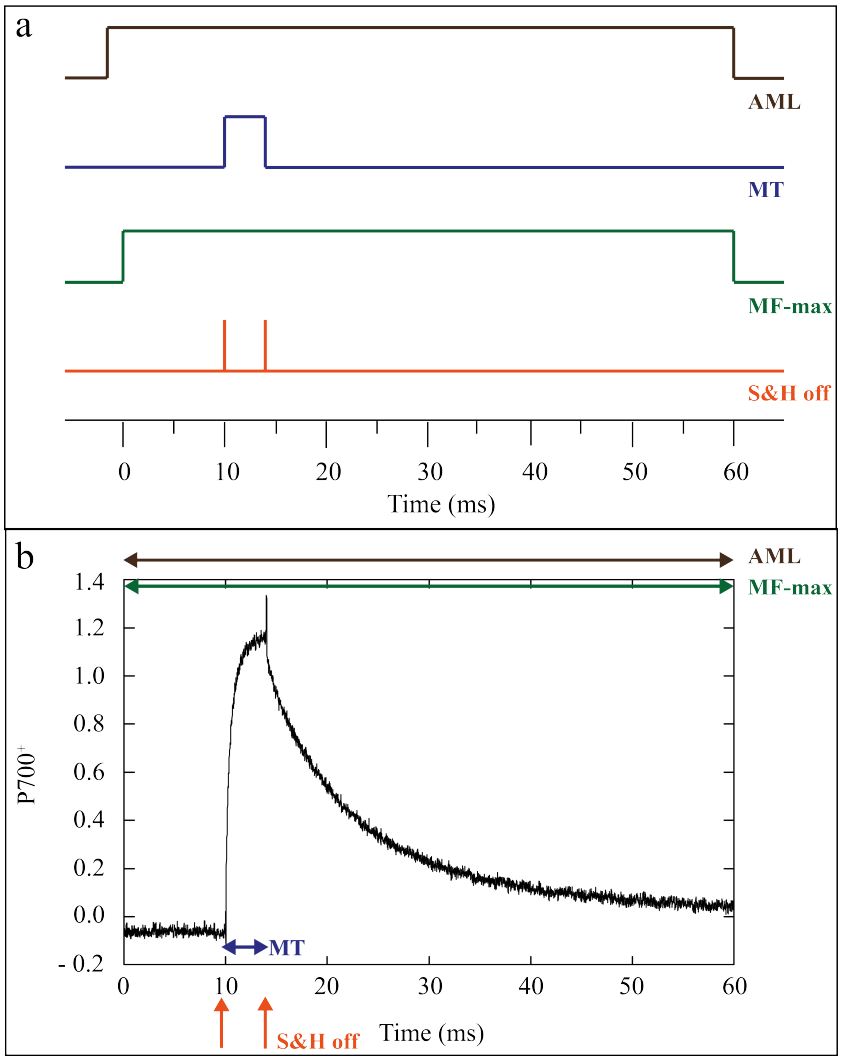

FIGURE 2.4: a) Principle of measuring the cross-section using the Saturation Pulse Method. AML = absorption measuring light on, MT = saturating multiple turnover flash, MF-max = measuring light pulse frequency, and S & H off = sample and hold amplifier. b) Example data of $P700^+$ against time (ms) annotated with cross-section pulse protocol.

Harvested whole cells were gently concentrated to increase signal to noise ratios to allow resolution of kinetic measurements of P700 oxidation at 7.5 μs time resolution over 50 ms timescales. Accurate estimates of absolute σ_{PSI} on cultures dense enough for ΔA_{820}

measurements require correction for absorption of the saturating pulse within the culture (Zipfel and Owens, 1991). Indeed even relative changes in σ_{PSI} between cultures would be susceptible to artefacts resulting from the need to make such measurements in optically dense situations. Culture absorption was thus measured at the wavelength, A_{635}, of the saturating pulse using a Varian Cary 50 Scan UV-Visible spectrophotometer (Agilent Technologies UK Ltd., Wokingham, Berkshire, U.K.). Raw ΔA_{820} measurements were analysed using custom software in a MATLAB$^{\mathrm{TM}}$ computing environment following Zipfel and Owens (1991). Briefly, the effective photochemical rate constant for P700 oxidation (K_{eff}) measured under monochromatic saturating light (E_{635}) will be related to the total absorption of the sample at that wavelength (A_{635}) and the functional absorption cross section according to (Zipfel and Owens, 1991):

$$K_{eff} = \sigma_{\mathrm{PSI}} E \frac{(1 - e^{-A})}{A} \tag{2.2}$$

Values for $\mathrm{K_{eff}}$ were derived from nonlinear least squares fitting of ΔA_{820} saturation kinetics as a function of time (t) to:

$$\Delta A_{820} = \Delta A_{820\ \mathrm{max}}(1 - e^{-K_{eff}t}) \tag{2.3}$$

Where $\Delta A_{820\ \mathrm{max}}$ is the maximum absorption change measured in a given sample under saturating light. Correction for re-reduction of $P700^{+}$ during the saturation flash (Zipfel and Owens, 1991) was not performed, as kinetic measurements indicated that the effective rate constant for this process was an order of magnitude lower than K_{eff} (Figure 2.4).

Formation of the IsiA-PSI supercomplex is expected to be capable of increasing σ_{PSI} by 70% (Bibby et al., 2001b). For further comparison with measured values of σ_{PSI}, absolute theoretical cross-sections for an isolated PSI (trimer) and the IsiA-PSI supercomplex (Bibby et al., 2001b) were calculated using the in vivo absorption of a single chl molecule (Bidigare et al., 1990; Johnsen et al., 1994), and assuming 100 chl molecules in a single PSI protein complex (Jordan et al., 2001) and that every IsiA protein binds at least 12 chl molecules (Ferreira et al., 2004; Murray et al., 2006).

2.8 Fluorescence spectroscopy

Fluorescence spectroscopy was undertaken on *Synechocystis* sp. PCC 6803 cultures using a Varian Cary 50 Scan^{TM} UV-Visible spectrophotometer, on samples that had been sonicated on a freeze thaw cycle using a Sonics & Material VibraCell^{TM} (Sonics and Materials Inc, Newtown, Connecticut, USA) in order to extract the thylakoid membranes. Scans were performed on a medium resolution from 250 nm to 800 nm on triplicate cultures from both treatments over the course of 5 days.

2.9 Nutrients

Seawater samples for concentrations of nitrate, phosphate and silicate on D350, D354 and PRISM were collected from the stainless steel CTD rosette system and the non-toxic underway supply system (intake depth 5-7 metres) on D350 and D354. Samples were collected unfiltered into either 40 mL diluvials or pre filtered through a 0.45 μm syringe filter into an acid washed 50 mL tube, and were refrigerated at 4°C until analysis, which commenced within 12 hours of sampling. Analysis was undertaken on a Skalar San Plus segmented flow autoanalyser on D350 and D354, and on a five-channel Lachat Instruments QuikChem FIA+ 8000s series autoanalyser on PRISM. The limit of detection calculated for nutrient analysis on the cruises is listed in Table 2.6.

TABLE 2.6: Limit detection for nutrients calculated on the cruises.

Nutrient	D350	D354	PRISM
Nitrate + Nitrite (μM)	0.12	0.09	0.07
Phosphate (μM)	0.010	0.020	0.025
Silicate (μM)	0.02	0.01	0.34

2.10 Dissolved Fe

During the cruises D350 and D354 trace metal water samples were collected using a titanium-frame CTD rosette system and from a tow fish deployed off the side of the ship. The trace metal clean niskin bottles were transferred to a dedicated clean chemistry container for sample processing. Trace metal clean water was pumped from a trace metal clean fish (Bowie et al., 2001) towed at a depth of $\sim$ 4 m, while the ship was steaming at no less than 5 knots, into a dedicated clean chemistry container using a

polytetrafluoroethylene (PTFE) diaphragm pump (Almatec - 15). Concentrations of dissolved iron for samples collected using the trace metal clean fish were determined by isotope dilution inductively coupled plasma mass spectrometry as described by (Milne et al., 2010). Analysis was performed on an Element II instrument (ThermoFisher Scientific, Bremen, Germany) following an offline pre-concentration and matrix removal step via solid phase extraction on a column filled with the chelating resin WAKO CM-PEHA. Accuracy of the method was verified by analysis of SAFe (Sampling and Analysis of iron) reference samples.

During PRISM, trace metal water samples were collected using a titanium-frame CTD rosette system with Teflon-lined, external closure 5L Niskin-X samplers (General Oceanics). Following collection of the samples, they were filtered (within 4 hours of collection) using 0.2 μm pore Supor Acropak filter capsules (Pall Corp.), then acidified to pH 1.7 with Seastar Baseline ultrapure hydrochloric acid (4.0 mL of 6 M acid per litre of sample). The samples were analysed by flow injection analysis with colourimetric detection, following in-line preconcentration on resin-immobilised 8-hydroxyquinoline. The method is modified from that described by Measures et al. (1995), with an updated version described in Sedwick et al. (2011), however samples were analysed within 24 h of collection. The accuracy of the method was verified by analysis of SAFe reference seawater samples (Johnson et al., 2007).

2.11 Protein Analysis

2.11.1 Culture Sample Collection

Harvested whole cells were gently concentrated by centrifugation; samples were spun down in 50 mL centrifuge tubes for 10 minutes at 4000 rpm at 4°C. The pellet was resuspended in 2 mL of supernatant and placed in a 2 mL eppendorf tube, before being spun down for a further 5 minutes at 13,500 rpm and the supernatant was removed. Pellets were flash frozen in liquid nitrogen and stored at -80°C until analysis.

2.11.2 Environmental Sample Collection

During PRISM, seawater samples were collected in 20 L niskin bottles mounted on a CTD rosette system and were decanted into 20 L acid rinsed polycarbonate carboys (nalgene) using acid cleaned silicone tubing. Samples were collected from the surface (5-10 m) and from a secondary biologically important depth, either the deep-chlorophyll maximum (DCM) or the bottom of the mixed layer. Samples were filtered onto glass fibre filters (Fisherbrand MF 300 or Whatmann), and four replicate samples of 0.5 - 4 L of seawater were filtered dependent upon the biomass. Filtering times were usually around 1.5 h and no more than 2 h, before filters were placed in cryo vials and flash frozen in liquid nitrogen. Filtering times were selected to prevent any protein degradation during sampling (Macey, A.I., *personal communication.* Samples were stored at -80°C until analysis.

2.11.3 Protein extraction

Protein extraction was performed in 1× denaturing extraction buffer (1× PSB), containing 140 mM Tris Base, 105 mM Tris-HCl, 0.5 mM ethylenediaminetetraacetic acid (EDTA), 2% lithium dodecyl sulphate (LDS), 10% glycerol and 0.1 mg ml^{-1} PefaBloc SC (AEBSF) protease inhibitor (Roche). 250-1000 μl 1× PSB was added to samples collected, before extraction began. For extraction, samples frozen in liquid nitrogen were sonicated for 15 seconds using a VibraCell solicitor (Sonics & Materials, Inc.) with a microtip attachment at a duty cycle setting of 35%. Samples were refrozen in liquid nitrogen immediately to avoid excess heating, and 4 sonication freeze/thaw cycles were used to extract samples.

A test was performed to look at how the number of sonication freeze/thaw cycles affects the protein concentrations (Figure 2.5), chlorophyll concentrations (Figure 2.6) and the concentration of specific peptide targets. A range of different sonication cycles were used (2, 4 and 6), and based upon the optimum return of the variables 4 sonications was determined to be ideal. This is also in good agreement with other studies that have examined protein extractions for immunodetection (Macey, A.I., *personal communication*).

Subsamples of extract were taken to determine Chl *a* total protein concentration. The sub-samples taken for Chl *a* analysis were diluted into 90% acetone and measured on

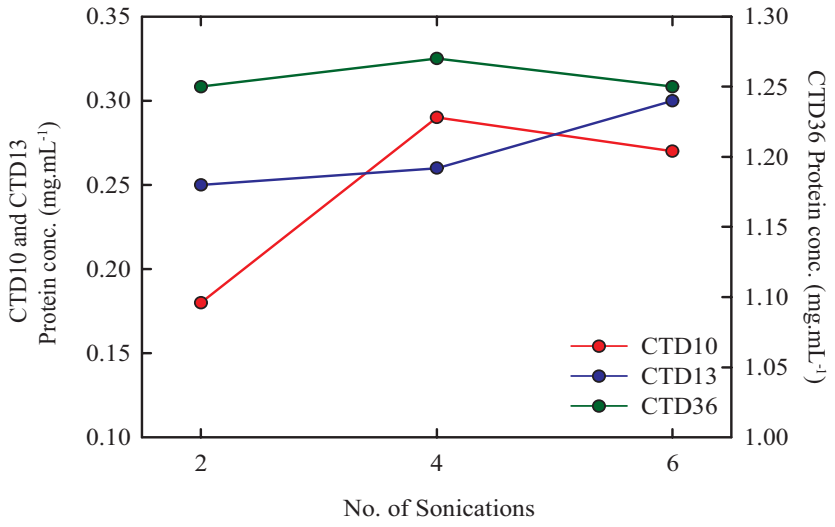

FIGURE 2.5: Protein concentration (mg.mL^{-1}) versus number of sonication cycles from three different CTD stations during the PRISM cruise.

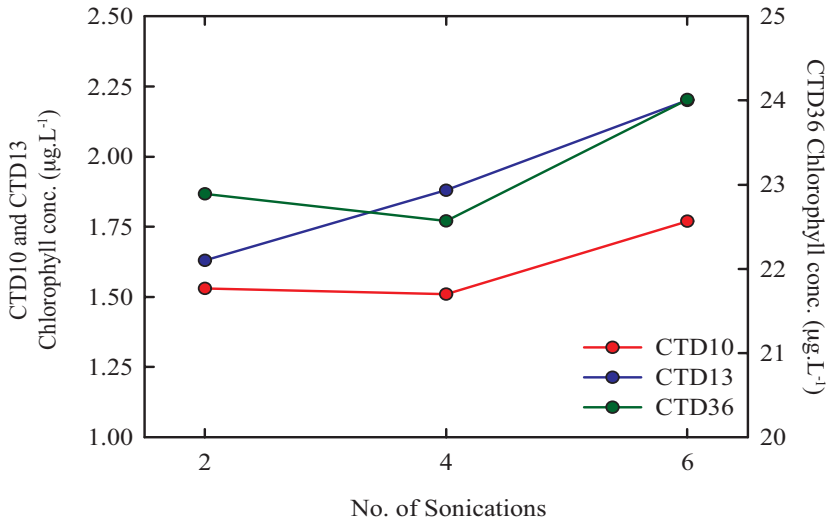

FIGURE 2.6: Chlorophyll concentration (μg.L^{-1}) versus number of sonication cycles from three different CTD stations during the PRISM cruise.

either a Turner Designs 10-AU fluorometer or a Turner Designs TD-700 fluorometer. Total protein concentration was measured with a modified Lowry assay (DC protein assay, Bio-Rad) (Lowry et al., 1951; Peterson, 1979) using bovine gamma globulin as a comparative protein standard. 96-well plates were used for total protein analysis and absorbance, at 750 nm, was measured using a FLUOstar Optima plate reader (BMG Labtech).

2.11.4 Electrophoresis, immunoblotting and quantification

To enable quantification of target subunits (IsiA, PsaC, PsbA and RbcL) in sample extracts, protein standards (Agrisera, Sweden) were run alongside samples on each gel to produce a standard curve. Each standard curve was formulated from either 3 or 4 points, and showed a good correlation (R^2 >0.95). This method was optimised for the use of the commercially available protein standards and antibodies developed by Agrisera.

Dithiothreitol (DTT) was added to a final concentration of 50 mM in the samples and standards, with a blue loading buffer, before being heated to 80°C for 5 minutes. Following heating, samples were spun down for 15-30 seconds in a microcentrifuge. Gel loading was based upon either total protein or Chl *a* concentrations (see Table 2.7). Proteins were separated by electrophoresis on 4-12% acrylamide mini-gels (NU-PAGE Bis-Tris gels, Invitrogen) in MES running buffer (Invitrogen) in an XCell Sure-Lock Tank (Invitrogen) at 200V for 35-40 minutes. Following electrophoresis, proteins were transferred to polyvinylidene difluoride (PVDF) (Immobilon-P, Millipore) membranes. Prior to transfer, the membranes were pre-washed in 100% methanol and equilibrated in 1× transfer buffer (Invitrogen). The transfers were performed using the XCell blot module (Invitrogen) for 55-70 minutes dependent upon protein size and number of transfers per blot module.

Once the transfer was complete, the blot membranes were blocked in 2% ECL Advance blocking reagent (GE Healthcare) in 20 mM Tris, 137 mM sodium chloride pH 7.6 with 0.1% (v/v) tween-20 (TSB-T) for either 1 hour at room temperature with agitation or overnight at 4°C. Blot membranes were incubated in a primary antibody, diluted in 2% ECL Advance blocking solution in TBS-T at a concentration dependent upon the target protein (see Table 2.7), for 1 hour at room temperature with agitation. The primary antibody was poured off and the blot membrane washed with TBS-T twice, followed by 4 subsequent washes at room temperature with agitation; 1 for 15 minutes and 3 for 5 minutes each. Membrane blots were incubated in horseradish peroxidase conjugated secondary antibody (Abcam), diluted in 2% ECL Advance blocking solution in TBS-T at a concentration dependent upon the target protein (see Table 2.7), for 1 hour at room temperature with agitation. The membrane blots were washed as before and developed with ECL Advance detection reagent (GE Healthcare) for 5 minutes in

the dark. Images were obtained using a CCD imager (VersaDoc 5000, Bio-Rad) and Quantity One software (Bio-Rad). Quantification of protein was performed using either Quantity One or Image lab software (Bio-Rad).

TABLE 2.7: Gel loadings based upon Chl *a* and total protein concentrations, and primary and secondary antibody dilutions for target proteins.

Target protein	Chl Loading Chl *a* (ng lane^{-1})	Protein Loading Total protein (μg lane^{-1})	Primary Antibody dilution	Secondary Antibody dilution
IsiA	3.66 - 45.83	2 - 4	1/5000 - 1/10000	1/5000 - 1/10000
PsaC	1.55 - 360.28	2 - 29	1/5000 - 1/10000	1/10000
PsbA	0.73 - 360.28	0.8 - 20	1/40000	1/40000
RbcL	0.73 - 74.32	0.8 - 12	1/10000	1/10000

2.11.5 Quality Control

In order to assess the inter/intra-gel variability when running the PRISM protein samples, a Synechocystis *sp.* extract was run on every gel for the following targets, PsaC/Chl (mol mol^{-1}) (Figure 2.7), PsbA/Chl (mol mol^{-1}) (Figure 2.8) and RbcL/Chl (mol mol^{-1}) (Figure 2.9). The average standard errors (%) are listed in Table 2.8, and demonstrate a wide degree of variability. Normality tests were performed on the concentrations to eliminate potential outliers. The RbcL concentrations have a normal distribution, whereas the PsaC and PsbA concentrations did not have a normal distribution. However, if the Syn 9 extract is removed from the PsbA concentrations then it has a normal distribution, and the standard error can be recalculated at 34.17%. Between samples differences of <50% are unlikely to be significant differences (p>0.05). The highest level of error was found for PsaC which did not have a normal distribution, so no PsaC numbers will be reported for PRISM protein samples. This is in part due to the lower available concentrations of PsaC available in field samples, and the method requirement for high biomass.

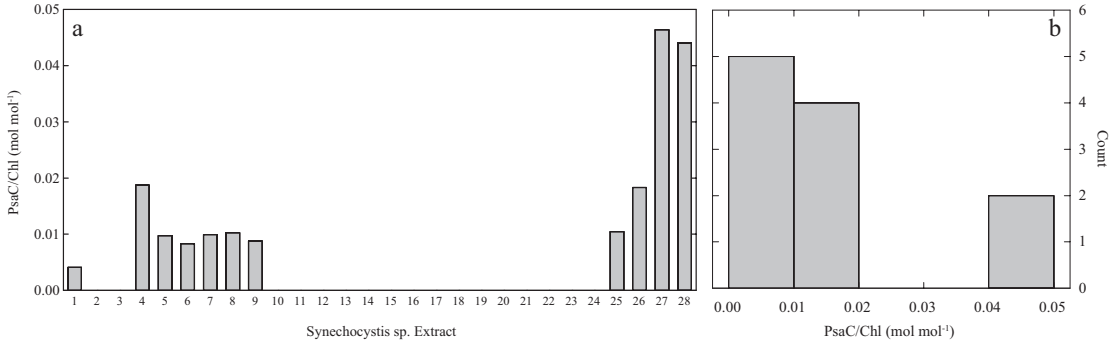

FIGURE 2.7: a) PsaC concentrations per unit chlorophyll (mol mol^{-1}) for a Synechocystis sp. extract run along in situ samples. b) PsaC concentrations histogram.

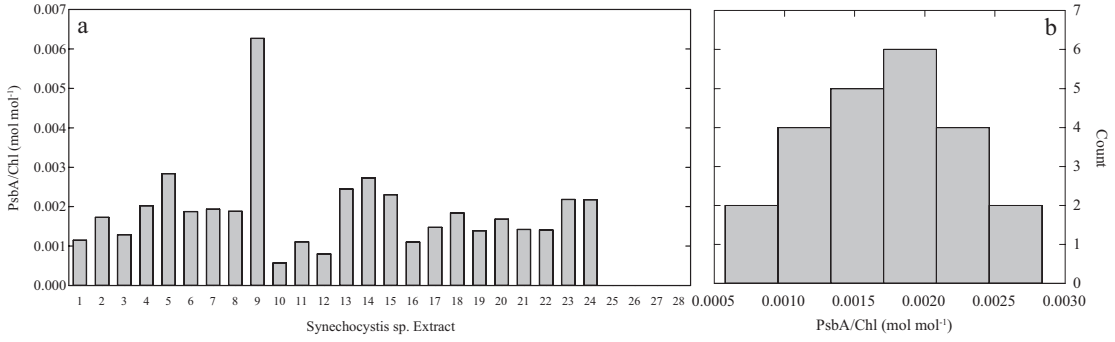

FIGURE 2.8: a) PsbA concentrations per unit chlorophyll (mol mol^{-1}) for a Synechocystis sp. extract run along in situ samples.b) PsbA concentrations histogram.

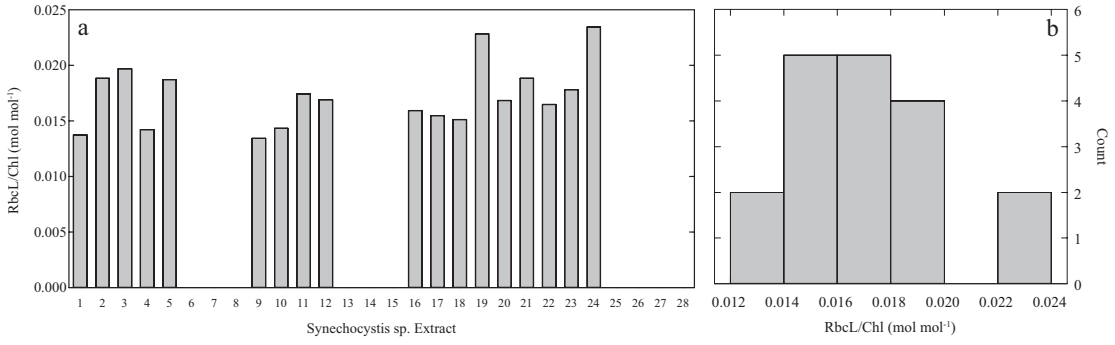

FIGURE 2.9: a) RbcL concentrations per unit chlorophyll (mol mol^{-1}) for a Synechocystis sp. extract run along in situ samples. b) RbcL concentrations histogram.

TABLE 2.8: Standard error of target protein concentrations calculated from extracts of Synechocystis *sp.* *Standard error not determined.

Target protein	*n*	Inter-Gel Variability	Intra-Gel Variability
PsaC	7	77.63%	11.14%
PsbA	24	54.75%	1.72%
RbcL	18	17.67%	*

2.12 Satellite Data

Satellite ocean color data, from D350 & D354, were used to place in situ and experimental data within the context of the annual spring bloom cycle. Moderate Resolution Imaging Spectroradiometer (MODIS) 8-day composites were first used to generate a 40-day running mean 0.42 degree, 8-day resolution time-series of surface chlorophyll for 2010. The date of the bloom peak was then pragmatically identified at each location as the first time at which the rate of change of the net chlorophyll growth rate dropped below 8×10^{-4} d^{-2}, provided the bloom had already reached >0.7 μg Chl L^{-1}. Visual inspection of the satellite chlorophyll time series and comparison with in situ data (see Results), confirmed that this criterion was a reasonable predictor of the early stage of the bloom peak in the region.

2.13 Person's Responsible for Sample Collection and Processing

The person's responsible for sample collection on the research cruises and post-processing are outlined below. All further interpretation following processing was conducted by myself.

TABLE 2.9: Person's responsible for sample collection and analysis during D350, D354 and PRISM. When more than one name is listed, the person/s responsible for sample collection at sea listed in italics and person/s responsible for sample processing and analysis are in bold.

Parameter	D350	D354	PRISM
Protein abundance	n/a	n/a	**T. Ryan-Keogh** *T. Bibby*
Chl *a*	**C. M. Moore** *M. Lucas*	**C. M. Moore** *M. Lucas* *A. Borero* *A. Macey*	**T. Ryan-Keogh** *T. Bibby* *L. Delizo* *A. Mosby*
Nutrients	**M. Stinchcombe** *D. Hembury*	**M. Stinchcombe**	**L. Ekern** *T. Ryan-Keogh* *T. Bibby*
FRRf	**T. Ryan-Keogh** *C. M. Moore*	**T. Ryan-Keogh** *C. M. Moore*	**T. Ryan-Keogh** *T. Bibby*
Dissolved Fe	**S. Steigenberger** *J. Klar*	**S. Steigenberger** *J. Klar*	**P. Sedwick** *C. Marsay*

Chapter 3

The Role and Function of the Iron-Stress-Inducible Gene, *isiA* in *Synechocystis* sp. PCC 6803

Published as:

Ryan-Keogh, T. J., Macey, A. I., Cockshutt, A. M., Moore, C. M. and Bibby, T. S., (2012), "The cyanobacterial chlorophyll-binding-protein IsiA acts to increase the *in vivo* effective cross-section of photosystem I under iron limitation", *Journal of Phycology*, Volume 48, Issue 1, Pages 145-154, doi: 10.1111/j.1529-8817.2011.01092.x

3.1 The Iron-Stress-Inducible Gene

In cyanobacteria there are two iron-stress-inducible genes, *isiA* and *isiB*, which are located on the *isiAB* operon. The *isiB* gene encodes a protein that replaces ferredoxin (two Fe atoms) with flavodoxin (no Fe atoms) (Strauss, 1994); the chloroplast ferredoxin is involved in both cyclic and non-cyclic photophosphorlyation reactions of photosynthesis (see Chapter 1 section for more details). Flavodoxin is a functionally equivalent non-iron containing protein and the accumulation of flavodoxin has been used as a biochemical marker of iron stress (La Roche et al., 1995; McKay et al., 1999); its detection within individual cells provided a new insight into the physiological response of natural phytoplankton on a molecular level (Erdner et al., 1999; La Roche et al., 1996a).

However, flavodoxin expression varies between species and it is not necessarily indicative of growth limitation (Geiss et al., 2001). Erdner et al. (1999) found that the only cyanobacteria representative of the coastal strains, *Synechococcus* CCMP 1334, showed no expression of flavodoxin under iron-deplete conditions.

The expression of *isiA* produces a protein, IsiA, with a sequence and structural motif homologous to the core antenna proteins of PSII (CP43 and CP47) (Burnap et al., 1993; Pakrasi et al., 1985) and to the light harvesting antenna proteins (Pcbs) of the marine cyanobacteria *Prochlorococcus* (Bibby et al., 2003; La Roche et al., 1996b); however IsiA and Pcbs lack the large hydrophilic loop that joins the luminal ends of helices V and VI of CP43 (Burnap et al., 1993) (Figure 3.1). *Prochlorococcus* can have multiple *pcb* genes, each of which has a specific function; for example, as specific light-harvesting antenna for PSII or PSI (expressed constitutively) or as a light-harvesting antenna system for PSI expressed under iron limitation (Bibby et al., 2001d, 2003; Garczarek et al., 2000). The IsiA protein is thought to bind 12 chlorophyll molecules in six transmembrane helices arranged in three sets of two dimers (Bricker and Frankel, 2002). This six trans-membrane chlorophyll-binding motif is therefore thought to be a core building block of photosynthesis that has been retained in some cyanobacteria because it offers a photosynthetic strategy advantageous under iron limitation (Chen and Bibby, 2005; Green, 2003).

It has been proposed, however, that the chlorophyll-binding protein IsiA, expressed in some cyanobacteria under iron stress (Burnap et al., 1993), is not directly involved in photosynthesis (Behrenfeld et al., 2006; Cadoret et al., 2004; Sarcina and Mullineaux, 2004; Singh and Sherman, 2007). Under iron limitation, IsiA can be the most abundant chlorophyll-binding protein in cyanobacteria cells (Burnap et al., 1993). IsiA-associated pigment may therefore significantly contribute to total chlorophyll in oceanic regions such as the Equatorial Pacific, where cyanobacteria comprise a substantial fraction of the total phytoplankton community and the availability of the trace metal iron has been shown to limit primary production (Behrenfeld and Kolber, 1999; Behrenfeld et al., 1996, 2006; Martin et al., 1994). A recent whole-community genomic study has revealed that the cyanobacterial *isiA* gene is present specifically in this region, suggesting it has a functional role that confers a selective advantage *in situ* (Bibby et al., 2009). In addition to expressing IsiA under iron stress, cyanobacterial cells can also undergo chlorosis (loss

of total chlorophyll per cell) (Boyer et al., 1987; Erdner et al., 1999; Guikema and Sherman, 1983; Moseley et al., 2002; Strauss, 1994), reduce the abundance of photosynthetic reaction centres (PSI and PSII) (Boekema et al., 2001; Küpper et al., 2008; Öquist, 1974; Strauss, 1994) and reduce their phycobilisome content (soluble light-harvesting systems that require iron-binding enzymes for synthesis) (Guikema and Sherman, 1983).

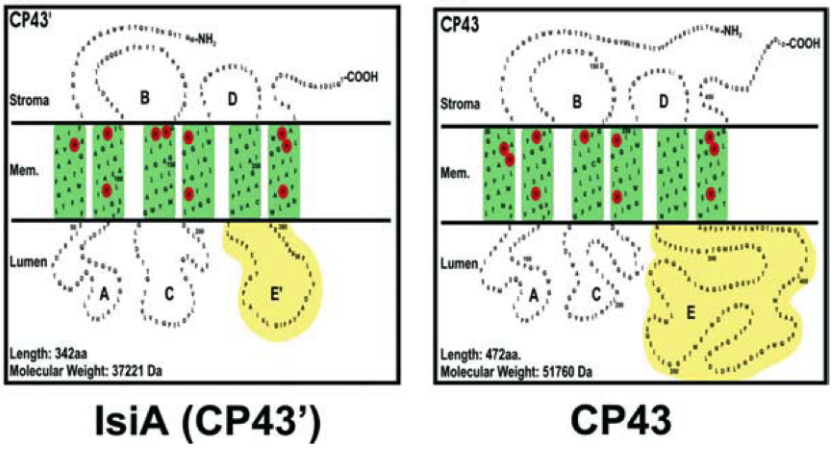

FIGURE 3.1: Comparison of the folding diagrams of IsiA (CP43') and CP43 based on the sequencing of the *psbC* and *isiA* gene of *Synechocystis* sp. PCC 6803 and hydropathy analyses (Chen and Bibby, 2005)

3.1.1 IsiA - Peripheral Antenna

The biochemical isolation of an IsiA-PSI supercomplex from iron-limited cells, of *Synechocystis* sp. PCC 6803 (Bibby et al., 2001a,b,c) and *Synechoccus* sp. PCC 7942 (Boekema et al., 2001), revealed 18 IsiA monomer proteins are functionally coupled to a PSI trimer (IsiA:PSI ratio 6:1). The organisation of IsiA in this antenna ring is controlled by two factors, first it is stabilised primarily by interactions between adjacent IsiA subunits and then it is stabilised with a localised specific interaction with the PSI monomer (Aspinwall et al., 2004). The antenna size of the IsiA-PSI supercomplex is composed of approximately 216 chlorophyll molecules, assuming that the IsiA unit binds to at least 12 chlorophyll molecules as does CP43 within its six-helix bundle (Zouni et al., 2001). The role of this protein was hypothesised to increase the functional antenna size (σ_{PSI}) of a restricted cellular quota of PSI reaction centres by $\sim$ 70% under iron limitation, thus compensating for a reduction in PSI per cell (Andrizhiyevskaya et al., 2002; Küpper et al., 2008; Melkozernov et al., 2003). However, an increase in the cross-section of PSI (σ_{PSI}) has not been established *in vivo* (Ivanov et al., 2006). It has also been shown that the trimeric organisation of PSI is not necessary for IsiA to associate

(Aspinwall et al., 2004), that a monomer of PSI can have 6 IsiA units associated with it. The results also show that due to the increased exposure of the edge of the PSI reaction centre it allows another IsiA unit to bind, forming a 7 IsiA-PSI supercomplex. Recently, Chauhan et al. (2011) demonstrated that IsiA can form a double ring around PSI in *Thermosynechoccus elongatus* (Figure 3.3), with 18 sub-units on the inner ring and 25 sub-units on the outer ring.

Evidence from culture studies have suggested that IsiA may have an alternative role in photoprotection or as a chlorophyll store for the cell (Guikema and Sherman, 1983; Park et al., 1999; Sandström et al., 2001, 2002; Singh and Sherman, 2007) and is, therefore, not directly involved in harvesting light for primary production (Behrenfeld et al., 2006).

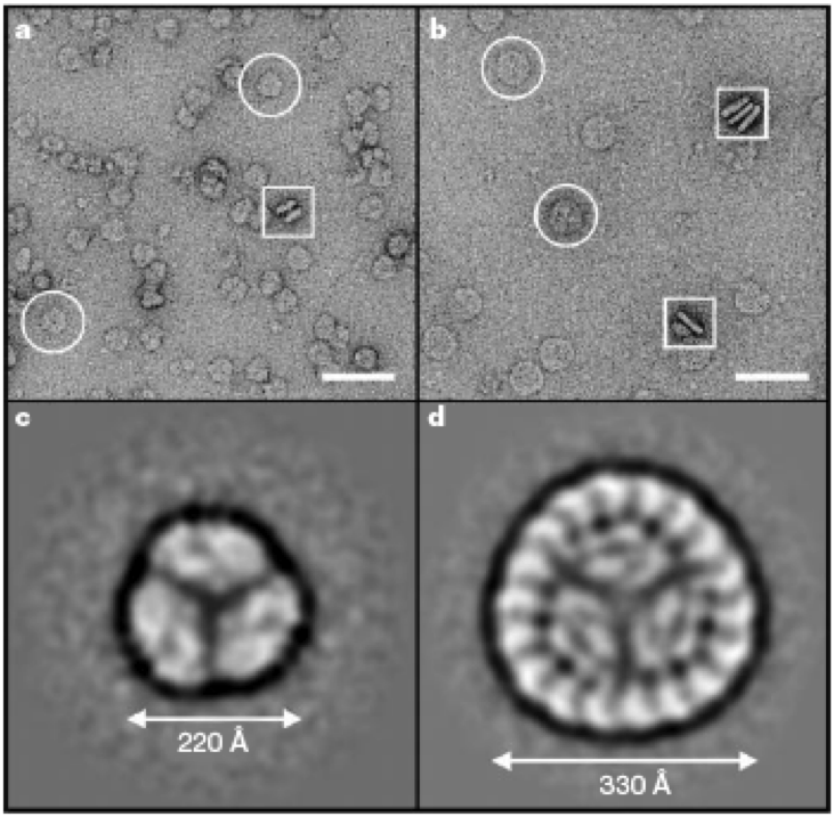

FIGURE 3.2: Supercomplex of IsiA-PSI (Bibby et al., 2001b). Typical electron micrographs of PSI trimers (a) and IsiA-PSI complex (b) in negative stain. Image processed top views of negatively stained PSI trimers (c) and IsiA-PSI complexes (d).

3.1.2 IsiA - Chlorophyll storage protein

The second role that has been proposed for IsiA is to donate chlorophyll upon the addition of iron and recovery of the cell. Behrenfeld et al. (2006) examined the effect

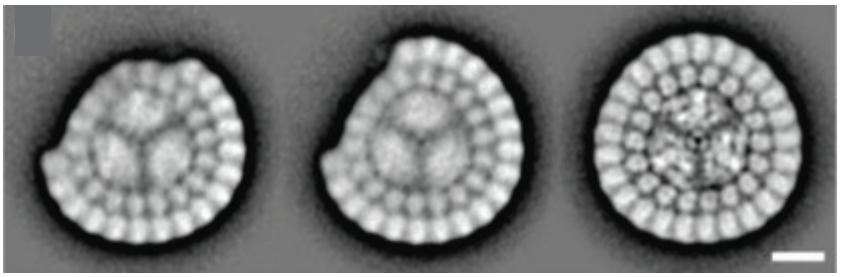

FIGURE 3.3: Structural comparison between the IsiA-PSI super complex and the PSI trimer (Chauhan et al., 2011), PSI-IsiA supercomplexes with incomplete and complete outer rings. The scale bar is 10 nm.

of this proposed variability, and the resulting changes in fluorescent properties upon satellite-based measurements of the tropical Pacific. This study examined the effects of iron starvation upon the acceptor side of PQ pool and the relative effects upon the apparent photosynthetic efficiency (F_v/F_m). The ratio of variable to maximal fluorescence (F_v/F_m) has frequently been used to establish and map phytoplankton iron stress in the field (Behrenfeld et al., 2006; Boyd and Abraham, 2001), however, the mechanistic basis of this response remains unclear (Suggett et al., 2009). The observed reduction of F_v/F_m within natural populations in low-iron regions (Behrenfeld et al., 2006; Schrader et al., 2011) and within cultures under iron-starvation conditions, although not necessarily steady-state iron limitation (Price, 2005), likely reflects accumulation of non-photochemically active chlorophyll. Consequently, rather than the original suggestion that lowered F_v/F_m reflects accumulation of damaged PSII reaction centers (Falkowski and Kolber, 1995), it has been suggested that accumulation of uncoupled chlorophyll-binding protein (such as IsiA) may be primarily responsible for the observed reduction of F_v/F_m under iron stress (Behrenfeld et al., 2006). Establishing the role of IsiA and the potential for excess accumulation of this protein is thus crucial for understanding the physiological basis of active fluorescence data and potentially for interpreting large-scale satellite based measurements of production (Behrenfeld et al., 2006, 2009).

Singh and Sherman (2007) examined the function of IsiA by looking at its role in the biogenesis of photosynthetic complexes; they examined the recovery of the thylakoid membranes upon iron addition. Under iron-stress the number of thylakoid membranes in the *Synechococcus elongatus* tends to decrease to only one concentric thylakoid membrane (Sherman and Sherman, 1983), which also increases the proportion of cytoplasmic to photosynthetic membrane. When iron is added back, the cells recover and by 15

hours the number of thylakoid membranes returns to that of a cell growing under normal conditions. Since IsiA is a major chlorophyll-containing protein under these types of conditions, it could deliver chlorophyll to the photosynthetic complexes. Sarcina and Mullineaux (2004) had also proposed this idea when examining the mobility of IsiA in the thylakoid membrane of *Synechococcus* sp. PCC 7942. Their results showed that the diffusion coefficient for PSII was below 2 x 10^{-13} cm^2 s^{-1}, while the diffusion coefficient for IsiA was $\sim$ 100 fold higher ($\sim$3 x 10^{-11} cm^2 s^{-1}). As the diffusion coefficient for PSII is below 1.5 x 10^{-12} cm^2 s^{-1} it is generally classed as immobile (Zhang et al., 1993). However, the reason why PSII is immobile while IsiA is mobile can be explained by interactions with the thylakoid lumen. PSII has a large domain on the lumenal side of the membrane mainly composed of the water-oxidizing complex and associated proteins (Zouni et al., 2001). This is best explained by the differences between IsiA and the homologous CP43 of PSII, where the largest hydrophilic loop of CP43 is truncated in IsiA (Burnap et al., 1993). The loss of this loop might facilitate migration of IsiA throughout the thylakoid membrane and this may also facilitate its role in donating chlorophyll for the biogenesis of new reaction centres.

3.1.3 IsiA - Non-photochemical quencher

The third proposed function of IsiA is that it acts as a non-photochemical quencher under high light stress. All photosynthetic organisms can adjust to changes in light intensity, known as photo-acclimation; however they also have to cope with fluxes that are too large or too fast for photo-acclimation to occur. This is particularly important for the oxygen-evolving PSII where over excitation can lead to a rapid inhibition when the destruction of the reaction centre protein D1 becomes faster than its production (Aro et al., 1993). The excess illumination can induce a change in the chlorophyll-binding antenna proteins which accelerates the thermal dissipation of excitation energy, known as non-photochemical quenching (NPQ) (Horton et al., 1996). NPQ appears to be triggered by excessive acidification of the thylakoid lumen when consumption of the proton gradient by ATP synthesis is faster than its production by electron transport (Cadoret et al., 2004). Cadoret et al. (2004) have demonstrated, in *Synechocystis* PCC 6803, that the accumulation of IsiA is accompanied by the appearance of a reversible, light-induced NPQ that provides an effective protection against photo-inhibition of PSII. There results showed that the NPQ associated with IsiA is induced only by excitation

of a blue light absorbing pigment and they argue that its primary function may not be to just cope with rapid light intensity fluctuations but to adjust the excitation rate of IsiA to an already photo-acclimated system.

3.1.4 Regulation of IsiA

The regulation of IsiA has long been assumed to be controlled at both transcriptional and post-transcriptional levels by Fur (ferric uptake regulator), a transcription repressor with iron as a co-factor (Ghassemian and Straus, 1996). Kunert et al. (2003) have suggested that a Fur binding site could be located in the upstream region of the IsiA promoter. After prolonged iron starvation, PSII can no longer be effectively protected from damage and this is when PSI is modified by the production of IsiA. The consequence of the PSI-IsiA supercomplex is an increase in cyclic electron flow, compensating for the decreased cyclic electron flow around PSII.

Many researchers have suggested the use of IsiA as biochemical marker to iron stress but this has previously been objected due to two reasons. The first is the non-ubiquitous distribution of the gene; Bibby et al. (2009) found that the *isiA*-like genes were found in only 4 of 11 sequenced marine *Synechococcus* genomes. This is also compounded by the fact that it shares a strong homology with the *psbC* gene product (CP43) (Laudenbach and Strauss, 1988) and the *pcb* gene family present in prochlorophytes (La Roche et al., 1996b). Any molecular probes targeting the *isiA* gene would need to be carefully designed in order to avoid detection of other gene products within this large and diverse gene family.

Second, is the poor understanding of the role and function of IsiA. Jeanjean et al. (2003) found that under iron-replete conditions the *isiA* gene in *Synechocystis* sp. PCC 6803 was induced in by salt stress or by treatment with methyl viologen, a non-selective herbicidal compound. Yousef et al. (2003) also discovered that the gene was inducible by hydrogen peroxide in *Synechococcus elongatus* PCC 7942, which suggests that IsiA synthesis may be a more general acclimation response to redox imbalance and derived oxidative stress. Havaux et al. (2005) hypothesised that the primary regulator of *isiA* induction is the redox state of the PQ pool which will become more reduced in high light or in conditions when the PSI level drops relative to PSII.

3.2 Aims and Objectives

In spite of all the efforts and advancement in trying to determine the specific role of the IsiA chlorophyll-binding protein, there has not yet been a definitive answer. Moreover, the IsiA protein has never been quantified in a phytoplankton species. Within this chapter, the absolute abundance of the chlorophyll-binding proteins PSII, PSI and IsiA in cultures of the model cyanobacteria *Synechocystis* sp. PCC 6803 will be quantified under conditions of increasing iron stress. Alongside these measurements, the *in vivo* cross-section of PSI (σ_{PSI}) will also be measured under conditions of increasing iron stress for the first time. A chlorophyll budget will also calculated for the iron-limited cyanobacterial cell and demonstrated that the primary function of IsiA *in vivo* is as a PSI antenna. As predicted by previous studies the cross-section of PSI will increase under iron-stress in parallel with an increase in the IsiA to PSI ratio to 6:1. While under iron-deplete conditions, there will be no expression of the IsiA protein and no change in the cross-section of PSI. The key role of IsiA is to act as a peripheral antenna protein for PSI, but any excess of IsiA beyond the 6:1 ratio will result in the adoption of a secondary role, either as chlorophyll storage or as a non-photochemical quencher.

3.3 Results

3.3.1 Physiological Response

Iron-stress was induced by growing *Synechocystis* cells in BG-11 media lacking iron. When compared with control cultures (BG-11 containing iron), a marked difference in total chlorophyll (Figure 3.4a) and cell numbers (Figure 3.4b) and a marked decline in F_v/F_m (Figure 3.5a) became apparent on day 2 after inoculation into low-iron media, indicating the point when the photophysiology switches to the iron-limited phenotype. This change was accompanied by a blue-shift of ∼8 nm in the red-absorption peak of chlorophyll (indicative of expression and accumulation of the IsiA protein) (Figure 3.6a), a decline in phycobilisome content (Figure 3.6b) and growth rates to ∼85% of iron-replete cultures (Figure 3.4d). Prolonged growth in iron-deplete media (>2 days) resulted in a continued reduction in F_v/F_m to 0.26, with significant differences from day 2 onwards (ANOVA, $p<0.05$) and further declines in growth rates to ∼32% of iron-replete

cultures, which had a μ^{max} of 1.38±0.1. Despite the clear differences in growth rates under iron stress conditions, there was not a significant difference (ANOVA, p>0.05) in cellular chlorophyll concentrations, which ranged from 75% to 90% of iron-replete cultures (Figure 3.4c). Alongside measurements of F_v/F_m, the absolute changes in F_o, F_m and F_v were calculated and normalized to chlorophyll. F_o Chl^{-1} (Figure 3.5b) and F_m Chl^{-1} (Figure 3.5c) remained relative constant in the iron-replete culture, but increased from day 2 onwards in the iron-deplete culture, with a statistically significant difference between the cultures on days 3 and 4 (ANOVA, p<0.05). F_v Chl^{-1} (Figure 3.5d) remained relatively constant within both the iron-replete and iron-deplete cultures, with no statistically significant difference (ANOVA, p>0.05).

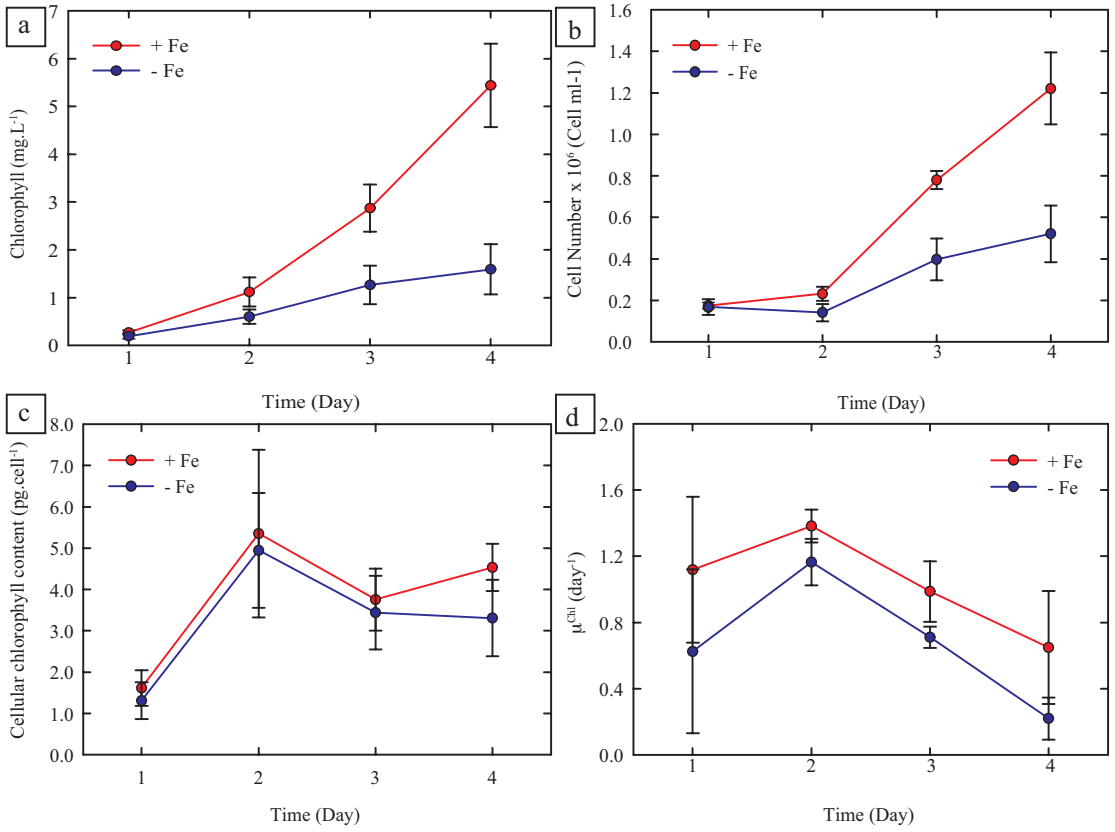

FIGURE 3.4: a) Average chlorophyll concentrations (mg L^{-1}) from three independent experiments. b) Average cell numbers (cells ml^{-1} enumerated using flow cytometry from three independent experiments. c) Average cellular chlorophyll content (pg.$cell^{-1}$). d) Growth rates (μ^{Chl} day^{-1}) calculated from chlorophyll concentrations. Displayed are results from two different treatments, iron-replete (+ Fe) and iron-deplete (- Fe), averaged from triplicates with ± standard errors.

Measurements of ΔA_{830} during high-intensity light pulses displayed first-order saturation kinetics (Figure 3.7a), with K_{eff} ranging from ~0.7 - 5 ms^{-1} (Figure 3.7d). In

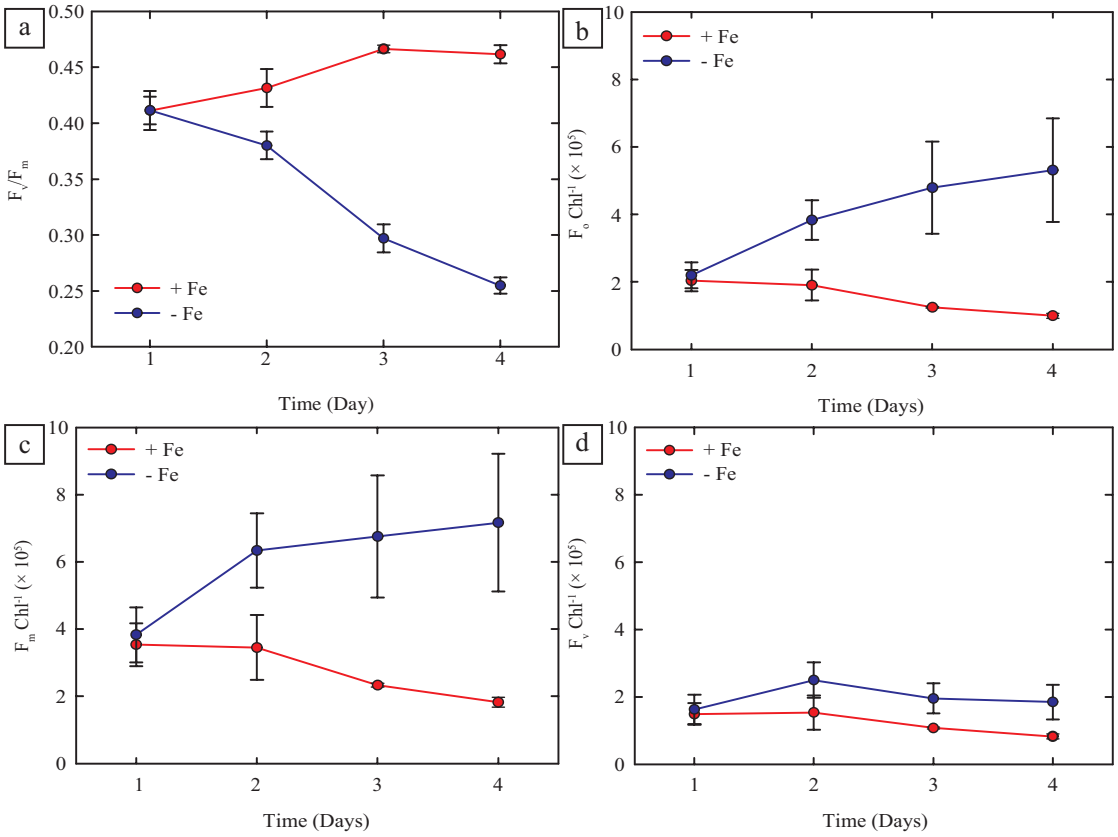

FIGURE 3.5: Average F_v/F_m, F_o Chl^{-1} (× 10^5), F_m Chl^{-1} (× 10^5) and F_v Chl^{-1} (× 10^5) from three independent experiments. Displayed are results from two different treatments, iron-replete (+ Fe) and iron-deplete (- Fe), averaged from triplicates with ± standard errors.

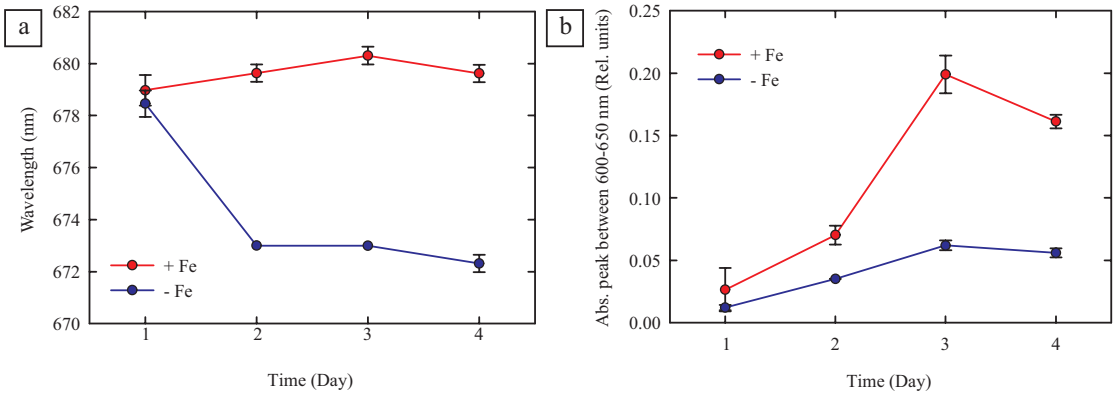

FIGURE 3.6: a) Wavelength shift of maximum absorption value between 670 nm and 685 nm measured at room temperature and b) phycobilisome content measured by maximum absorption value (Rel. units) between 600 - 650 nm at room temperature. Displayed are results from two different treatments, iron-replete (+ Fe) and iron-deplete (- Fe), averaged from triplicates with ± standard errors.

contrast, first-order rate constants estimated from post-light pulse ΔA_{830} relaxation kinetics ranged from 0.07 - 0.1 ms^{-1} (Figure 3.7a). The rate of ΔA_{830} saturation normalized to cumulative photon dose at different saturation pulse intensities confirmed measurements of a photochemical absorption cross-section (Figure 3.7b) and further confirmed the relative insensitivity of saturation kinetics to $P700^+$ re-reduction. When corrected for samples absorption, K_{eff} thus conformed to the expected linear function of excitation intensity (Figure 3.7d), with a slope that will be equal to σ_{PSI} (Equation 2.2).

Clear differences in saturation kinetics were observed between iron-replete and iron-deplete cultures (Figures 3.7c & 3.7d) Measured values of σ_{PSI} indicated a significant shift between the two cultures from 48 h onwards (Figure 3.8), with the iron-replete culture remaining relatively constant at around 1.2 $\pm$ 0.1 nm^2, higher than but still in reasonable agreement with the theoretical cross-section for a PSI complex receiving absorption from only 100 chlorophyll molecules (Ferreira et al., 2004; Jordan et al., 2001). In contrast, σ_{PSI} increased from day 2 onwards in the iron-starved culture to a maximum value of 1.90$\pm$0.01 nm^2 on 72 h, $\sim$60% larger than the iron-replete value at the same timepoint. Differences between treatments were significant from 48 h onwards (t-test, $p<0.05$).

3.3.2 Protein Concentrations

The absolute concentrations of the key photosynthetic proteins PsaC, PsbA and IsiA, representing the vast majority of the chlorophyll-binding complexes in the cyanobacterial cell, were measured by quantitative Western blotting (Figure 3.9) (Brown et al., 2008). The subunits PsaC and PsbA are used to infer PSI and PSII concentrations respectively. In agreement with physiological measurements (Figure 3.10a, b) protein abundances normalized to total protein concentration, indicated that the IsiA protein was only detectable from day 2 onwards (Figure 3.10a), increasing to a maximum of 0.53$\pm$0.15 pmol IsiA μg^{-1} total protein by day 4. PSI decreased throughout to a final value of 0.028$\pm$0.012 pmol PSI μg^{-1} total protein. PSII decreased between day 2 and day 3, remaining relatively constant until day 4 with a value of 0.035$\pm$0.018 pmol PSII μg^{-1} total protein. Under iron-replete conditions (Figure 3.10b), PSI decreased between day 1 and day 3, before increasing again until to a final value of 0.07$\pm$0.03 pmol PSI μg^{-1}. PSII

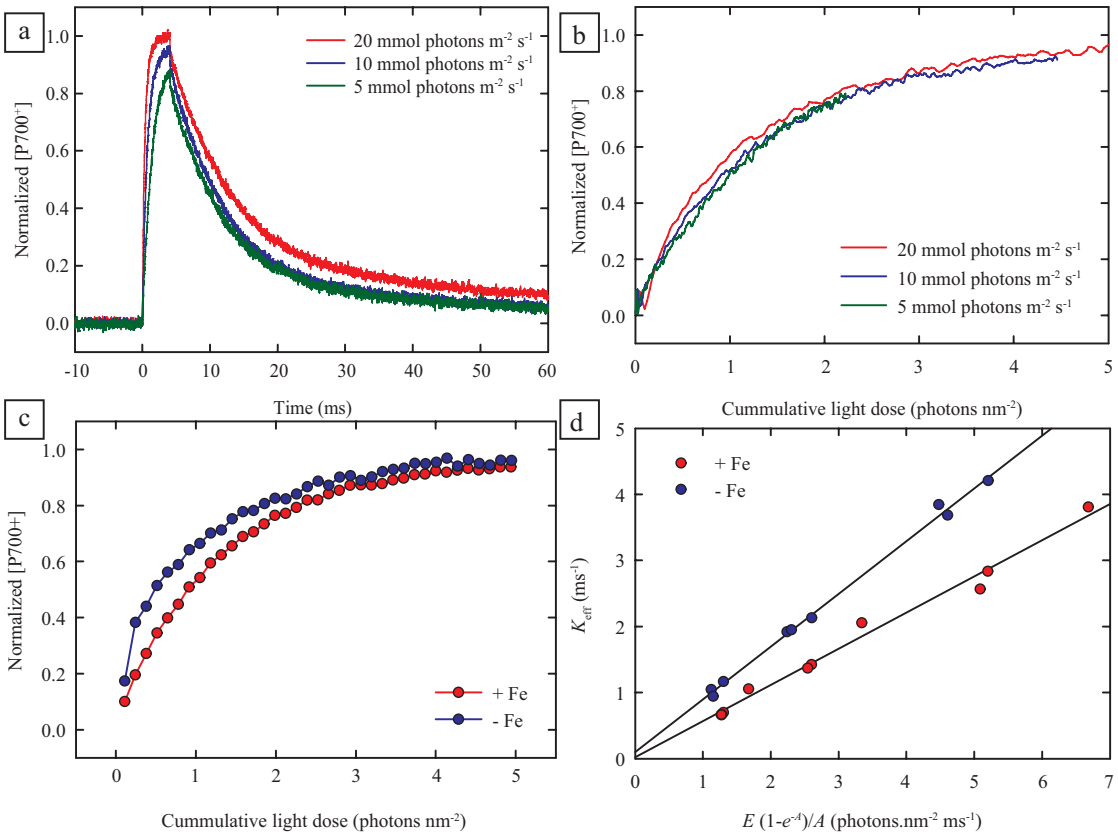

FIGURE 3.7: a) Measurements of ΔA_{830} kinetics over a range of different light intensities on the same sample. Light intensities are 5, 10 and 20 mmol photons m^{-2} s^{-1}. b) The rate of ΔA_{830} saturation normalized to cumulative photon dose. c) Example measurements of ΔA_{830} normalized to cumulative photon dose of iron-replete (+ Fe) and iron-deplete (- Fe) cultures. d) K_{eff} (ms^{-1}) as a function of mean light intensity within the measurement cuvette for an iron-replete (+ Fe) and iron-deplete (- Fe) culture measured at multiple excitation intensities and cell densities.

also decreased between day 1 and day 3 before increasing to a final value of 0.011±0.002 pmol PSII μg^{-1}.

When normalized to total cellular chlorophyll, IsiA:chl increased from 0.017±0.002 to a maximum of 0.094±0.041 mol mol^{-1} on day 4 (Figure 3.10c, d). This increase in IsiA:chl occurs alongside a decrease in PSI:chl, while PSII:chl remained relatively constant, with final values of 0.0035±0.0012 mol mol^{-1} and 0.0015±0.0006 mol mol^{-1} respectively (Figure 3.10c). Under iron-replete conditions (Figure 3.10d), PSI:chl and PSII:chl both decreased throughout the experiment to final values of 0.004±0.001 mol mol^{-1} and 0.0006±0.0002 mol mol^{-1}. These measured values of protein abundance to total cellular chlorophyll were in good agreement with previously measured values (Brown et al., 2008), even though these values were measured within Trichodesmium. Thus suggesting that this method can be universally applied across different organisms, both in culture

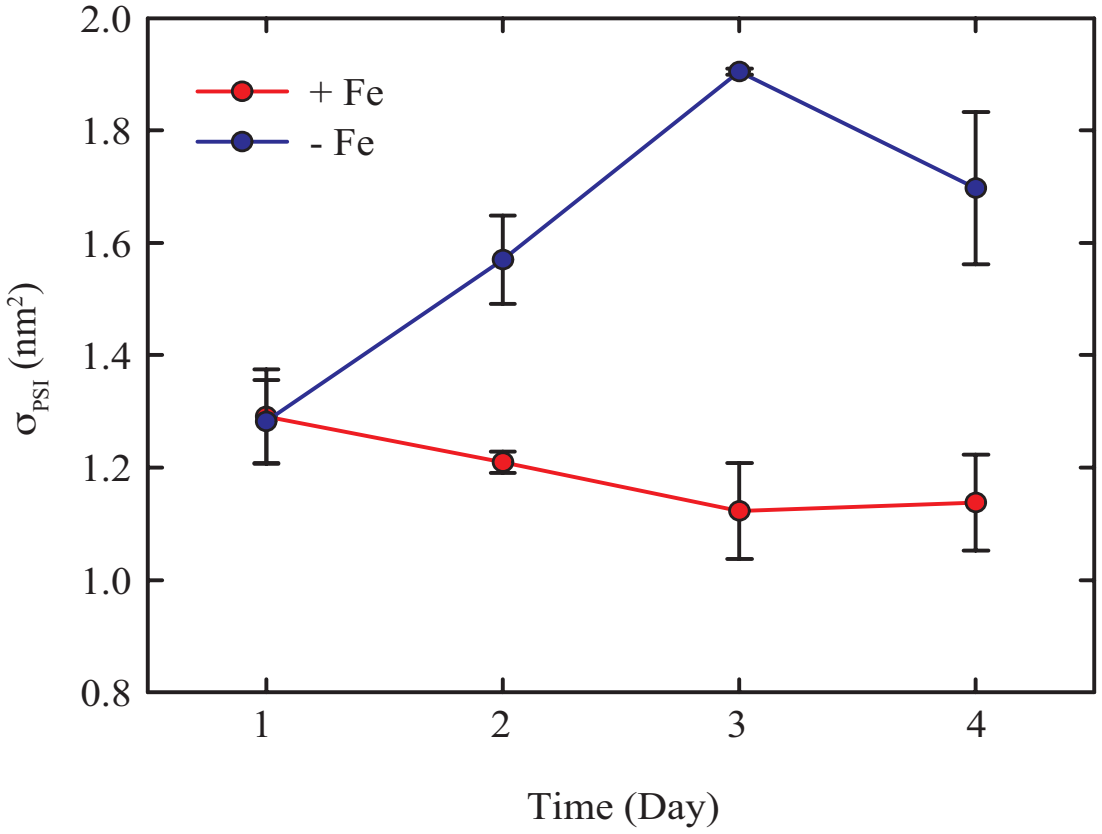

FIGURE 3.8: The *in vivo* effective absorption cross-section of photosystem I (σ_{PSI}) measured on *Synechocystis* PCC 6803 under iron-replete (+ Fe) and iron-deplete (- Fe) conditions. Displayed are results averaged from triplicate bottles from three independent experiments with ± standard errors.

and in the field.

These changes led to marked shifts in relative protein ratios, with the IsiA:PSI ratio increasing past the predicted ratio of 6:1 for an IsiA:PSI supercomplex after 2 days of growth to a maximum of 27:1 at the end of the experiment; PSII:PSI increased slightly from 0.4:1 to a final value of 0.8:1 under iron-deplete conditions while under iron-replete conditions (Figure 3.11) it decreased from 0.4:1 to 0.2:1, in agreement with previous findings (Küpper et al., 2008).

The relative contribution of each protein complex (PSI, PSII and IsiA) to the total cellular chlorophyll content was calculated using the protein ratios combined with numbers of chlorophyll molecules per complex (100, 36 and 12 per PSI, PSII and IsiA, respectively) taken from structural studies that used the CP43 protein of PSII as a homolog for IsiA (Ferreira et al., 2004; Murray et al., 2006). Based on the relative protein abundance and predicted chlorophyll budget, the amount of IsiA protein that could be structurally

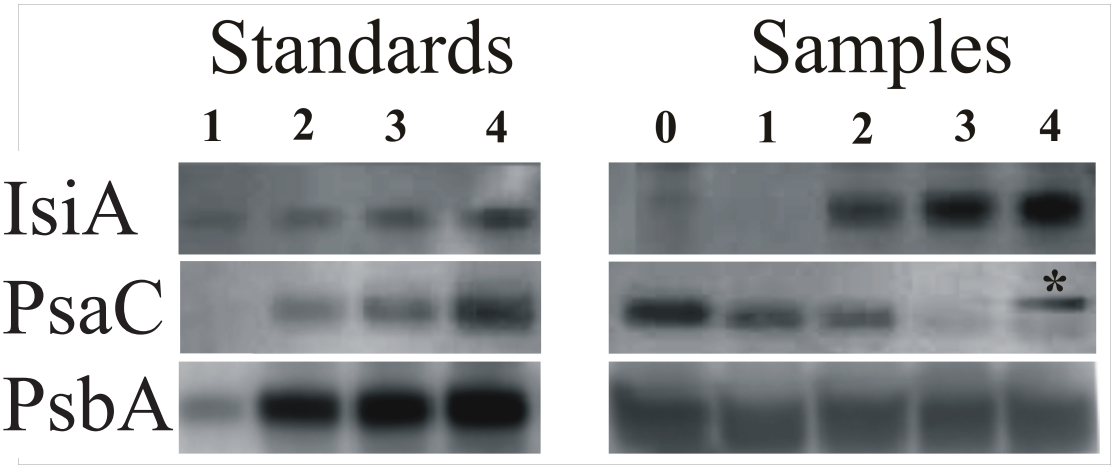

FIGURE 3.9: Example of quantitative Western-blot detection of the chlorophyll-binding proteins (IsiA, PsaC and PsbA). The left panel shows the specific peptide standards at increasing concentrations (1-4). The right panel shows detection of specific peptide targets from total protein extracted from *Synechocystis* PCC 6803. The '*' indicates a band present under severe iron limitation that cross-reacts with PSI-specific global antibody, not considered in quantification of this target.

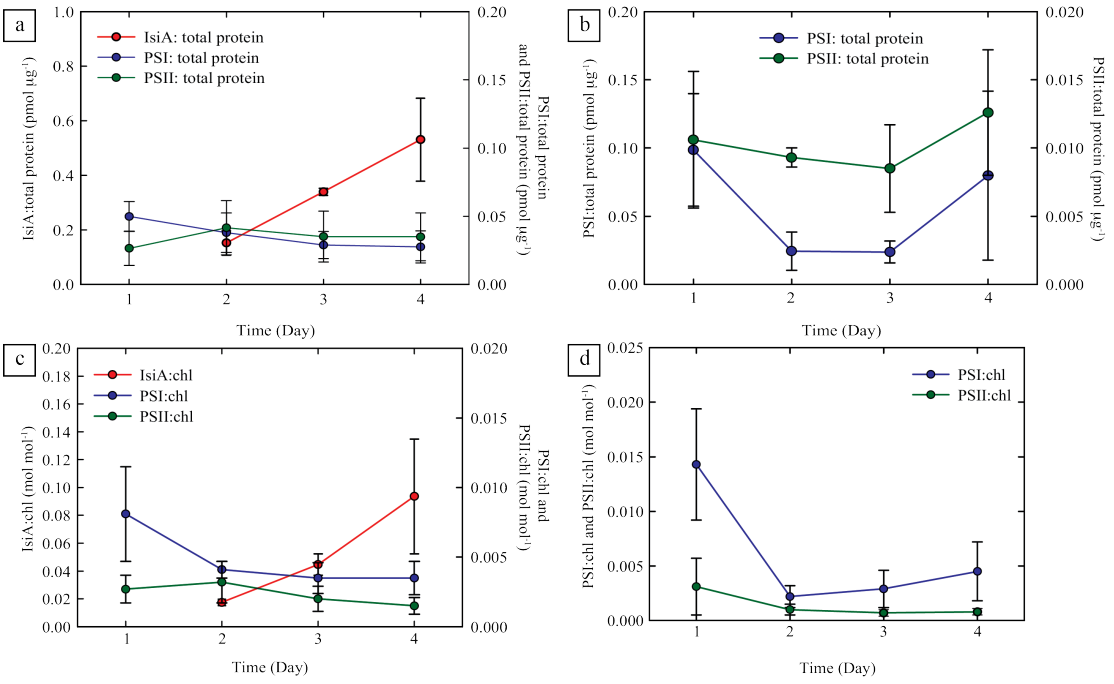

FIGURE 3.10: Results from the protein quantification experiment, protein concentrations determined by immunodetection on an iron-deplete culture (- Fe) (a, c) and iron-replete culture (+ Fe) (b, d). Measurements normalised to total protein concentration in pmol μg^{-1} (a, b) and normalised to chlorophyll in mol mol^{-1} (c, d). Displayed are results averaged from three independent experiments with ± standard errors.

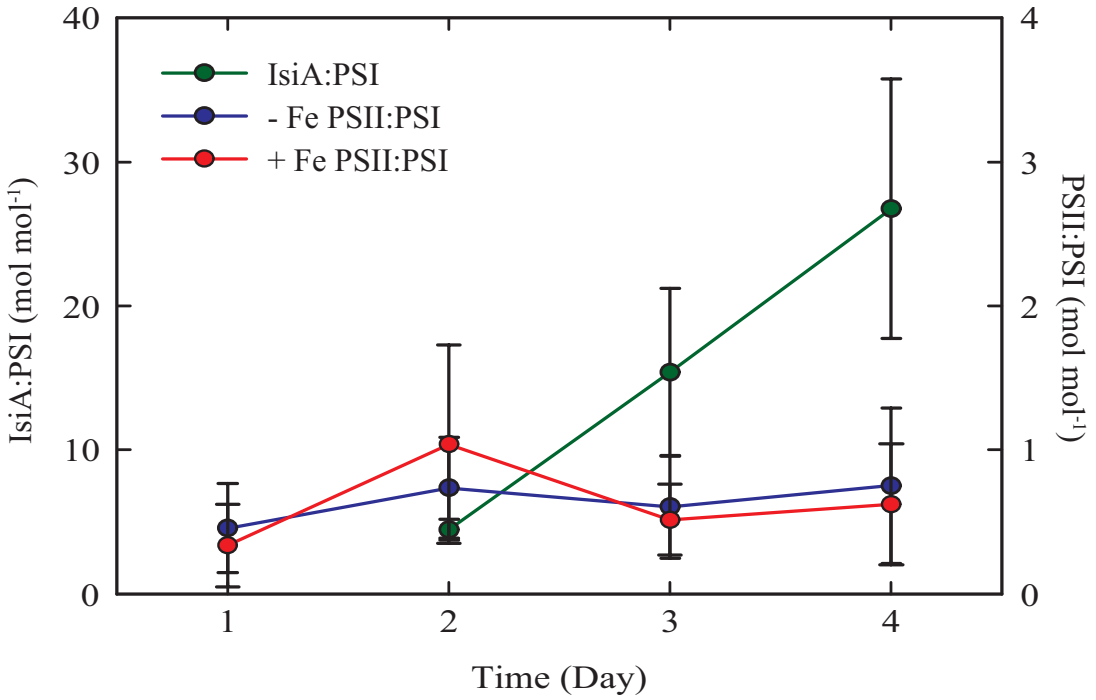

FIGURE 3.11: Protein ratios of an iron-deplete culture (- Fe) calculated from protein abundances normalized to chlorophyll, ratios in mol mol^{-1}. Displayed are results averaged from three independent experiments with ± standard errors.

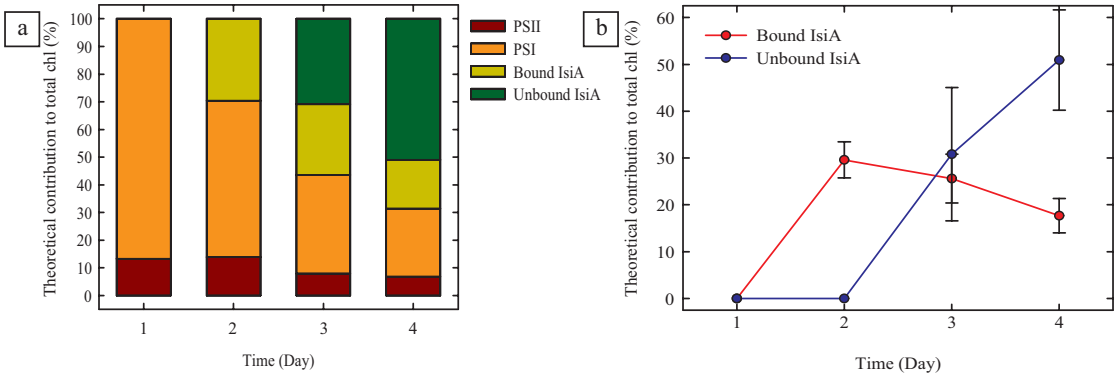

FIGURE 3.12: a) The contribution of total chlorophyll content (%) by PSI, PSII and IsiA proteins in an iron-deplete culture (- Fe) and b) plotted against time. Displayed are results averaged from three independent experiments with ± standard errors.

coupled to PSI was inferred from a theoretically IsiA:PSI ratio of 6:1 for IsiA:PSI supercomplex combined with the observed ∼60% increase in the functional PSI cross-section (from day 3 under Fe limitation), which suggested conversion of >80% of the total PSI pool to this state (Figure 3.12a). Under iron-replete conditions PSI was the major pool of chlorophyll throughout the experiment with a value ∼90%, while PSII was ∼10%.

Using these calculations it is clear that the IsiA protein is a substantial fraction of the total cellular chlorophyll content from day 2 onwards. However, unbound IsiA was only

inferred to represent a substantial fraction of total chlorophyll on days 3 and 4. The potential contribution of bound and unbound IsiA thus shows differing trends (Figure 3.12b). In particular, bound IsiA, as indicated by increased σ_{PSI}, becomes significant at the onset of iron-stress. In contrast, the proportion of unbound IsiA, only becomes significant after prolonged growth under iron stress.

3.4 Discussion

In this chapter, the photosynthetic physiology of the cyanobacteria *Synechocystis* PCC 6803, grown under conditions of increasing iron stress, is described at both biophysical and molecular levels. Biophysical measurements confirmed the development of increased iron-stress physiology over time. When compared with Fe-replete cultures, iron-depleted *Synechocystis* PCC 6803 showed a blue shift in the red chlorophyll absorption peak (Figure 3.6a), indicative of accumulation of the iron-stress-induced protein IsiA (Burnap et al., 1993), and reductions in F_v/F_m (the photosynthetic energy conversion efficiency) (Figure 3.5a), growth rates (Figure 3.4d) and cellular chlorophyll concentrations (Figure 3.4c). These are well characterized responses of iron limitation and reflect an acclimation to growth under iron-limited conditions; the resulting different photosynthetic strategy enables photosynthesis to continue with a lower demand for iron (Behrenfeld et al., 1996; Bibby et al., 2001a).

Alongside clear evidence of iron stress, the first demonstration of an increase of approximately 60% in σ_{PSI} *in vivo* (Figure 3.8) was provided. This increase is consistent with the notion that the IsiA protein forms an antenna ring around PSI trimers, forming the IsiA-PSI supercomplex that has been biochemically isolated and shown to be energetically coupled (Andrizhiyevskaya et al., 2004; Melkozernov et al., 2003). Formation of this IsiA-PSI supercomplex has previously been proposed to represent a strategy to minimize the number of iron-containing PSI reaction centers required under iron-stress conditions (Bibby et al., 2001b,c; Küpper et al., 2008). The increased effective cross-section was temporally correlated with both the ∼8 nm blue shift in the red peak of the chlorophyll absorption ($R^2 = 0.70$) and a reduction in F_v/F_m ($R^2 = 0.63$) (Figures 3.6a & 3.5a).

In parallel with this physiological measurement, the abundance of the photosynthetic reaction centers PSI and PSII and the iron-stress chlorophyll-binding protein IsiA were quantified, together representing the major pools of chlorophyll in the cell. The PSII:PSI ratio showed no significant difference between iron-replete and iron-deplete cultures (Figure 3.11), thus suggesting that the specific response to iron stress is to express IsiA rather than reduce the expression of PSI. Coincident with the initial increase in σ_{PSI}, the IsiA:PSI ratio increased from undetectable levels (no IsiA present) past the 6:1 ratio after day 2 (Figure 3.11). This is the ratio of PSI reaction centers to IsiA antenna proteins revealed in the 10-Å structure of the IsiA-PSI supercomplexes (Bibby et al., 2003). At this point in progressive iron-stress development (day 2), the culture shows many signs of an iron-limited photophysiology, including a shift in the red absorption peak of chlorophyll (indicative of the accumulation of IsiA), and reductions in phycobillisomes (Figure 3.6b), F_v/F_m and growth rate. At least 80% of the chlorophyll associated with expressed IsiA appears to be associated with PSI (Figure 3.12a) if we are to account for the measured increase in σ_{PSI} (Figure 3.8).

Under more severe iron stress (>2 days into iron limitation), while no further increase in σ_{PSI} or blue shift in the red absorption peak of chlorophyll is observed, IsiA continues to accumulate in the cell and F_v/F_m becomes severely reduced, alongside further reductions in growth rate. Cellular IsiA concentrations and Isia:PSI ratios continued to increase to a maximum of 27:1 without a parallel increase in σ_{PSI}. The increase in IsiA:PSI ratios beyond 6:1 thus appears to represent the accumulation of IsiA that was functionally uncoupled from PSI *in vivo*. This pool of IsiA is, therefore, likely to be inactive in photosynthesis and may have an alternative role in cell, such as a chlorophyll store or in photoprotection. It has been shown that IsiA can form a double ring around PSI (Chauhan et al., 2011). Theoretically, a double ring would have a cross-section of >2 nm^2 at 635 nm based upon an approximated 18-IsiA inner ring and an 24-IsiA outer ring. This value is higher than the maximal observed values of σ_{PSI} measured in this study (Figure 3.8). The lack of a further increase in σ_{PSI} beyond 2-3 days suggests that the proportion of double ring complexes remains small *in vivo*.

Our estimated levels of uncoupled IsiA under progressive iron-stress conditions provide further evidence that this protein may not act solely in its primary role as a peripheral antenna for PSI. A number of alternative roles have previously been suggested, including protecting PSII from excess light (Park et al., 1999) or acting as an alternate antenna

for PSII (Pakrasi et al., 1985). The most likely alternative role would be as a chlorophyll storage protein (Sarcina and Mullineaux, 2004; Singh and Sherman, 2007) with ∼50% of the total chlorophyll content in unbound IsiA, there is at least the possibility that this pool could act to rapidly increase photosynthesis under conditions of iron re-supply (Behrenfeld et al., 2006). If transient spikes of iron were added to iron-stressed cultures this could result in the reduction of this unbound IsiA pool. However, it has also been shown that an IsiA ring can form without a PSI trimer (Aspinwall et al., 2004), although whether such structures act as chlorophyll storage proteins or as a mechanism for protecting PSII via non-photochemical quenching (Wilson et al., 2007, 2008) remains unclear. Irrespective of the functional role, increased levels of unbound IsiA observed under high iron-stress conditions should act to lower F_v/F_m by increasing F_o and F_m, as confirmed by the biophysical measurements (Figure 3.5b and 3.5c).

The potential accumulation of significant amounts of unbound and hence photochemically inactive IsiA, within natural iron-stressed phytoplankton populations where cyanobacteria dominate, would have major implications for the interpretation of both *in situ* and remotely sensed data (Behrenfeld et al., 2006, 2009; Schrader et al., 2011). As discussed above, unbound IsiA will likely have a high and non-variable fluorescence yield, which will depress F_v/F_m as a result of increase in F_o (Behrenfeld et al., 2006; Schrader et al., 2011), thereby invalidating the strict interpretation of F_v/F_m as a measure of the photochemical quantum efficiency of PSII (Suggett et al., 2009). In addition, highly fluorescent unbound chlorophyll might contribute to the inferred high quantum yields of chlorophyll fluorescence in low-iron oceanic regions (Behrenfeld et al., 2009). The recent description of a eukaryotic chlorophyll-binding protein expressed under iron-stress conditions, Tidi (thylakoid iron-deficiency-induced) (Varsano et al., 2003, 2006), suggests that eukaryotic phytoplankton in oceanic regions could also potentially have a depressed F_v/F_m due to accumulation of non-photosynthetically active chlorophyll. However, analogous to the IsiA-PSI supercomplex, Tidi has also only been shown to be an antenna system for PSI to date (Varsano et al., 2003, 2006). It is clear that a more detailed understanding of the role of iron-stress-induced chlorophyll-binding proteins in a range of marine phytoplankton may be required to interpret satellite-derived production estimates based on chlorophyll levels in large oceanic regions (Behrenfeld et al., 2006).

Establishing the contribution of unbound IsiA in natural populations will require an increased understanding of the levels of iron stress experienced by natural populations and

how these relate to culture conditions. The batch culture experiments employed here and elsewhere (Bibby et al., 2001a,d; Ivanov et al., 2006; Wang et al., 2010; Yeremenko et al., 2004) will drive *Synechocystis* PCC 6803 into increasing levels of iron stress/starvation. Under these conditions it appears that the primary role of IsiA is a functioning PSI antenna (Figure 3.8). However, subsequent excess accumulation may result from continued IsiA expression combined with down-regulation of the photosynthetic complexes (Figures 3.10,a 3.10c & 3.11). Within natural populations, iron-limited growth is more likely to approach a steady-state balance between iron uptake and resupply by regeneration owing to tight coupling between growth and loss terms (Cullen, 1991; Morel et al., 1991). The relative contributions of bound and unbound IsiA to total chlorophyll (Figures 3.12a & 3.12b), suggests that unbound IsiA only increases under more severe cases of iron stress. Although it is difficult to directly extrapolate from these laboratory measurements on a monoculture of a model organism, grown photoheterotrophically, to natural populations; it can be proposed that the time required under iron-starvation to accumulate large cellular pools of unbound IsiA may have limited ecological relevance. Although *in situ* growth rates of autotrophic prokaryotes clearly vary greatly in iron-limited systems (Mann and Chisholm, 2000), given the high mortality rates reported (Landry et al., 1997) organisms with very low iron-limited growth rates would likely be outcompeted by other species. In order to provide more direct ecological relevance, cultures of *Synechocystis* sp. PCC 6803 could be grown under steady-state iron limitation to keep the growth rate constant.

Given the apparent role of IsiA as a functioning PSI antenna in combination with evidence for subsequent expression of uncoupled IsiA only under longer term iron-stress conditions, it may thus be premature to ascribe large-scale biophysical/biogeochemical patterns to the *in situ* expression of this protein and potential eukaryotic proteins with similar function (Behrenfeld et al., 2006, 2009; Schrader et al., 2011). The role of chlorophyll-binding proteins, such as Tidi, which apparently acts as a functioning PSI antenna in eukaryotic algae, also need to be studied further in culture and their presence verified in iron-limited oceanic regions (Varsano et al., 2006). In addition to model culture work to determine the functional role and identify the environmental conditions under which bound and unbound IsiA dominate, it is clearly necessary to obtain absolute quantification of IsiA and functionally similar proteins from iron-limited regions before it will be possible to determine whether a significant fraction of *in situ* chlorophyll is

dominated by unbound pigment-protein complexes having no direct role in photosynthesis. Chlorophyll-binding proteins within iron-limited regions may or may not dominate the total chlorophyll pool, thereby directly influencing any measurements that rely on chlorophyll concentrations such as primary productivity estimates. However, there are no such direct ways to estimate the abundance of these chlorophyll-binding proteins within mixed communities. Yet their presence or absence can be estimated using time resolved fluorescence measurements such as fast repetition rate fluorometry. If under iron-stress conditions F_v/F_m decreases due to an increase in F_o resulting from an increase in IsiA, then iron-stressed populations supplied with iron will display an increase in F_v/F_m due to a decrease in F_o.

Chapter 4

Spatial and temporal development of phytoplankton iron stress in relation to bloom dynamics in the high latitude North Atlantic Ocean

Published as:

Ryan-Keogh, T. J., Macey, A. I., Nielsdóttir, M. C., Lucas, M. I., Steigenberger, S. S., Stinchcombe, M. C., Achterberg, E. P., Bibby, T. S. and Moore, C. M., (2013), "Spatial and temporal development of phytoplankton iron stress in relation to bloom dynamics in the high latitude North Atlantic Ocean", *Limnology and Oceanography* ,Volume 58, Issue 2, Pages 533-545, dpi:10.4319/lo.2013.58.2.0533

4.1 Introduction

The high latitude (>∼50°N) North Atlantic (HLNA) is characterized by a pronounced spring phytoplankton bloom, representing one of the largest annual productivity cycles in the oceans (Siegel et al., 2002). Deep winter overturning (>600 m) injects nitrate

into the surface waters, with an associated annual drawdown of macronutrients (e.g. >10 μmol L^{-1} nitrate) (Ducklow and Harris, 1993; Sanders et al., 2005). Enhanced export production further indicates that the biological carbon pump (BCP) (Eppley and Peterson, 1979; Volk and Hoffert, 1985) of the HLNA is one of the strongest of any large open oceanic region (Falkowski et al., 1998; Laws et al., 2000). Increasing incident surface irradiance in the spring results in the shoaling of the mixed layer to less than the critical depth (Siegel et al., 2002; Sverdrup, 1953). The combination of the high nutrients and increasing light intensity provides the ideal situation for the onset of a large phytoplankton bloom, with chlorophyll concentrations peaking at >2.0 mg m^{-3} in parts of the high latitude North Atlantic. Although the annual bloom cycle removes a large proportion of the macronutrients available at the end of winter, further indicating a highly efficient BCP, residual concentrations of both nitrate and phosphate (e.g., > 1 μmol L^{-1} nitrate) are frequently observed during summer in the region (Nielsdóttir et al., 2009; Sanders et al., 2005).

The large seasonal removal of macronutrients resulting from the North Atlantic spring bloom contrasts strongly with the other high-latitude systems of the sub-polar North Pacific and Southern ocean, which are both characterized by year round high-nitrate, low-chlorophyll (HNLC) conditions, at least partly as a consequence of low iron availability (de Baar et al., 1990; Maldonado et al., 1999; Martin et al., 1990). Consequently, despite some early evidence to the contrary (Martin et al., 1993) iron had not been considered to be a potentially limiting micronutrient in the HLNA. However, it was recently demonstrated that summer phytoplankton communities in the Iceland basin are prone to iron limitation (Nielsdóttir et al., 2009). Consequently, as suggested for the Southern Ocean (Boyd, 2002), the dominant bottom-up influences on phytoplankton growth may transition from irradiance during winter to iron during summer in the HLNA. From the perspective of a Liebig-type limit on biomass and nutrient drawdown (Cullen, 1991), such observations are consistent with the relative input ratios of iron and nitrate being lower than phytoplankton requirements at higher latitudes in the North Atlantic (Measures et al., 2008; Nielsdóttir et al., 2009), partly due to low atmospheric iron supply (Jickells et al., 2005; Moore et al., 2006a) (Figure 4.1), at least in many regions removed from potentially significant sources (Prospero et al., 2012).

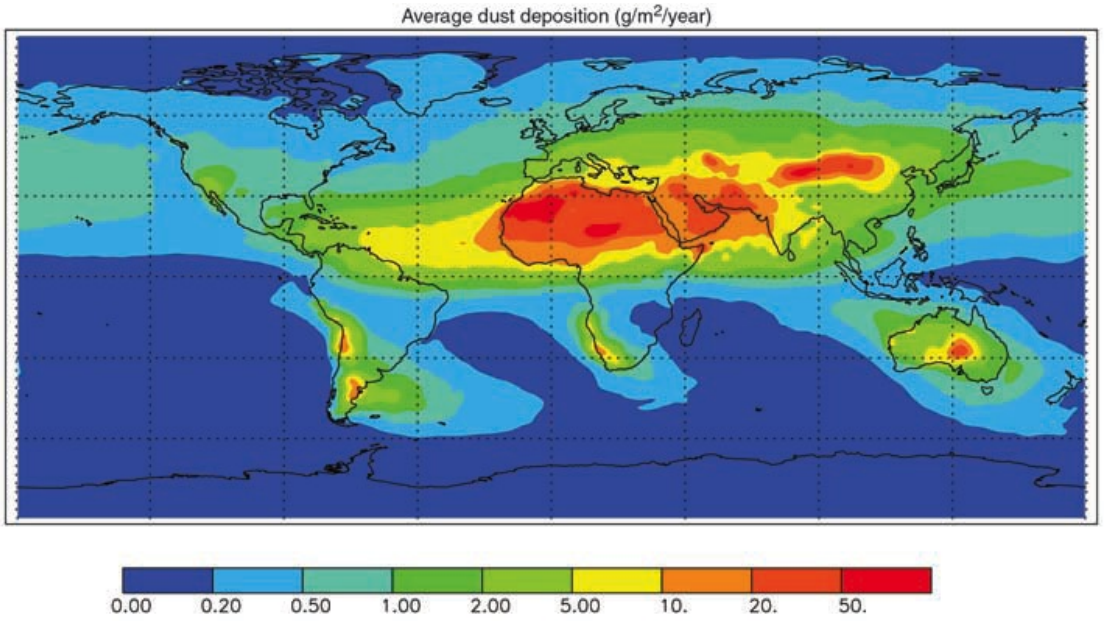

FIGURE 4.1: Dust fluxes to the world oceans based on a composite of three published modelling studies that match satellite optical depth, *in situ* concentration and deposition observations (Jickells et al., 2005).

Top-down factors may also influence accumulation of phytoplankton biomass and nutrient drawdown (Banse, 2002; Walsh, 1976). In addition to a proposed role of predator-prey dynamics during bloom initiation (Behrenfeld, 2010), zooplankton grazing (Walsh, 1976), which may be particularly high for small phytoplankton groups, likely plays a major role in the subsequent progression and termination of the bloom (Banse, 2002). Silicate limitation of large diatoms, which may otherwise have been able to escape grazing control (Cullen, 1991), has also been hypothesised to contribute to incomplete nutrient drawdown in the HLNA (Henson et al., 2006). Sinking (Walsby and Reynolds, 1980) and viral lysis (Bratbak et al., 1993) are also likely to contribute to incomplete nutrient drawdown. Rather than acting alone, within the classical HNLC regions these mechanisms likely interact with iron stress in maintaining residual macronutrients and constraining the overall phytoplankton biomass (Cullen, 1991; Price et al., 1994).

Nielsdóttir et al. (2009) demonstrated that, in a region of the Iceland basin during summer 2007, the phytoplankton community was limited by the availability of iron. Nutrient addition experiments demonstrated enhanced chlorophyll and F_v/F_m with the addition of iron (Figure 4.2). Experiments consistently showed that iron and not light availability was limiting the extent of biomass accumulation and nutrient drawdown. Beyond this available evidence for a limited region of the Iceland Basin during summer

(Nielsdóttir et al., 2009), the seasonal and spatial extent of any potential iron stress in the HLNA remains poorly resolved. Consequently, the effect of iron availability on the large-scale biogeochemistry of the region is currently difficult to assess. In this study, changes in phytoplankton standing stocks and photophysiology were assessed in both 48 - 120 h grow-out experiments and high spatial resolution short-term (24 h) incubations, in order to investigate the response of natural populations to the relief of potential nutrient stress.

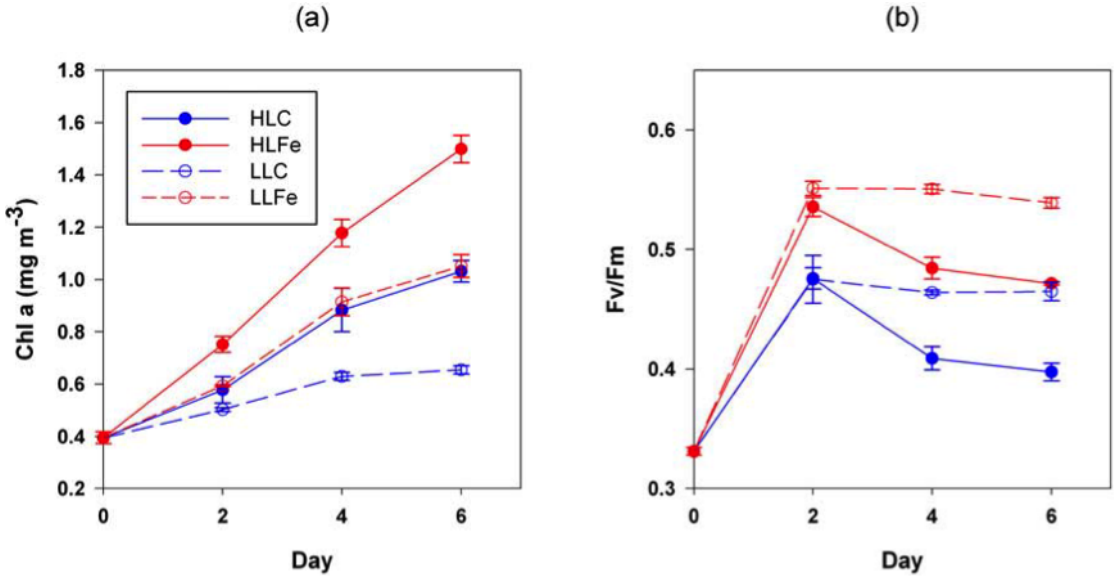

FIGURE 4.2: Results of incubation experiment B set up in the Iceland basin (Nielsdóttir et al., 2009), a) Chlorophyll concentration (mg m^{-3}) and b) F_v/F_m. Shown are mean values ($\pm$1 SE, n = 3). High light (HL) and low light (LL) correspond to 35% and 4% of E_0 respectively.

The apparent maximal photochemical yield of photosystem II (PSII) as measured using variable chlorophyll fluorescence (F_v/F_m) is particularly sensitive to iron stress (Greene et al., 1991) and hence variability in this parameter can provide a powerful diagnostic for investigating iron stress in the field (Behrenfeld et al., 2006; Boyd and Abraham, 2001; Kolber et al., 1994). The value of F_v/F_m is frequently observed to be suppressed within HNLC systems. More significantly, F_v/F_m increases rapidly following iron re-supply to iron-stressed field populations both *in situ* (Boyd and Abraham, 2001; Kolber et al., 1994) and in bottle incubations(Greene et al., 1994; Moore et al., 2007; Nielsdóttir et al., 2009) resulting from a decrease in F_o (Behrenfeld and Kolber, 1999; Behrenfeld et al., 2006; Greene et al., 1994; Kolber et al., 1994; Olson et al., 2000). Previous interpretations of increases in F_v/F_m were thought to be the result of an increase in

the variable fluorescence, F_v (Behrenfeld et al., 2004; Greene et al., 1994; Kolber et al., 1994).

Measurement of such rapid photophysiological changes (24 h) following deliberate experimental manipulations avoids potential problems in the interpretation of, for example, the absolute value of F_v/F_m in situ, where any physiological signal will be superimposed over taxonomic variability (Campbell et al., 1998; Fishwick et al., 2006; Moore et al., 2005, 2006b; Prasil et al., 2008; Suggett et al., 2009, 2004). In addition, because physiological changes will precede resultant changes in biomass accumulation ($>$ 24 h), the ability to restrict experimental time when monitoring sensitive changes to the photosynthetic apparatus minimizes the influence of bottle effects on biomass accumulation and the potential confounding influence of shifts in community structure on physiological measurements (Geider and La Roche, 1994; Greene et al., 1994).

The current study thus aimed to establish the seasonal cycle of iron stress across both the Iceland and Irminger basins of the HLNA. Previous studies to the region have only sampled a small region of the Iceland basin in late summer, thus making it difficult to ascribe any basin wide or seasonal conclusions about iron stress. Within this study the employment of different incubation experiments across both basins during spring and summer cruises will allow an extensive spatial and temporal sampling regime which can map the degree of iron stress within the seasonal cycle of the high latitude North Atlantic. By combining *in vitro* incubation experiments, with *in situ* measurements of phytoplankton physiology, macronutrients and chlorophyll, we mapped the development of physiological iron-stress. Moreover, contrasting seasonal responses to iron addition in two different biogeographical regions allowed us to describe the seasonal progression of iron stress over the HLNA.

Alongside the description of the seasonal progress of iron limitation in the HLNA, a specific analysis will be performed upon the FRRf data collected from the incubation experiments. It can be hypothesised that in experiments that display a high degree of iron limitation will show an increase in F_v/F_m following iron limitation due to a decrease in F_o. However, in those experiments that do not display any signs of iron limitation there should not be any change in F_o.

4.2 Results

4.2.1 Bloom Timing

Satellite data were used to derive the timing of the spring bloom in both the Iceland and Irminger Basins of the HLNA during 2010 (Figure 4.3). The criterion chosen to identify the date of the peak indicated a later bloom in the Central Irminger Basin than elsewhere in the region (Figure 4.3). This difference in bloom timing during 2010 was confirmed by in situ measurements of chlorophyll and macronutrients. Also indicated on Figure 4.3 are the defined geographic regions of the HLNA.

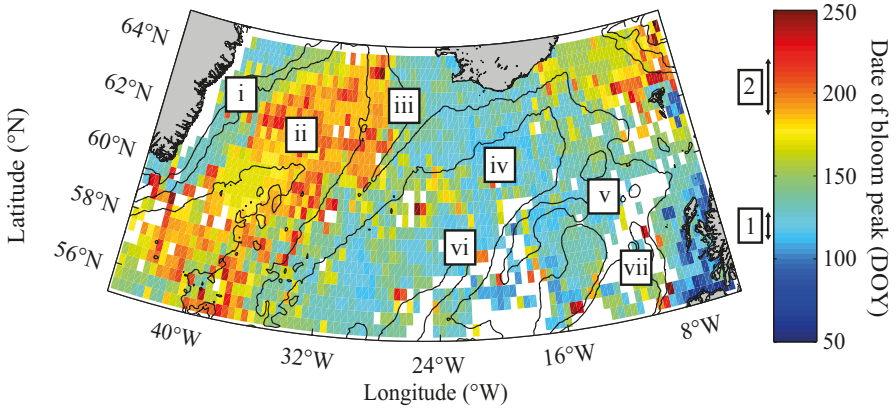

FIGURE 4.3: Date of bloom peak for the HLNA calculated using MODIS data. Black contours correspond to bathymetry in 1000 m isobaths. Indicated on colorbar are approximate timings of both cruises, where 1 = D350 (spring) and 2 = D354 (summer). Geographic regions of the HLNA include i = Western Irminger Basin, ii = Central Irminger Basin, iii = Reykjanes Ridge, iv = Iceland Basin, v = Rockhall Bank, vi = Hatton Bank, and vii = Rockhall Trough.

4.2.2 General Oceanography

In situ chlorophyll concentrations peaked during the spring cruise in the Iceland Basin (Figure 4.4a) and the summer cruise in the Central Irminger Basin (Figure 4.4b). Overall, the transition from spring to summer in the Iceland Basin corresponded to a decrease in average in situ chlorophyll concentrations from ~2 to ~1.5 μg L^{-1}, compared with an increase from ~1.0 to ~2.5 μg L^{-1} in the Central Irminger Basin. Sea surface values of in situ F_v/F_m, measured during the period of darkness (local midnight ±4 h) also displayed marked changes in both basins across the seasons, with generally higher values in spring. Superimposed onto this seasonal signal, in situ values of F_v/F_m were higher in the Irminger Basin than the Iceland Basin in spring (Figure 4.4c), but lower in

the Irminger Basin and Rockall region than the Iceland Basin in summer (Figure 4.4d). Initial dissolved (<0.4 μm) (Figure 4.4e and f) iron concentrations at experimental locations were frequently lower in summer, with >50% of samples measured at the summer stations being below the minimum value encountered during spring 0.07 nmol L^{-1}.

Alongside these changes in chlorophyll concentration and F_v/F_m, there were marked decreases in the in situ dissolved inorganic nitrogen (DIN) (Figure 4.5a,b), silicate (Figure 4.5c,d) and phosphate (Figure 4.5e,f) concentrations from spring (Figure 4.5a,c,e) to summer (Figure 4.5b,d,f). Both basins showed a decrease in macronutrient concentrations from spring to summer, with the Iceland Basin having lower concentrations than the Irminger Basin for both seasons. In particular, summer DIN concentrations in the central Iceland Basin were <1 μmol L^{-1} (Figure 4.5b), with silicate <0.3 μmol L^{-1} (Figure 4.5d) and phosphate <0.1 μmol L^{-1} (Figure 4.5f).

By combining these in situ sea surface variables with the bloom timings, different regions of the HLNA could be defined (solid black lines on Figures 4.4 and 4.5) and ascribed to the different bloom stages and conditions during both cruises. Satellite derived bloom timing was first used to separate the temporal progression of bloom into broad pre-bloom, bloom and post-bloom periods. Regions and periods sampled under post-bloom conditions were then further differentiated on the basis of observed residual macro-nutrient (DIN) concentrations. Consequently, we identify 4 broad conditions encountered in different regions over different periods during the two cruises, namely: pre-bloom (labeled A in Figure 4.4): bloom (labeled B), post-bloom high DIN (labeled C), and post-bloom low DIN (labeled D). These regions, defined on the basis of in situ observations and satellite derived bloom timings, subsequently provided context for the analysis of the experimental observations.

4.2.3 Long-term (>24 h) incubation experiments

Data from 48 - 120 h experiments indicated variable responses to iron addition to the extant phytoplankton communities. During spring, an experiment set up in the Central Irminger Basin (D350 Experiment 1) provided some evidence that the in situ phytoplankton community had the potential to become iron stressed, with relative decreases in F_v/F_m in the control treatment (Figure 4.6a) and an increased chlorophyll concentration seen within the iron addition treatment compared with the control treatment after

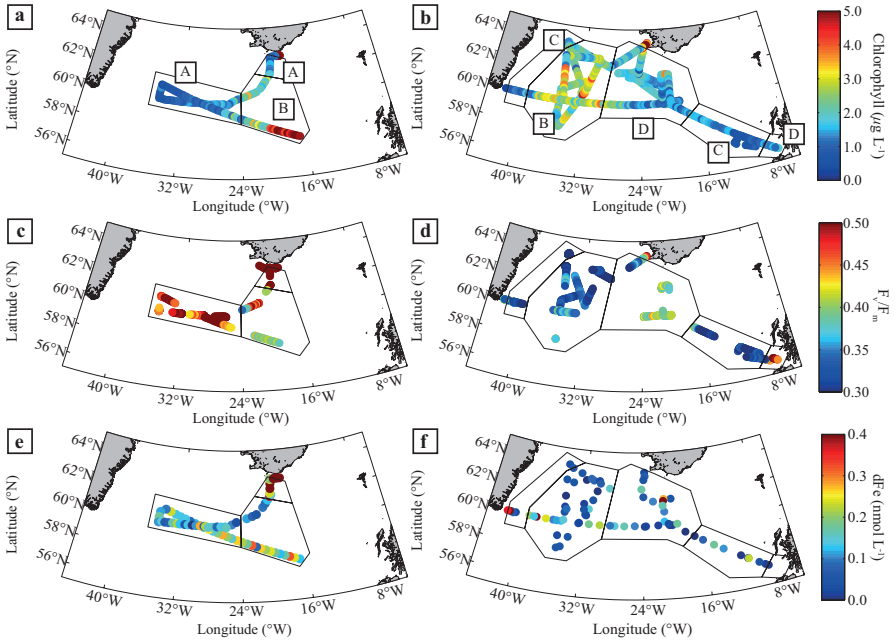

FIGURE 4.4: (a,b) Sea surface chlorophyll concentrations (μg L^{-1}), (c, d) night-time F_v/F_m values and (e, f) sea surface dissolved iron concentrations (nmol L^{-1}) during the (a,c,e) spring and (b,d,f) summer cruises. Solid black lines delineate regions on the basis of in situ sea surface variables and bloom timing during both cruises. (a,b) Regions are labeled according to conditions which correspond to: (A) pre-bloom, (B) bloom, (C) post-bloom, high DIN, and (D) post-bloom, low DIN.

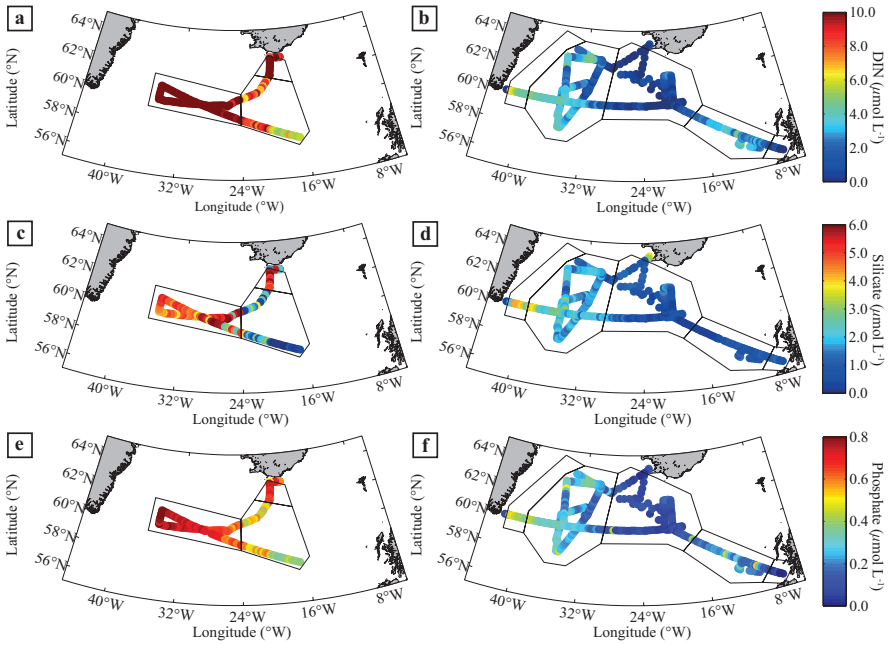

FIGURE 4.5: (a,b) dissolved inorganic nitrogen (DIN) concentrations (μmol L^{-1}), (c,d) silicate concentrations (μmol L^{-1}) and (e,f) phosphate concentrations (μmol L^{-1}) during the (a,c,e) spring and (b,d,f) summer cruises. Solid black lines delineate regions on the basis of in situ sea surface variables and bloom timing during both cruises. (a,b) Regions are labeled in according to conditions which correspond to: (A) pre-bloom, (B) bloom, (C) post-bloom, high DIN, and (D) post-bloom, low DIN.

120 h of incubation. During the same season, no evidence for iron stress was observed for an experiment initiated over the Reykjanes Ridge (D350 Experiment 2) (Figure 4.6b), with no significant differences in F_v/F_m (Analysis of Variance (ANOVA), $p>0.05$) or chlorophyll concentrations (ANOVA, $p>0.05$) observed between the iron addition and control bottles at any timepoint.

Some level of enhanced nutrient drawdown was also evident within the iron addition treatment of Experiment 1 (Figure 4.7a), while in Experiment 2 both treatments showed levels of enhanced nutrient drawdown (Figure 4.7b). Nitrate drawdown, calculated as the difference between the initial concentration and the final concentration (ΔNO_3^- (μmol L^{-1} d^{-1})), was slightly higher in the iron addition treatment of Experiment 1, at 0.26±0.01 μmol L^{-1} d^{-1} compared with 0.21±0.01 μmol L^{-1} d^{-1} for the control treatment (Figure 4.13). Experiment 2 also had a slightly higher ΔNO_3^- in the iron addition treatment, at 1.52±0.03 μmol L^{-1} d^{-1} compared to 1.47±0.04 μmol L^{-1} d^{-1} in the control treatment. Net growth rates, estimated from increases in chlorophyll concentrations at 72 h (Figure 4.12), were similar between iron and control treatments, with no significant difference (ANOVA, $p>0.05$). However, net growth rates in the iron addition treatment at 120 h in Experiment 1 were significantly higher than in the control treatment.

During the summer, iron addition had a more pronounced influence on phytoplankton community responses, particularly in the Irminger basin. Rapid increases in F_v/F_m were frequently observed within 24 h of iron amendment, as illustrated by Figure 4.8. Experiment 3 (Figure 4.8a) displayed an increase in F_v/F_m with iron addition, which increased from 0.30±0.01 to 0.44±0.004, while the control treatment remained relatively constant around ∼0.30. Biomass accumulation, inferred from bulk chlorophyll concentrations, also increased with iron addition, from 2.32±0.12 μg L^{-1} to 5.04±0.74 μg L^{-1}; while the control treatment remained constant around ∼2 μg L^{-1}.

Experiment 4 exhibited a similar pattern, with significant increases in the iron addition treatment (Figure 4.8b). The F_v/F_m and chlorophyll increased to 0.47±0.002 and 4.83±0.05 μg.L^{-1} respectively with iron addition, while both remained relatively constant in the control treatment. Experiment 6 also displayed a similar response, with significant increases in iron addition treatments (Figure 4.8c). F_v/F_m increased from 0.28±0.003 to 0.44±0.03 in the iron addition treatment, while chlorophyll concentrations increased from 1.50±0.07 to 6.98±0.18 μg L^{-1}.

Nutrient drawdown following iron addition were frequently higher than that in controls, particularly in the Central and Western Irminger basins (Figure 4.9). ΔNO_3^- at 72 h was significantly higher in the iron addition treatment in all experiments (ANOVA $p<0.05$), excepting experiment 6 where there was no significant difference at 72 h (Figure 4.13). Net growth rates were frequently higher in the iron addition treatment in comparison to the controls. Experiments in the Irminger basin exhibited the greatest difference in growth rates between iron and control treatments, $\Delta\mu^{Chl}$ (d^{-1}), with values frequently >0.24 at both 72 and 120 h.

In contrast, within the Iceland Basin during the summer cruise, where surface DIN concentrations were frequently undetectable (<0.03 μmol L^{-1}) (Figure 4.5b), no significant chlorophyll increases were observed on addition of nitrate alone. Indeed, nitrate addition often resulted in a net decrease in F_v/F_m as displayed in Figure 4.10a. The greatest increases in chlorophyll were typically observed only following the combined addition of both iron and nitrate, in Experiment 7 (Figure 4.10b) chlorophyll concentrations doubled from 0.99 ± 0.03 μg L^{-1} to 2.05 ± 0.03 μg L^{-1}; however iron addition resulted in the same increase in F_v/F_m as the combined treatment (+FeN) (Figure 4.10b). Experiment 5, set up in the Irminger Basin, under conditions of enhanced nitrate concentrations, was used as a control to test whether the different experimental design would have an effect upon results. F_v/F_m and chlorophyll concentrations in the iron addition (+ Fe) were not significantly differently to the combined treatment (+ FeN). Moreover ΔNO_3^- and net chlorophyll growth rates at 72 h were not significantly different between the two treatments (ANOVA $p>0.05$).

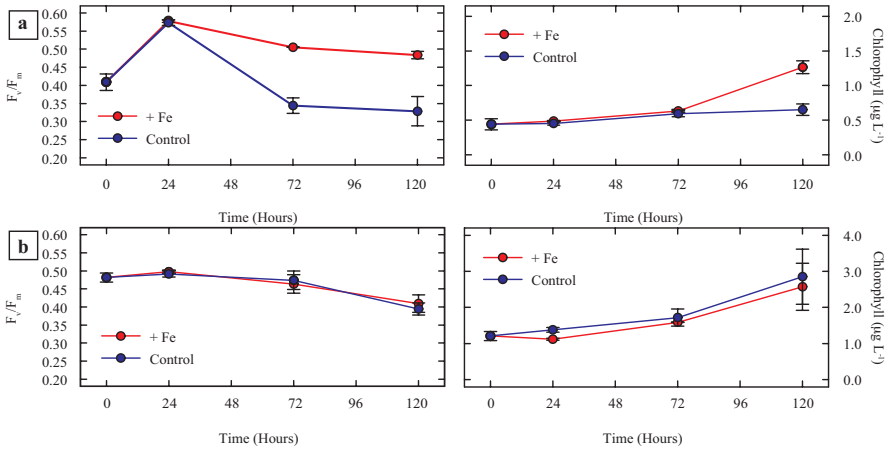

FIGURE 4.6: F_v/F_m and chlorophyll responses (μg L^{-1}) from iron addition long-term (>24 h) experiments on the spring cruise (D350) initiated over (a) the Irminger basin (Experiment 1), (b) the Reykjanes ridge (Experiment 2). Shown are averages with ± standard errors, where n = 3, 2, 2, and 5 for time points 0, 24, 72, and 120 h respectively.

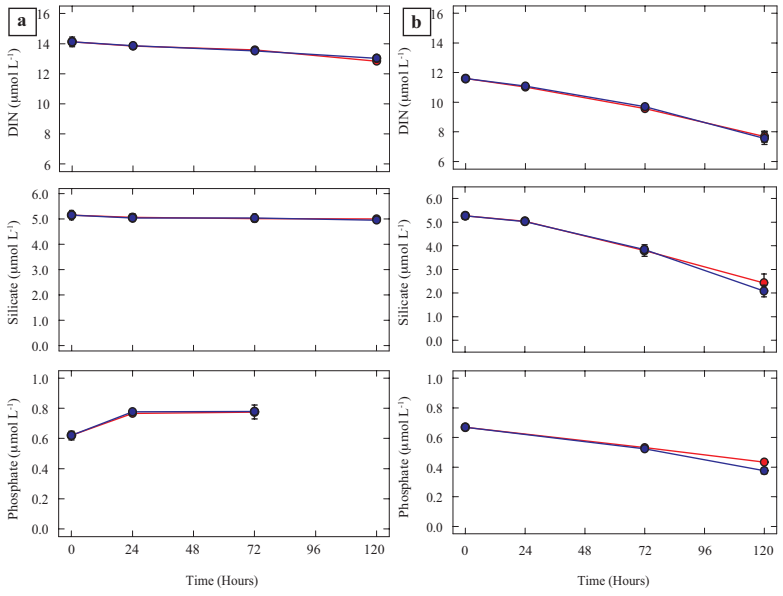

FIGURE 4.7: Nutrient drawdown responses, DIN (μmol L^{-1}), Silicate (μmol L^{-1}) and Phosphate (μmol L^{-1}), from iron addition long-term (>24 h) experiments on the spring cruise (D350) initiated over (a) the Irminger basin (Experiment 1), (b) the Reykjanes ridge (Experiment 2). Shown are averages with ± standard errors, where n = 3, 2, 2, and 5 for time points 0, 24, 72, and 120 h respectively.

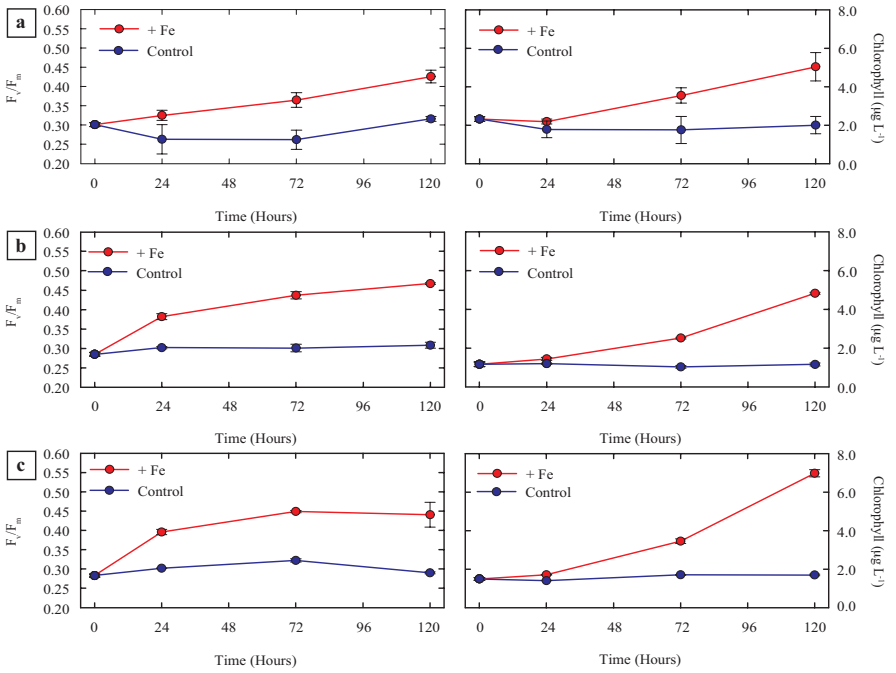

FIGURE 4.8: F_v/F_m and chlorophyll responses (μg L^{-1}) from iron addition long-term (>24 h) experiments on the summer cruise (D354) initiated over (a) the Central Irminger basin (Experiment 3), (b) the Northern Irminger basin (Experiment 4) and (c) the Western Irminger basin (Experiment 6). Shown are averages with ± standard errors, where n = 3, 2, 2, and 5 for time points 0, 24, 72, and 120 h respectively.

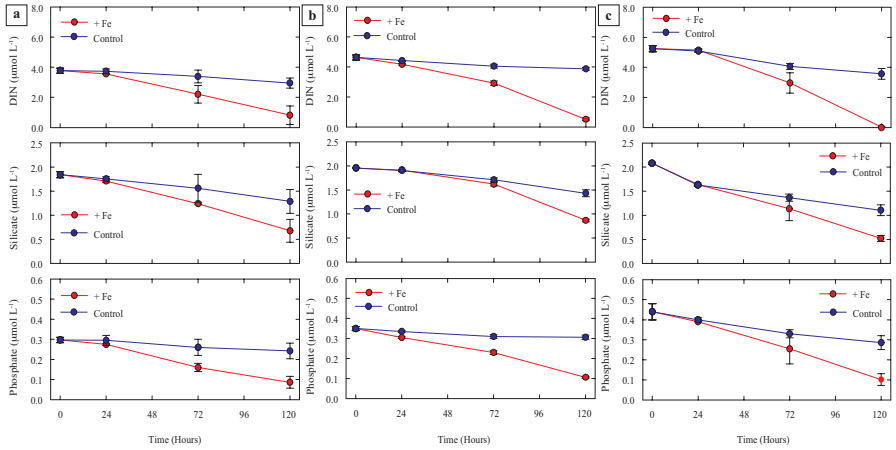

FIGURE 4.9: Nutrient drawdown responses, DIN (μmol L^{-1}), Silicate (μmol L^{-1}) and Phosphate (μmol L^{-1}), from iron addition long-term (>24 h) experiments on the summer cruise (D354) initiated over (a) the Central Irminger basin (Experiment 3), (b) the Northern Irminger basin (Experiment 4) and (c) the Western Irminger basin (Experiment 6). Shown are averages with ± standard errors, where n = 3, 2, 2, and 5 for time points 0, 24, 72, and 120 h respectively.

4.2.3.1 Size-Fractionated Measurements

Size-fractionated F_v/F_m measurements performed on the initial samples from incubation experiments, revealed a consistent pattern throughout both basins, with the <5 μm

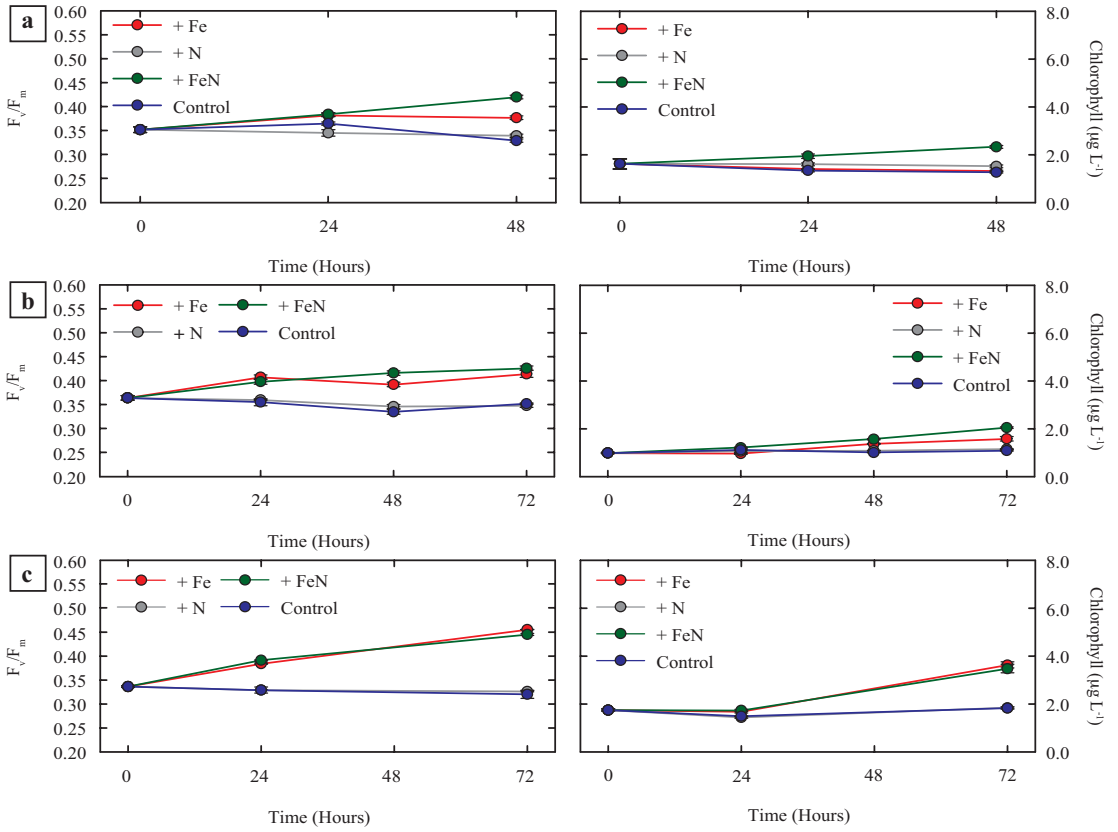

FIGURE 4.10: F_v/F_m and chlorophyll responses (μg L^{-1}) from iron and nitrate addition long-term (>24 h) experiments on the summer cruise (D354) initiated over (a) the Central Iceland basin (Experiment 2), (b) the Central Iceland basin (Experiment 7) and (c) the Southern Irminger basin (Experiment 5). Shown are averages with ± standard errors, where $n = 3$ for all timepoints.

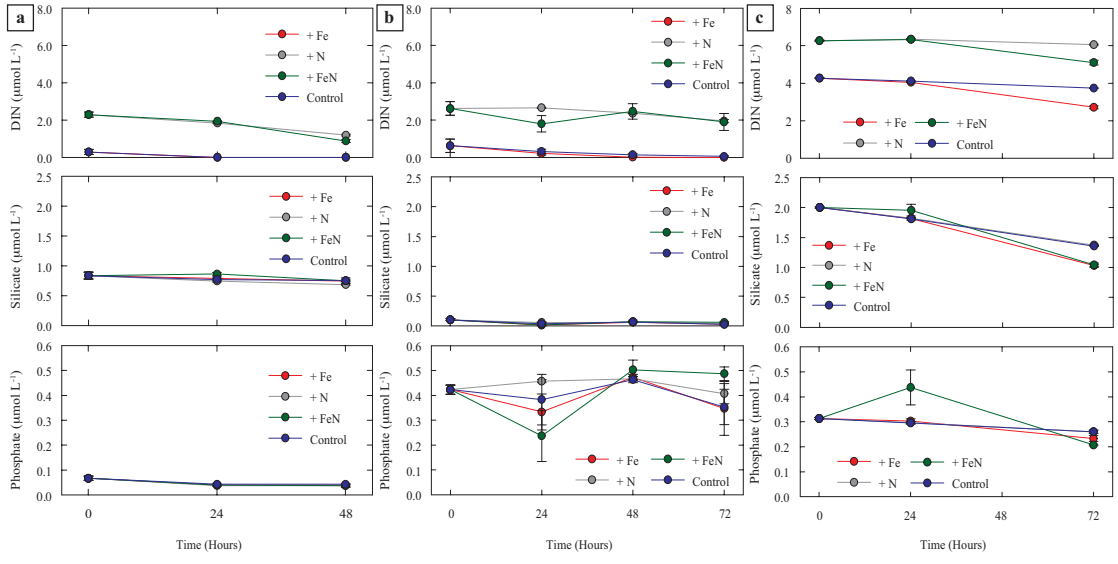

FIGURE 4.11: Nutrient drawdown responses, DIN (μmol L^{-1}), Silicate (μmol L^{-1}) and Phosphate (μmol L^{-1}), from iron addition long-term (>24 h) experiments on the summer cruise (D354) initiated over (a) the Central Iceland basin (Experiment 2), (b) the Central Iceland basin (Experiment 7) and (c) the Southern Irminger basin (Experiment 5). Shown are averages with ± standard errors, where $n = 3$ for all timepoints.

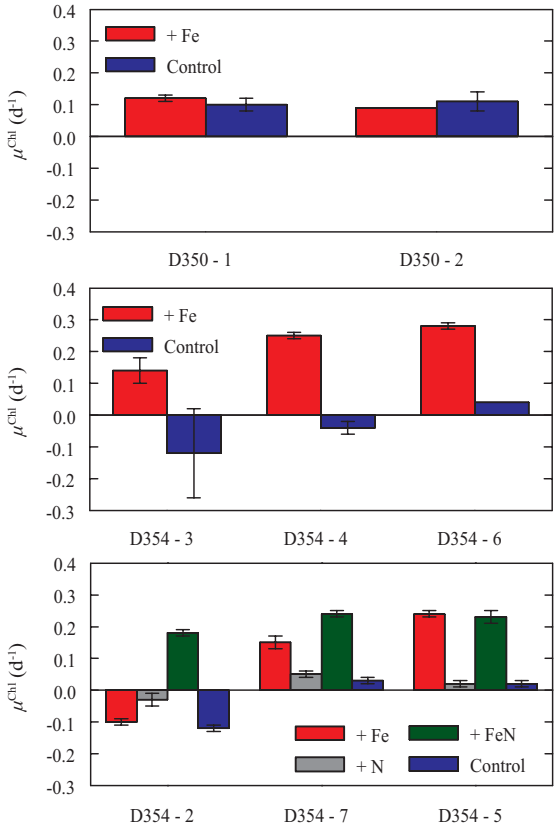

FIGURE 4.12: Net chlorophyll growth rates, μ^{Chl} (d^{-1}), calculated from chlorophyll concentrations from long-term experiments on both the spring and summer cruises. Shown are averages with ± standard errors where $n = 5$ for all iron addition only experiments and $n = 3$ for iron and nitrate addition experiments.

size-fraction having a higher *in situ* F_v/F_m than the >5 μm size-fraction. Overall, F_v/F_m values for the <5 μm and >5 μm fractions were, respectively, 10% higher and 25% lower than those of the bulk community (Figure 4.14). Although both size-classes physiologically responded to the addition of Fe (Figure 4.15), the response of the >5 μm size-fraction was generally larger. For example, in a longer timescale experiment (Experiment 6) performed in the Western Irminger Basin, the value of F_v/F_m for the >5 μm fraction had nearly increased to that of the iron amended <5 μm fraction after 120 h (Figure 4.15a). The addition of iron also resulted in a net chlorophyll derived growth rate for the >5 μm fraction (over 120 h) which was double that of the <5 μm size-fraction (0.45±0.01 $\mu^{Chl>5}$ (d^{-1}) compared with 0.22±0.01 $\mu^{Chl<5}$ (d^{-1})) (Figure 4.16a).

However, within the Iceland Basin, although F_v/F_m was also lower for the >5 μm size-fraction than the <5 μm size-fraction (Figure 4.15b), the increase was less pronounced and F_v/F_m >5 μm did not increase to a value equivalent to that of the initial or control

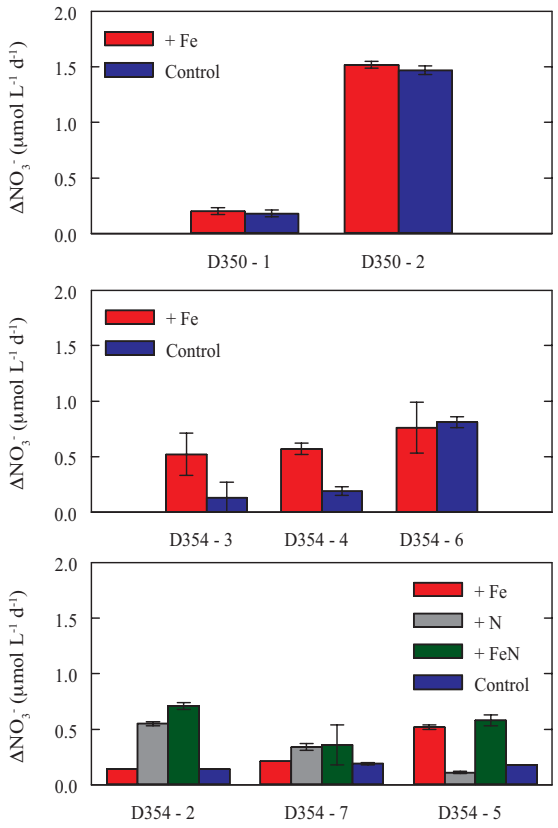

FIGURE 4.13: Net nitrate drawdown, ΔNO_3^- (μmol L^{-1} d^{-1}), calculated from DIN concentrations from long-term experiments on both the spring and summer cruises. Shown are averages with $\pm$ standard errors, where $n = 5$ for all iron addition only experiments and $n = 3$ for iron and nitrate addition experiments.

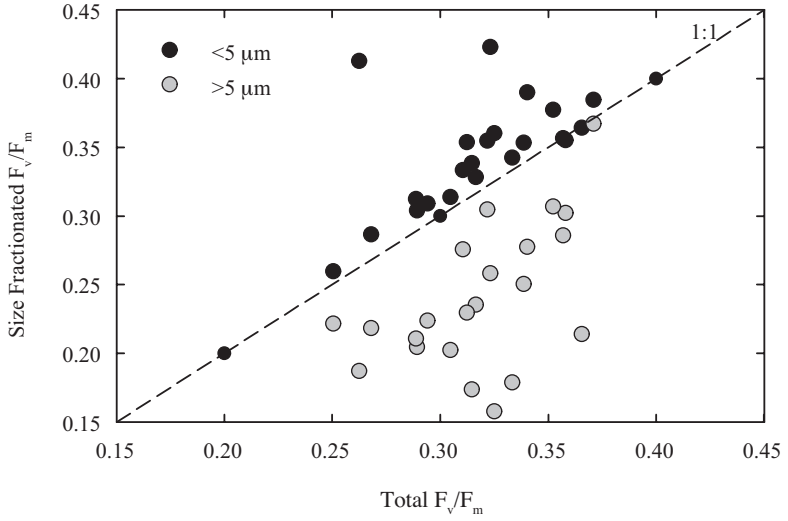

FIGURE 4.14: Size-fractionated F_v/F_m against total F_v/F_m from initial samples of experiments on the summer cruise. Dashed line represents the 1:1 line.

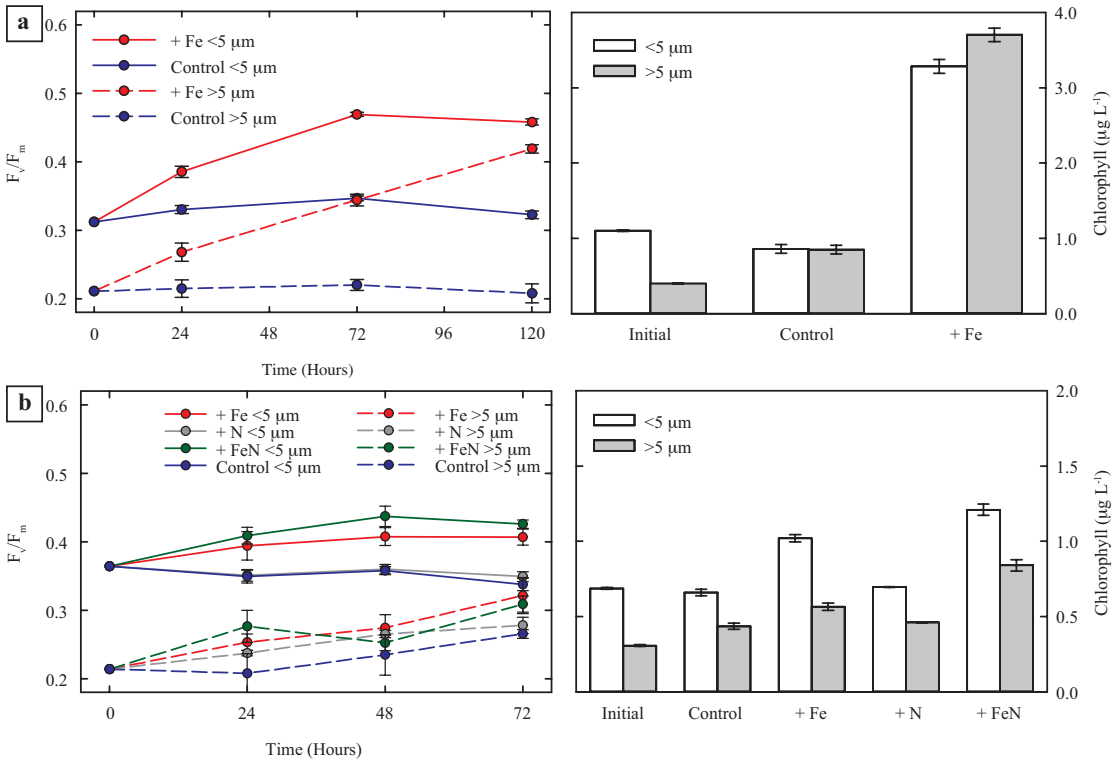

FIGURE 4.15: Size-fractionated F_v/F_m and chlorophyll responses (μg L^{-1}) from long-term (>24 h) experiments set up in (a) the Irminger basin (Experiment 6) and (b) the Iceland basin (Experiment 7) during the summer cruise (D354). Shown are averages with ± standard errors, where n=3 for all timepoints of Experiment 7, and n=3, 2, 2, and 5 for 0, 24, 72, and 120 h timepoints in Experiment 6.

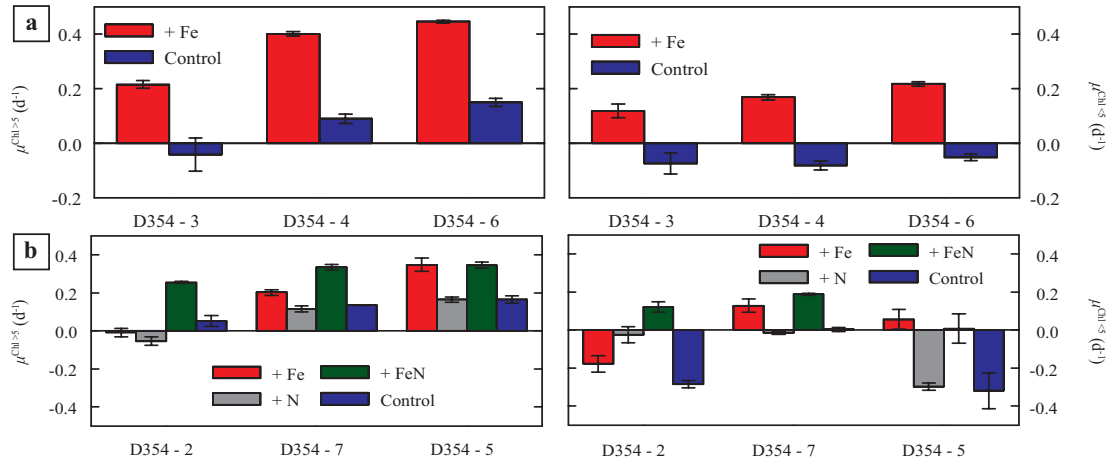

FIGURE 4.16: Size-fractionated net growth rates, μ^{Chl} (d^{-1}), calculated from size-fractionated chlorophyll measurements from long-term (>24 h) experiments during the summer cruise (D354). Shown are averages with ± standard errors, where $n = 5$ for all iron addition alone experiments and $n = 3$ for all iron and nitrate addition experiments.

<5 μm size-fraction. The chlorophyll concentration in the <5 μm size-fraction also remained higher than that for the >5 μm size-fraction in this experiment. The differences in the net chlorophyll derived growth rate for the combined treatment (+ FeN) was significantly higher than the iron alone and control treatment in both size fractions, but in the<5 μm fraction it was ∼30% and ∼100% higher respectively.

4.2.3.2 Absolute Changes in Fluorescence

Alongside measurements of F_v/F_m, the absolute changes in F_o, F_m and F_v (normalised to chlorophyll) were calculated. Overall, by the end of experiments across both cruises F_o Chl^{-1} was generally lower when iron was added. On the spring cruise in D350 Experiment 1, the absolute changes in fluorescence occurred within the F_o Chl^{-1} (Figure 4.17a) component with an increase in the control treatment, while the iron addition remained relatively constant. This increase was significantly different at 120 h (ANOVA, p <0.05), while there were no significant differences in the F_m Chl^{-1} (Figure 4.17c) or F_v Chl^{-1} (Figure 4.17e). In experiment 2, both treatments showed increases in F_o Chl^{-1} (Figure 4.17b), F_m Chl^{-1} (Figure 4.17d) and F_v Chl^{-1} (Figure 4.17f) across both treatments; with no significant differences found at any time point.

The absolute changes in fluorescence for the iron and nitrate experiments from the summer cruise at low ambient nitrate concentrations (Experiments 2, 5 and 7 - Figure 4.18) showed a decrease in F_o Chl^{-1} and F_m Chl^{-1} within the iron and combined iron and nitrate treatments. Within experiment 2, although there slight decreases in both F_o Chl^{-1} (Figure 4.18a) and F_m Chl^{-1} (Figure 4.18d), these decreases were not significant between treatments. The decreases in F_o Chl^{-1} (Figure 4.18b) and F_m Chl^{-1} (Figure 4.18e) within experiment 7 for both the iron and combined iron and nitrate treatments were significantly different from the controls (ANOVA, p <0.05). Experiment 5 that was set up in the Irminger basin, with enhanced ambient nitrate concentrations, also displayed a similar pattern with significant differences (ANOVA, p <0.05) in F_o Chl^{-1} (Figure 4.18c) and F_m Chl^{-1} (Figure 4.18f). Across all experiments, F_v Chl^{-1} did not show any significant difference between treatments (ANOVA, p >0.05). The nitrate treatment had a similar response to the control across all experiments.

The absolute changes in fluorescence for the iron addition experiments from the summer cruises at high ambient nitrate concentrations (Exeriments 3, 4 and 6 - Figure 4.19)

showed a very consistent response across the experiments, with a general decrease in F_o Chl^{-1} (Figure 4.19a, b and c) and in F_m Chl^{-1} (Figure 4.19d, e and f) with the addition of iron. The differences were significant from 24 h onwards (ANOVA, p <0.05) in experiments 4 and 6, whereas in experiment 3 they were significant from 72 h. Within F_v Chl^{-1} (Figure 4.19g, h and i) there were very little changes across the experiments with time in comparison to F_o Chl^{-1} and F_m Chl^{-1}, excepting in experiment 6 where the iron addition treatment was significantly different (ANOVA, p <0.05) from 24 h onwards.

If the F_o Chl^{-1} from the initial and end time points of both treatments from the iron addition experiments performed in the Irminger basin during summer is plotted against F_v/F_m then the consistent pattern can be observed more clearly (Figure 4.20). The control treatment does not differ significantly from the initial time point (t-test, p >0.05) whereas the iron treatment did differ significantly (t-test, p <0.05). As the F_v/F_m increased with iron addition, consistently across all experiments F_o Chl^{-1} decreased.

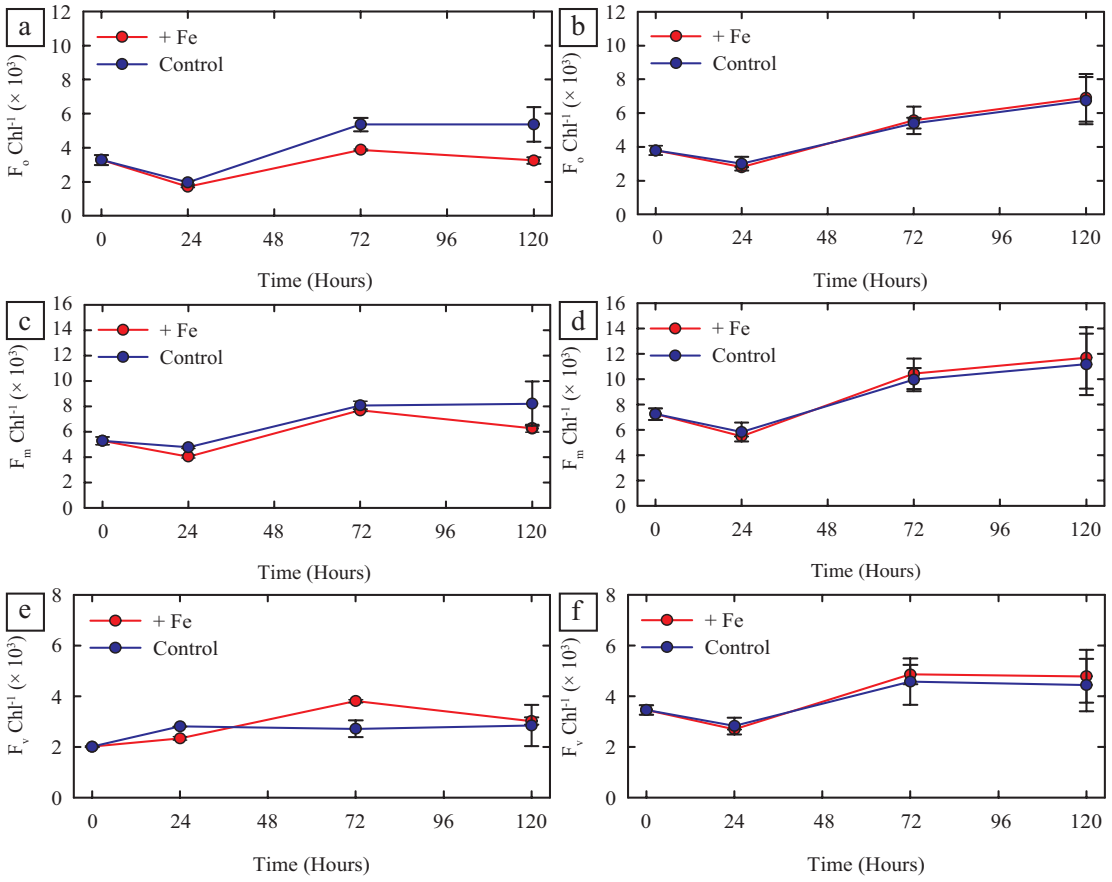

FIGURE 4.17: The absolute changes in F_o Chl^{-1} (× 10^3) (a, b), F_m Chl^{-1} ($\times 10^3$)$(c, d) and F_v Chl^{-1}(\times\ 10^3)$ (e, f) for D350 Experiment 1 (a, c and e) and D350 Experiment 2 (b, d and f).

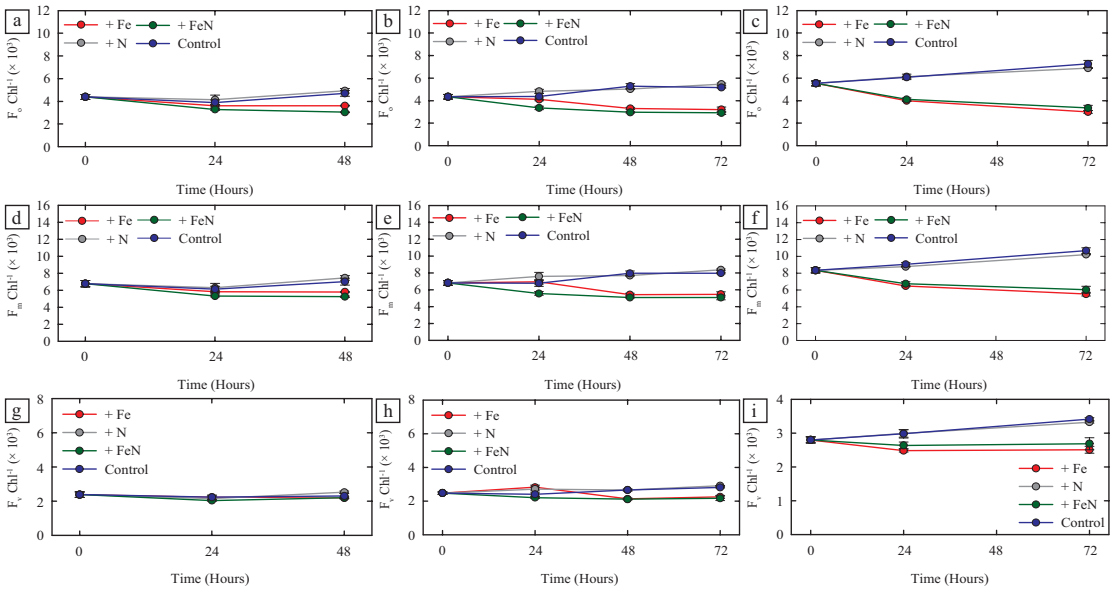

FIGURE 4.18: The absolute changes in F_o Chl^{-1} ($\times 10^3$) (a, b and c), F_m Chl^{-1} ($\times 10^3$) (d, e and f) and F_v Chl^{-1} ($\times 10^3$) (g, h and i) for D354 Experiment 2 (a, d and g), D354 Experiment 7 (b, e and h) and D354 Experiment 5 (c, f and i).

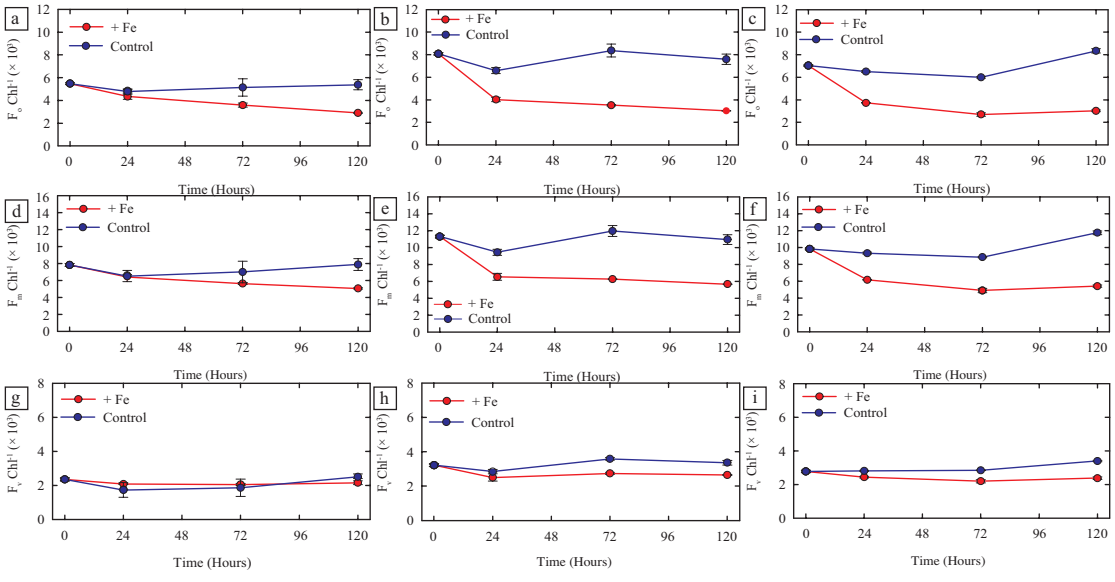

FIGURE 4.19: The absolute changes in F_o Chl^{-1} ($\times 10^3$) (a, b and c), F_m Chl^{-1} ($\times 10^3$) (d, e and f) and F_v Chl^{-1} ($\times 10^3$) (g, h and i) for D354 Experiment 3 (a, d and g), D354 Experiment 4 (b, e and h) and D354 Experiment 6 (c, f and i).

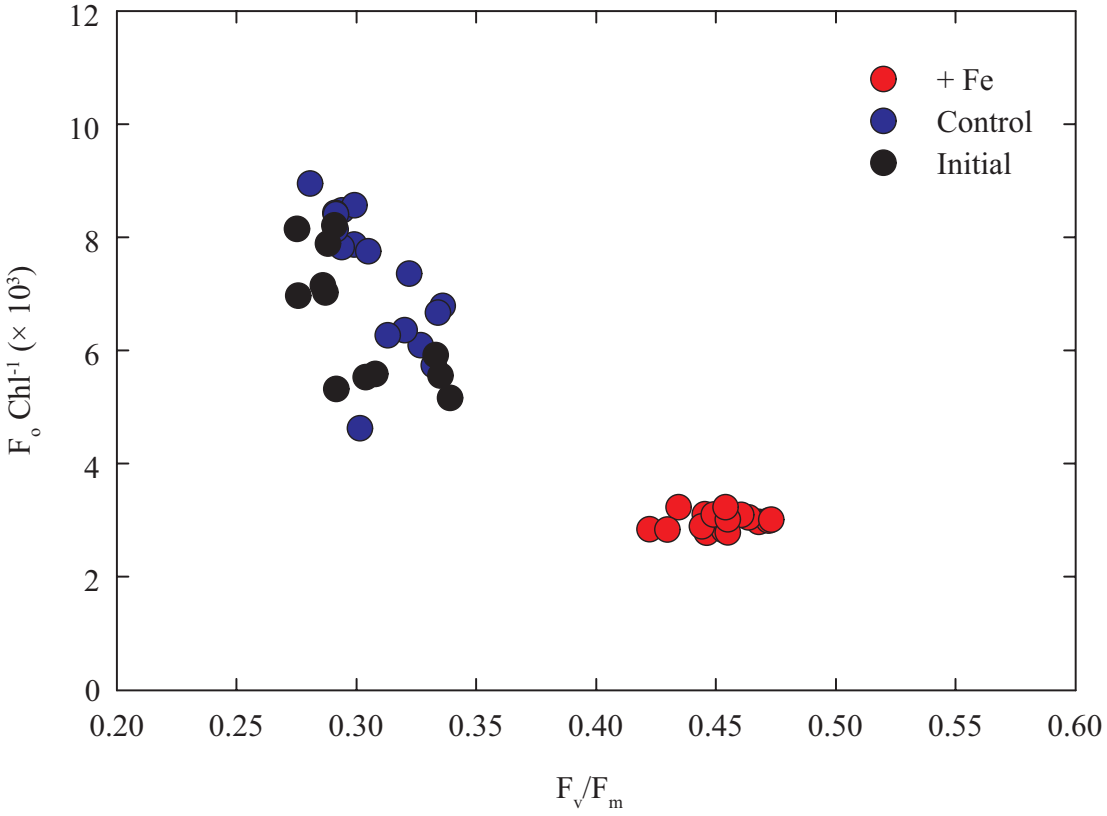

FIGURE 4.20: The absolute changes in fluorescence normalised to Chl^{-1} from the end time points of the iron addition experiments set up on the summer cruise.

4.2.4 Short-term (24 h) incubation experiments

The 25 short-term 24-h incubation experiments conducted over both cruises further revealed variability between basins and seasons. Significant (ANOVA, p <0.05) rapid changes in photophysiology (F_v/F_m) were often observed in these experiments, despite the lack of significant changes in other variables such as chlorophyll or nutrient concentration over the short 24-h time scale. In order to contrast relative changes in PSII photophysiology between the large numbers of experiments, we calculated the difference in F_v/F_m between control and treatment bottles ($\Delta(F_v/F_m)$). $\Delta(F_v/F_m)$ was calculated for all the different nutrient addition treatments performed during both cruises over the two seasons (Figure 4.21). For simplicity calculated values of $\Delta(F_v/F_m)$ are hereafter subscripted '+ 1.0 N', '+ FeN', '+ 0.2 Fe', or '+ 2.0 Fe' corresponding to the 1 μmol L^{-1} nitrate, 1 μmol L^{-1} nitrate and 2.0 nmol L^{-1} and 0.2 nmol L^{-1} and 0.2 nmol L^{-1} iron additions respectively.

Values of $\Delta(F_v/F_m)_{\ +\ 1.0\ N}$ were frequently indistinguishable from zero (Figure 4.24) or slightly negative, due to a small drop in F_v/F_m following N addition in some experiments,

as previously observed in some other systems (Behrenfeld et al., 2006). In contrast, $\Delta(F_v/F_m)$ was frequently positive following iron addition (Figures 4.21 and 4.23), with the values calculated for the two iron alone treatments (+ 0.2 Fe and + 2.0 Fe) being highly correlated ($r^2 = 0.960$, $p < 0.001$, n = 23) (Figure 4.22a) and hence displaying consistent spatial patterns (Figure 4.23). Moreover, within those natural populations displaying significant responses (ANOVA, $p < 0.05$), the addition of 2.0 nmol L^{-1} iron consistently resulted in a larger change in F_v/F_m (on average 40% higher) than the addition of 0.2 nmol L^{-1} iron (Figure 4.21 and 4.23a, b). Consequently the observed variability of $\Delta(F_v/F_m)$ following iron addition ($\Delta(F_v/F_m)_{\text{ + 0.2 Fe or + 2.0 Fe}}$) indicated spatially and temporally coherent physiological responses that scaled with increasing iron enrichment (Figure 4.23). We thus interpret $\Delta(F_v/F_m)_{\text{ + 0.2 Fe or + 2.0 Fe}}$ as a relative measure of the degree of iron stress, providing a means to compare and contrast the inter/intra-basin and seasonal variability.

Values of $\Delta(F_v/F_m)_{\text{ + 0.2 Fe or + 2.0 Fe}}$ were lowest under the pre-bloom conditions (labeled A in Figure 4.4), suggesting a lack of physiological iron stress for these populations (Figures 4.21; 4.23a,c), consistent with the lack of a treatment response in longer term grow out experiments performed under the same conditions (Figure 4.6a). Low $\Delta(F_v/F_m)$ was also observed following iron addition within the post-bloom low DIN conditions (labeled D in Figure 4.4) encountered in the Iceland Basin (Figure 4.23b,d), where the + FeN treatment also tended to have a higher $\Delta(F_v/F_m)$ than that for iron alone (Figure 4.24d) and where longer term experiments indicated the potential for co-limitation of chlorophyll accumulation by iron and nitrate (Figure 4.10). Higher values of $\Delta(F_v/F_m)_{\text{ + 0.2 Fe or + 2.0 Fe}}$ were observed during the bloom conditions (labeled B in Figure 4.4) encountered in the Iceland Basin during the spring cruise (Figure 4.23a,c) and the Central Irminger Basin during the summer cruise (labeled B in Figure 4.4) (Figure 4.23b,d), while the highest values were observed under post-bloom high DIN conditions (labeled C in Figure 4.4), as encountered in the Western Irminger Basin and Rockall region during the summer cruise (Figure b,d). These regions corresponded to the clearest influence of iron addition on chlorophyll accumulation and nitrate drawdown in longer term experiments (Figure 4.8c).

To provide a more quantitative comparison of short-term (24 h) physiological responses to nutrient amendment with longer-term biomass responses inferred from bulk chlorophyll accumulation, we compared the value of $\Delta(F_v/F_m)_{\text{ + 2.0 Fe}}$ observed after 24 h in

the long-term experiments with differences in chlorophyll derived net growth rates over 72 h between iron amended and control treatments (Figure 4.22b). The values were highly correlated ($R^2 = 0.87$, $p < 0.05$, $n = 8$) indicating that the observed short-term physiological responses were predictive of subsequent biomass responses in experiments.

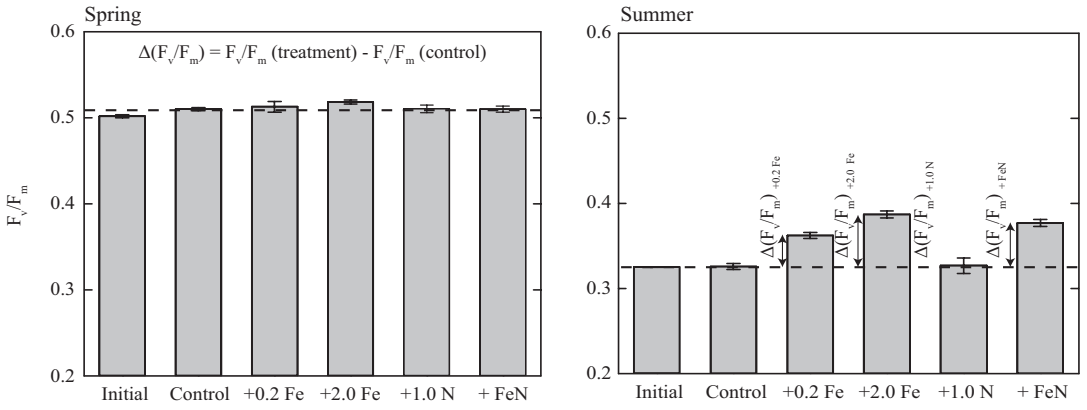

FIGURE 4.21: Representative data from two short-term experiments set up during D350 (Spring) and D354 (Summer). $\Delta(F_v/F_m)$ is calculated as the difference between the F_v/F_m of the nutrient amended treatment and the control treatment at the 24 h time point. Four different values were calculated, $\Delta(F_v/F_m)_{+\ 0.2\ Fe}$, $\Delta(F_v/F_m)_{+\ 2.0\ Fe}$, $\Delta(F_v/F_m)_{+\ 1.0\ N}$ and $\Delta(F_v/F_m)_{+\ FeN}$. The dashed line represents level of control treatment. Shown are averages with ± standard errors, where n = 3 for all treatments.

4.3 Discussion

The annual cycle of phytoplankton growth in the HLNA results in significant seasonality in surface macronutrient concentrations. During winter, photosynthesis is likely limited by low mean irradiance, with net phytoplankton growth occurring rapidly following the onset of stratification (Sverdrup, 1953), although alternative controlling factors have been suggested for bloom initiation (Behrenfeld, 2010). Behrenfeld (2010) utilised a nine-year satellite record of phytoplankton biomass in the subarctic Atlantic to reevaluate seasonal dynamics. The results of this study were in direct contradiction to the Critical Depth Hypothesis (Sverdrup, 1953). The study found that bloom initiation occurs in winter rather than spring when mixed layer depths are maximum, coupling between growth and loss terms increases with stratification rather than decreasing, that maximal net growth rates are as likely to occur during winter as in spring and these net growth rates are inversely related to phytoplankton growth.

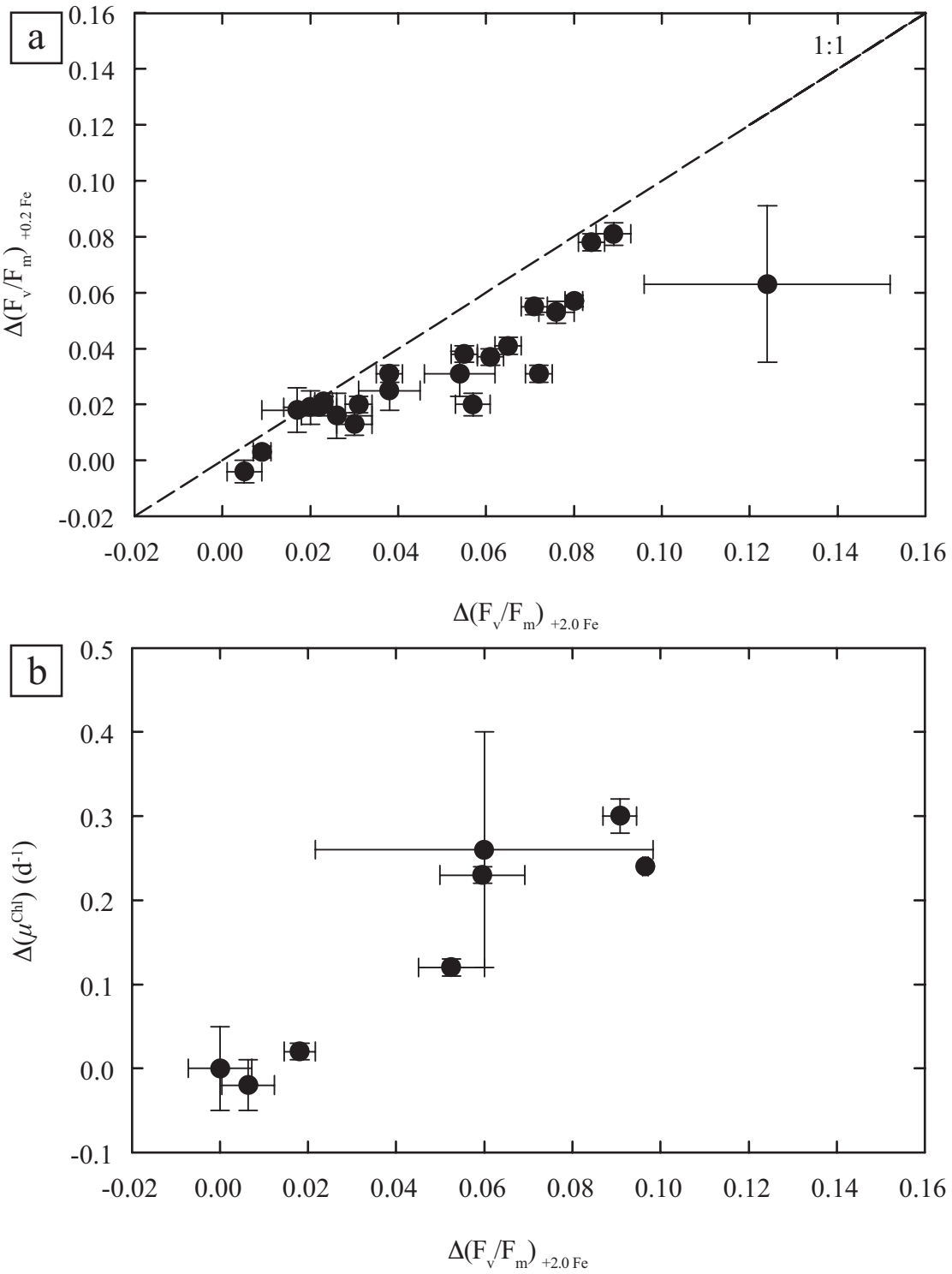

FIGURE 4.22: a) The $\Delta(F_v/F_m)$ from the + 2.0 Fe treatment plotted against the + 0.2 Fe treatment. b) The $\Delta(F_v/F_m)_{+\ 2.0\ Fe}$ plotted against the difference in chlorophyll derived net growth rates over 72 h ($\Delta\mu^{Chl}$ (d^{-1}) for all long-term experiments, where $\Delta\mu^{Chl}$ (d^{-1}) is μ^{Chl} for the + Fe treatment minus the μ^{Chl} from the control treatment. *Growth rate calculated over 48 h only due to shortened experimental duration. Dashed line represents the 1:1 line. Shown are averages with ± standard errors, where n = 2 or 3 for $\Delta(F_v/F_m)_{+\ 2.0\ Fe\ or\ +0.2\ Fe}$ and n = 3 or 5 for $\Delta\mu^{Chl}$.

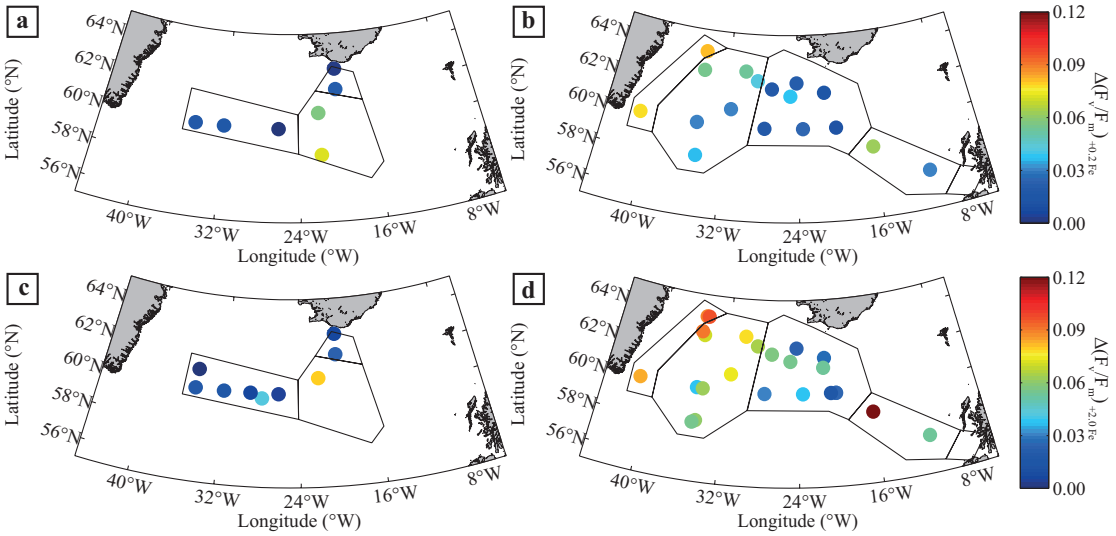

FIGURE 4.23: Experimental values of $\Delta(F_v/F_m)$ calculated after 24 h for (a,b) the 0.2 nmol L^{-1} iron (+ 0.2 Fe) and (c,d) the 2.0 nmol L^{-1} iron (+ 2.0 Fe) addition treatments during (a,c) the spring and (b,d) summer cruises.

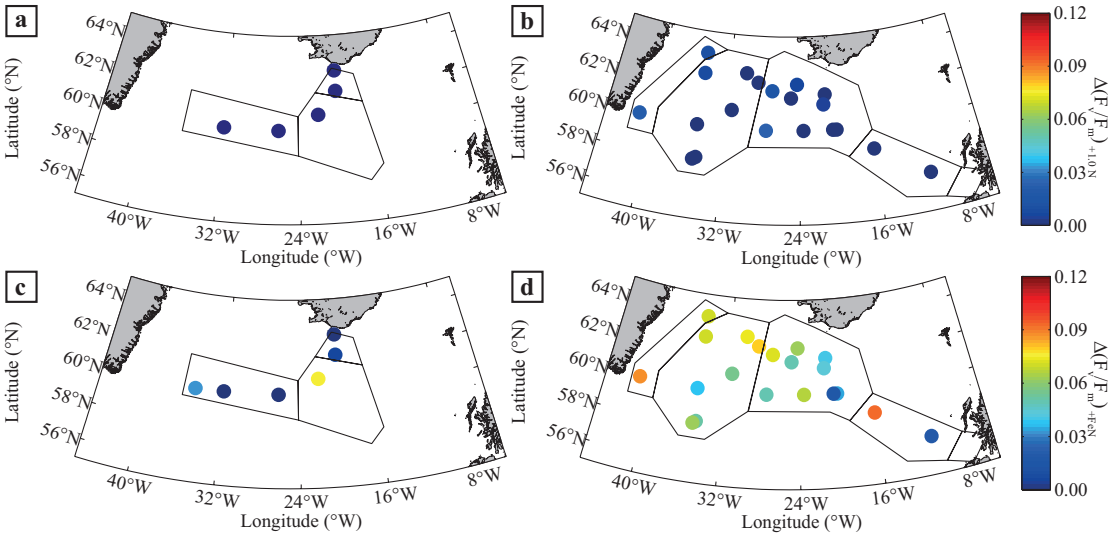

FIGURE 4.24: Experimental values of $\Delta(F_v/F_m)$ calculated after 24 h for (a,b) the 1.0 μmol L^{-1} nitrate (+ 1.0 N) and (c,d) the 1.0 μmol L^{-1} iron and 2.0 nmol L^{-1} iron (+ FeN) addition treatments during (a,c) the spring and (b,d) summer cruises.

In contrast to the majority of high-latitude open ocean systems, where large seasonal macronutrient drawdown appears to be restricted by the availability of iron (Boyd et al., 2007; de Baar et al., 1990; Martin and Fitzwater, 1988), macronutrient drawdown over the growing season in the HLNA can be substantial. However, despite the magnitude of the bloom, residual DIN concentrations have frequently been observed in the HLNA at the end of the growing season (Nielsdóttir et al., 2009; Sanders et al., 2005), suggesting that some factor is constraining the complete utilization of this nutrient resource

(Cullen, 1991; Greene et al., 1994). Although a lack of bioavailable iron is one possibility (Nielsdóttir et al., 2009), zooplankton grazing (Frost, 1991; Walsh, 1976) or silicate limitation (Henson et al., 2006) could also play a role.

Satellite derived estimates of bloom timing (Figure 4.3) enabled the placement of the observed spatial and temporal variability of *in situ* variables and experimental indices of iron stress within the annual bloom cycle (Figure 4.26). *In situ* observations of chlorophyll and nutrients confirmed the temporal progression of a classical spring-bloom, with macronutrient drawdown accompanying the peak accumulation of phytoplankton biomass, as inferred by bulk chlorophyll (Figure 4.26). Clear spatial differences in bloom timing and progression were observed within the HLNA during 2010. The Iceland basin, Western Irminger Basin and Rockall region bloomed earlier in the spring (Figures 4.3, 4.4a). However, while there was near complete nutrient drawdown in the Iceland Basin by summer (Figure 4.5b), there was incomplete nutrient drawdown (residual nitrate >1 μmol L^{-1}) in the Western Irminger Basin and Rockall region. In contrast, the Central Irminger Basin bloomed later in the growing season (Figures 4.3, 4.4b) with incomplete nutrient drawdown where the bloom was still underway (Figure 4.5b). The almost complete nutrient drawdown observed in the Iceland Basin in the present study is anomalous for this region, with values (<1 μmol L^{-1} DIN) being lower than typically recorded for the summer period (Henson et al., 2003; Nielsdóttir et al., 2009; Sanders et al., 2005), possibly indicative of an additional source of iron to this basin in 2010.

Indeed, prior to the start of the first cruise (D350) the Eyjafjallajokull volcano located in Iceland began to erupt, discharging $\sim 270 \pm 70\ 10^6$ m^3 of volcanic ash particles (tephra) into the atmosphere to a height of up to 10 km (Gudmundsson et al., 2012). Modelled estimates of the iron input indicated that the high latitude North Atlantic could have accumulated > 0.2 nM DFe over the course of the eruption (Achterberg et al., 2013) (Figure 4.25). Combined with this were direct measurements of highly elevated DFe concentrations (10.2 nM) directly under the plume (Achterberg et al., 2013). The low residual nitrate concentrations observed within the Iceland basin during summer may be the direct result of this volcanic eruption, but other causes of this interannual variability cannot be excluded.

Grow-out bioassay incubation experiments (Figures 4.6, 4.8 and 4.10) demonstrated the development of iron limitation of the *in situ* phytoplankton population in the Central and

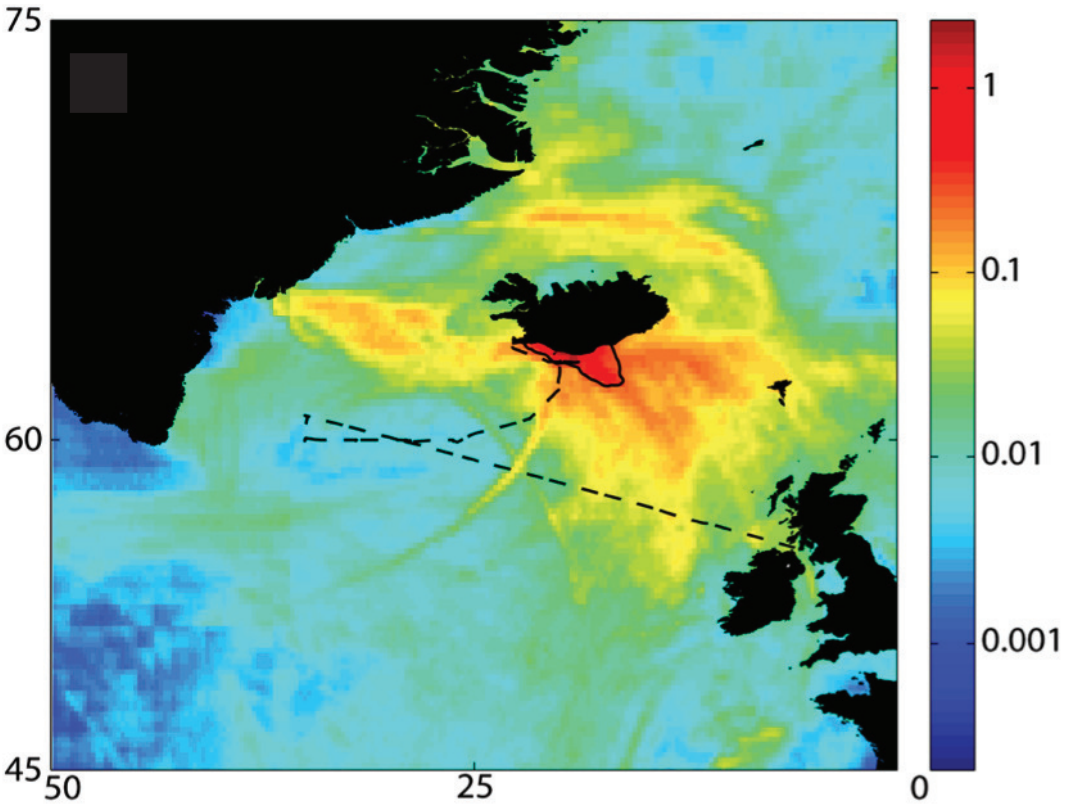

FIGURE 4.25: Modelled DFe enhancement (nM) as result of ash deposition (15th April to 23rd May) using midrange estimates of salt layer thickness (20 nm) of volcanic particles as obtained through leaching experiments (Achterberg et al., 2013). Black contour marks 0.2 nM DFe enhancement. The dashed line is the cruse track of D350.

Western Irminger Basin from spring to summer, but evidence of an iron and nitrate co-limited system in the Iceland Basin by summer (Figure 4.10). Size-fractionated analysis of the phytoplankton community *in situ* and during bioassay experiments suggested that, the larger size fraction (>5 μm) was experiencing greater iron stress and consequently responded more strongly to iron addition (Figure 4.15). Such observations are consistent with the similar responses found during an *in situ* iron release in HNLC systems (Kolber et al., 1994) and suggest that smaller cells might be less susceptible to iron stress when availability is low (Cullen, 1991; Price et al., 1994). Community-level characteristics of iron stress development within the HLNA spring bloom thus appear consistent with the hypothesis that iron limitation develops principally through broadly increasing levels of stress for larger cell sizes (de Baar et al., 2005; Hudson and Morel, 1990; Sunda and Huntsman, 1997). Subsequent iron limitation of macronutrient drawdown may then represent a combined effect of grazer control of the small-celled populations, combined with restrictions on the growth rates of the larger, less heavily grazed cells, resulting from low iron availability (Cullen, 1991; Price et al., 1994; Sunda and Huntsman, 1997).

The absolute changes in fluorescence showed overall a consistent pattern within the incubation experiments. An increase in F_v/F_m was generally accompanied by a decrease in F_o Chl^{-1} and F_m Chl^{-1}, with relatively small changes in F_v Chl^{-1}. These changes were most prevalent within experiments that were conducted in the Irminger basin (Figure4.19). One suggested reason for this depression of F_v/F_m is the presence of disconnected light-harvesting complexes (LHCs) which act to elevate F_o (Benesova et al., 2000; Berera et al., 2009; Davey and Geider, 2001; Desquilbet et al., 2003; Greene et al., 1992; Guikema and Sherman, 1983; Lin et al., 2001; Morales et al., 2001; Moseley et al., 2002; Price, 2005; Riethman and Sherman, 1988; Vassiliev et al., 1995). Indeed, these responses are found across several different phytoplankton strains (Desquilbet et al., 2003; Greene et al., 1991; Moseley et al., 2002; Petroutsos et al., 2009; Varsano et al., 2003) when grown into iron limitation, and has been found in low iron waters in the field. Behrenfeld et al. (2006) suggested that in the equatorial Pacific, a known HNLC region, depressed values of F_v/F_m could be explained by elevated F_o levels. This study also demonstrated that if you further enrich the community with nitrate then you can elevate F_o even further and depress F_v/F_m, and this same response was found within the iron and nitrate experiments conducted here (Figure 4.18). The results presented here along with other studies (Behrenfeld et al., 2006; Schrader et al., 2011) demonstrate a regulatory role for nitrate in iron-stress thylakoid restructuring and photophysiological responses. Indeed the role of chlorophyll-binding-proteins, such as IsiA, have demonstrated a capacity for over expression when grown into severe iron limitation (Ryan-Keogh et al., 2012) (Figure 3.10a and c). Yet, an elevated F_o signal is not definitive evidence of the presence of disconnected light-harvesting complexes.

Short duration iron-addition experiments conducted over the growing season enabled the mapping of the spatial/temporal extent of iron-stress throughout the HLNA using the derived variable $\Delta(F_v/F_m)_{\,+\,0.2\text{ Fe or }+\,2.0\text{ Fe}}$ (Figures 4.21 and 4.23). Moreover, the value of $\Delta(F_v/F_m)_{\,+\,2.0\text{ Fe}}$ was well correlated with observed differences in net growth rates inferred from chlorophyll accumulation following iron addition in the longer term grow-out experiments (Figure 4.22a). Such an empirical relationship between $\Delta(F_v/F_m)$ + 2.0 Fe and $\Delta\mu^{Chl}$ should not be taken to infer any universal relationship between the absolute value of F_v/F_m and phytoplankton growth rates (Kruskopf and Flynn, 2006; Parkhill et al., 2001; Price, 2005). For example, high values of F_v/F_m have been observed under steady-state iron or nitrogen limitation in culture (Parkhill et al., 2001; Price,

2005) and nitrogen (iron) (co-)limitation *in situ* (Behrenfeld et al., 2006). However, the observed correlation between these two independent measures of the relative level of iron stress within the studied natural communities studied provided empirical evidence that physiological iron stress, as indicated by the short-term response of a biomass-independent measure of phytoplankton physiology (F_v/F_m) was likely accompanied by a significant repression of phytoplankton community growth rates (Figure 4.22).

Placing the experimental results within the seasonal cycle resolved using satellite derived bloom timing alongside the *in situ* chlorophyll and DIN concentrations (Figure 4.26), the four broad stages representing pre-bloom (A), bloom (B), post-bloom high DIN (C), and post-bloom low DIN (D) conditions (as defined in Figure 4.5) could be related to differing levels of iron stress (Figure 4.26). Low levels of iron stress (inferred from measurements of $\Delta(F_v/F_m)$ (Figures 4.26a-e) and $\Delta\mu^{Chl}$ (Figure 4.26f) were observed under pre-bloom conditions (e.g. spring in the Central Irminger Basin), when chlorophyll was low (Figure 4.26e), DIN (Figure 4.26a), Phosphate (Figure 4.26b) and Silicate (Figure 4.26c) were all high and *in situ* F_v/F_m was high (Figure 4.4c). Low levels of iron stress were also observed under post-bloom conditions (summer in Iceland Basin) when chlorophyll was low, DIN, Phosphate and Silicate were depleted and *in situ* F_v/F_m was intermediate (Figure 4.4d), with long-term grow-out experiments indicating a condition approximating Fe and N co-limitation in this system (Figure 4.10a, b). Between these two conditions, higher levels of iron stress coincided with the peak of the bloom (Figure 4.26e), while the highest levels were observed under post-bloom high macronutrient conditions (Figures 4.26a-c), coincident with the lowest *in situ* values of F_v/F_m (Figure 4.4d). In 2010 such conditions prevailed during summer in the Western side of the Irminger Basin and the Rockall region (Figure 4.5b).

Resource availability and loss terms are both crucial determinants of net community growth and hence ultimately biomass accumulation and/or (macro-) nutrient removal (Banse, 1991, 2002; Frost, 1991). Although significant levels of iron stress developed within the HLNA during the peak of the phytoplankton bloom, nitrate removal appeared to continue beyond this stage in some regions (Figure 4.26a), indicating that the community retained a capacity for net growth (Figure 4.26f). Consequently, although physiological iron stress appears to develop at some stage in the bloom cycle throughout the HLNA (Figures 4.23, 4.24 and 4.26) and is likely linked to restriction of net community growth rates (Figure 4.22a), with $\mu^{Chl,\ net}$ up to 0.3 d^{-1} higher following

the addition of iron (Figure 4.26f), the development of iron stress may not necessarily correspond to an ultimate restriction on overall biomass and nutrient drawdown, i.e., Liebig-type limitation (Cullen, 1991), in all cases. Indeed, continued net community phytoplankton growth and nutrient drawdown beyond the point where some degree of iron stress develops, only requires that any suppression of growth still leaves the gross rate higher than the combined loss terms including, e.g., grazing (Walsh, 1976), sinking (Walsby and Reynolds, 1980) and viral lysis (Bratbak et al., 1993).

Although loss rates within long-term grow-out experiments will likely differ from *in situ* values (Banse, 1991), mortality might be expected to be reasonably consistent between controls and nutrient amended treatments, at least over short timescales. Excepting when resources are limited *in situ*, as the loss rates could be even greater within these conditions. Recognising the additional caveats involved in inferring net phytoplankton growth rates from chlorophyll accumulation, due to increases in cellular chlorophyll following relief of iron stress (Geider and La Roche, 1994; Greene et al., 1991; Moore et al., 2007), the calculated values of $\Delta\mu^{\mathrm{Chl}}$ (Figure 4.22a) potentially provide an upper bound on the level of iron limitation of phytoplankton growth rates (Figure 4.26f). Maximal phytoplankton growth rates at the in situ temperatures (6-14°C) would likely lie in the range from 1-2 d^{-1} (Eppley, 1972). However, loss terms will be significant *in situ* (Banse, 2002) and maximal net community growth rates within the bloom are typically <0.1 d^{-1} (Behrenfeld, 2010). Consequently, levels of growth rate iron limitation (Blackman, 1905) approaching 0.3 d^{-1}, as were suggested by our long-term experiments (Figures 4.8, 4.10, 4.22a), would not only be sufficient to significantly influence bloom dynamics, but could also potentially act to terminate the bloom before complete macronutrient removal under some circumstances (Figures 4.5b and 4.26). Such a scenario is entirely consistent with the apparent level of physiological iron stress (Figures 4.8, 4.10, 4.15) and hence potential growth rate limitation (Figure 4.22), being highest under those post-bloom conditions where macronutrients remain elevated (Figure 4.26).

The observations of near complete nitrate drawdown in the Iceland Basin (Figure 4.5b), in marked contrast to previous observations (Nielsdóttir et al., 2009), alongside incomplete removal of nitrate in the Western Irminger Basin and Rockall regions in the same growing season (Figure 4.5b), provide some indication of how finely poised the HLNA system may be between having sufficient or insufficient iron to drive complete macronutrient drawdown. It can be speculated that variability in the overall supply ratios of

iron and macronutrients (Nielsdóttir et al., 2009), combined with shifts in community composition between large cells experiencing greater iron stress and smaller cells experiencing lower iron stress (Figure 4.22) may both interact with group specific variability in grazing mortality and other loss terms (Cullen, 1991; Price et al., 1994) to dictate whether complete surface macronutrient removal occurs over the annual cycle.

The following conceptual model is proposed for the influence of iron availability on the bloom dynamics of the HLNA (Figure 4.26f). Low chlorophyll (Figure 4.4a), high DIN (Figure 4.5a), high F_v/F_m (Figure 4.4c) and a low $\Delta(F_v/F_m)_{\ +0.2\ Fe\ and\ +2.0\ Fe}$ (Figure 4.23a, c) characterize the winter or pre-bloom condition (labeled A in Figures 4.4a and 4.26), likely representing a nutrient replete, and possibly light-limited, system. As light limitation (Chiswell, 2011; Sverdrup, 1953) and/or grazing pressure (Behrenfeld, 2010) is reduced, a bloom is initiated. Macronutrients are then consumed as the bloom develops (Figures 4.26a-c, labeled B Figure 4.4), however restricted iron (bio-) availability in the HLNA results in the development of iron stress during the bloom. Ecosystem dynamics (Banse, 2002; Cullen, 1991; Price et al., 1994) interacting with group-specific susceptibility to iron stress (Figure 4.22) may then combine with variable iron supply either inter-annually, inter-basin or intra-basin (Figures 4.23 and 4.24) to dictate whether the macronutrients (e.g., DIN) are completely removed (Figures 4.5b, 4.26a and 4.26f). Consequently, the post-bloom condition either tends towards complete nitrate removal (labeled D in Figure 4.4) and a N-limited or Fe and N co-limited system (Figure 4.10), as observed in the Iceland Basin during 2010, or incomplete nitrate removal (labeled C in Figure 4.4) and a Fe-limited system, as observed in the same basin in 2007 (Nielsdóttir et al., 2009) and in the Western Irminger Basin and Rockall region in 2010 (Figure 4.8).

The current study represents the first extensive spatial and temporal mapping of the degree of iron stress in a large oceanic region using rapid experimentally induced changes in photophysiology ($\Delta(F_v/F_m)$) placed in the context of the seasonal cycle. The results suggest that the development of iron stress in the HLNA is closely linked to the accumulation of phytoplankton biomass and hence presumably increasing iron requirements, alongside the tendency for cumulative whole community uptake to reduce iron availability. Consequently, in this system, the seasonal progression of the bloom appears to be a crucial control on the development of iron stress, which then plays a significant role in dictating overall macronutrient drawdown. Observed regional contrasts in the degree of iron stress were hence at least partially dictated by variability

in the temporal development of the bloom. The North Atlantic clearly differs from the other high-latitude oceanic regions, where a lack of iron contributes to restricted major macronutrient removal, resulting in the HNLC condition. However, even in the highly productive HLNA system, iron availability appears to influence the overall extent of macronutrient removal and hence ultimately both the local strength and efficiency of the biological carbon pump.

This chapter has provided evidence that the observed depression of F_v/F_m within iron-limited regions is due to an increase in F_o. It can be hypothesised that the cause of this increased signal is the expression of chlorophyll-binding proteins, in the same manner as IsiA in *Synechocystis* sp. PCC 6803. This potential pool of chlorophyll-binding proteins could dominate the chlorophyll signal within the HLNA, yet this cannot be determined with the current data available. One such way in which this theory can be tested is by measuring the ratio of photosynthetic proteins to total chlorophyll. A high chlorophyll to photosynthetic protein ratio would be indicative of a iron limited phytoplankton community, whereas a low chlorophyll to protein ratio would be indicative of an iron replete community. The Ross Sea, a known iron limited region, has a unique taxonomic community with which to study the potential shifts in protein ratios.

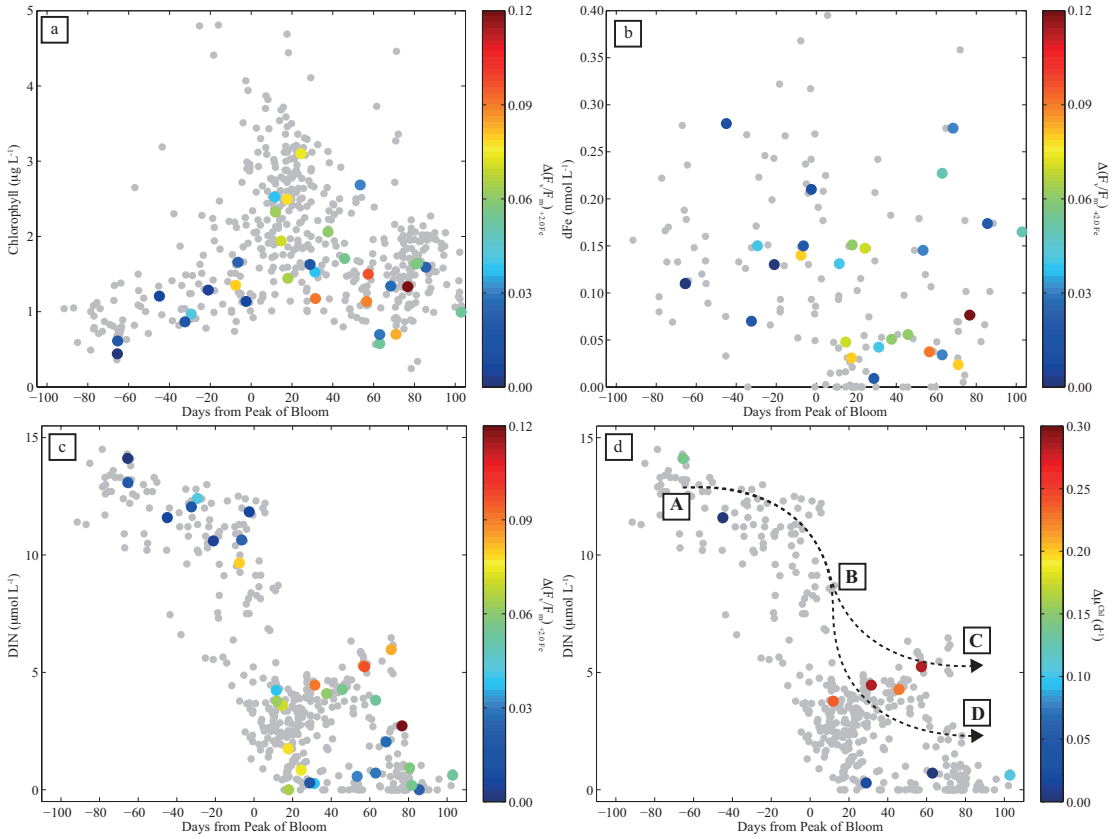

FIGURE 4.26: (a) In situ DIN (μmol L^{-1}) data and relative degree of Fe stress ($\Delta(F_v/F_m)_{+\ 2.0\ Fe}$), (b) in situ dFe (nmol L^{-1}) and $\Delta(F_v/F_m)_{+\ 2.0\ Fe}$, (c) in situ chlorophyll (μg L^{-1}) and $\Delta(F_v/F_m)_{+\ 2.0\ Fe}$ and (d) in situ DIN (μmol L^{-1}) and net chlorophyll growth rate ($\Delta\mu^{Chl}$ (d^{-1})) relative to time of peak of bloom. Superimposed on (d) is a conceptualised model of bloom dynamics, demonstrating two different post-bloom scenarios (low DIN and high DIN) associated with different degrees of Fe stress and iron limited growth rates. Bloom timing as indicated in Figure 4.3, with regions associated with different conditions defined as in Figure 4.4.

Chapter 5

The Ross Sea - Processes Regulating Iron Supply on the Mesoscale

5.1 The Ross Sea

The Ross Sea is the most productive region in the entire Southern Ocean (Arrigo and van Dijken, 2004; Arrigo et al., 1998; Peloquin and Smith, 2007; Smith and Gordon, 1997), with annual productivity estimates that exceed 200 g C m^{-2} (Smith et al., 2006). The continental shelf in this region has an average depth of around 600m, with four central banks that shoal to depths ∼300 m (Figure 5.1). A persistent polynya opens from the southern Ross Sea in early spring, reaching an average area of ∼400,000 km^2 by late summer (Arrigo and van Dijken, 2003; Reddy et al., 2007). This polynya hosts large seasonal phytoplankton blooms, which are typically dominated by colonial *Phaeocystis antarctica* in spring through early summer (November-December), with an increasing abundance of diatoms in mid- to late summer (Arrigo and van Dijken, 2004; Arrigo et al., 1998; Bunt and Wood, 1963; Comiso et al., 1993; DiTullio and Smith, 1996; Elsayed et al., 1983; Goffart et al., 2000; Smith and Gordon, 1997; Smith et al., 2000).

The bloom is initiated in late October (Arrigo et al., 1998; Smith and Gordon, 1997), with peaks in algal biomass and production in late December (Smith et al., 2000). A significant fraction of annual production can occur in January and early February, when

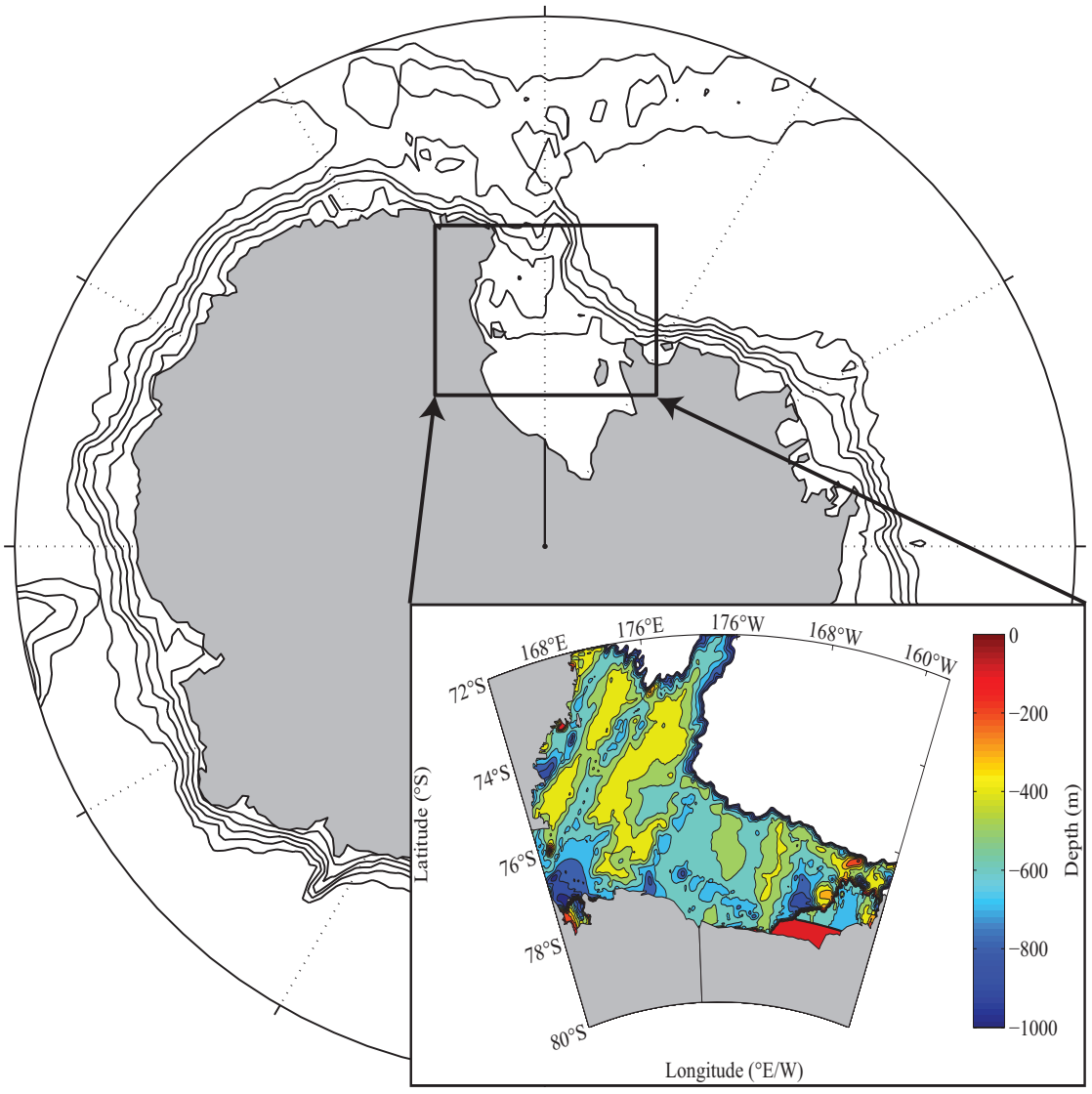

FIGURE 5.1: Map of Antarctica and the Southern Ocean, with inset map of the Ross Sea to denote study area. Ross Sea map includes bathymetry and 100 m isobaths.

much of the southern Ross Sea is typically ice free (Arrigo and van Dijken, 2003, 2004; Peloquin and Smith, 2007; Smith et al., 2006, 2000). Arrigo et al. (2008) (Figure 5.2) estimated through modelling that the Ross Sea continental shelf accounts for a net air-sea CO_2 that can be ∼27% of the estimated total Southern Ocean CO_2 sink, an estimate that does not include the Antarctic continental margins. An understanding of the controls on net primary productivity is needed to quantify this potentially important CO_2 sink, given the particular importance of Southern Ocean phytoplankton mediating changes in atmospheric carbon dioxide concentrations over glacial-interglacial timescales (Brovkin et al., 2007; Kohfeld et al., 2005; Kumar et al., 1995; Martin et al., 1990; Sigman and Boyle, 2000; Watson and Liss, 1998). Moreover the potential future changes

in the Southern Ocean as a result of climate change, due to changes in stratification, sea-ice cover and atmospheric dust inputs (Boyd and Doney, 2002; Boyd et al., 2008; Mahowald and Luo, 2003; Sarmiento et al., 2004, 1998; Tagliabue et al., 2008), highlight the importance of understanding the connections between environmental forcing and phytoplankton dynamics.

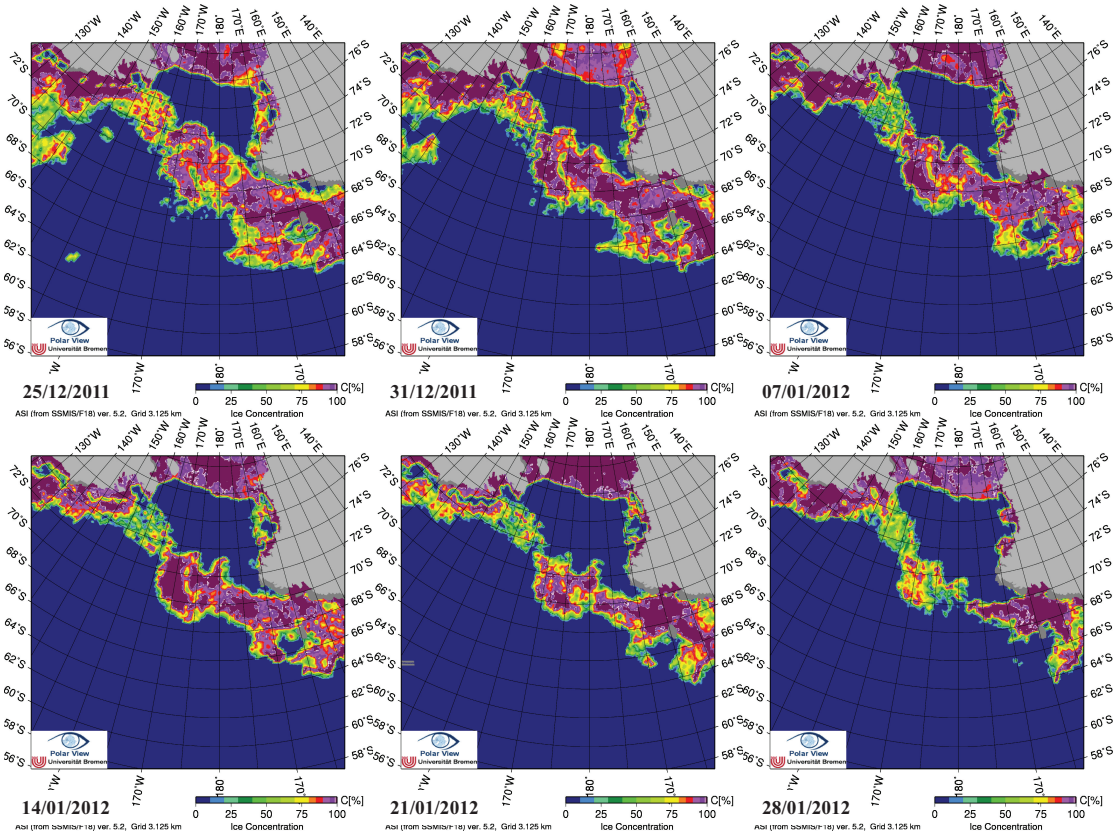

FIGURE 5.2: Mean sea ice concentrations for the Ross Sea from from 25/12/2011 to 28/01/2012. Data accessed from (iup, 2013).

Mesoscale processes, including currents, fronts and eddies, in the Ross Sea are relatively unknown, excepting a study by Hales and Takahashi (2004) which observed significant variability at length scales on the order of 10 km or less in nearly all the quantities measured. The mechanisms responsible for generating this patchiness thus far are unknown, yet it can be assumed the expression of these processes would be analogous to those in other ocean regions. The effect of these mesoscales processes on biogeochemical cycling in other ocean regions, including the net transport of nutrients into the euphotic zone, has been well documented (Angel and Fasham, 1983; Falkowski et al., 1991; McGillicuddy et al., 2003; Oschlies, 2002; Oschlies and Garcon, 1998; Tranter et al., 1980; Venrick, 1990; Williams and Follows, 2003). It is possible that fronts and eddies in the Ross Sea may provide a vertical supply of nutrients to the surface, but they may

also provide horizontal transport from shallow coastal areas similar to that of the Haida Eddies in the Gulf of Alaska (Johnson et al., 2005). Another mesoscale process that may be of importance in the Ross Sea is the mechanism by which the circumpolar deep water (CDW) mixes vertically after intrusion onto the continental shelf. Surface waters in the west Antarctica Peninsular provide evidence of a modified CDW (MCDW), with mixing of CDW with a fresher and cooler version of CDW (Hoffman and Klinck, 1998; Peloquin and Smith, 2007). Preliminary modelling results suggest that the flow of MCDW onto the shelf takes place on the western side of the Ross Sea (Dinniman et al., 2003).

The dissolved iron concentrations in surface waters of the Ross Sea display significant horizontal gradients (Sedwick et al., 2011), with values ranging from less than 0.1 nM up to 0.3 nM, which are suggested to be limiting and sufficient for algal growth respectively (Garcia et al., 2009; Sedwick et al., 2007b, 2011; Timmermans et al., 2001, 2004). Localised inputs of dissolved iron from melting sea ice, biological uptake and inputs from other sources, including shelf sediments and mesoscale processes, are likely responsible for these horizontal variations. The other sources include CDW, which has been proposed as a potential source of iron to surface waters (Dinniman et al., 2003; Prézelin et al., 2000, 2004; Sambrotto et al., 2003). The CDW may be enriched in dissolved iron relative to the surface waters or it may also mobilise sedimentary iron from the shelf (Boye et al., 2001; Sohrin et al., 2000). Along the ice shelf in the Ross Sea, intrusions of Ice Shelf Water (ISW) from several areas under the ice shelf (Jacobs et al., 1970; Smethie and Jacobs, 2005) may potentially carry iron derived from the glacial ice and sub-glacial debris (Fitzwater et al., 2000). Combining modelling studies, *in situ* measurements of dissolved iron and assimilation ratios of C:Fe for phytoplankton, may yield the relative contribution of each source to the total annual net primary production for the Ross Sea.

Irradiance and dissolved iron are assumed to be the major controls on phytoplankton productivity in the Ross Sea, given the lack of significant macronutrient removal and low microzooplankton grazing pressure (Arrigo and van Dijken, 2003; Arrigo et al., 1998; Caron et al., 2000; Coale et al., 2003; Fitzwater et al., 2000; Sedwick et al., 2000, 2007b; Smith et al., 2000, 2003; Tagliabue and Arrigo, 2003). Evidence for the role of iron in limiting phytoplankton growth in the Ross Sea is from both shipboard iron addition experiments (Bertrand et al., 2007; Coale et al., 2003; Cochlan et al., 2002; Martin et al., 1990; Olson et al., 2000; Sedwick and DiTullio, 1997; Sedwick et al., 2000) and measurements of low dissolved iron (<0.2 nM) in surface waters during summer

(Coale et al., 2005; Fitzwater et al., 2000; Martin et al., 1991; Sedwick and DiTullio, 1997; Sedwick et al., 2000). Iron concentrations in the Ross Sea likely follows a seasonal pattern of elevated concentrations during spring, due to vertical re-supply by winter mixing, and depleted concentrations in the summer due to biological uptake. Elevated Silicate/Nitrate drawdown ratios (Arrigo et al., 2000; Smith et al., 2006) and high levels of flavodoxin (Maucher and DiTullio, 2003) also imply that iron availability limits phytoplankton growth in the Ross Sea during summer. However, this depletion in the summer may be moderated by episodic inputs from melting sea ice around the perimeter of the polynya (Arrigo and van Dijken, 2003; Coale et al., 2005; Sedwick et al., 2000), which is also suggested to increase growth through stratification (Smith and Nelson, 1985). Sedwick et al. (2011) have also suggested that the pattern of seasonal iron concentrations may vary significantly from year to year, with potentially limiting iron concentrations (<0.2 nM) as early as November.

The Ross Sea is characterised by taxonomic heterogeneity, with the phytoplankton assemblages having distinctly different compositions in two different regions, *P. antarctica* in the Southern Ross Sea and diatoms along the coast and near ice edges (Arrigo et al., 1999; DiTullio and Smith, 1996; Smith and Asper, 2001). There is also a well defined seasonal succession between the two groups, with *P. antarctica* dominant in spring with increasing abundances of diatoms in summer (Arrigo and van Dijken, 2004; Arrigo et al., 1998; Bunt and Wood, 1963; Comiso et al., 1993; DiTullio and Smith, 1996; Elsayed et al., 1983; Goffart et al., 2000; Smith and Gordon, 1997; Smith et al., 2000). This seasonal succession may be the result of a tendency for *P. antarctica* to dominate in waters with a deeper mixed layer, whereas diatoms dominated in waters with shallower mixed layers (Arrigo et al., 1999; Smith and Asper, 2001). Preferentially inhabiting different depths was originally thought to be driven by the efficiency of light harvesting complexes, however van Hilst and Smith (2002) found no differences in photosynthetic responses between diatoms and colonial *P. antarctica*. Instead it is now believed that this characteristic variability of the Ross Sea is driven by complex interactions of vertical mixing processes and iron limitation. *P. antarctica* has been suggested to have a higher iron quotient when compared to diatoms (Coale et al., 2003; Sedwick et al., 2007b; Strzepek et al., 2012) and, in the late summer, dissolved iron concentrations may potentially be limiting. Regardless of the mechanism, the distribution patterns of different phytoplankton assemblages has profound biogeochemical consequences on vertical

flux and elemental ratios of biogenic material (Arrigo et al., 1999; DeMaster et al., 1992; Smith and Dunbar, 1998).

Beyond the available evidence (Bertrand et al., 2007; Coale et al., 2003; Cochlan et al., 2002; Martin et al., 1990; Olson et al., 2000; Sedwick and DiTullio, 1997; Sedwick et al., 2000), the short-term physiological response and the abundance of photosynthetic proteins in the Ross Sea remain poorly constrained, particularly in reference to the seasonal progression of the community composition. In this chapter, the changes in phytoplankton standing stocks and photophysiology were assessed in both 168 h grow-out experiments and high spatial resolution short-term (24-48 h) incubations in order to investigate the response of natural phytoplankton populations to the relief of potential iron stress. Protein samples were collected and quantitatively assessed for photosynthetic protein abundance.

The current study thus aimed to investigate both regional and mesoscale sources of iron to the Ross Sea and to establish the spatial and temporal phytoplankton response to relief from iron limitation, in combination with the quantification of key photosynthetic proteins. By combining *in vitro* incubation experiments with *in situ* physiological data, protein concentrations, chlorophyll and macronutrients the differential response of physiological iron stress were elucidated. The variety of different sources of iron to the Ross Sea, and subsequent fluxes, should produce different responses to iron limitation. However, as most of these sources have not yet been studied in great detail it is difficult to hypothesise which may display a greater degree of iron limitation. One further objective of this study was to determine whether the different taxonomic assemblages of the Ross Sea would have different responses to relief from iron limitation. Based upon the different ecological niches the assemblages occupy, *P. antarctica* at depth and diatoms in the surface, it would be expected that the diatoms would exhibit a greater response to relief from iron limitation. By combining the bulk experimental responses with the taxonomic responses, it can be determined whether the same photophysiological response exhibited in both *Synechocystis* sp. PCC 6803 and the HLNA is present in the Ross Sea.

5.2 Results

5.2.1 General Oceanography

In situ chlorophyll concentrations peaked close to the ice shelf (Figure 5.3a), with a maximum value recorded in the Western Ross Sea surface waters of 24.59 μg L^{-1}. In general the offshore waters had the lowest concentrations recorded in the surface water throughout the study at 0.22 μg L^{-1}. The F_v/F_m displayed an inverse relationship to this (Figure 5.3b), with the highest values measured in the offshore waters (> 0.35); however there was a high degree of variability throughout the Ross Sea. In contrast to this, σ_{PSII} showed a band of high values along the Ross Ice shelf (Figure 5.3c), which ranged from 2.20 - 2.70 nm^{-2}. The lowest values, ~1.4 nm^{-2}, followed the same pattern as the chlorophyll concentrations and were found in the offshore waters. Alongside these patterns in chlorophyll, F_v/F_m and σ_{PSII} there were marked differences in the macronutrient concentrations across the Ross Sea (Figure 5.4). High values of DIN (μmol L^{-1}) (Figure 5.4a) and phosphate (μmol L^{-1}) (Figure 5.4b) were both found in the offshore waters. Mid-range values of DIN (~20 μmol L^{-1}) and phosphate (~1.2 μmol L^{-1}) were found along the Ross Ice shelf. The Silicate concentrations (μmol L^{-1}) displayed a different pattern (Figure 5.4c), with the offshore concentrations and the measurements close to the Ross Ice shelf falling within the same range (40 - 55 μmol L^{-1}). All three macronutrients had the lowest concentrations measured in the Western Ross Sea where chlorophyll concentrations were high, F_v/F_m was low and σ_{PSII} was high. Dissolved iron (dFe) concentrations did not display any marked variability across the Ross Sea with average concentrations of ~0.2 nmol L^{-1} (Figure 5.4d), excepting two stations which peaked at around 0.7 and 0.8 nmol L^{-1} in the Western Ross Sea.

5.2.2 Long-term (>24 h) incubation experiments

Data from three long-term (168 h) experiments, established in different regions across the Ross Sea (Figure 2.2), indicated variable responses to iron addition to the extant phytoplankton communities (For initial conditions and raw data please refer to Appendix C). Within an anticyclonic (downwelling) eddy, an experiment provided evidence that the in situ phytoplankton community were potentially iron limited (Figure 5.5a). Both F_v/F_m and chlorophyll concentrations were higher under the iron addition treatment,

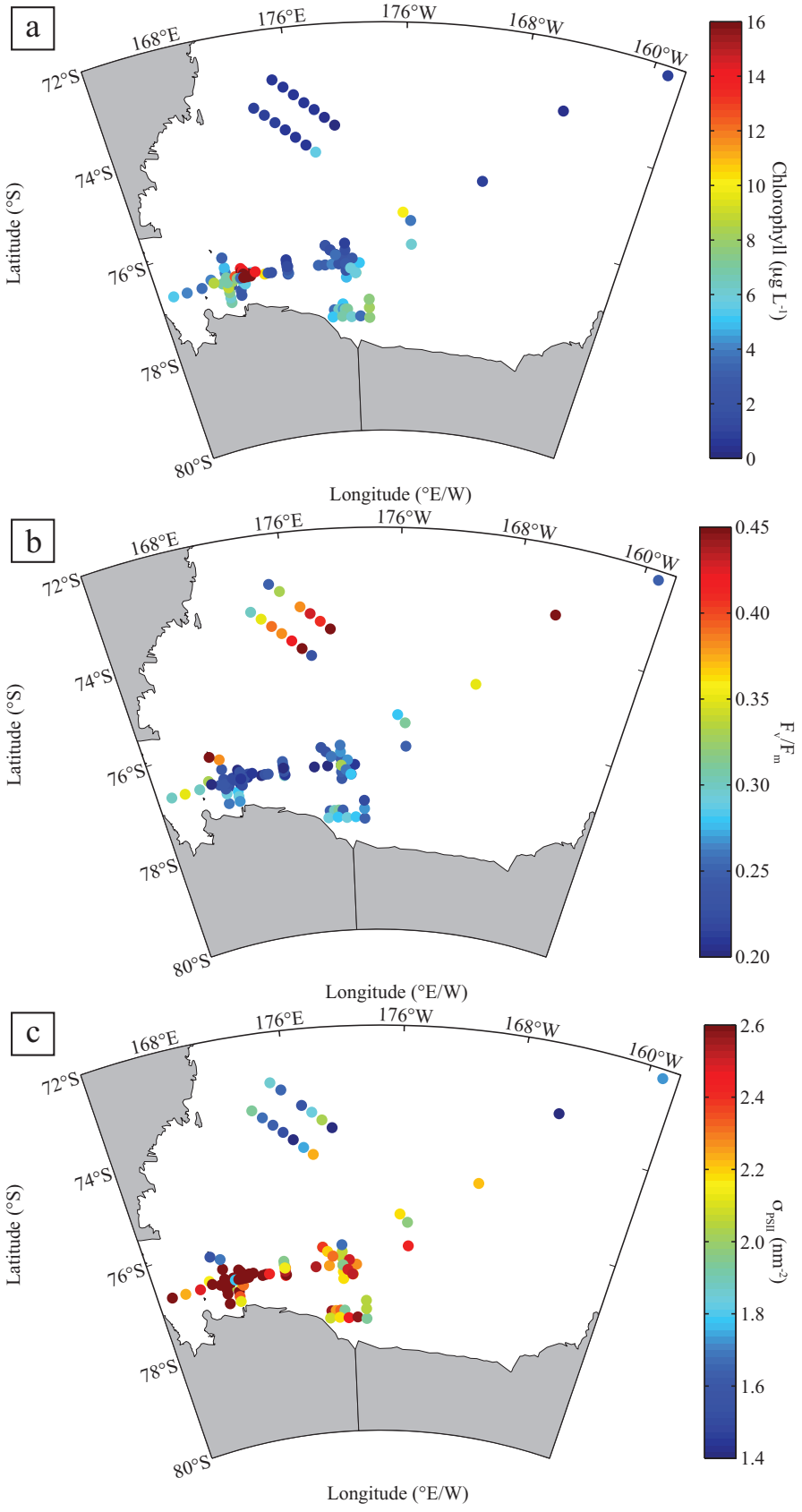

FIGURE 5.3: (a) Sea surface chlorophyll concentrations (μg L^{-1}), (b) F_v/F_m values and (c) σ_{PSII} (nm^{-2}) values from the Ross Sea.

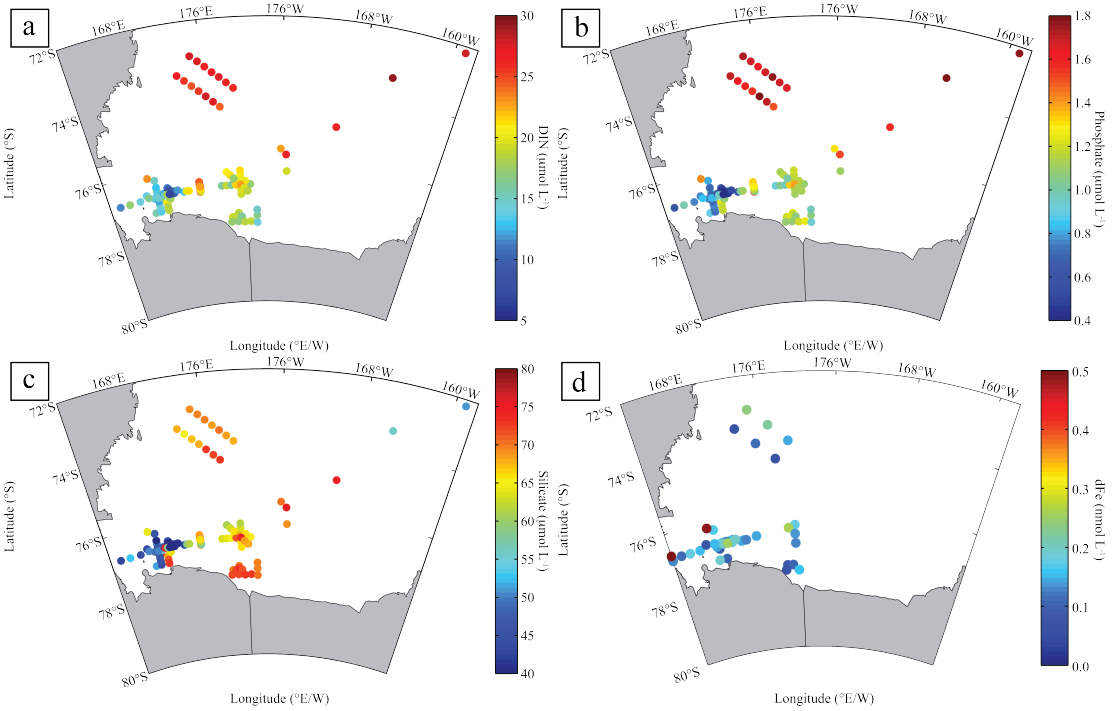

FIGURE 5.4: (a) Sea surface DIN concentrations (μmol L^{-1}), (b) Phosphate concentrations (μmol L^{-1}), (c) Silicate concentrations (μmol L^{-1}) and (d) dissolved Iron concentrations (nmol L^{-1}) values from the Ross Sea.

with significant differences from 72 h for F_v/F_m and 168 h for chlorophyll (ANOVA, $p<0.05$). Experiment 2 that was set up over the Ross Bank showed very similar responses between both treatments (Figure 5.5b), with a significant difference for both F_v/F_m and chlorophyll at the final time point (168 h) (ANOVA, $p<0.05$). Experiment 3, set up in proximity to the Ross Ice shelf (Figure 5.5c), also displayed evidence of iron limitation. Both F_v/F_m and chlorophyll were higher in the iron addition treatment, with significant differences at 72 h and 120 h respectively (ANOVA, $p<0.05$). Growth rates (Table 5.1) at the final time point (168 h) (μ^{Chl} d^{-1}) of the iron control treatments were significantly higher (t-test, $p<0.05$) in all experiments compared to the control treatments.

Nutrient drawdown within experiments were highly variable (Table 5.1), with Experiment 1 (Figure 5.6a) displaying the highest levels of nutrient drawdown with iron addition throughout all the experiments. The DIN drawdown (ΔNO_3^-) for the iron addition and the control treatments were significantly different (t-test, $p<0.05$), at 2.53±0.13 μmol L^{-1} d^{-1} and 1.61±0.34 μmol L^{-1} d^{-1}. Experiment 3 also had significant differences in ΔNO_3^- (t-test, $p<0.05$), whereas Experiment 2 had no significant differences in ΔNO_3^- (t-test, $p>0.05$). Phosphate drawdown ΔPO_4^{3-} was also significant for experiments 1 and 3 (t-test, $p<0.05$), whereas the silicate drawdown $\Delta Si(OH)_4$ for all experiments was

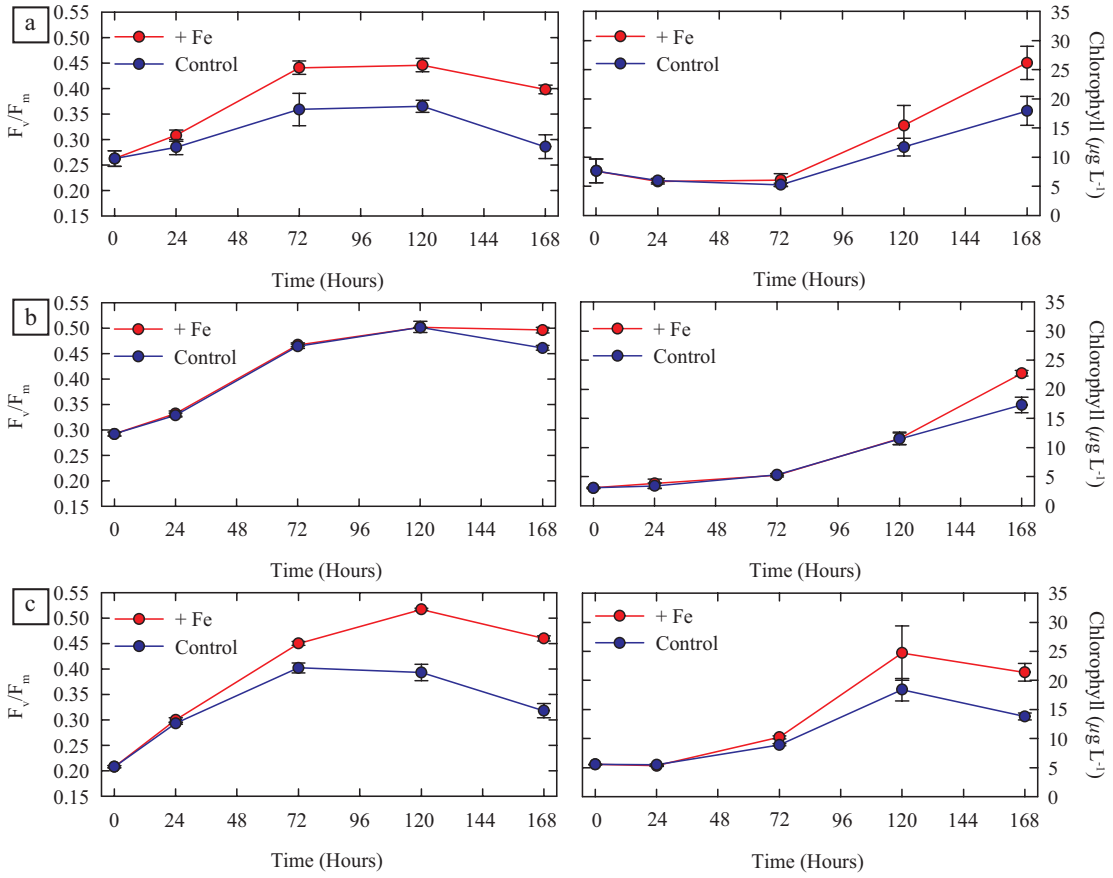

FIGURE 5.5: F_v/F_m and chlorophyll responses (μg L^{-1}) from iron addition long-term (>24 h) experiments during the PRISM cruise initiated over (a) an anti-cyclonic Eddy (Experiment 1), (b) the Ross Bank (Experiment 2) and (c) adjacent to the Ross Ice Shelf. Shown are averages with ± standard errors, where n = 3, 5, 5, 2, and 5 for time points 0, 24, 72, 120 and 168 h respectively.

not significantly different between treatments (t-test, p>0.05). This resulted in different DIN:Silicate drawdown ratios ($\Delta Si(OH)_4/\Delta NO_3^-$) for the experiments, which can be indicative of different communities preferentially growing. A $\Delta Si(OH)_4/\Delta NO_3^-$ ratio of <0.5 is indicative of a *Phaeocystis* dominated community whereas a ratio of >1.0 is indicative of a diatom dominated community (Hutchins and Bruland, 1998; Sweeney et al., 2000; Takeda, 1998). In all experiments the $\Delta Si(OH)_4/\Delta NO_3^-$ ratio for the iron treatment were lower than the control treatment, with a significant difference (t-test, p<0.05) in experiment 2.

5.2.2.1 Absolute Changes in Fluorescence

Alongside measurements of F_v/F_m, the absolute changes in F_o, F_m and F_v (normalised to chlorophyll) were calculated. Overall, by the end of the experiments F_o Chl^{-1} was

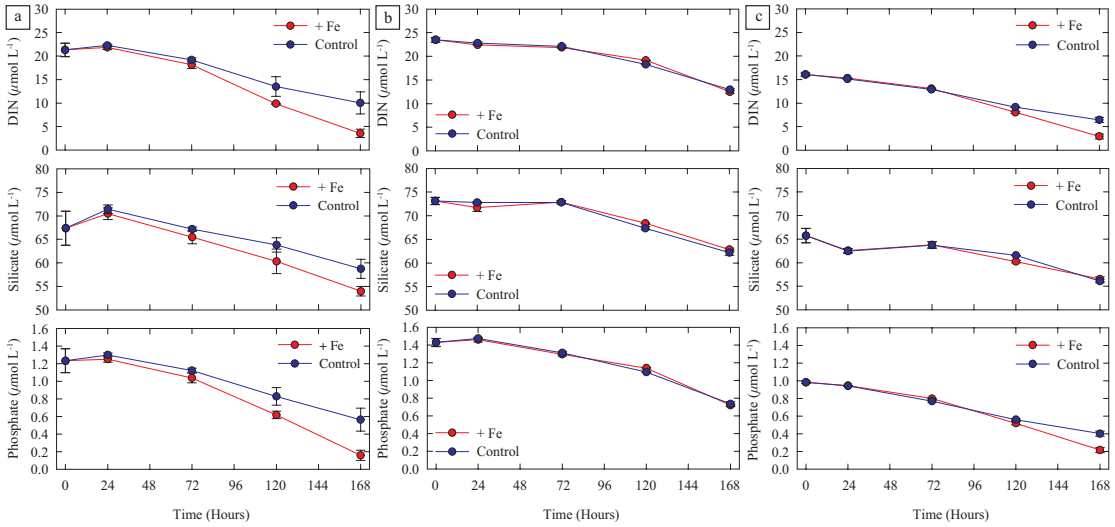

FIGURE 5.6: Nutrient drawdown responses, DIN (μmol L^{-1}), Silicate (μmol L^{-1}) and Phosphate (μmol L^{-1}), from iron addition long-term (>24 h) experiments during the PRISM cruise initiated over (a) an anti-cyclonic Eddy (Experiment 1), (b) the Ross Bank (Experiment 2) and (c) adjacent to the Ross Ice Shelf. Shown are averages with $\pm$ standard errors, where n = 3, 5, 5, 2, and 5 for time points 0, 24, 72, 120, and 168 h respectively.

TABLE 5.1: Growth Rates and Nutrient Drawdown for Long-Term Experiments.

	Experiment		
	1	2	3
+Fe μ^{Chl}	0.17±0.02	0.29±0.00	0.19±0.01
Control μ^{Chl}	0.12±0.03	0.25±0.01	0.13±0.01
+ Fe ΔNO_3^-	2.53±0.13	1.57±0.05	2.93±0.07
Control ΔNO_3^-	1.61±0.34	1.50±0.05	2.43±0.08
+ Fe $\Delta Si(OH)_4$	1.92±0.15	1.47±0.04	2.37±0.07
Control $\Delta Si(OH)_4$	1.24±0.29	1.57±0.08	2.43±0.06

generally lower when iron was added (Figure 5.7a and e). In experiments 1 and 3, where there was an iron limitation response, the difference in F_o Chl^{-1} between the iron addition and control treatment was significant (ANOVA, p<0.05) at the end timepoint (168 h). However in experiment 2, where there no iron limitation response, there was no significant difference in F_o Chl^{-1} between the treatments (t-test, p>0.05) (Figure 5.7c). F_m Chl^{-1} (not shown) followed the same pattern as F_o Chl^{-1}, with significant differences at 168 h in experiments 1 and 3 (ANOVA, p<0.05) and no significant differences in experiment 2 (ANOVA, p>0.05). F_v Chl^{-1} did not have any significant differences between treatments (ANOVA, p>0.05) across all experiments (Figure 5.7b, d and f).

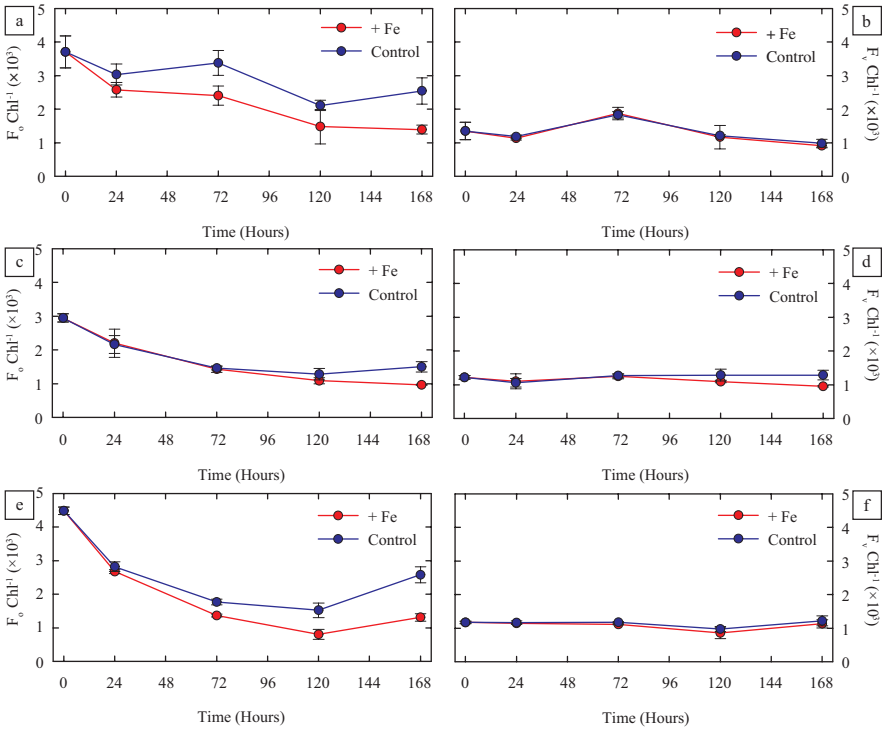

FIGURE 5.7: The absolute changes in F_o Chl^{-1} ($\times 10^3$) (a, c, e) and F_v Chl^{-1} ($\times 10^3$) (b, d, f) for Experiment 1 (a and b), Experiment 2 (c and d) and Experiment 3 (e and f).

5.2.3 Short-term incubation experiments

The 29 short-term (24-48 h) incubation experiments conducted further revealed variability across the Ross Sea; the extended incubation time was due to the colder sea surface temperatures. Significant (t-test, $p<0.05$) rapid changes in photophysiology (F_v/F_m) were often observed in these experiments, over both 24 and 48 h. These changes were significant despite no significant changes in other variables, such as chlorophyll, over the short time scale. In order to contrast these relative changes, the same approach used in the HLNA was applied to calculate the difference in F_v/F_m between the control and iron addition bottle ($\Delta(F_v/F_m)$). $\Delta(F_v/F_m)$ was calculated for both time scales (24 and 48 h), for simplicity calculated values of $\Delta(F_v/F_m)$ are hereafter subscripted '24 h' or '48 h' corresponding to the 24 h and 48 h time scales respectively. Values of $\Delta(F_v/F_m)$ were frequently positive following iron addition (Figure 5.8a and b). No clear spatial differences in $\Delta(F_v/F_m)_{24\ h}$ or $\Delta(F_v/F_m)_{48\ h}$ could be observed between the different regions of the Ross Sea, yet within this highly dynamic environment it can still be used as a relative measure of the degree of iron stress. The highest value for $\Delta(F_v/F_m)_{24\ h}$

was found in the Western Ross Sea, at 0.17±0.05, whereas the lowest value was found in near to the Ross Ice shelf at -0.03±0.02.

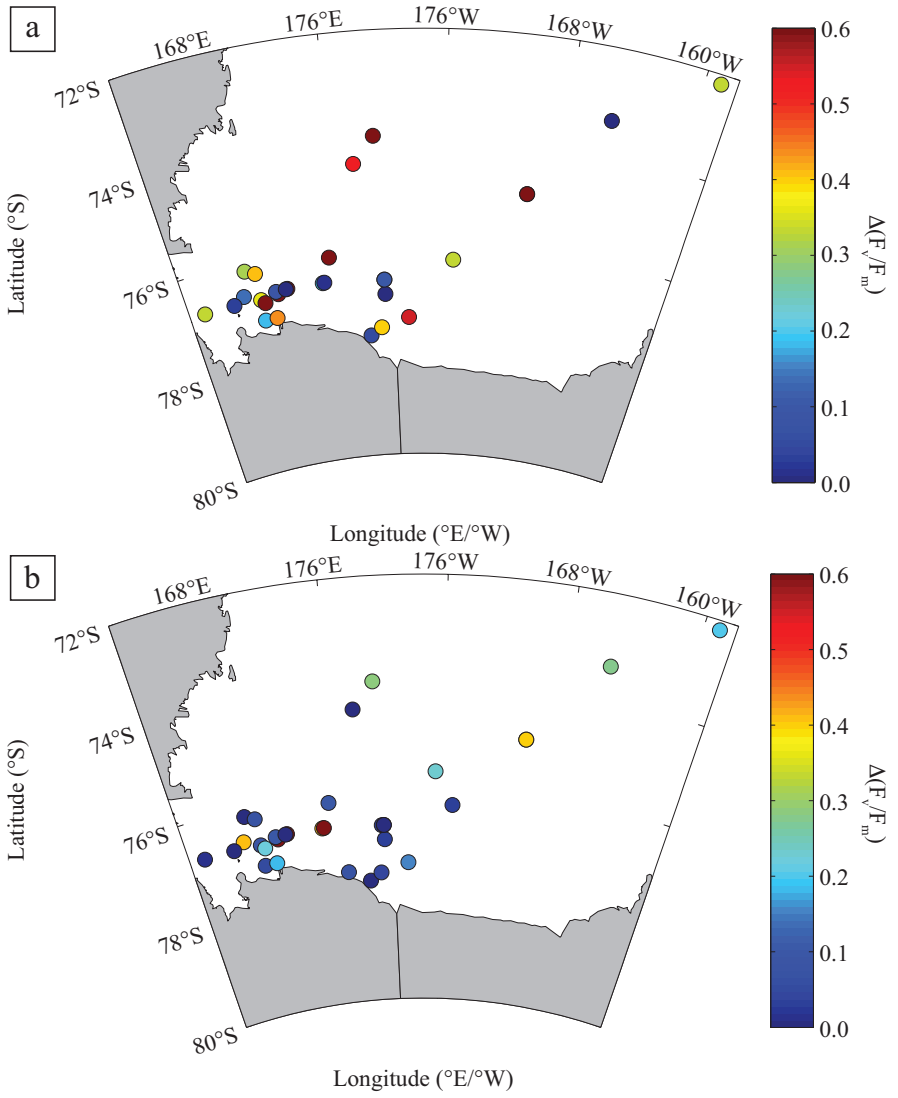

FIGURE 5.8: Experimental values of $\Delta(F_v/F_m)$ calculated after (a) 24 hr and (b) 48 h with a 2.0 nmol L^{-1} iron addition.

5.2.4 Community Composition

The relative ratio $\Delta Si(OH)_4/\Delta NO_3^-$ can be used to provide a relative indication of the phytoplankton community structure, for comparing and contrasting *P. antarctica* and diatom dominated waters (Hutchins and Bruland, 1998; Sweeney et al., 2000; Takeda, 1998). The absolute ratios of diatoms versus *P. antarctica* can be calculated by using the pigment data from HPLC (data not available) and determining whether 19'-hex and fucoxanthin are dominant. In order to calculate the $\Delta Si(OH)_4/\Delta NO_3^-$ ratio for

the short-term experiments, deep water concentrations of DIN and silicate were used as the pre-bloom or winter concentrations, and the *in situ* concentrations measured in the surface waters as the bloom/post-bloom concentrations. The difference between these values were used to calculate the relative drawdown ratios for the surface waters, which could be further interpreted into a percentage of community structure, following the ratios of Sweeney et al. (2000). Figure 5.9 shows the spatial $\Delta Si(OH)_4/\Delta NO_3^-$ ratio represented as % community composition, ranging between 100% diatoms to 100% phaeocystis. The results show some clear spatial patterns of diatom dominated versus *P. antarctica* dominated regions (Figure 5.9), with the offshore and Western Ross Sea being dominated by diatoms. The potential differences in community structure can be used to explain the variability in both sea surface variables, photophysiology and experimental results.

Alongside the clear spatial patterns, the community composition followed the expected pattern of *P. antarctica* dominating in waters with a deeper mixed layer, whereas diatoms dominated in waters with shallower mixed layers (Arrigo et al., 1999; Smith and Asper, 2001). Mixed layer depths were calculated as the depth at which the density (σ_T) changed by 0.1 from a stable surface value, stable surface values were taken from (Smith and Asper, 2000). The mixed layer depths were lowest in the eastern Ross Sea, with an average depth of ∼10 m; in the central Ross Sea the mixed layer depth was at its maximum at >80 m. The mixed layer depths were binned into 5 m intervals and the average community composition was calculated for each interval (Figure 5.11). Diatoms exhibited dominance (>90 %) in mixed layer depths of <20 m, whereas *P. antarctica* dominated in mixed layer depths of >60 m.

5.2.5 Protein Concentrations

In combination with incubation experiments, samples for quantitative protein concentrations were collected in the Ross Sea. A total of 22 stations were processed to quantitatively measure the protein targets PsaC, PsbA and RbcL which are used to infer abundances of PSI, PSII and Rubisco respectively. Unfortunately, due to low abundance in natural communities, PsaC quantification was not possible; thus only results from PsbA and RbcL will be reported. The subunits, PsbA and RbcL, were normalised

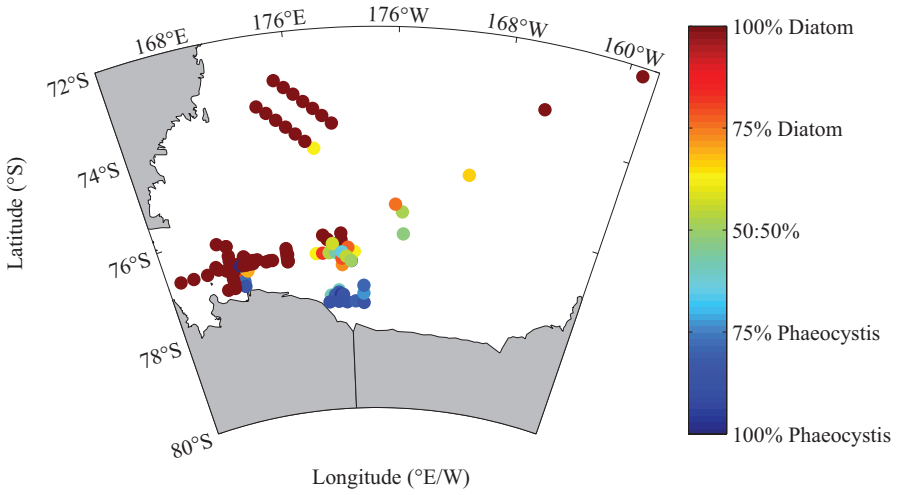

FIGURE 5.9: $\Delta Si(OH)_4/\Delta NO_3^-$ ratio represented as % community composition, ranging between 100% diatoms to 100% *Phaeocystis*.

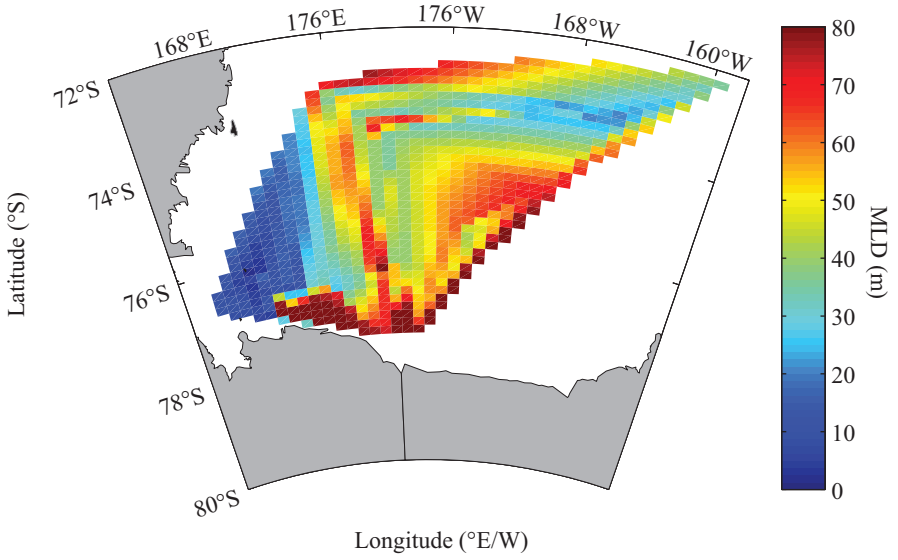

FIGURE 5.10: Mixed layer depths (m) for the Ross Sea calculated as the depth at which density (σ_T) changes by 0.1 from a stable surface value.

to both μg total protein (reflecting the abundance of target protein to the total community protein pool) and to chlorophyll (reflecting the ratio of target protein to cellular chlorophyll). Spatial distribution maps of the protein data show similar patterns between the two target proteins (Figure 5.12 and 5.13).

In general there were higher ratios of PsbA normalised to total protein (fmol μg^{-1}) (Figure 5.12a) and PsbA normalised to chlorophyll (mmol mol^{-1}) (Figure 5.12b) in the offshore region; with maximum ratios of 8.5±3.0 (fmol μg^{-1}) and 13.7±0.8 (mmol mol^{-1}). The RbcL ratios followed the same general pattern, with lower ratios in Western Ross Sea and near to the Ross ice shelf and higher ratios in the offshore region (Figure 5.13).

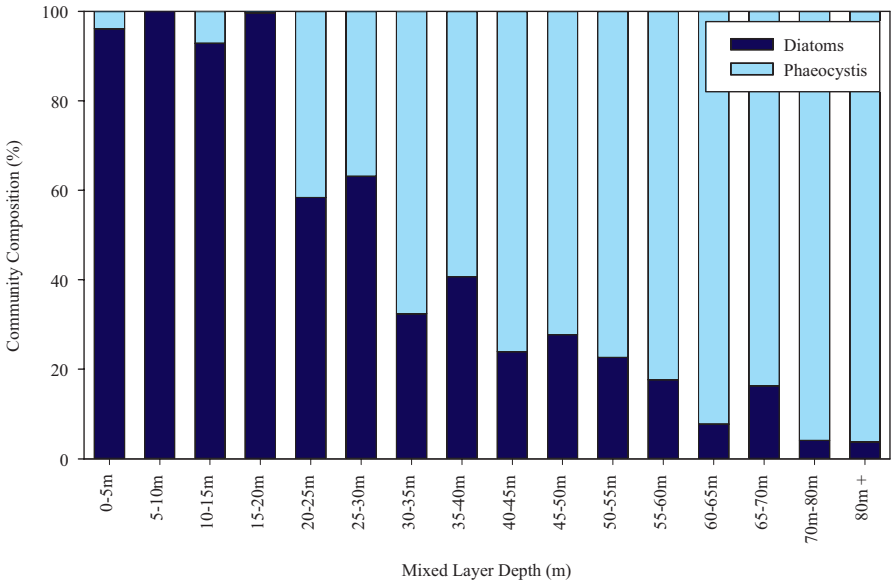

FIGURE 5.11: Average community composition (%) against mixed layer depths (m) for the Ross Sea; mIxed layer depths binned into 5 m intervals.

Maximum ratios normalised to total protein (fmol μg^{-1}) (Figure 5.13a) and chlorophyll (mmol mol^{-1}) (Figure 5.13b) in the offshore region were 260±66 and 278±72 respectively. A relationship was observed between the RbcL ratios and sea surface temperature, which showed a negative correlation (Figure 5.14). Variation in the RbcL:PsbA ratio was observed throughout the Ross Sea (Figure 5.15)., with the maximum ratio almost 50 times greater than minimum ratio (270±14 mol mol^{-1} and 6±0.5 mol mol^{-1}).

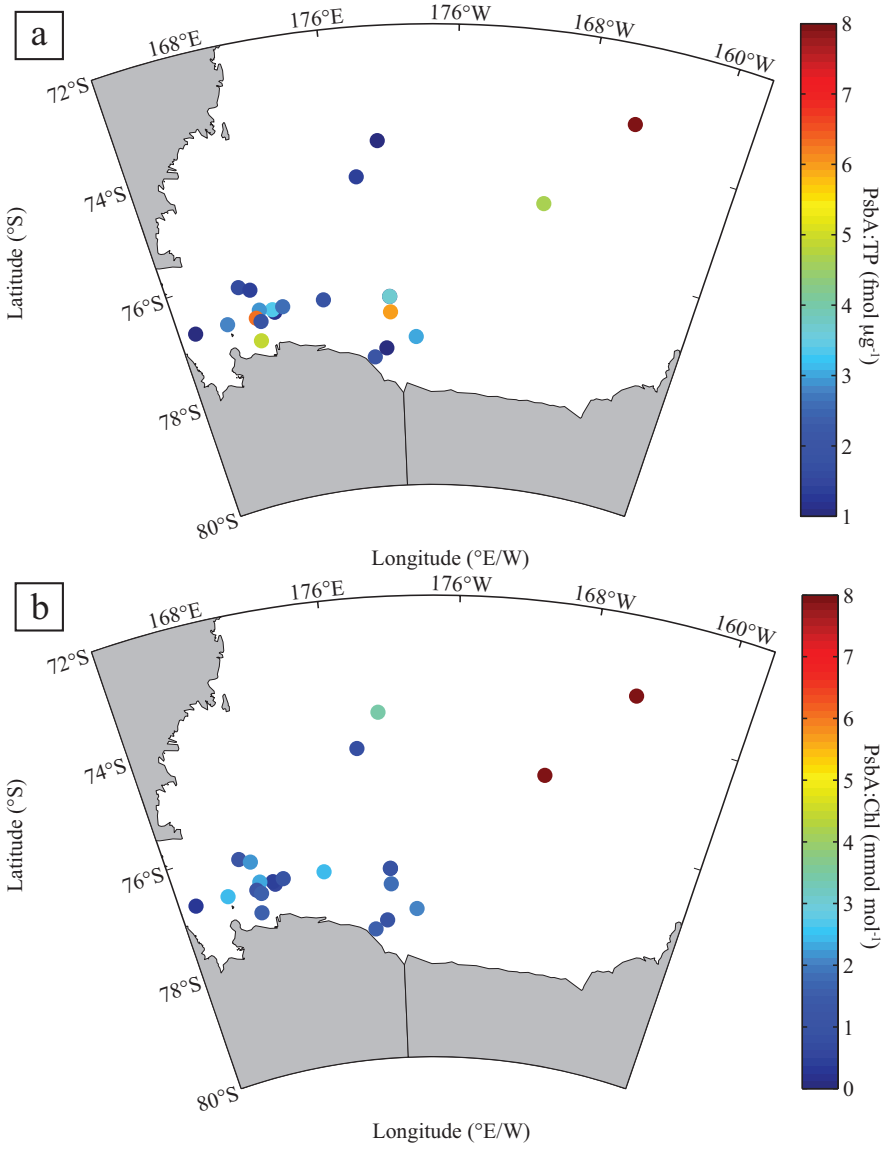

FIGURE 5.12: Sea surface ratios of (a) PsbA normalised to TP (fmol μ^{-1}) and (b) PsbA normalised to Chl (mmol mol^{-1}).

5.3 Discussion

The Ross Sea is the most productive region in the entire Southern Ocean, yet it has been demonstrated here within this chapter and elsewhere (Bertrand et al., 2007; Coale et al., 2003; Cochlan et al., 2002; Martin et al., 1990; Olson et al., 2000; Sedwick and DiTullio, 1997; Sedwick et al., 2000) that iron can be potentially limiting micronutrient, at least spatially. *In situ* measurements of chlorophyll, nutrients and photophysiology revealed a high degree of spatial variability (Figure 5.3a and 5.3b). The variability followed the retreat of the sea ice, with the Western Ross Sea becoming ice free later in the growing season. As such the offshore region presented 'post-bloom' conditions, low chlorophyll,

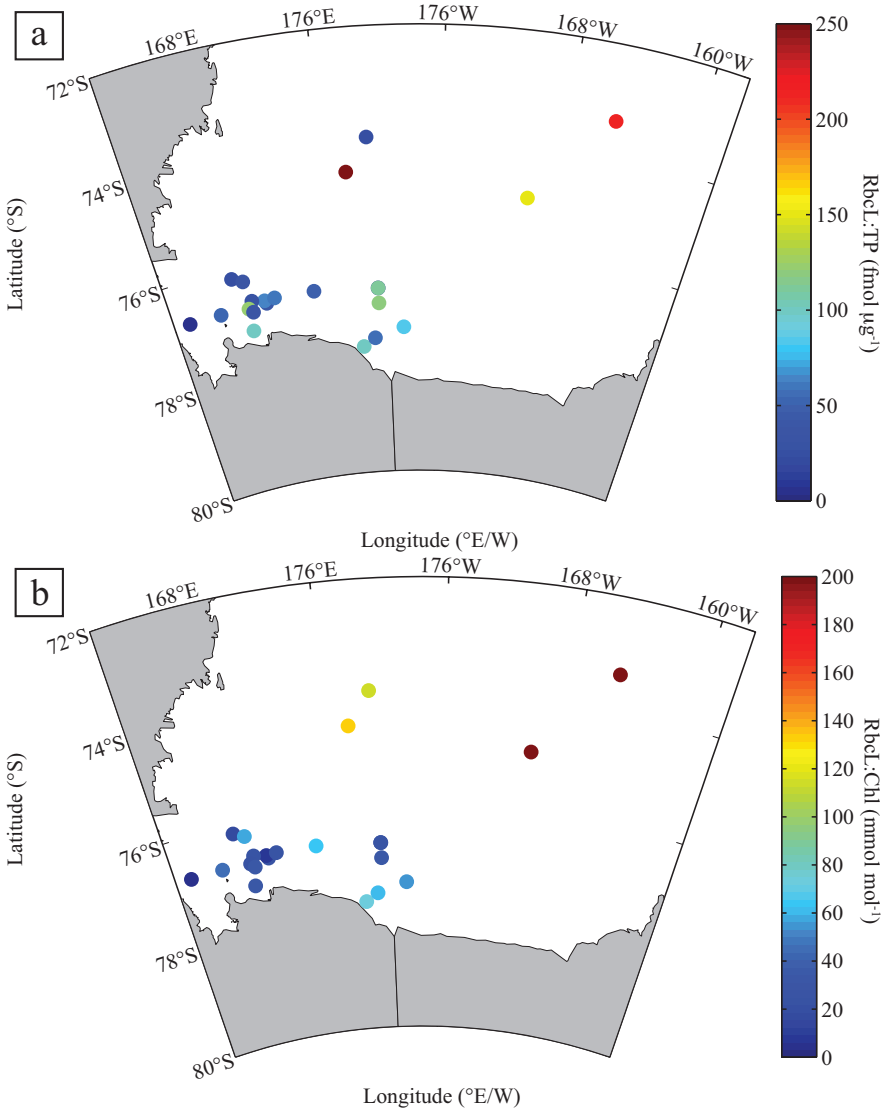

FIGURE 5.13: Sea surface ratios of (a) RbcL normalised to total protein (pmol/μg) and (b) RbcL normalised to Chl (mmol mol^{-1}).

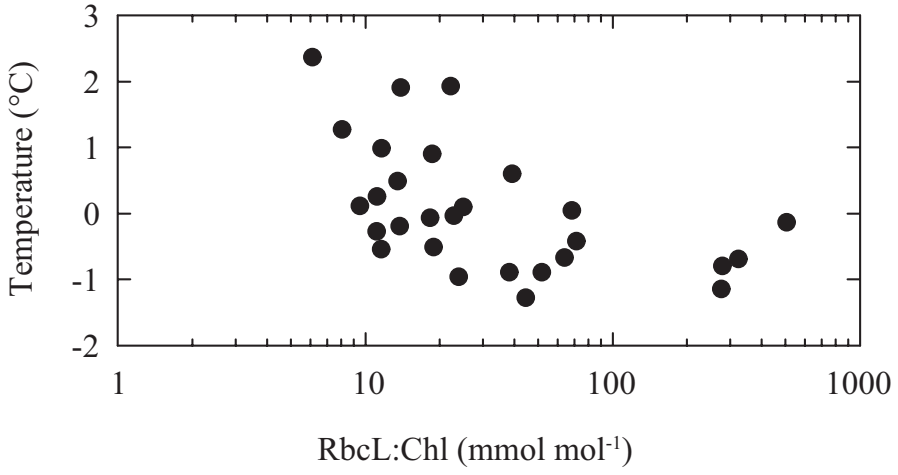

FIGURE 5.14: Sea surface protein ratio of RbcL normalised to Chl (mmol mol^{-1} against sea surface temperature (°C).

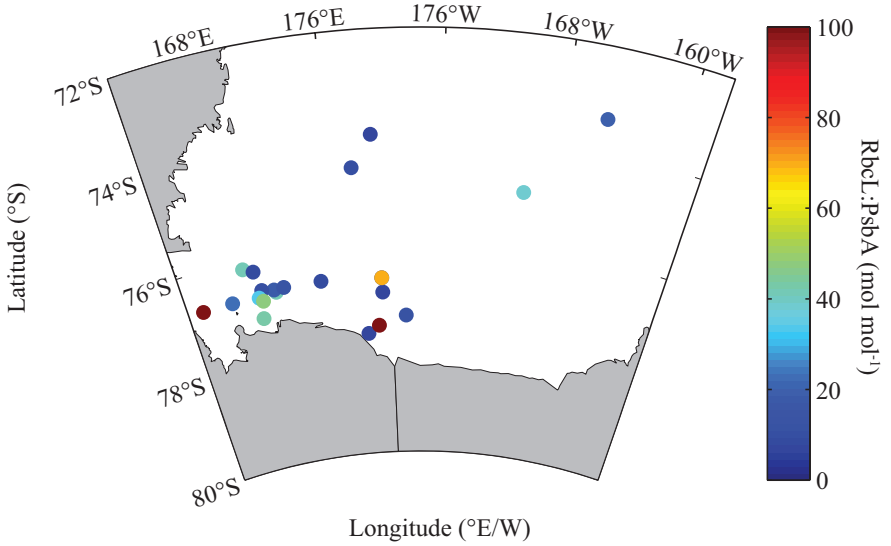

FIGURE 5.15: Sea surface protein ratio of RbcL to PsbA (mol mol^{-1}).

high F_v/F_m, and the Western Ross Sea presenting 'bloom' conditions, high chlorophyll, low F_v/F_m.

Grow-out bioassay experiments demonstrated the development of iron limitation of the *in situ* phytoplankton population in the Ross Sea (Figure 5.5). The results of such were significant differences in growth rates (Table 5.1) and nutrient drawdown (Figure 5.6), with potential implications for the biological carbon pump of this highly productive region. The annual cycle of phytoplankton growth in the Ross Sea is a balance between light to iron limitation and community succession, which may be coupled. In combination with the classical increase in growth rates and F_v/F_m following relief from iron limitation, specific changes in the F_o Chl^{-1} and F_v Chl^{-1} were observed (Figure 5.7). Consistent with the significant increases in F_v/F_m with iron addition, there were significant decreases in F_o Chl^{-1} with no significant changes in F_v Chl^{-1}. One potential explanation of this is that an increased F_o is the direct result of unbound chlorophyll-binding-proteins (Behrenfeld et al., 1996). Iron addition causes a rapid incorporation of pigment from these proteins into the photosynthetic apparatus.

The Ross Sea, although highly productive, lacks complete macronutrient removal like other high-latitude regions due to the availability of iron (Boyd et al., 2007; de Baar et al., 1990; Martin and Fitzwater, 1988). Nutrient removal and subsequent conversion to particulate matter, can be highly efficient in the Ross Sea (Smith and Asper, 2000), yet iron limitation can alter the nitrate uptake. Hutchins and Bruland (1998) and Takeda (1998) found an elevated silicate:nitrate uptake ratio under iron limitation, which

preferentially suppresses nitrate uptake in favour of silicate uptake. The cause of this change in the ratio is a switch in the phytoplankton from phaeocystis to diatoms; as phaoecystis are hypothesised to have higher iron requirements and there is a degree of silicification by diatoms. Indeed, the silicate:nitrate ratios decreased in the incubation experiments with the addition of iron (Table 5.1).

P. antarctica tend to dominate areas with deep mixed layer depths (MLDs), where iron concentrations tend to be lower, as iron inputs from melting sea ice increases surface concentrations where diatoms dominate (Sedwick et al., 2000). The result of deeper MLDs also results in decreased irradiance which are expected to increase cellular iron requirements (Raven, 1990; Sunda and Huntsman, 1997). Boyd (2002) has speculated that phaeocystis growth will be limited by iron from spring through late summer, and by low irradiance from autumn through early spring. Sedwick et al. (2007b) has proposed a different scenario to explain changes in cellular iron requirements and community succession; that as iron availability decreases during spring, it is mitigated by increases in irradiance, thereby decreasing cellular iron requirements.Strzepek et al. (2012) continued this discussion by examining the relationship of light and intracellular iron requirements in Southern Ocean diatoms and *P. antarctica*. The results found no difference in intracellular iron requirements for Southern Ocean species at low light and high light, 10 & 100 μmol quanta m^{-2} s^{-1} for diatoms and 3 & 570 μmol quanta m^{-2} s^{-1} for *P. antarctica*. Strzepek et al. (2012) suggested that Southern Ocean species increase the size of photosynthetic units (PSU) ('sigma'-type response), rather than the number of units ('n'-type response), thereby not increasing cellular iron requirements (Figure 5.16). An increase in the number of photosynthetic units would increase the cellular concentrations of iron-rich protein complexes, whereas an increase in photosynthetic unit size is accomplished through an increase in light-harvesting pigments and their specific arrangement (Strzepek et al., 2012). The result of such an increase in PSU would be reflected in the functional absorption cross-section for σ_{PSI} and σ_{PSII}. This model, however, assumes that the photosystems and light-harvesting complexes change together, whereas the components may change independently (Suggett et al., 2007); moreover these different strategies are not mutually exclusive (Falkowski and La Roche, 1991).

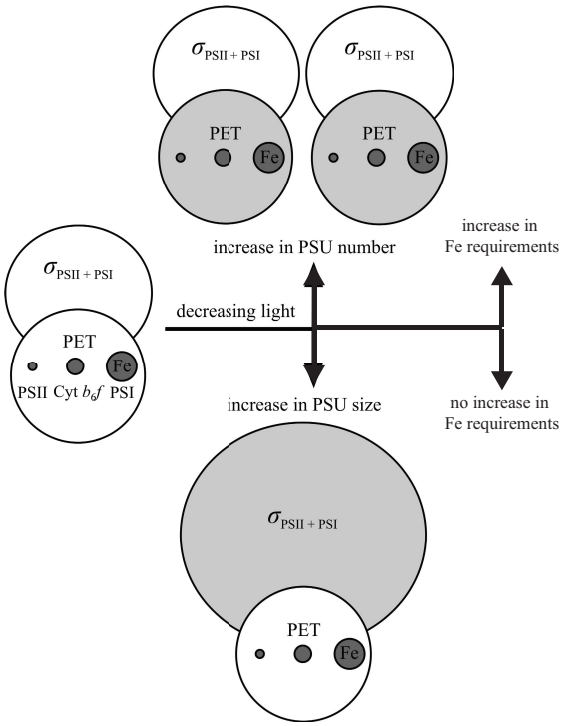

FIGURE 5.16: Schematic of how photoacclimation may alter intracellular iron requirements for photosynthesis, redrawn from Strzepek et al. (2012).Photosynthetic units - PSU, photosynthetic electron transport (PET).

The results presented here can support this hypothesis, with a conceptualised model of the Ross Sea seasonal progression. As the bloom progresses in the Ross Sea DIN (μmol L^{-1}) and F_v/F_m decrease while chlorophyll concentrations (μg L^{-1}) increase in an 'L-shaped' curve (Figure 5.17a). At the same time the community composition switches from phaeocystis dominated to diatom dominated (Figure 5.17b). The result of this is a conceptualised model of differential iron limitation dependent upon the community composition. At the start of the bloom (Figure 5.17c, labelled 'A') the Ross Sea is characterised by high DIN, high F_v/F_m, low chlorophyll and phaeocystis dominated with low levels of iron stress ($\Delta(F_v/F_m)$. As the bloom progresses there is an increase in iron stress (labelled 'B'), with a small decrease in DIN, a large decrease in F_v/F_m and a small increase in chlorophyll, which is coupled with a community shift towards diatoms. As the season progresses further there is a complete switch to a diatom dominated community (labelled 'C'), which results in a large decrease in DIN, a large increase in chlorophyll and a second stage of high levels of iron stress.

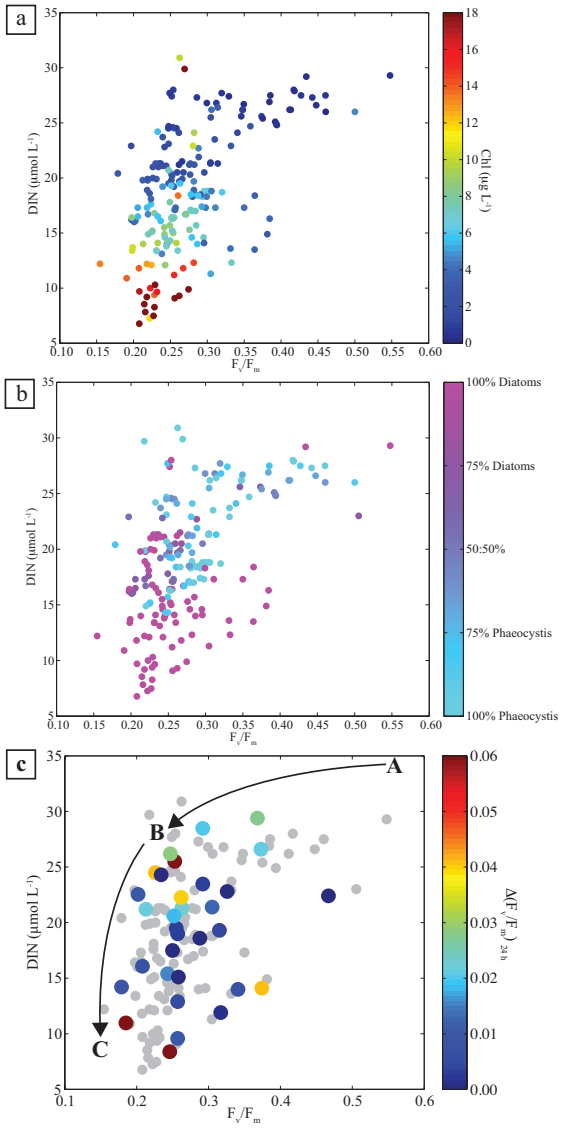

FIGURE 5.17: Seasonal progression of the Ross Sea. a) *In situ* DIN (μmol L^{-1}) and F_v/F_m with chlorophyll concentration (μg L^{-1}), b) *in situ* DIN (μmol L^{-1}) and F_v/F_m with %community composition and c) *in situ* DIN (μmol L^{-1}) and F_v/F_m with the relative degree of Fe stress $\Delta(F_v/F_m)_{24\ h}$ with conceptualised model of Ross Sea.

Protein concentrations throughout the Ross Sea revealed spatial variability (Figure 5.12 and 5.13), which can also be examined within the context of this seasonal model. Under initial bloom conditions, both PsbA:Chl and RbcL:Chl (mmol mol^{-1}) were at their maximum levels under phaeocystis dominated community (Figure 5.18a and 5.18b). When the community switches to diatom dominated both proteins ratios have depleted to their minimum values. One potential explanation for this decrease in PsbA is the increase in irradiance, which is hypothesised to decrease the abundance of photosynthetic reaction centres. An alternative hypothesis is iron limitation, as PSII requires 3 atoms, and one method of coping with iron limitation is to reduce the number of reaction centres. The

high levels of RbcL at the start of the season may be a product of low temperatures (Figure 5.14), as the catalytic rates of Rubisco are affected by temperature. One way to overcome low temperatures is to increase the substrate for reactions, Li and Morris (1982) found that in *Phaeodactylum tricornutum* the reduced specific activity of Rubisco was compensated by an increase in Rubisco abundance, whereas Anning et al. (2001) found the opposite in *Chaetoceros calcitrans*. Regardless of the previous results from culture studies, in the Ross Sea as the season progressed, sea surface temperatures increased and the RbcL ratios decreased, but a causal relationship cannot be assumed.

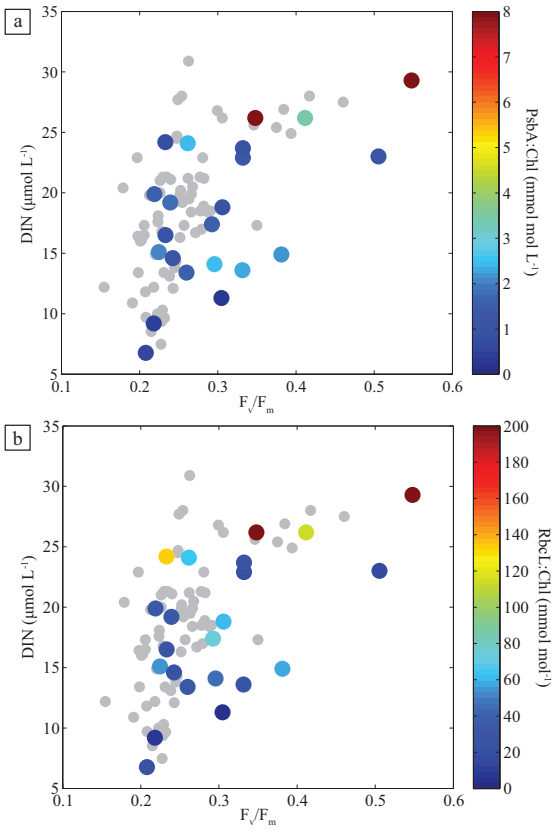

FIGURE 5.18: Seasonal progression of the Ross Sea proteins a) *In situ* DIN (μmol L^{-1}) and F_v/F_m with PsbA:Chl (mmol mol^{-1}) and b) *in situ* DIN (μmol L^{-1}) and F_v/F_m with RbcL:Chl (mmol mol^{-1}).

The current study of the Ross Sea represents the first extensive spatial mapping of the degree of iron stress in this highly productive region using the rapid experimentally induced changes in photohysiology ($\Delta(F_v/F_m)$). The results presented here suggest that the development of iron limitation is intrinsically linked to the community composition coupled with specific cellular iron requirements and irradiance. Consequently, in this polar system, the progression of community composition appears to be a crucial control on the development of iron stress, which then affects the extent of macronutrient removal

and the abundance of photosynthetic proteins. The major control over the carbon fixation protein, Rubisco, appears to be temperature. The Ross Sea clearly differs from other high latitude regions, due to the taxonomic heterogeneity, yet iron availability still contributes to reduced growth rates and macronutrient drawdown. Even though the Ross Sea is one of the most productive regions in the Southern Ocean, iron availability still exerts an ultimate control over productivity.

The Southern Ocean is thought to be particularly sensitive to climate change (Marinov et al., 2006), as it is the only iron-limited HNLC region where the cyrosphere plays a central role. Boyd et al. (2012) demonstrated through modelling studies that climate change mediated changes to the MLD and light availability due to reduced sea-ice cover may increase iron utilisation in some regions in the future. In combination, there is some indirect evidence that some supply mechanisms, which display a high inter annual variability such as Australian dust (Mackie et al., 2008), may also be altered in response to climate change. An understanding of iron limitation is this dynamic is thus important, particularly if climate mediated variability is expected to increase.

While iron limitation within the Ross Sea has been studied previously, this is the first attempt to characterise the fluorescence parameters and the relative ratios of photosynthetic proteins to total chlorophyll. While no clear spatial patterns where observed, a temporal pattern was observed within the bloom cycle similarly to the HLNA. A higher $\Delta F_v/F_m$ value was observed within the latter stages of the bloom, which was also characterised by an increased chlorophyll to photosynthetic protein ratio. Coupled with the observation of an elevated F_o signal, this suggests the presence of chlorophyll-binding proteins. Thus indicating that this genotypic response to iron limitation could be ubiquitous to all iron limited regions, but until such a time these proteins can be observed directly it may be premature to ascribe the notion that the total chlorophyll pool within the iron limited ocean regions is dominated by chlorophyll-binding proteins.

Chapter 6

Synthesis: Photophysiological Changes in Fluorescence under Iron Stress

The objectives of this thesis were to determine the potential role of unbound chlorophyll-binding proteins upon the chlorophyll fluorescence signature as determined by fast repetition rate fluorometry. By utilising the model organism *Synechocystis* PCC 6803 a study was performed on the iron-stress-induced protein IsiA, a well documented chlorophyll-binding protein. Alongside determining for the first time that the primary role for IsiA is to form an antenna for PSI, thereby increasing σ_{PSI}, the abundance of this protein was measured under increasing iron stress. A chlorophyll budget was determined which indicated that under severe iron stress the amount of unbound IsiA, and therefore unbound chlorophyll, could be as much as 50% of total chlorophyll. This increase in unbound chlorophyll was temporally correlated with a reduction in F_v/F_m due to an increase in F_o. To determine whether a decreased F_v/F_m under iron stress is due to an increased F_o iron addition experiments were performed in 2 iron limited oceanic regions, the high latitude North Atlantic and the Ross Sea. Experiments confirmed that the phytoplankton community in these regions are limited by the availability of iron. These experiments for the first time tried to establish the differences in physiological and taxonomic signals of F_v/F_m. By utilising short-term experiments the difference in F_v/F_m between the iron-amended treatment and the control treatment could be calculated, $\Delta(F_v/F_m)$.

$\Delta(F_v/F_m)$ could be used as a proxy for the relative degree of iron stress. Alongside this objective the specific changes in fluorescence were also studied to determine whether the decreased *in situ* F_v/F_m frequently measured in iron limited oceanic regions is due to presence of unbound chlorophyll-binding proteins. In all experiments where there was a strong response to the addition of iron, F_v/F_m increased due to a decrease in the F_o signal. Elucidating the cause and function of these chlorophyll-binding proteins remains a task in the field of phytoplankton physiology.

$\Delta F_v/F_m$ relies on the assumption that a change in F_v/F_m for a given organism will to first order be dependent upon the magnitude of differences in any uncoupled antenna (and hence F_o and F_m). Taxonomy could potentially negate the effectiveness of this iron limitation proxy, if the effective differences in the magnitude of F_v Chl^{-1} are sufficiently large enough. Figure 6.1 displays the $\Delta F_v/F_m$ against the initial F_v/F_m and the F_v/F_m from the iron addition treatments of experiments during D354. This demonstrates that taxonomy is not a first order effect, as they are highly correlated. At least within this study, the treatment effect dominates over any differences in community structure between experiments.

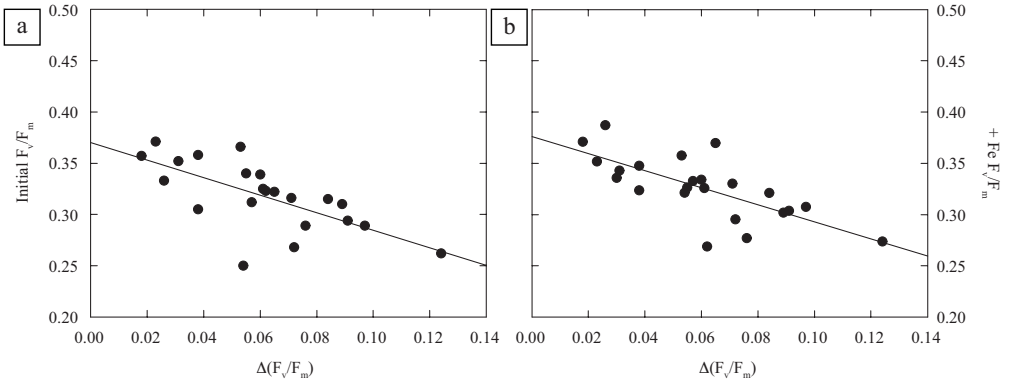

FIGURE 6.1: $\Delta F_v/F_m$ against a) initial F_v/F_m and b) iron addition F_v/F_m from experiments during D354.

Iron as a primary limiting nutrient for phytoplankton growth and productivity was first considered in the 1930s (Gran, 1931, 1933; Hart, 1934; Harvey, 1938; Hendey, 1937) to explain oceanic regions with elevated surface macronutrient concentrations and relatively low chlorophyll concentrations (HNLC). With the establishment of ultra-clean trace metal techniques and high-sensitivity analytical methods in the 1970s (Bender and Gagner, 1976; Bender et al., 1977; Boyle and Edmond, 1975; Knauer and Martin, 1973), the testing of this hypothesis became a possibility. The work of de Baar (1994);

de Baar et al. (1990, 1995); Martin and Fitzwater (1988); Martin et al. (1989, 1990, 1994) demonstrated that in HNLC waters the chlorophyll accumulation by phytoplankton was limited by the availability of iron. Recognition of the importance of iron in regulating biogeochemical cycles and phytoplankton ecology has increased over the years, given that iron stress may affect between 30% and 60% of the global ocean surface area (Behrenfeld et al., 2009), at least seasonally.

The dominant reason for the importance of iron is the photosynthetic apparatus, which represents a major cellular iron sink in phytoplankton (∼23/24 atoms per linear electron transport chain (ETC)) (Shi et al., 2007). As such phytoplankton have evolved different adaptive strategies to iron stress: retrenchment, acquisition/storage and compensation. Retrenchment, a reduction of physiological activities is most commonly observed as chlorosis, a reduction in chlorophyll concentrations (Greene et al., 1991, 1992). Although this response is not unique to iron limitation (Davey and Geider, 2001; Moseley et al., 2002). Acquisition, the excretion of siderophores by prokaryotic organisms in order to chelate and solubilise aqueous iron (Haygood et al., 1993; Raiswell and Canfield, 2012; Sunda, 2001). Eukaryotic organisms may also be able to access this pool of iron through membrane transporter systems (Amin et al., 2009; Maldonado and Price, 2001; Maldonado et al., 1999). Storage refers to the production of ferritin, an iron-storage protein to safely concentrate and store iron while reducing cell damage from potential oxidative stress (Marchetti et al., 2009). The strategy that will be discussed here specifically is compensation, while is sub-divided into alteration of the thylakoid membrane, alteration of the PSII:PSI ratio (an increase in PSII relative to PSI) and over-expression of photosynthetic pigments.

The first notable alteration of the thylakoid membrane is the replacement of iron-containing proteins by an alternative protein without iron as a cofactor, such as ferredoxin and flavodoxin (Ferreira and Straus, 1994; La Roche et al., 1996a). An elevated PSII:PSI ratio is proposed to enhance ATP production through a PSII-MOX pathway (midstream oxidase) (Bailey et al., 2008; Behrenfeld and Milligan, 2013; Behrenfeld et al., 2008; Cardol et al., 2008; Desquilbet et al., 2003; Mackey et al., 2008). This chapter will focus on the third mechanism, the over-expression of photosynthetic pigments and the potential consequences of such on observed variable chlorophyll fluorescence.

Variable chlorophyll fluorescence measured following iron enrichment results in an increase in F_v/F_m, however this does not appear to be the result of an increase in the efficiency of PSII except under cases of severe iron limitation (Behrenfeld et al., 2004; Benesova et al., 2000; Desquilbet et al., 2003; Garcia-Mendoza and Colombo-Pallotta, 2007; Greene et al., 1994; Guikema and Sherman, 1983; Kolber et al., 1994; Morales et al., 2001; Moseley et al., 2002; Sandström et al., 2002; Schrader et al., 2011; Vassiliev et al., 1995). There is a growing body of evidence that this increases is the result of a decrease in F_o and F_m (Behrenfeld and Kolber, 1999; Behrenfeld et al., 2006; Greene et al., 1994; Kolber et al., 1994; Olson et al., 2000). These multiple studies suggest that this increase in F_v/F_m following iron addition is the result of rapid incorporation of pigment from a disconnected storage pool of unbound chlorophyll-binding proteins (Behrenfeld and Milligan, 2013; Behrenfeld et al., 1996, 2006; Ryan-Keogh et al., 2012, 2013).

Such a potential pool of unbound chlorophyll-binding proteins is likely a result of a separation between growth rates and pigment synthesis. There is strong evidence that pigment synthesis is over expressed relative to growth rate during iron stress when macronutrient concentrations are high. Milligan (1998) found that *T. wiessfloggi* decreased its growth rate 3.5 fold compared to an only 2.5-fold decrease in chlorophyll concentration. Allen et al. (2008) found that *Phaeodactylum tricornutum* under iron stress displayed an 80% decrease in growth accompanied by only a 27% decrease in chlorophyll per unit of cell volume. The results of the *Synechocystis* experiment within this thesis found a 70% reduction in growth rates under iron stress (Figure 3.4b), with only a 25% reduction in chlorophyll production (Figure 3.4a). This disparity between growth rates and pigment synthesis is an area of iron stress that is still not fully understood, with the question remaining as to why phytoplankton may over express these proteins and accumulate these pigments.

An area where excess accumulation of antenna complexes has been throughly studied is the chlorophyll- and carotenoid-binding, iron-stress-induced protein IsiA of cyanobacteria. The role of this protein has been discussed in detail in Chapter 3, with inferences about the potential role of overexpression and its influence on fluorescence. Under severe iron limitation of *Synechocystis* PCC. 6803 the relative expression of IsiA increased beyond the proposed 6:1 IsiA:PSI ratio (Bibby et al., 2001a,b,c; Boekema et al., 2001), characteristic of an IsiA:PSI supercomplex, without a concurrent increase σ_{PSI}. As this

pool of potentially unbound IsiA continued to increase, F_v/F_m decreased (Figure 3.5a) as a result of increasing F_o Chl^{-1} (Figure 3.5b) suggesting a population of photosynthetically uncoupled chlorophyll.

Further studies of iron stress in the field within this thesis have demonstrated that increases in F_v/F_m following relief from iron limitation are consistently due to decreases in F_o. By examining *in situ* surface measurements of F_v/F_m from CTD stations, a relationship became apparent. This relationship is not as strong during D350 (Figure 6.2a), which can be ascribed to the relative lack of iron stress during spring. However, during D354 (Figure 6.2c) and PRISM (Figure 6.2e), where iron stress was present, a clear negative relationship can be determined between F_v/F_m and F_o Chl^{-1} (Figure 6.2a, c and e). Within all three cruises, there was no relationship between F_v/F_m and F_v Chl^{-1} (Figure 6.2d, d and f).

Moreover, the increase in F_v/F_m and decrease in F_o Chl^{-1} is most evident within the experiments which displayed clear signs of iron stress. Experiments 4 (Figure 4.8b) and 6 (Figure 4.8c) from D354 showed a strong increase in F_v/F_m following iron addition. This was deemed to be due to the decrease in F_o Chl^{-1}, which is clearly demonstrated in Figures 6.3a and 6.3b. The same pattern was observed in experiments 1 (Figure 6.3c) and 3 (Figure 6.3d) in the Ross Sea, despite some evidence of a small increase in the F_v/F_m in the control treatments. In all cases, the F_v/F_m, F_o Chl^{-1} and F_v Chl^{-1} of the control treatment remain relatively consistent with the initial measurements. Where as the iron addition treatment resulted in the same negative relationship with F_o Chl^{-1} and no relationship with F_v Chl^{-1}.

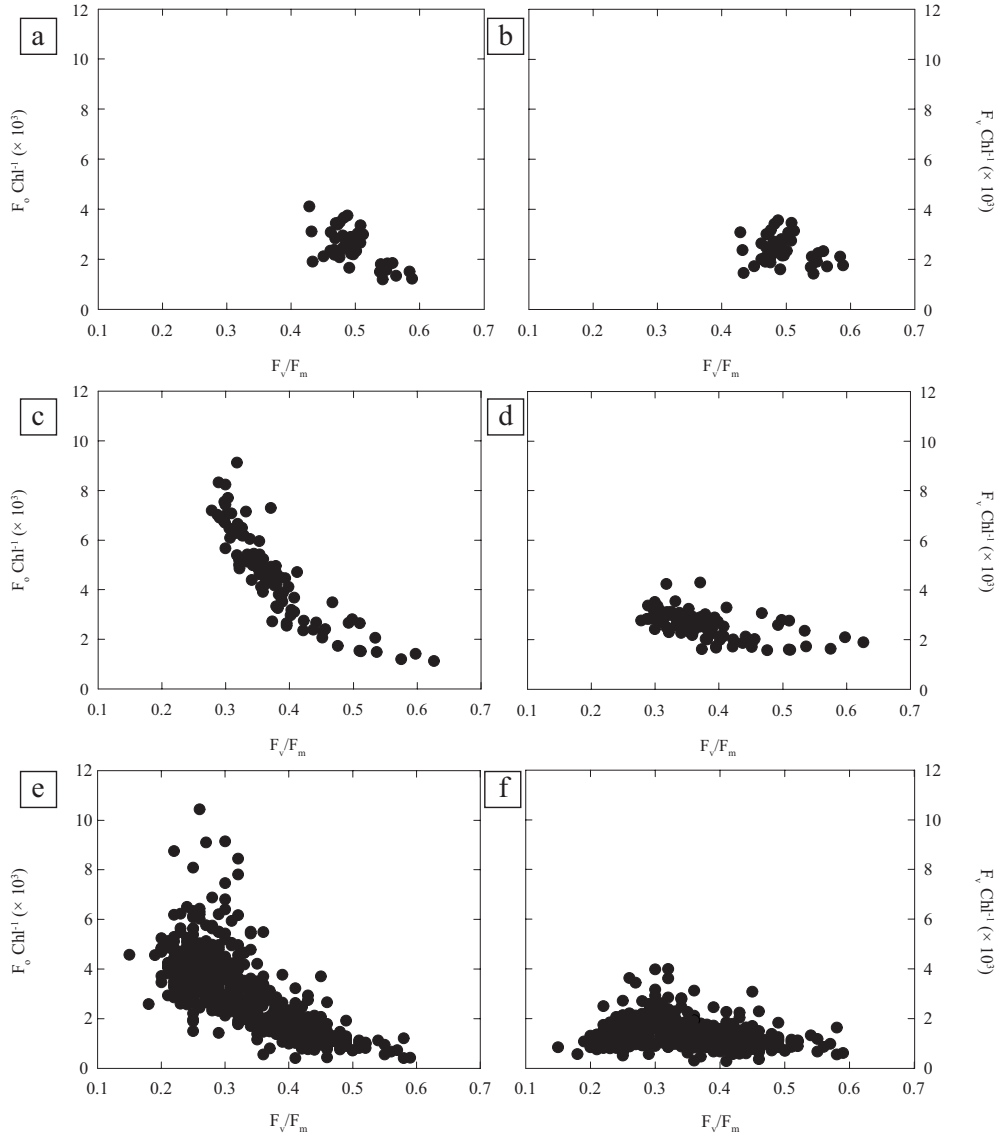

FIGURE 6.2: F_o Chl^{-1} (a, c and e) and F_v Chl^{-1} (b, d and f) against F_v/F_m from surface *in situ* measurements of the high latitude North Atlantic during the spring (D350) (a, b), the high latitude North Atlantic during the summer (D354) (c, d) and the Ross Sea (PRISM) (e, f).

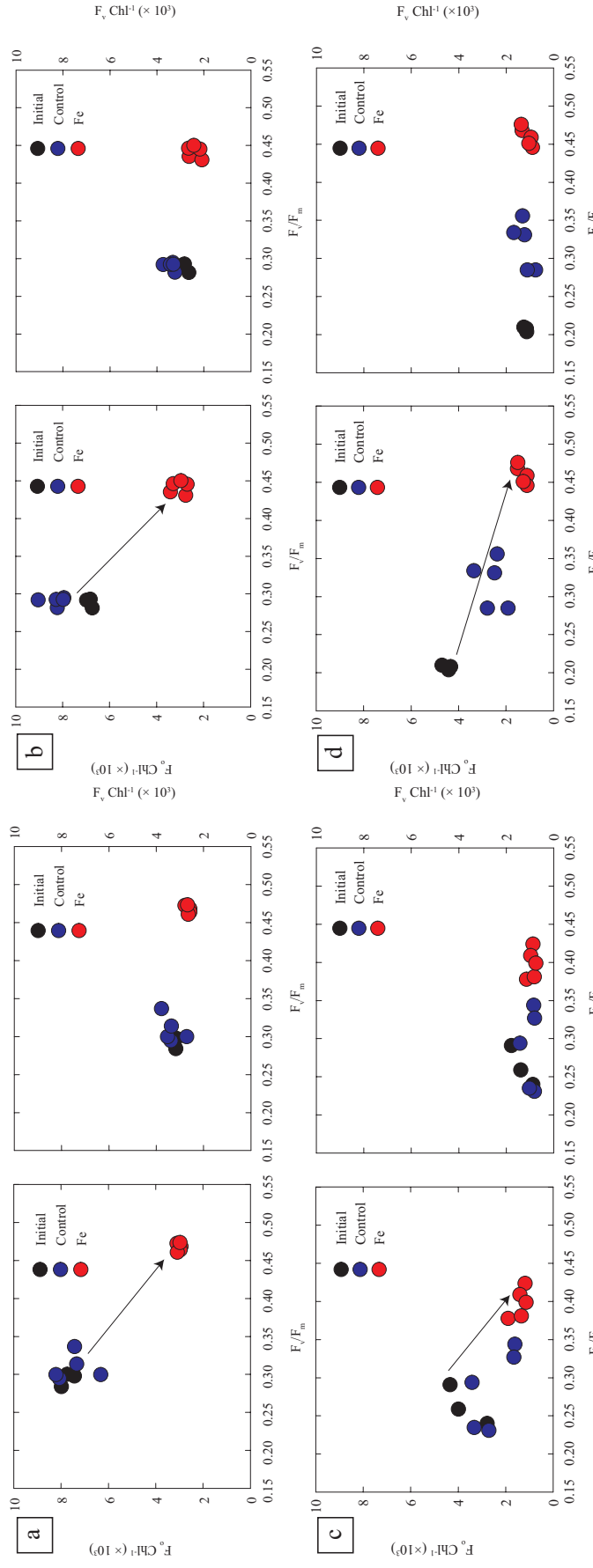

FIGURE 6.3: F_o Chl^{-1} and F_v Chl^{-1} against F_v/F_m from the initial and end time points of a) Experiment 4 in the high latitude North Atlantic (D354), b) Experiment 6 in the high latitude North Atlantic (D354), c) Experiment 1 in the Ross Sea (PRISM) and d) Experiment 3 in the Ross Sea (PRISM). Black arrows denote the shift in F_o Chl^{-1} relative to F_v/F_m.

This can be further interpreted by examining the specific differences between the photophysiological parameters of the iron addition treatment against the control treatment. Within this thesis, the parameter $\Delta(F_v/F_m)$ has already been described (Chapter 4 - Section 4.24) and used to determine a relative degree of iron stress. Similar calculations can be performed for the individual fluorescence parameters, $\Delta(F_o\ Chl^{-1})$ and $\Delta(F_v\ Chl^{-1})$, by calculating the difference in these parameters between the iron addition and control treatment.

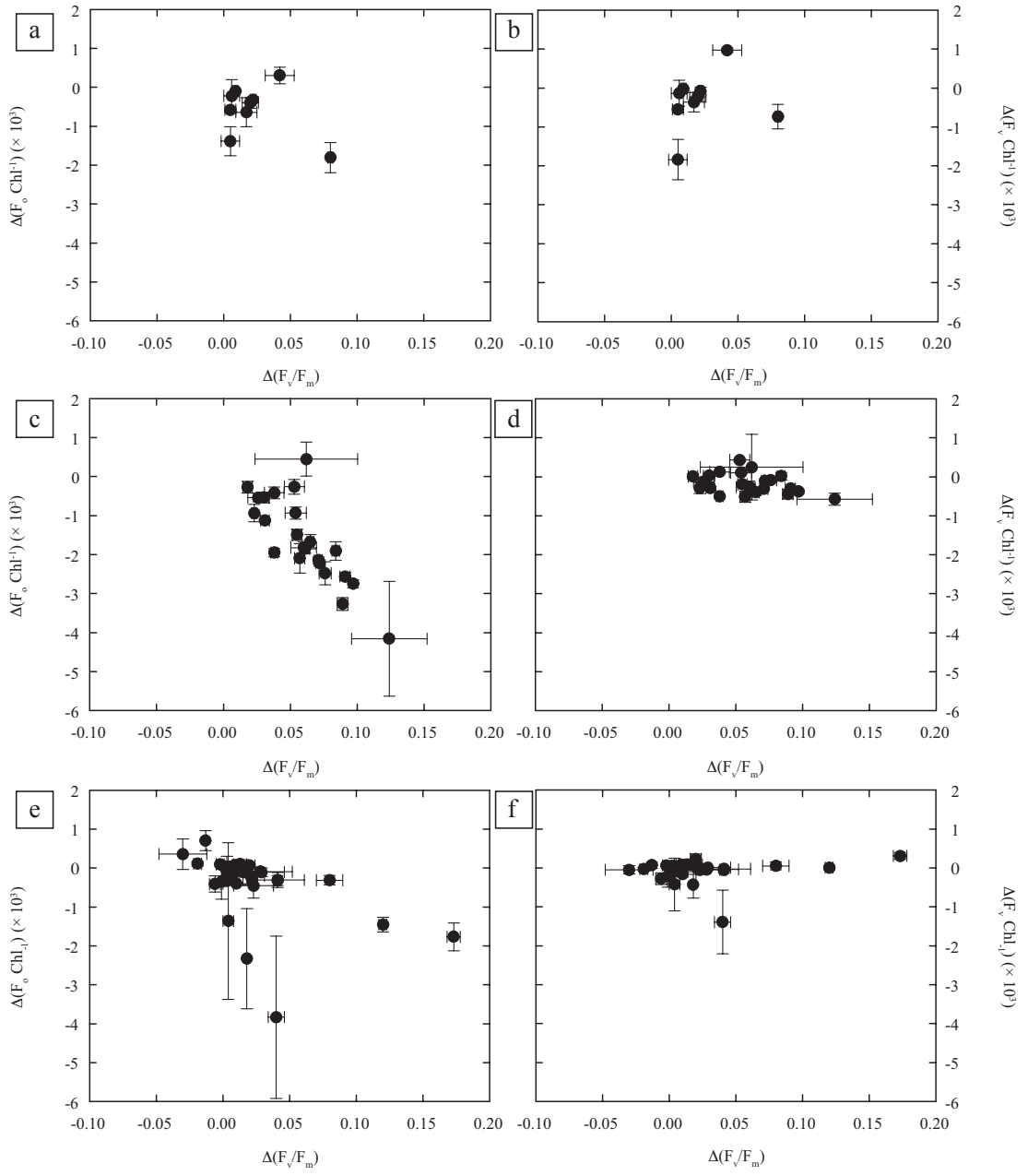

FIGURE 6.4: $\Delta(F_o\ Chl^{-1})$ (a, c and e) and $\Delta(F_v\ Chl^{-1})$ (b, d and f) against $\Delta(F_v/F_m)$ from all iron addition experiments set up in the high latitude North Atlantic during spring (D350) (a, b), the high latitude North Atlantic during summer (D354) (c, d) and the Ross Sea (PRISM) (e, f).

The results from D350 (Figure 6.4a and b), where iron stress was not as prevalent, show no clear relationship between the change in F_v/F_m and either F_o Chl^{-1} or F_v Chl^{-1}. However, the results from D354 (Figure 6.4c and d) display a relative strong correlation ($R^2 = 0.641$) between $\Delta(F_v/F_m)$ and $\Delta(F_o$ Chl$^{-1})$. A similarly strong relationship was evident from the results of the experiments from the PRISM cruise (Figure 6.4e and f), with the possibility of two separate slopes based upon the distinct community structure of the Ross Sea. Indeed, when the relative percentage of diatoms and *Phaeocystis* are plotted on this figure (6.5) it appears as if the contribution of unbound chlorophyll is greater in *Phaeocystis* than the diatoms.

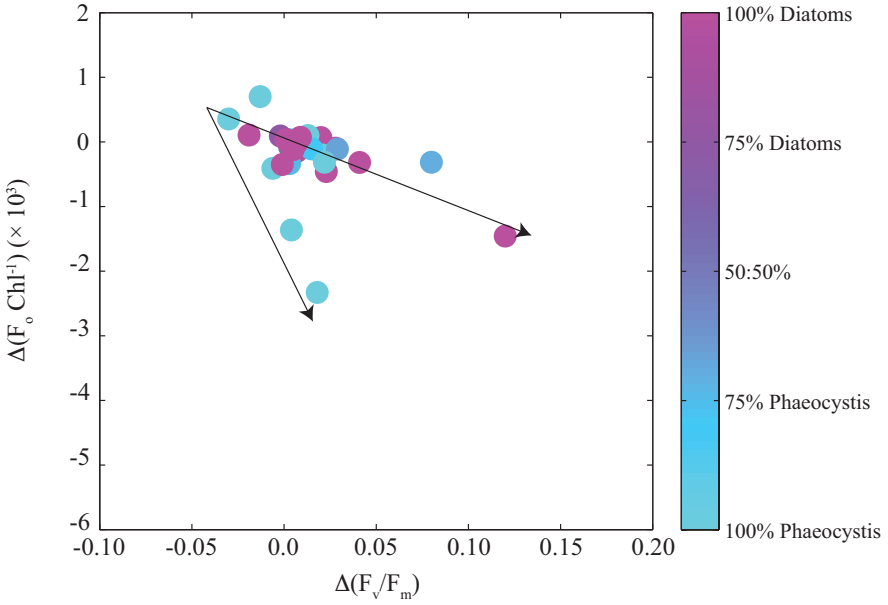

FIGURE 6.5: $\Delta(F_o$ Chl$^{-1})$ against $\Delta(F_v/F_m)$ with community from all experiments set up in the Ross Sea (PRISM).

One hypothesis to explain the resource investment in over-expressed pigments, is that unbound chlorophyll-binding proteins will provide a rapid source chlorophyll upon iron re-supply (Behrenfeld and Milligan, 2013; Schrader et al., 2011). Schrader et al. (2011) demonstrated that in an iron-stressed culture of *Synechocystis* PCC 6803 nitrate addition decreases F_v/F_m by increasing the resource investment in unbound IsiA complexes. Within field studies in the Pacific, the same response was observed with nitrate addition (Figure 6.6); the increase in the fluorescence yield from natural populations was ascribed to an increase in the abundance of unbound complexes. In agreement with these findings are the results of nitrate addition experiments performed in the HLNA (Figure 6.7). In intermediate DIN water (4.27 μmol L^{-1}) (Figure 6.7a), the nitrate addition resulted in a decrease in F_v/F_m and an increase in Fo Chl^{-1}, displaying an inverse relationship to

the iron addition treatment. The low DIN water (0.64 μmol L^{-1}) experiment (Figure 6.7b) followed the same pattern as above. Upon nitrate addition, the F_v/F_m decreased to that of the intermediate DIN experiment, whereas the F_o Chl^{-1} increased to that of the intermediate DIN experiment. Overall this resulted in a $\Delta(F_o\ Chl^{-1})$ at t = 72 h of -0.37±0.32 and 0.29±0.06 ($\times\ 10^3$) respectively for each experiment. Consistent with these findings, the specific differences in $\Delta(F_v/F_m)$ and $\Delta(F_o\ Chl^{-1})$ across all short-term experiments (Figure 6.8) demonstrated an increase in $\Delta(F_o\ Chl^{-1})$ and a decrease in $\Delta(F_v/F_m)$ with nitrate addition. Given the pattern of resource investment of nitrate demonstrated here, it appears as though there is an ecological advantage to such unbound complexes, with one possibility that it permits a rapid response to a resource with particularly episodic availability, iron.

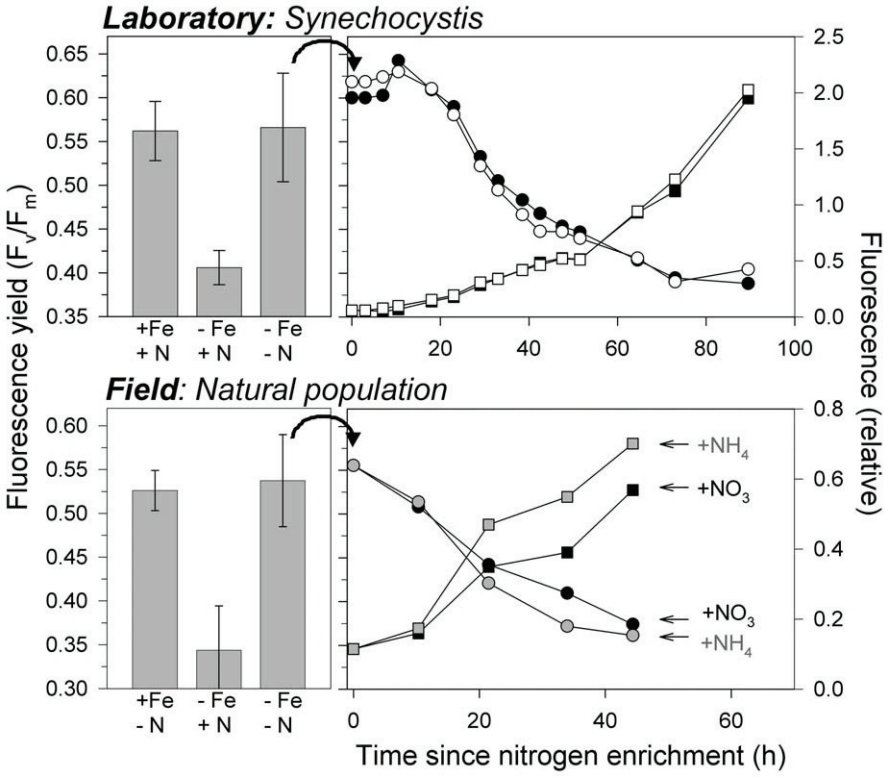

FIGURE 6.6: Comparison of laboratory experiments on wild type Synechocystis with analogous experiments using mixed populations in the field from Schrader et al. (2011).

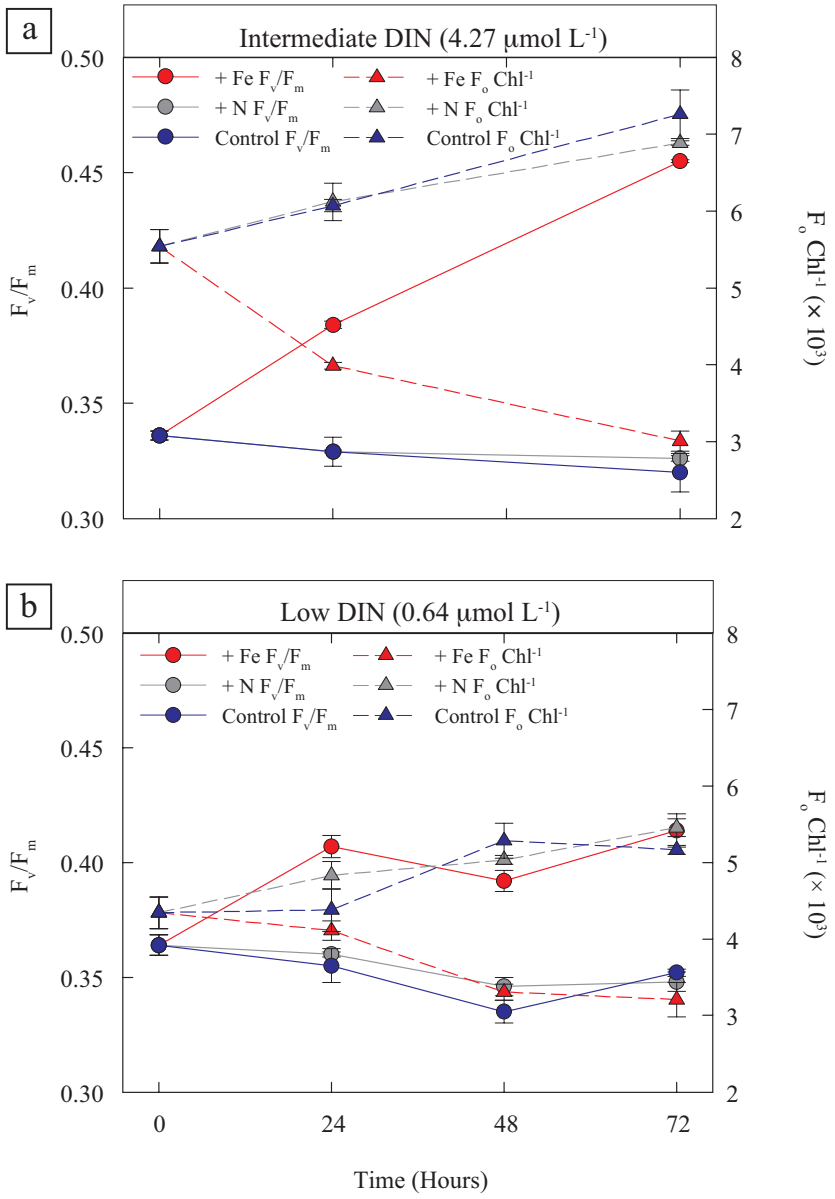

FIGURE 6.7: Effects of iron and nitrate addition on F_v/F_m and F_o $Chl^{-1}$from experiments in a) intermediate DIN water, Experiment 5 from the Irminger basin of the HLNA and b) low DIN water, Experiment 7 from the Iceland basin of the HLNA. Both experiments performed in summer 2010. Shown are averages with ± standard errors, where n = 3 for all timepoints.

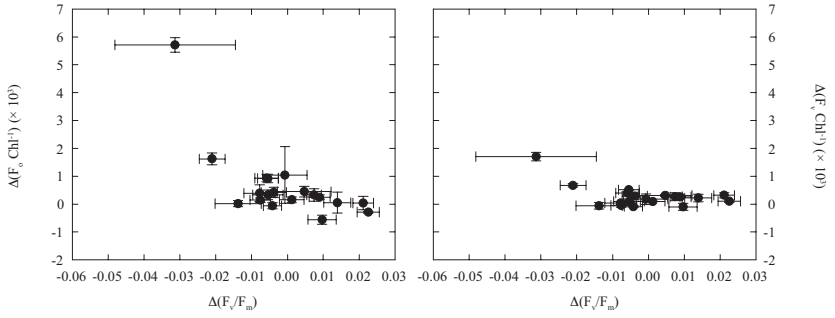

FIGURE 6.8: $\Delta(F_o\ Chl^{-1})$ against $\Delta(F_v/F_m)$ from all nitrate addition treatment experiments in the HLNA during summer (D354).

The results presented here are consistent with previous observations (Behrenfeld and Kolber, 1999; Behrenfeld et al., 2006; Greene et al., 1994; Kolber et al., 1994; Olson et al., 2000; Schrader et al., 2011), depressed F_v/F_m values measured in culture and in the field are the result of an elevated F_o (Figure 6.9) and not a reduced F_v. The potential consequences of this finding has many different implications for the study of photophysiology and the use of fluorescence data to infer iron limitation of phytoplankton. F_m can also be used to track potential unbound chlorophyll binding proteins as it follows the same variations as F_o, yet in the basis of this study only F_o was examined. The most important finding to take away from these results is that there is F_v does not vary when iron is added to the experiments, the only variation comes from F_o and F_m.

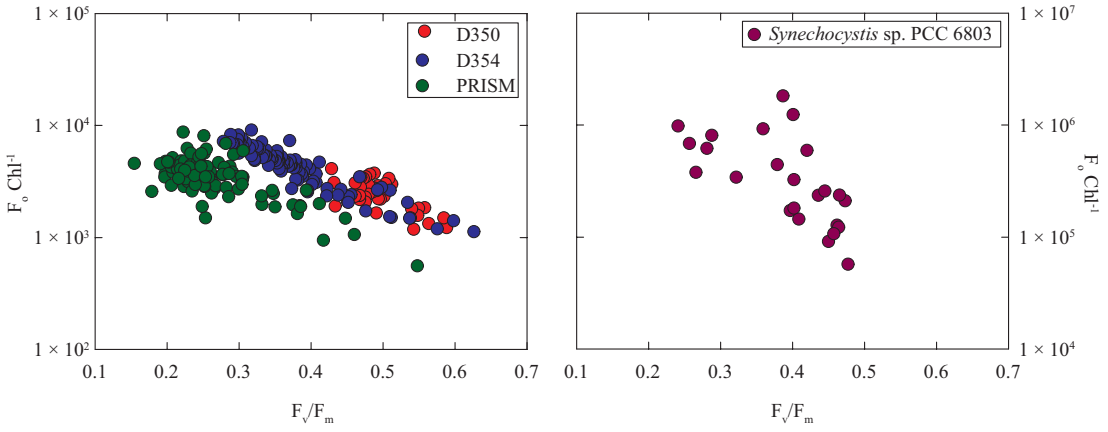

FIGURE 6.9: F_o Chl^{-1} against F_v/F_m from CTD stations of all three cruises and the *Synechocystis* experiment.

One of the first implications that must be considered is that increased F_o may be the direct result of unbound chlorophyll-binding proteins and therefore energetically disconnected from the electron transport chain (ETC), thereby invalidating the strict interpretation of F_v/F_m as a measure of the photochemical quantum efficiency of PSII (Suggett et al., 2009). The consistent presence of this elevated F_o under iron stress, suggests that expression of these proteins is a result of iron limitation. Furthermore, it can inferred that iron limitation responses, such as the expression of IsiA protein, may not be limited to cyanobacteria but may be a more generic response across all phytoplankton. Indeed, the recently described Tidi protein has been suggested to also act as an antenna protein for PSI (Varsano et al., 2006) and could possibly, under cases of overexpression, act as an unbound chlorophyll-binding protein. Several genomic studies (Armbrust et al., 2004; Marchetti et al., 2012; Mock et al., 2008) identified genes within different phytoplankton species which are up-regulated under iron limitation and have been hypothesised to act

within the capacity as a PSI antenna, and therefore could also contribute to pools of unbound chlorophyll.

The second implication that must be considered is that as these unbound complexes contain chlorophyll but may not contribute to photosynthesis, they will act to decrease apparent assimilation efficiencies (i.e. carbon fixed per unit chlorophyll or light absorption) in productivity estimates (Behrenfeld and Milligan, 2013). P vs E relationships are frequently used to link indices of phytoplankton biomass (e.g. chlorophyll) and rates of primary production, and this feature can manifest itself in these relationships. Physiological effects upon P vs E relationships will manifest itself as F_k-independent variability (Behrenfeld et al., 2004; Davey and Geider, 2001; Kolber et al., 1994; Park et al., 1999; van Leeuwe and de Baar, 2000), parallel changes in the light-limited slope and light-saturated rate of chlorophyll-normalised carbon fixation. As opposed to E_k-dependent variability, changes in the light saturation index E_k. However, E_k-independent variability may also be controlled growth rate (Halsey et al., 2010) or other mechanisms (Behrenfeld et al., 2004) and therefore may not be a consequence of such unbound complexes.

Moreover, the chlorophyll in unbound complexes will contribute to the bulk chlorophyll signal measured from space by absorption and estimates calculated utilising satellite will need to take into account the presence of such complexes. Behrenfeld et al. (2006) attempted this by utilising fluorescence data measured by satellites for the Pacific to infer the relative proportion of chlorophyll involved in photosynthesis and that of unbound complexes. This was achieved by calculating the difference between the dawn maxima (calculated by satellite measured fluorescence) and the assumed maximum potential of an oligotrophic region (calculated *in situ*), and applying this correction to two different satellite productivity models: the Carbon-based Production Model (CbPM) (Behrenfeld et al., 2005) and the Vertically Generalized Production Model (VGPM) (Behrenfeld and Falkowski, 1997). The results of this study suggested that around 50% of chlorophyll in the Pacific is not directly involved in photosynthesis, with a respective over-estimate of primary productivity for the equatorial Pacific. Despite the obvious caveats of this approach, it highlights the need for corrections for such unbound complexes.

One of the underlying objectives of this thesis has been to link iron-related fluorescence properties to specific physiological impacts of iron limitation under both culture and field studies. Despite the clear advancements made here, there are still many questions

that remain unanswered, primarily around the function of the unbound pigment-protein complexes. These proteins would clearly provide a rapid source of pigment following iron re-supply, yet is this their only role? Many studies of IsiA have suggested that the over expression of this protein is a more general oxidative response rather than a specific PSI antenna or pigment storage (Berera et al., 2009; Cadoret et al., 2004; Havaux et al., 2005; Ihalainen et al., 2005; Jeanjean et al., 2003; Michel and Pistorius, 2004; Singh and Sherman, 2006; Wilson et al., 2006, 2007; Yeremenko et al., 2004). Do unbound chlorophyll-binding proteins provide other advantages, and if so, how is their synthesis over growth rates justified. The recent discovery of such potential complexes in eukaryotes in laboratory studies (Armbrust et al., 2004; Marchetti et al., 2012; Mock et al., 2008; Varsano et al., 2003, 2006) also raises the question of ecological importance, yet these complexes have not yet been studied in eukaryotes in the field. The role of fluorescence properties in understanding the story of iron stress in the contemporary oceans has provided a valuable insight, yet it is clear that further investigations both in culture and in the field are required.

Irrespective of the underlying causes for unbound pigment-protein complexes, the potential large scale expression of such complexes provides a powerful diagnostic tool with which to investigate nutrient stress *in situ*. The reduction in F_o following iron addition in a short timescale (24 h) is assumed to be the rapid incorporation of these complexes into the photosynthetic electron transport chain. As such it has allowed the construction of an experimental design which negates one of the previous caveats of FRRf interpretation, the effect of community structure. The rapid responses can be used to understand the physiological state of phytoplankton, without measuring the effect of a potential community shift within iron addition experiments; as any FRRf measurement will contain both a physiological signal superimposed over a taxonomic signal (Campbell et al., 1998; Fishwick et al., 2006; Moore et al., 2005, 2006b; Prasil et al., 2008; Suggett et al., 2009, 2004). Measurements of rapid iron addition responses allows mapping of the degree of iron limitation, $\Delta(F_v/F_m)$ in different ocean regions. Such mapping allows much greater spatial and temporal resolution of unambiguous iron stress indication to be achieved, allowing seasonal and sub-basin scale variability to be resolved for the first time.

The unique seasonally-resolved data from the high latitude North Atlantic cruises has allowed the first extensive spatial and temporal study of iron limitation in the field. Iron limited areas of the oceans are assumed to be limited due to inefficient supplies

(Martin and Fitzwater, 1988) and this limitation may persist in large open ocean areas (Martin and Fitzwater, 1988; Martin et al., 1990). The data presented here demonstrate that iron limitation is highly dynamic with a high degree of spatial and temporal variability. Measurements of $\Delta(F_v/F_m)$ were generally lower in pre-bloom conditions, increasing during the bloom, with the highest values measured in post-bloom conditions with residual macronutrients (Figure 4.23). Inter- and intra-basin differences were also highly significant in the HLNA. Furthermore, these responses were further correlated with observed differences in net growth rates (Figure 4.22), indicating that these independent measures of iron stress provided empirical evidence of iron stress within the HLNA. The consequences of such highlighted that even the highly productive region of the HLNA may potentially experience iron stress throughout the growing season.

The results of this study demonstrate that the HNLC classification needs to be reexamined within a seasonal context, which was further investigated in the Ross Sea. This highly productive region of the Southern Ocean is known to be limited by the availability of iron (Bertrand et al., 2007; Coale et al., 2003; Cochlan et al., 2002; Martin et al., 1990; Olson et al., 2000; Sedwick and DiTullio, 1997; Sedwick et al., 2000, 2007b) , yet the extent to which this occurs has not yet been described. Also, the taxonomic heterogeneity (Arrigo et al., 1999; DiTullio and Smith, 1996; Smith and Asper, 2001) provided a unique opportunity to examine the rapid responses within the two distinctly different groups *in situ*. The results demonstrated a high degree of variability across the Ross Sea, which could be further linked to the seasonal succession of the phytoplankton community. Dependent on whether diatoms or *Phaeocystis* were dominant, the extent to which unbound pigment-protein complexes are rapidly incorporated and F_v/F_m increases would be affected. One hypothesis to explain this is whether the phytoplankton exhibit a 'n'-type or 'sigma'-type response (Falkowski and Owens, 1980; Strzepek et al., 2012). A 'n-type' response, increasing the number of photosynthetic units, is a generalist strategy that enables an ecotype to exploit a wide range of irradiances. Whereas, a 'sigma-type' response, increasing the size of photosynthetic units, is more specialised and confines the ecotype to a narrower range of irradiances. Conversely, by employing a 'n-type' strategy to cope with large fluctuations in irradiance will result in an increase in the intra-cellular iron requirements which may limit the distribution and specific growth rate of this ecotype. Strzepek et al. (2012) demonstrated in culture experiments that *Phaeocystis antarctica* and Southern Ocean diatoms employ a 'sigma-type'

response. However it was noted that the Southern Ocean diatoms contained less cellular chlorophyll, thereby overcoming the potential problem of decreased light absorption and reductions in photochemical efficiency due to self-shading. The biophysical measurements of this unique phytoplankton community, placed within the seasonal context of the Ross Sea, reaffirm the idea that rapid responses provide a powerful diagnostic tool for studying iron limitation within the ocean.

In order to verify the presence of unbound chlorophyl-binding proteins molecular markers needed to be developed for use in the field. One such method for achieving this may be by examining the biomolecular structure of IsiA and Tidi, 2 known chlorophyll-binding proteins, to determine any potential similarity in genetic markers for a molecular probe. By combining the use of novel molecular probes with the continued use of biophysical measurements the abundance of unbound chlorophyll in the field can be established. By measuring this abundance across different nutrient regimes it can be determine whether or not current primary productivity measurements are accurate.

6.1 Conclusion

This thesis aimed to reconcile the physiological response of phytoplankton to iron addition experiments. By combining photophysiology data from culture and field experiments with *in situ* measurements of photophysiology, a comprehensive picture of the underlying basis of biophysical measurements has been constructed.

The biophysical datasets collected throughout this thesis allowed a deeper understanding of the basis of biophysical measurements. Originally a depressed F_v/F_m was thought to be a result of a decreased F_v value, yet it became clear that this was not the case. Instead, an elevated F_o value is responsible for a depressed F_v/F_m under iron limitation. Data presented in iron limitation experiments in a culture study and iron addition experiments in the field demonstrated consistently that under iron limitation F_o is the dominant factor resulting in a depressed F_v/F_m. Further analysis of this work hinted that an elevated F_o may be the result of unbound light-harvesting complexes. IsiA, a PSI antenna pigment-protein complex in cyanobacteria expressed under iron limitation, was found to be overexpressed under severe iron limitation and therefore could be energetically disconnected from photosynthesis. Evidence has suggested that similar

proteins may be present within eukaryotes, however these proteins are yet to be detected in the field. If phytoplankton express pigment-protein complexes to such a degree that they are disconnected from photosynthesis, then a reevaluation of interpreting fluorescence measurements in the field are required. Fluorescence measurements have become a powerful diagnostic tool for investigating iron limitation in the field and determining the photochemical efficiency across several different phytoplankton species and oceanic regions. Yet the role of unbound pigment-protein complexes in interpreting fluorescence measurements is only starting to be understood.

Appendix A

IsiA Experiment Summary

Table A.1: IsiA Experiment Summary 1 - Physiology (*Blank and Gain Corrected)

Expt.	Treatment	Time (Day)	σ_{PSI}	Spectral Shift	F_o*	F_m*	F_v*	F_v/F_m	Chl (μg L^{-1})	Cell No. (cells ml^{-1})
1	+ Fe	1	1.18	677.96	237884	433760	195876	0.401	0.191	202149
1	+ Fe	2	1.18	679.97	377905	699925	322020	0.420	0.639	296346
1	+ Fe	3	1.21	679.97	402144	674155	272011	0.473	1.904	847764
1	+ Fe	4	1.28	679.96	411755	705312	293557	0.477	7.187	1457076
1	- Fe	1	1.20	677.96	201764	354457	152693	0.387	0.111	239316
1	- Fe	2	1.44	673.00	431112	715319	284208	0.359	0.465	213857
1	- Fe	3	1.91	673.00	735024	1214021	478997	0.288	0.911	540527
1	- Fe	4	1.83	671.97	1151216	1738207	586991	0.241	1.175	739267
2	+ Fe	1	1.45	679.99	61987	104105	42118	0.397	0.359	148062
2	+ Fe	2	1.20	679.97	245031	420251	175221	0.409	1.692	185701
2	+ Fe	3	0.95	680.98	405592	758076	352485	0.462	3.178	696927
2	+ Fe	4	1.15	679.96	425334	777512	352178	0.450	4.640	882898
2	- Fe	1	1.43	678.97	55259	91909	36650	0.402	0.305	155162
2	- Fe	2	1.56	673.00	291907	469492	177585	0.402	0.898	141638
2	- Fe	3		673.00	709405	1023131	313726	0.322	2.072	449553
2	- Fe	4	1.56	672.99	995316	1347831	352515	0.266	2.634	554573
3	+ Fe	1	1.24	678.97	60010	106405	46395	0.436	0.255	172988
3	+ Fe	2	1.24	678.95	242187	452582	210395	0.465	1.025	214080
3	+ Fe	3	1.21	679.97	431013	803988	372975	0.464	3.535	793467
3	+ Fe	4	0.98	678.94	480782	885797	405016	0.457	4.493	1320519
3	- Fe	1	1.22		42297	76272	33975	0.445	0.164	109591
3	- Fe	2	1.71	673.00	192449	324671	132222	0.379	0.436	68988
3	- Fe	3	1.90	673.00	502865	699214	196349	0.281	0.816	202915
3	- Fe	4		671.97	660190	888349	228159	0.257	0.964	268901

TABLE A.2: IsiA Experiment Summary - Protein (**Undetectable)

Expt.	Treatment	Time (Day)	IsiA:chl (mol mol^{-1})	PsaC:chl (mol mol^{-1})	PsbA:chl (mol mol^{-1})	IsiA:TP (pmol μg^{-1})	PsaC:TP (pmol μg^{-1})	PsbA:TP (pmol μg^{-1})
1	+ Fe	1	**	0.0091	0.0083	**	0.0176	0.0159
1	+ Fe	2	**	0.0038	0.0021	**	0.0186	0.0105
1	+ Fe	3	**	0.0023	0.0012	**	0.0279	0.0143
1	+ Fe	4	**	0.0034	0.0013	**	0.0207	0.0082
1	- Fe	1	**	0.0115	0.0017	**	0.0390	0.0057
1	- Fe	2	0.0148	0.0029	0.0006	0.0643	0.0126	0.0026
1	- Fe	3	0.0579	0.0022	0.0004	0.3275	0.0121	0.0021
1	- Fe	4	0.1689	0.0038	0.0006	0.2309	0.0052	0.0008
2	+ Fe	1	**	0.0093	0.0009	**	0.1524	0.0152
2	+ Fe	2	**	0.0026	0.0004	**	0.0512	0.0080
2	+ Fe	3	**	0.0003	0.0003	**	0.0084	0.0080
2	+ Fe	4	**	0.0097	0.0004	**	0.2033	0.0078
2	- Fe	1	**	0.0047	0.0036	**	0.0608	0.0491
2	- Fe	2	0.0154	0.0051	0.0031	0.1890	0.0629	0.0681
2	- Fe	3	0.0449	0.0057	0.0019	0.3666	0.0464	0.0664
2	- Fe	4	0.0853	0.0053	0.0015	0.7226	0.0452	0.0450
3	+ Fe	1	**	0.0012	0.0001	**	0.0060	0.0006
3	+ Fe	2	**	0.0023	0.0006	**	0.0352	0.0093
3	+ Fe	3	**	0.0027	0.0006	**	0.0153	0.0032
3	+ Fe	4	**	0.0018	0.0005	**	0.0722	0.0219
3	- Fe	1	**	**	**	**	**	0.0250
3	- Fe	2	0.0221	0.0042	0.0058	0.2039	0.0385	0.0539
3	- Fe	3	0.0314	0.0027	0.0036	0.3250	0.0283	0.0372
3	- Fe	4	0.0267	0.0014	0.0025	0.6386	0.0325	0.0594

Appendix B

HLNA Experiment Summary

Table B.1: HLNA Long-Term Experiment Summary Metadata.

Cruise	Experiment	DOY	Time (GMT)	Lat °N	Lon °W
D350	1	121	02:00	60.9712	-34.8567
D350	2	124	03:00	59.9945	-29.1957
D354	1	193	02:22	59.9938	-19.9051
D354	2	195	01:18	59.9999	-20.4745
D354	3	198	02:50	60.0016	-34.3769
D354	4	204	01:05	63.0273	-35.2885
D354	5	208	02:41	58.1550	-35.0315
D354	6	212	01:27	63.8401	-34.7382
D354	7	216	02:04	61.3675	-21.1584

The following lists the associated variables with their respective units for each long-term and short-term experiment summary.

F_o, F_m, F_v (blank and gain corrected)- a.u.

F_v/F_m - a.u.

σ_{PSII} - nm^{-2}

Chlorophyll - $\mu g\ L^{-1}$

DIN - $\mu mol\ L^{-1}$

Silicate - $\mu mol\ L^{-1}$

Phosphate - $\mu mol\ L^{-1}$

B.1 D350 Long-Term Experiment Summary

Table B.2: D350 Experiment 1 Summary.

Bottle	Treatment	Time (h)	σ_{PSII}	F_o	F_m	F_v	F_v/F_m	Chl	DIN	Phosphate	Silicate
	Initial	0	2.120	1024.600	1611.465	586.865	0.364	0.285	14.760	0.676	5.500
	Initial	0	1.880	1506.047	2634.540	1128.493	0.428	0.560	13.820	0.579	4.950
	Initial	0	1.970	1680.935	2610.912	929.977	0.356	0.475	13.760	0.603	4.990
4	Fe	24	1.700	808.383	1918.346	1109.963	0.579	0.488	13.780	0.766	4.930
5	Fe	24	1.600	844.133	1997.507	1153.374	0.577	0.480	13.880	0.786	5.180
12	Control	24	1.830	877.330	2075.817	1198.487	0.577	0.427	13.750	0.766	4.900
13	Control	24	1.740	881.586	2208.604	1327.018	0.601	0.471	13.960	0.768	5.170
4	Fe	72	2.440	2338.907	4630.541	2291.634	0.495	0.611	13.420	0.763	4.910
5	Fe	72	2.520	2544.874	5056.873	2511.999	0.497	0.649	13.610	0.795	5.110
12	Control	72	2.580	3145.978	4602.546	1456.568	0.316	0.547	13.490	0.821	4.880
13	Control	72	2.440	3155.177	4920.095	1764.918	0.359	0.635	13.650	0.730	5.180
1	Fe	120	1.970	4295.092	8667.563	4372.471	0.504	1.514	12.610	n/a	5.050
2	Fe	120	1.930	4065.187	8061.987	3996.800	0.496	1.404	12.610	n/a	4.990
3	Fe	120	2.010	3970.867	7841.729	3870.862	0.494	1.276	12.830	n/a	5.020
4	Fe	120	2.050	3474.617	6275.807	2801.190	0.446	0.996	12.970	n/a	5.010
5	Fe	120	2.140	4379.229	8373.885	3994.656	0.477	1.123	12.890	n/a	5.030
9	Control	120	2.080	4179.335	7820.829	3641.493	0.466	0.880	12.890	n/a	4.760
10	Control	120	2.140	2728.097	3842.249	1114.152	0.290	0.570	13.040	n/a	4.860
11	Control	120	2.100	3791.338	6009.460	2218.122	0.369	0.412	13.130	n/a	5.070
12	Control	120	2.140	2445.674	3421.562	975.888	0.285	0.776	13.040	n/a	4.750
13	Control	120	2.050	3024.990	3937.105	912.115	0.232	0.614	13.290	n/a	5.210

TABLE B.3: D350 Experiment 2 Summary.

Bottle	Treatment	Time (h)	σ_{PSII}	F_o	F_m	F_v	F_v/F_m	Chl	DIN	Phosphate	Silicate
	Initial	0	2.100	4545.399	8633.704	4088.305	0.474	1.070	11.440	0.662	5.040
	Initial	0	2.030	4747.133	8937.582	4190.449	0.469	1.241	11.660	0.682	5.350
	Initial	0	2.010	4309.617	8484.745	4175.128	0.492	1.311	11.680	0.662	5.400
4	Fe	24	1.680	3042.315	6011.841	2969.526	0.494	1.098	11.010	n/a	5.030
5	Fe	24	1.650	3197.490	6243.404	3045.914	0.488	1.135	11.020	n/a	5.050
12	Control	24	1.670	4547.275	8755.004	4207.729	0.481	1.330	11.010	n/a	5.030
13	Control	24	1.700	3685.812	7248.444	3562.632	0.492	1.426	11.170	n/a	5.030
4	Fe	72	1.940	7520.771	14609.965	7089.194	0.485	1.584	9.640	0.530	4.050
5	Fe	72	2.040	10072.504	18324.363	8251.859	0.450	1.576	9.490	0.531	3.550
12	Control	72	2.140	9526.546	17004.868	7478.321	0.440	1.876	9.560	0.513	3.720
13	Control	72	1.940	8809.609	16793.795	7984.187	0.475	1.543	9.820	0.533	3.960
1	Fe	120	2.240	14795.411	24416.092	9620.681	0.394	3.612	8.220	0.463	3.030
2	Fe	120	2.030	11302.023	19031.442	7729.419	0.406	2.812	6.770	0.400	1.720
3	Fe	120	2.210	13393.303	22200.048	8806.745	0.397	2.195	6.850	0.383	1.350
4	Fe	120	2.350	20425.628	37054.870	16629.242	0.449	2.222	8.330	0.475	2.880
5	Fe	120	2.250	22406.007	36534.031	14128.023	0.387	2.013	8.240	0.446	3.160
9	Control	120	2.310	14593.412	23816.037	9222.625	0.387	2.829	7.600	0.373	2.200
10	Control	120	2.270	13019.011	20724.666	7705.654	0.372	3.817	6.450	0.347	1.320
11	Control	120	2.150	16755.986	27582.718	10826.732	0.393	3.347	6.870	0.346	1.740
12	Control	120	2.480	22643.653	37005.361	14361.708	0.388	2.352	8.150	0.361	2.460
13	Control	120	2.380	19932.514	34345.712	14413.198	0.420	1.904	8.700	0.447	2.710

B.2 D354 Long-Term Experiment Summary

TABLE B.4: D354 Experiment 1 Summary.

Bottle	Treatment	Time (h)	σ_{PSII}	F_o	F_m	F_v	F_v/F_m	Chl	Chl >5μm	Chl <5μm	DIN	Phosphate	Silicate
	Initial	0	1.690	4461.432	5221.349	759.917	0.146	0.431	0.480	-0.050	0.670	0.090	0.620
	Initial	0	1.730	3871.398	4602.912	731.514	0.159	0.293	0.395	-0.102	1.200	0.100	0.610
	Initial	0	1.650	7183.307	9242.801	2059.493	0.223	1.366	0.536	0.830	0.250	0.100	0.830
1	Fe	48	1.960	3815.247	5926.754	2111.507	0.356	1.073	0.456	0.617	0.000	0.050	0.830
2	Fe	48	1.760	3480.824	5284.151	1803.327	0.341	0.971	0.405	0.565	0.000	0.050	0.810
3	Fe	48	1.930	3743.922	5691.918	1947.997	0.342	1.080	0.396	0.684	0.000	0.050	0.800
4	FeN	48	1.740	4719.602	7495.918	2776.316	0.370	1.823	0.547	1.275	1.240	0.050	0.830
5	FeN	48	1.700	4576.951	7116.412	2539.461	0.357	1.403	0.525	0.877	1.420	0.40	0.770
6	FeN	48	1.680	4354.899	7031.628	2676.729	0.381	1.756	0.567	1.189	1.390	0.040	0.760
7	N	48	1.720	5276.749	7662.793	2386.043	0.311	1.019	0.558	0.462	1.600	0.040	0.780
8	N	48	1.940	5163.705	7520.141	2356.437	0.313	1.195	0.454	0.741	1.710	0.040	0.750
9	N	48	1.790	5212.152	7466.311	2254.158	0.302	1.070	0.512	0.558	1.770	0.040	0.760
10	Control	48	1.910	4052.102	6232.243	2180.141	0.350	0.978	0.543	0.435	0.000	0.050	0.760
11	Control	48	1.830	3908.778	5731.618	1822.840	0.318	0.796	0.429	0.367	0.020	0.050	0.770
12	Control	48	1.840	4191.389	6126.601	1935.212	0.316	0.880	0.513	0.367	0.000	0.050	0.740

Table B.5: D354 Experiment 2 Summary.

Bottle	Treatment	Time (h)	σ_{PSII}	F_o	F_m	F_v	F_v/F_m	Chl	Chl >5μm	Chl <5μm	DIN	Phosphate	Silicate
	Initial	0	1.850	4943.672	7516.777	2573.105	0.342	1.241	0.636	0.605	0.020	0.050	0.720
	Initial	0	1.890	8783.143	13755.749	4972.606	0.361	1.972	0.697	1.275	0.470	0.080	0.910
	Initial	0	1.840	7913.105	12188.604	4275.499	0.351	1.667	0.612	1.055	0.370	0.070	0.880
1	Fe	24	1.670	5220.900	8538.886	3317.987	0.389	1.421	n/a	n/a	0.000	0.040	0.820
2	Fe	24	1.670	5181.200	8378.740	3197.540	0.382	1.395	n/a	n/a	0.000	0.040	0.810
3	Fe	24	1.630	4767.377	7647.989	2880.613	0.377	1.390	n/a	n/a	0.000	0.040	0.740
4	FeN	24	1.740	6664.907	10694.804	4029.897	0.377	1.987	n/a	n/a	1.920	0.040	0.910
5	FeN	24	1.770	6487.939	10642.992	4155.053	0.390	2.090	n/a	n/a	1.950	0.040	0.860
6	FeN	24	1.790	5984.622	9711.049	3726.427	0.384	1.760	n/a	n/a	1.940	0.040	0.820
7	N	24	1.770	6716.719	10307.223	3590.504	0.348	0.404	n/a	n/a	1.870	0.030	0.780
8	N	24	1.810	7057.871	10565.610	3507.740	0.332	1.554	n/a	n/a	1.790	0.040	0.730
9	N	24	1.770	6202.636	9612.808	3410.172	0.355	1.661	n/a	n/a	1.850	0.040	0.730
10	Control	24	1.700	5289.534	8348.461	3058.927	0.366	1.246	n/a	n/a	0.000	0.050	0.810
11	Control	24	1.700	4852.833	7692.400	2839.567	0.369	1.392	n/a	n/a	0.000	0.040	0.760
12	Control	24	1.680	5563.397	8666.734	3103.337	0.358	1.405	n/a	n/a	0.000	0.040	0.740
1	Fe	48	1.630	5068.828	8032.878	2964.050	0.369	1.398	0.586	0.812	0.000	0.040	0.740
2	Fe	48	1.650	4647.604	7504.665	2857.062	0.381	1.313	0.683	0.630	0.000	0.040	0.740
3	Fe	48	1.610	4696.724	7587.430	2890.706	0.381	1.275	0.647	0.628	0.000	0.040	0.760
4	FeN	48	1.570	7322.314	12510.915	5188.602	0.415	2.443	1.090	1.353	0.710	0.030	0.840
5	FeN	48	1.610	7082.095	12189.277	5107.183	0.419	2.337	1.063	1.274	0.920	0.050	0.730
6	FeN	48	1.620	6870.809	11997.506	5126.696	0.427	2.220	1.093	1.127	1.000	0.030	0.680
7	N	48	1.700	7852.546	11792.276	3939.731	0.334	1.525	0.798	0.727	1.290	0.030	0.700
8	N	48	1.620	7238.203	10898.688	3660.484	0.336	1.415	0.658	0.757	1.160	0.040	0.660
9	N	48	1.750	7354.612	11238.493	3883.881	0.346	1.619	0.712	0.908	1.120	0.030	0.700
10	Control	48	1.690	5902.531	8853.123	2950.592	0.333	1.310	0.538	0.772	0.000	0.040	0.800
11	Control	48	1.720	6399.118	9572.435	3173.317	0.332	1.225	0.628	0.597	0.000	0.050	0.730
12	Control	48	1.710	5654.237	8341.732	2687.495	0.322	1.292	0.586	0.706	0.000	0.040	0.730

TABLE B.6: D354 Experiment 3 Summary.

Bottle	Treatment	Time (h)	σ_{PSII}	F_o	F_m	F_v	F_v/F_m	Chl	Chl >5μm	Chl <5μm	DIN	Phosphate	Silicate
	Initial	0	1.840	13459.140	18998.726	5539.585	0.292	2.533	1.134	1.399	3.450	0.270	1.740
	Initial	0	1.890	11787.006	16930.357	5143.351	0.304	2.133	1.321	0.812	3.890	0.310	1.960
	Initial	0	1.980	12848.760	18565.305	5716.544	0.308	2.303	1.520	0.783	3.990	0.310	1.820
1	Fe	24	1.750	9539.379	14405.680	4866.301	0.338	2.323	n/a	n/a	3.530	0.270	1.750
2	Fe	24	1.740	9491.712	13795.371	4303.659	0.312	2.075	n/a	n/a	3.580	0.280	1.670
6	Ash (2.0 mg)	24	1.850	8100.854	11106.435	3005.581	0.271	1.713	n/a	n/a	3.830	0.300	1.760
7	Ash (2.0 mg)	24	1.670	8033.610	10894.487	2860.878	0.263	1.618	n/a	n/a	3.960	0.310	1.880
11	Control	24	1.610	6176.295	7962.109	1785.814	0.224	1.360	n/a	n/a	3.890	0.320	1.800
12	Control	24	1.820	11135.592	15939.131	4803.539	0.301	2.219	n/a	n/a	3.580	0.270	1.710
1	Fe	72	1.650	13442.812	21827.737	8384.924	0.384	3.952	n/a	n/a	1.630	0.140	1.220
2	Fe	72	1.730	11847.275	18130.601	6283.326	0.347	3.147	n/a	n/a	2.780	0.180	1.260
6	Ash (2.0 mg)	72	1.720	7110.417	9642.982	2532.565	0.263	1.537	n/a	n/a	3.650	0.260	1.790
7	Ash (2.0 mg)	72	1.720	6524.400	9054.401	2530.000	0.279	1.341	n/a	n/a	3.780	0.260	1.900
11	Control	72	1.750	4626.580	6062.768	1436.189	0.237	1.057	n/a	n/a	3.810	0.300	1.850
12	Control	72	1.870	14501.660	20332.330	5830.670	0.287	2.459	n/a	n/a	2.970	0.220	1.270
1	Fe	120	1.760	17292.669	31185.027	13892.358	0.445	5.822	3.200	2.622	0.180	0.040	0.410
2	Fe	120	1.820	16890.652	29232.374	12341.722	0.422	5.948	4.472	1.475	0.650	0.080	0.410
3	Fe	120	1.740	16078.697	29034.336	12955.639	0.446	5.793	4.058	1.734	0.000	0.050	0.410
4	Fe	120	1.730	15625.190	28586.770	12961.580	0.453	5.535	3.950	1.585	0.020	0.060	0.540
5	Fe	120	1.750	6492.941	10212.677	3719.737	0.364	2.100	1.309	0.791	3.220	0.200	1.620
6	Ash (2.0 mg)	120	1.910	7297.323	10683.390	3386.067	0.317	1.593	0.906	0.687	3.860	0.250	1.810
7	Ash (2.0 mg)	120	1.900	7378.187	10978.756	3600.569	0.328	1.492	3.470	-1.978	3.900	0.260	1.900
8	Ash (2.0 mg)	120	2.200	15076.625	22487.203	7410.578	0.330	2.782	2.029	0.752	2.420	0.200	0.950
9	Ash (2.0 mg)	120	2.020	16233.166	25111.205	8878.039	0.354	3.010	1.835	1.174	2.150	0.180	0.740
10	Ash (2.0 mg)	120	2.000	16506.458	26913.350	10406.891	0.387	4.009	2.766	1.243	1.130	0.130	0.520
11	Control	120	1.950	4261.018	6099.217	1838.199	0.301	0.921	0.504	0.417	3.770	0.340	1.890
12	Control	120	2.210	19118.578	28398.634	9280.056	0.327	3.140	2.074	1.066	2.350	0.180	0.700
13	Control	120	2.120	15581.621	22918.925	7337.304	0.320	2.451	1.674	0.777	2.390	0.160	0.890
14	Control	120	2.140	14613.216	21885.168	7271.951	0.332	2.547	1.568	0.979	2.480	0.200	1.100
15	Control	120	1.940	4026.477	5760.115	1733.638	0.301	0.990	0.531	0.459	3.750	0.330	1.860

Table B.7: D354 Experiment 4 Summary.

Bottle	Treatment	Time (h)	σ_{PSII}	F_o	F_m	F_v	F_v/F_m	Chl	Chl >5μm	Chl <5μm	DIN	Phosphate	Silicate
	Initial	0	1.860	9163.397	12873.124	3709.727	0.288	1.162	0.371	0.791	4.840	0.360	1.950
	Initial	0	1.930	9519.880	13424.518	3904.638	0.291	1.160	0.468	0.692	4.310	0.330	1.970
	Initial	0	1.980	9810.965	13537.361	3726.397	0.275	1.204	0.385	0.819	4.770	0.360	1.950
1	Fe	24	1.880	5830.708	9322.324	3491.615	0.375	1.523	n/a	n/a	4.110	0.300	1.910
2	Fe	24	1.940	5821.345	9549.594	3728.249	0.390	1.377	n/a	n/a	4.250	0.310	1.910
6	Ash (9.0 mg)	24	2.000	7522.039	10952.369	3430.329	0.313	1.208	n/a	n/a	4.390	0.320	1.920
7	Ash (9.0 mg)	24	2.000	7782.506	11417.974	3635.468	0.318	1.222	n/a	n/a	4.350	0.320	1.910
11	Control	24	2.040	7703.345	11080.900	3377.555	0.305	1.219	n/a	n/a	4.440	0.330	1.920
12	Control	24	2.000	8099.152	11549.059	3449.907	0.299	1.179	n/a	n/a	4.420	0.340	1.920
22	Ash (2.0 mg)	24	1.980	8426.012	12238.529	3812.517	0.312	1.412	n/a	n/a	4.350	0.310	1.890
23	Ash (2.0 mg)	24	2.010	7085.375	10685.092	3599.718	0.337	1.323	n/a	n/a	4.290	0.300	1.880
1	Fe	72	1.730	9208.278	16096.855	6888.577	0.428	2.569	n/a	n/a	2.770	0.220	1.660
2	Fe	72	1.770	8597.898	15546.743	6948.845	0.447	2.481	n/a	n/a	3.070	0.240	1.580
6	Ash (9.0 mg)	72	2.000	6997.701	9999.026	3001.325	0.300	1.084	n/a	n/a	3.780	0.270	1.730
7	Ash (9.0 mg)	72	1.920	8293.225	12167.029	3873.803	0.318	1.273	n/a	n/a	3.670	0.270	1.670
11	Control	72	2.070	8653.282	12553.473	3900.191	0.311	1.110	n/a	n/a	3.930	0.300	1.750
12	Control	72	2.070	8597.954	12122.766	3524.812	0.291	0.962	n/a	n/a	4.190	0.320	1.820
22	Ash (2.0 mg)	72	2.030	8776.706	12553.473	3776.767	0.301	1.108	n/a	n/a	3.810	0.280	1.720
23	Ash (2.0 mg)	72	2.000	9215.924	13883.896	4667.972	0.336	1.362	n/a	n/a	3.600	0.250	1.670
1	Fe	120	1.920	14187.493	26661.819	12474.325	0.468	4.782	3.090	1.692	0.670	0.110	0.910
2	Fe	120	1.920	15037.666	28481.419	13443.753	0.472	5.033	3.360	1.673	0.690	0.120	0.780
3	Fe	120	1.860	14395.228	26837.495	12442.268	0.464	4.727	2.984	1.743	0.470	0.100	0.920
4	Fe	120	1.880	14974.833	27758.195	12783.362	0.461	4.844	3.168	1.676	0.230	0.090	0.830
5	Fe	120	1.820	14401.639	27331.185	12929.546	0.473	4.789	2.612	2.177	0.530	0.110	0.890
6	Ash (9.0 mg)	120	2.250	9003.108	14074.650	5071.542	0.360	1.571	1.128	0.444	3.150	0.250	1.310
7	Ash (9.0 mg)	120	2.240	9255.724	13940.007	4684.284	0.336	1.794	1.165	0.628	3.090	0.310	1.220
8	Ash (9.0 mg)	120	2.050	9749.414	15033.819	5284.405	0.352	1.746	0.995	0.751	3.250	0.260	1.360
9	Ash (9.0 mg)	120	2.110	11234.330	17686.921	6452.591	0.365	2.093	1.280	0.813	2.990	0.230	1.350
10	Ash (9.0 mg)	120	2.010	12344.812	19993.799	7648.988	0.383	2.430	1.453	0.977	2.630	0.220	1.270
11	Control	120	2.170	8706.894	13114.199	4407.304	0.336	1.283	0.720	0.563	3.720	0.310	1.480
12	Control	120	1.990	7414.325	10576.504	3162.180	0.299	0.943	0.468	0.475	4.170	0.340	1.690
13	Control	120	2.170	9457.047	13396.307	3939.261	0.294	1.116	0.717	0.399	3.960	0.290	1.630
14	Control	120	2.200	9628.876	13741.249	4112.373	0.299	1.124	0.615	0.509	3.620	0.280	1.600
15	Control	120	2.170	8601.745	12521.771	3920.026	0.313	1.373	0.732	0.642	3.920	0.310	1.540
22	Ash (2.0 mg)	120	2.150	9936.631	14599.115	4662.484	0.319	1.403	0.751	0.651	3.670	0.280	1.420
23	Ash (2.0 mg)	120	2.090	10673.960	15769.866	5095.906	0.323	1.612	0.869	0.743	3.070	0.250	1.360
24	Ash (2.0 mg)	120	2.260	918.264	1166.661	248.398	0.213	0.133	0.100	0.033	4.300	0.380	1.880
25	Ash (2.0 mg)	120	2.170	11261.259	16853.419	5592.160	0.332	1.502	0.815	0.687	3.280	0.260	1.280
26	Ash (2.0 mg)	120	2.130	3968.754	5640.888	1672.134	0.296	0.666	0.205	0.462	4.430	0.340	1.910

Table B.8: D354 Experiment 5 Summary.

Bottle	Treatment	Time (h)	σ_{PSII}	F_o	F_m	F_v	F_v/F_m	Chl	Chl >5μm	Chl <5μm	DIN	Phosphate	Silicate
	Initial	0	1.980	9851.999	14826.084	4974.086	0.335	1.774	1.002	0.772	4.220	0.310	2.010
	Initial	0	1.770	9894.315	14833.778	4939.464	0.333	1.674	0.825	0.849	4.300	0.320	2.010
	Initial	0	1.850	9295.475	14068.238	4772.763	0.339	1.803	0.891	0.912	4.290	0.310	1.980
13	Fe	24	1.940	6942.434	11229.201	4286.767	0.382	1.777	n/a	n/a	4.100	0.300	1.810
14	Fe	24	1.890	6829.591	11135.592	4306.002	0.387	1.682	n/a	n/a	4.050	0.290	1.820
15	Fe	24	1.860	6352.571	10280.291	3927.720	0.382	1.588	n/a	n/a	4.000	0.320	1.820
4	Fe+N	24	1.940	7098.876	11693.398	4594.522	0.393	1.810	n/a	n/a	6.360	0.530	2.150
5	Fe+N	24	1.800	6997.573	11431.806	4434.233	0.388	1.745	n/a	n/a	6.270	0.300	1.860
6	Fe+N	24	1.960	7260.447	11930.625	4670.178	0.391	1.650	n/a	n/a	6.380	0.480	1.850
7	N	24	2.090	9132.622	13583.525	4450.903	0.328	1.385	n/a	n/a	6.370	0.300	1.840
8	N	24	2.070	8511.983	12670.519	4158.536	0.328	1.435	n/a	n/a	6.270	0.300	1.810
9	N	24	2.010	8808.197	13141.127	4332.930	0.330	1.511	n/a	n/a	6.400	0.290	1.810
16	Control	24	1.940	9296.758	13992.582	4695.824	0.336	1.512	n/a	n/a	4.110	0.300	1.830
17	Control	24	n/a	n/a	n/a	n/a	n/a	n/a	n/a	n/a	n/a	n/a	n/a
18	Control	24	1.980	8842.819	13064.189	4221.369	0.323	1.476	n/a	n/a	4.120	0.290	1.790
1	Fe	72	1.750	10767.569	19743.749	8976.180	0.455	3.869	3.121	0.748	2.640	0.250	1.020
2	Fe	72	1.670	10382.875	19067.971	8685.095	0.455	3.446	2.177	1.269	2.880	0.210	1.070
3	Fe	72	1.700	11533.109	21111.975	9578.866	0.454	3.572	2.518	1.053	2.630	0.240	1.000
4	Fe+N	72	1.680	11904.979	21626.182	9721.203	0.450	3.779	2.752	1.027	4.870	0.200	1.000
5	Fe+N	72	1.650	11998.588	21587.712	9589.125	0.444	3.155	2.610	0.546	5.280	0.210	1.010
6	Fe+N	72	1.610	10806.038	19380.855	8574.816	0.442	3.498	2.350	1.148	5.160	0.210	1.110
7	N	72	2.080	12355.070	18280.631	5925.561	0.324	1.810	1.334	0.475	6.100	0.240	1.390
8	N	72	2.070	12457.655	18444.767	5987.112	0.325	1.800	1.614	0.186	5.990	0.260	1.350
9	N	72	2.090	13264.229	19741.184	6476.955	0.328	1.919	1.537	0.382	6.080	0.260	1.380
10	Control	72	2.100	13300.134	19612.953	6312.819	0.322	1.808	1.445	0.363	3.770	0.260	1.350
11	Control	72	2.020	12765.410	19171.838	6406.428	0.334	1.914	1.607	0.307	3.730	0.250	1.350
12	Control	72	2.140	13775.871	19833.510	6057.639	0.305	1.777	1.411	0.366	3.720	0.270	1.370

TABLE B.9: D354 Experiment 6 Summary.

Bottle	Treatment	Time (h)	σ_{PSII}	F_o	F_m	F_v	F_v/F_m	Chl	Chl >5μm	Chl <5μm	DIN	Phosphate	Silicate
	Initial	0	2.010	10394.416	14351.629	3957.213	0.276	1.492	0.390	1.102	5.630	0.410	2.040
	Initial	0	2.040	10516.236	14751.710	4235.475	0.287	1.497	0.385	1.112	5.140	0.390	2.120
	Initial	0	2.170	10768.851	15081.264	4312.413	0.286	1.507	0.416	1.092	4.960	0.520	2.080
1	Fe	24	2.030	6406.970	10481.656	4074.686	0.389	1.706	n/a	n/a	5.050	0.390	1.670
2	Fe	24	1.970	6382.285	10678.283	4295.998	0.402	1.723	n/a	n/a	5.250	0.390	1.610
6	Ash (9.0 mg)	24	2.140	7418.193	11185.597	3767.404	0.337	1.499	n/a	n/a	5.060	0.400	1.620
7	Ash (9.0 mg)	24	2.130	7932.317	12207.886	4275.569	0.350	1.556	n/a	n/a	5.040	0.400	1.630
11	Control	24	2.070	9334.241	13389.349	4055.109	0.303	1.418	n/a	n/a	5.180	0.410	1.640
12	Control	24	2.100	9040.577	12944.173	3903.595	0.302	1.406	n/a	n/a	5.000	0.390	1.620
27	Fe + Ash (9.0 mg)	24	2.010	6628.281	10883.422	4255.140	0.391	1.716	n/a	n/a	5.040	0.390	1.650
28	Fe + Ash (9.0 mg)	24	2.060	6350.791	10351.423	4000.632	0.386	1.672	n/a	n/a	4.990	0.400	1.600
1	Fe	72	1.890	9551.938	17235.548	7683.610	0.446	3.341	n/a	n/a	2.290	0.180	0.890
2	Fe	72	1.910	9155.703	16685.436	7529.733	0.451	3.586	n/a	n/a	3.650	0.330	1.380
6	Ash (9.0 mg)	72	2.110	9163.397	15105.628	5942.231	0.393	2.198	n/a	n/a	3.870	0.310	1.290
7	Ash (9.0 mg)	72	2.070	9398.060	14747.863	5349.803	0.363	1.915	n/a	n/a	4.270	0.350	1.440
11	Control	72	2.100	10077.685	14953.033	4875.348	0.326	1.701	n/a	n/a	2.670	0.180	0.780
12	Control	72	2.080	10448.273	15303.104	4854.831	0.317	1.718	n/a	n/a	2.980	0.170	0.920
27	Fe + Ash (9.0 mg)	72	1.890	9489.104	17425.330	7936.225	0.455	3.382	n/a	n/a	2.340	0.180	0.940
28	Fe + Ash (9.0 mg)	72	1.880	9135.186	16720.058	7584.872	0.454	3.597	n/a	n/a	3.190	0.290	1.320
1	Fe	120	1.930	23880.599	42225.127	18344.528	0.434	7.398	3.761	3.637	0.000	0.020	0.340
2	Fe	120	1.880	23078.498	41611.755	18533.257	0.445	7.441	3.919	3.522	0.000	0.110	0.500
3	Fe	120	1.770	19316.486	33870.692	14554.206	0.430	6.816	3.751	3.066	0.000	0.070	0.440
4	Fe	120	1.730	18923.299	34046.840	15123.541	0.444	6.556	3.371	3.184	0.130	0.200	0.690
5	Fe	120	1.810	20785.432	37730.214	16944.782	0.449	6.708	3.709	2.999	0.010	0.110	0.630
6	Ash (9.0 mg)	120	2.090	19383.949	30384.954	11001.005	0.362	3.303	1.402	1.901	1.730	0.140	0.580
7	Ash (9.0 mg)	120	2.070	18502.680	28612.515	10109.834	0.353	3.246	1.697	1.549	2.520	0.230	0.830
8	Ash (9.0 mg)	120	2.070	20784.077	32228.687	11444.610	0.355	3.694	1.877	1.817	1.550	0.130	0.560
9	Ash (9.0 mg)	120	2.010	18084.820	28339.223	10254.402	0.362	3.030	1.486	1.544	1.800	0.140	0.600
10	Ash (9.0 mg)	120	1.990	18029.370	27747.089	9717.719	0.350	3.148	1.681	1.467	1.950	0.140	0.560
11	Control	120	2.150	13629.688	19300.069	5670.381	0.294	1.741	3.546	-1.805	3.700	0.310	1.190
12	Control	120	2.050	15504.427	21872.386	6367.958	0.291	1.839	4.119	-2.280	3.960	0.330	1.190
13	Control	120	2.120	14120.813	19630.905	5510.092	0.281	1.578	3.924	-2.345	4.030	0.310	1.200
14	Control	120	2.000	14202.881	20046.374	5843.493	0.291	1.690	3.884	-2.194	4.000	0.330	1.280
15	Control	120	2.070	13675.851	19298.787	5622.936	0.291	1.681	3.744	-2.062	2.170	0.150	0.660
27	Fe + Ash (9.0 mg)	120	1.900	23449.666	42501.931	19052.264	0.448	6.750	0.961	5.789	0.000	0.000	0.310
28	Fe + Ash (9.0 mg)	120	1.810	21445.986	38790.246	17344.260	0.447	6.679	0.825	5.854	0.000	0.030	0.170
29	Fe + Ash (9.0 mg)	120	1.780	21065.381	37443.974	16378.593	0.437	6.374	0.643	5.730	0.000	0.070	0.270
30	Fe + Ash (9.0 mg)	120	1.750	18866.680	34147.495	15280.815	0.447	6.214	0.854	5.360	0.000	0.000	0.170
31	Fe + Ash (9.0 mg)	120	1.790	18998.791	34713.685	15714.894	0.453	6.164	0.952	5.212	0.000	0.100	0.520

TABLE B.10: D354 Experiment 7 Summary.

Bottle	Treatment	Time (h)	σ_{PSII}	F_o	F_m	F_v	F_v/F_m	Chl	Chl >5μm	Chl <5μm	DIN	Phosphate	Silicate
	Initial	0	1.740	4329.762	6794.174	2464.412	0.363	0.967	0.319	0.648	0.080	0.400	0.100
	Initial	0	1.840	4129.305	6578.119	2448.814	0.372	1.047	0.298	0.749	0.470	0.460	0.080
	Initial	0	1.870	4452.232	6924.154	2471.922	0.357	0.966	0.303	0.662	1.310	0.410	0.130
13	Fe	24	1.910	4306.655	7381.104	3074.449	0.417	1.002	n/a	n/a	0.130	0.460	0.040
14	Fe	24	1.720	3783.848	6338.379	2554.531	0.403	0.980	n/a	n/a	0.400	0.330	0.000
15	Fe	24	1.810	3842.195	6419.255	2577.061	0.401	0.921	n/a	n/a	0.110	0.210	0.000
4	Fe+N	24	1.920	3817.932	6462.004	2644.072	0.409	1.249	n/a	n/a	0.980	0.110	0.000
5	Fe+N	24	1.760	4017.234	6588.518	2571.284	0.390	1.174	n/a	n/a	2.460	0.440	0.050
6	Fe+N	24	1.870	4374.244	7222.240	2847.996	0.394	1.222	n/a	n/a	1.970	0.160	0.000
7	N	24	1.860	4880.876	7600.625	2719.749	0.358	1.016	n/a	n/a	2.690	0.450	0.070
8	N	24	1.830	5427.945	8496.617	3068.672	0.361	1.198	n/a	n/a	2.690	0.450	0.060
9	N	24	1.860	5229.221	8188.132	2958.912	0.361	1.014	n/a	n/a	2.600	0.470	0.040
16	Control	24	1.860	5033.963	7763.533	2729.570	0.352	1.062	n/a	n/a	0.470	0.500	0.070
17	Control	24	1.790	5147.189	7855.962	2708.773	0.345	1.125	n/a	n/a	0.400	0.470	0.040
18	Control	24	1.910	4463.208	7078.396	2615.188	0.369	1.167	n/a	n/a	0.060	0.180	0.000
13	Fe	48	1.700	4616.295	7483.354	2867.059	0.383	1.364	n/a	n/a	0.000	0.450	0.050
14	Fe	48	1.800	4364.424	7259.212	2894.788	0.399	1.408	n/a	n/a	0.040	0.480	0.060
15	Fe	48	1.670	4675.797	7712.696	3036.899	0.394	1.364	n/a	n/a	0.000	0.490	0.080
4	Fe+N	48	1.890	4593.188	7975.544	3382.356	0.424	1.598	n/a	n/a	2.130	0.470	0.050
5	Fe+N	48	1.790	4478.228	7661.282	3183.054	0.415	1.516	n/a	n/a	1.980	0.460	0.050
6	Fe+N	48	1.840	4925.357	8320.423	3395.065	0.408	1.596	n/a	n/a	3.290	0.580	0.120
7	N	48	1.720	5728.342	8698.230	2969.888	0.341	1.113	n/a	n/a	2.410	0.480	0.060
8	N	48	2.000	5263.882	8146.539	2882.657	0.354	1.062	n/a	n/a	2.350	0.470	0.060
9	N	48	1.820	5423.901	8247.634	2823.733	0.342	1.086	n/a	n/a	2.330	0.450	0.070
16	Control	48	1.760	5696.569	8499.506	2802.936	0.330	1.004	n/a	n/a	0.240	0.480	0.080
17	Control	48	1.800	5436.033	8119.388	2683.355	0.330	1.025	n/a	n/a	0.180	0.470	0.070
18	Control	48	1.830	4923.047	7513.972	2590.925	0.345	1.008	n/a	n/a	0.000	0.440	0.050
1	Fe	72	1.650	5062.847	8456.757	3393.910	0.401	1.393	0.578	0.815	0.000	0.450	0.050
2	Fe	72	1.750	4904.561	8543.987	3639.427	0.426	1.702	0.600	1.101	0.000	0.130	0.000
3	Fe	72	1.680	5158.743	8810.301	3651.558	0.414	1.660	0.517	1.143	0.000	0.460	0.050
4	Fe+N	72	1.650	5679.816	9779.082	4099.265	0.419	2.088	0.852	1.237	1.270	0.470	0.050
5	Fe+N	72	1.710	5705.235	9944.300	4239.066	0.426	1.988	0.770	1.218	1.650	0.450	0.040
6	Fe+N	72	1.720	6547.502	11557.779	5010.277	0.433	2.073	0.899	1.174	2.780	0.540	0.090
7	N	72	1.810	6435.431	9858.803	3423.372	0.347	1.167	0.458	0.709	1.860	0.340	0.020
8	N	72	1.750	6244.216	9484.461	3240.245	0.342	1.112	0.460	0.652	2.130	0.480	0.060
9	N	72	1.740	6225.153	9668.166	3443.013	0.356	1.188	0.465	0.723	1.860	0.400	0.040
10	Control	72	1.790	5637.645	8714.983	3077.337	0.353	1.070	0.399	0.671	0.000	0.490	0.060
11	Control	72	1.790	5857.166	9074.882	3217.715	0.355	1.155	0.474	0.682	0.050	0.250	0.000
12	Control	72	1.840	5473.582	8410.542	2936.960	0.349	1.060	0.434	0.626	0.100	0.320	0.010

B.3 D350 Short-Term Experiment Summary

TABLE B.11: D350 Short-Term Experiment Initial Conditions. (*Data not available.)

Experiment	DOY	Time (GMT)	Lat °N	Lon °W	F_v/F_m	Chl	DIN	Phosphate	Silicate
1	119	4:28	58.570	-21.808	0.447	1.852	9.120	0.585	1.890
2	120	4:42	59.724	-27.962	0.495	0.970	12.410	0.720	5.780
3	122	2:47	59.973	-35.001	0.458	0.611	13.080	0.516	3.693
4	123	2:11	59.989	-31.998	0.467	0.864	12.050	0.732	5.060
5	125	2:07	59.978	-26.234	0.491	1.288	10.600	*	5.813
6	126	2:11	60.807	-21.996	0.444	1.352	9.653	*	3.863
7	127	4:31	62.025	-19.974	0.515	1.657	10.640	0.616	4.663
8	128	4:36	63.109	-19.934	0.502	1.137	11.837	0.777	5.657

TABLE B.12: D350 Short-Term Experiment Summary. (*Data not available.)

Experiment	$\Delta(F_v/F_m)_{+2.0\ Fe}$	Std. err	$\Delta(F_v/F_m)_{+0.2\ Fe}$	Std. err
1	*	*	0.072	0.022
2	0.042	0.011	*	*
3	0.020	0.006	0.019	0.006
4	0.017	0.008	0.018	0.008
5	0.005	0.004	-0.004	0.004
6	0.080	0.002	0.057	0.002
7	0.022	0.002	0.019	0.002
8	0.009	0.002	0.003	0.002

B.4 D354 Short-Term Experiment Summary

TABLE B.13: D354 Short-Term Experiment Initial Conditions.

Experiment	DOY	Time (GMT)	Lat °N	Lon °W	F_v/F_m	Chl	DIN	Phosphate	Silicate
1	191	2:30	57.029	-10.901	0.250	0.576	3.807	0.233	0.703
2	192	2:29	58.790	-16.201	0.262	1.332	2.723	0.187	0.190
3	193	2:22	59.994	-19.905	0.189	0.697	0.707	0.097	0.687
4	194	2:28	61.895	-21.001	0.333	1.340	2.040	0.147	1.123
5	196	2:24	60.004	-23.496	0.358	1.528	0.267	0.067	0.830
6	197	1:25	60.001	-27.661	0.352	2.684	0.567	0.077	1.503
7	199	2:07	60.017	-34.996	0.305	2.524	4.230	0.350	2.787
8	200	2:24	60.000	-41.224	0.315	0.701	5.963	0.470	3.837
9	203	3:48	62.832	-34.981	0.316	1.940	3.590	0.287	1.670
10	205	2:25	63.000	-30.083	0.289	2.495	1.750	0.220	1.743
11	206	2:33	60.929	-31.479	0.268	3.100	0.833	0.140	1.723
12	207	2:14	58.264	-34.686	0.325	2.059	4.093	0.297	1.827
15	211	2:43	63.844	-34.994	0.310	1.136	5.280	0.423	2.083
16	213	2:08	62.531	-28.622	0.322	1.442	-0.173	1.027	0.073
17	215	2:25	62.453	-24.138	0.371	1.589	-0.177	1.173	0.157
18	217	2:40	61.744	-24.849	0.340	1.645	0.183	0.473	0.070
19	218	2:50	62.116	-26.977	0.312	1.632	0.933	0.840	0.097

Table B.14: D354 Short-Term Experiment Summary.

Experiment	$\Delta(F_v/F_m)$ $_{+2.0\ Fe}$	Std. err	$\Delta(F_v/F_m)$ $_{+0.2\ Fe}$	Std. err
1	0.054	0.008	0.031	0.008
2	0.124	0.028	0.063	0.028
3	0.030	0.004	0.013	0.004
4	0.026	0.008	0.016	0.008
5	0.038	0.007	0.025	0.007
6	0.031	0.003	0.020	0.003
7	0.038	0.003	0.031	0.003
8	0.084	0.003	0.078	0.003
9	0.071	0.003	0.055	0.003
10	0.076	0.004	0.053	0.004
11	0.072	0.003	0.031	0.003
12	0.061	0.003	0.037	0.003
15	0.089	0.004	0.081	0.004
16	0.065	0.003	0.041	0.003
17	0.023	0.002	0.021	0.002
18	0.055	0.003	0.038	0.003
19	0.057	0.004	0.020	0.004

Appendix C

PRISM Experiment Summary

Table C.1: Long-Term Experiment Summary Metadata.

Experiment	DOY	Time (GMT)	Lat °N	Lon °W
1	9	11:25	-75.7203	183.3979
2	22	17:00	-76.7162	179.0814
3	23	05:00	-77.5484	175.9698

The following lists the associated variables with their respective units for each long-term and short-term experiment summary.

F_o, F_m, F_v (blank and gain corrected)- a.u.

F_v/F_m - a.u.

σ_{PSII} - nm^{-2}

Chlorophyll - $\mu g\ L^{-1}$

DIN - $\mu mol\ L^{-1}$

Silicate - $\mu mol\ L^{-1}$

Phosphate - $\mu mol\ L^{-1}$

C.1 PRISM Long-Term Experiment Summary

TABLE C.2: PRISM Experiment 1 Summary.

Bottle	Treatment	Time (h)	σ_{PSII}	F_o	F_m	F_v	F_v/F_m	Chl	DIN	Phosphate	Silicate
	Initial	0	2.730	37631.295	49536.994	11905.699	0.240	13.551	22.900	1.420	72.200
	Initial	0	2.020	27237.547	36749.525	9511.977	0.259	6.827	22.600	1.310	69.600
	Initial	0	1.890	36483.692	51431.085	14947.393	0.291	8.401	18.400	0.969	60.300
1	Fe	24	2.380	18782.661	26752.227	7969.565	0.298	6.491	21.300	1.210	73.300
2	Fe	24	2.150	12922.498	19213.518	6291.020	0.327	6.543	21.300	1.190	67.000
3	Fe	24	2.050	10574.770	15681.109	5106.339	0.326	4.556	23.000	1.350	73.300
4	Fe	24	2.330	15865.403	23347.690	7482.287	0.320	6.453	20.800	1.190	68.700
5	Fe	24	2.410	15794.876	21589.641	5794.765	0.268	4.904	22.700	1.320	70.000
1	Control	24	2.230	19930.710	28418.329	8487.619	0.299	7.292	21.600	1.220	73.600
2	Control	24	2.140	22481.227	30050.711	7569.484	0.252	5.549	22.500	1.300	73.600
3	Control	24	2.300	12986.993	19322.894	6335.901	0.328	5.614	22.600	1.300	69.200
4	Control	24	2.270	13331.935	18936.918	5604.983	0.296	5.072	22.900	1.350	70.500
5	Control	24	2.000	21283.548	28433.717	7150.168	0.251	6.208	21.700	1.330	70.100
1	Fe	72	1.450	14786.271	26288.605	11502.333	0.438	6.246	17.000	0.997	66.800
2	Fe	72	1.430	13562.946	25197.358	11634.411	0.462	9.911	17.000	0.972	63.000
3	Fe	72	1.490	11663.843	21191.417	9527.574	0.450	4.336	19.900	1.150	68.400
4	Fe	72	1.610	15124.801	28191.555	13066.753	0.463	6.091	16.500	0.887	61.400
5	Fe	72	1.800	11471.496	18912.749	7441.253	0.393	3.717	20.400	1.190	67.700
1	Control	72	1.590	19272.853	30713.636	11440.782	0.372	6.066	17.700	1.030	66.700
2	Control	72	1.740	17594.308	25086.853	7492.546	0.299	4.517	19.900	1.170	68.400
3	Control	72	1.610	13011.327	22983.862	9972.536	0.434	4.594	18.900	1.100	65.800
4	Control	72	1.690	12849.755	21974.683	9124.928	0.415	5.240	20.100	1.160	67.900
5	Control	72	2.030	25983.189	35774.919	9791.730	0.274	5.756	19.200	1.150	67.100
1	Fe	120	1.320	23848.420	42052.063	18203.643	0.433	11.976	10.000	0.661	62.900
2	Fe	120	1.270	18188.497	33675.061	15486.563	0.460	18.842	9.700	0.575	57.700
1	Control	120	1.500	26541.482	42596.414	16054.932	0.377	13.577	11.400	0.728	62.300
2	Control	120	1.510	22210.393	34356.057	12145.664	0.354	9.808	15.600	0.928	65.300
1	Fe	168	1.860	54839.819	88125.698	33285.879	0.378	28.994	2.760	0.072	57.200
2	Fe	168	1.620	41885.288	72761.468	30876.181	0.424	35.447	1.310	0.027	51.100
6	Fe	168	1.590	33845.402	54659.144	20813.741	0.381	25.295	3.090	0.175	53.200
7	Fe	168	1.510	31200.041	52809.592	21609.552	0.409	22.283	4.050	0.166	53.200
8	Fe	168	1.420	21216.239	35304.912	14088.673	0.399	18.670	6.590	0.362	55.000
1	Control	168	2.120	74301.716	105307.670	31005.954	0.294	21.767	4.800	0.332	57.100
2	Control	168	2.360	60147.609	78247.741	18100.132	0.231	22.197	9.780	0.575	60.700
6	Control	168	2.300	55794.087	72960.584	17166.497	0.235	16.777	8.800	0.422	54.500
7	Control	168	1.680	32200.308	49091.617	16891.309	0.344	20.004	7.860	0.435	55.700
8	Control	168	1.670	14456.522	21479.742	7023.220	0.327	8.733	18.800	1.060	65.600

TABLE C.3: PRISM Experiment 2 Summary.

Bottle	Treatment	Time (h)	σ_{PSII}	F_o	F_m	F_v	F_v/F_m	Chl	DIN	Phosphate	Silicate
	Initial	0	2.670	9418.046	13186.301	3768.255	0.286	3.072	22.500	1.340	71.600
	Initial	0	2.580	8652.819	12254.239	3601.420	0.294	3.201	23.900	1.460	73.600
	Initial	0	2.570	8934.566	12722.398	3787.832	0.298	2.908	24.000	1.490	74.200
1	Fe	24	2.200	7483.817	10917.009	3433.193	0.314	6.078	22.600	1.530	73.500
2	Fe	24	2.190	6976.608	10419.043	3442.435	0.330	5.175	22.200	1.520	73.800
3	Fe	24	2.100	7144.137	10906.033	3761.896	0.345	3.381	22.600	1.430	70.700
4	Fe	24	2.090	6965.054	10471.613	3506.559	0.335	2.129	22.300	1.400	70.300
5	Fe	24	2.190	6906.708	10385.537	3478.830	0.335	2.271	22.400	1.420	70.300
1	Control	24	2.010	7016.468	10414.999	3398.531	0.326	4.749	22.400	1.530	72.900
2	Control	24	2.240	7076.547	10576.174	3499.626	0.331	4.130	22.300	1.480	72.600
3	Control	24	2.160	6870.313	10040.081	3169.767	0.316	2.723	23.500	1.480	73.100
4	Control	24	2.050	6861.070	10220.897	3359.826	0.329	2.323	22.500	1.420	72.200
5	Control	24	2.140	6840.274	10378.027	3537.754	0.341	3.175	23.300	1.460	73.200
1	Fe	72	1.540	7820.520	14357.046	6536.526	0.455	4.672	22.300	1.330	73.500
2	Fe	72	1.620	7208.750	13685.774	6477.024	0.473	5.240	22.200	1.330	73.500
3	Fe	72	1.570	7065.484	13220.159	6154.675	0.466	5.678	21.900	1.310	72.700
4	Fe	72	1.580	7246.877	13547.129	6300.252	0.465	4.439	21.500	1.250	72.200
5	Fe	72	1.600	7438.092	14205.692	6767.601	0.476	6.143	21.500	1.260	72.400
1	Control	72	1.600	7761.823	14541.555	6779.732	0.466	5.007	22.100	1.330	72.400
2	Control	72	1.590	7723.118	14639.184	6916.066	0.472	4.852	21.400	1.270	72.200
3	Control	72	1.580	7295.629	13327.257	6031.628	0.453	5.446	22.800	1.360	74.000
4	Control	72	1.610	7700.010	14568.706	6868.696	0.471	5.807	21.800	1.270	72.500
5	Control	72	1.690	8082.439	14960.955	6878.516	0.460	5.420	22.500	1.330	73.000
1	Fe	120	1.520	12366.795	24292.083	11925.288	0.491	10.505	19.200	1.150	68.500
2	Fe	120	1.510	12601.643	25913.318	13311.675	0.514	12.622	19.100	1.130	68.300
1	Control	120	1.550	14890.518	29860.221	14969.703	0.501	10.273	18.400	1.090	67.700
2	Control	120	1.530	14185.247	28374.022	14188.776	0.500	12.699	18.200	1.100	67.000
1	Fe	168	1.340	21373.390	41630.686	20257.296	0.487	22.603	13.300	0.739	63.500
2	Fe	168	1.330	21751.643	41753.470	20001.827	0.479	21.573	13.100	0.738	63.200
6	Fe	168	1.370	22931.948	46405.380	23473.432	0.506	23.253	11.900	0.679	62.000
7	Fe	168	1.390	22181.385	44783.450	22602.065	0.505	24.229	11.600	0.698	62.300
8	Fe	168	1.360	21686.290	43735.829	22049.539	0.504	22.115	12.500	0.748	63.200
1	Control	168	1.440	26484.748	49956.199	23471.451	0.470	19.459	12.700	0.720	61.500
2	Control	168	1.490	28031.424	52661.397	24629.973	0.468	14.743	12.200	0.675	60.800
6	Control	168	1.470	25660.911	46811.358	21150.447	0.452	21.410	12.900	0.719	62.700
7	Control	168	1.490	25548.029	46860.867	21312.838	0.455	16.640	13.200	0.753	62.000
8	Control	168						14.364	13.800	0.812	63.900

TABLE C.4: PRISM Experiment 3 Summary.

Bottle	Treatment	Time (h)	σ_{PSII}	F_o	F_m	F_v	F_v/F_m	Chl	DIN	Phosphate	Silicate
	Initial	0	2.630	23938.182	30237.767	6299.585	0.208	5.524	16.500	1.010	64.100
	Initial	0	2.530	24171.867	30370.453	6198.586	0.204	5.472	16.200	0.968	64.300
	Initial	0	2.140	26548.321	33610.353	7062.031	0.210	5.653	15.500	0.971	68.800
1	Fe	24	2.430	14913.220	20973.424	6060.204	0.289	5.136	15.200	0.949	62.700
2	Fe	24	2.330	13997.650	20150.180	6152.530	0.305	4.930	15.200	0.934	62.200
3	Fe	24	2.340	13982.262	19847.554	5865.292	0.296	6.066	15.300	0.949	61.200
4	Fe	24	2.300	13460.361	19461.579	6001.217	0.308	5.678	15.500	0.950	63.900
5	Fe	24	2.490	14588.795	20915.720	6326.924	0.302	5.549	15.300	0.947	62.800
1	Control	24	2.140	15403.063	21728.705	6325.642	0.291	5.420	14.900	0.944	63.700
2	Control	24	2.170	16160.909	22669.922	6509.013	0.287	5.394	14.900	0.938	63.700
3	Control	24	2.220	15136.342	21513.277	6376.935	0.296	4.930	15.100	0.954	61.400
4	Control	24	2.220	14751.649	20988.812	6237.163	0.297	5.394	15.300	0.933	62.100
5	Control	24	2.300	15122.237	21432.491	6310.254	0.294	5.420	15.500	0.947	61.300
1	Fe	72	1.630	13856.842	24501.309	10644.467	0.434	8.311	13.000	0.806	65.300
2	Fe	72	1.690	14533.902	26626.099	12092.197	0.454	9.085	12.800	0.808	65.200
3	Fe	72	1.700	14925.007	27119.789	12194.781	0.450	8.905	13.400	0.791	62.600
4	Fe	72	1.650	13522.158	24819.322	11297.163	0.455	9.395	12.900	0.803	63.300
5	Fe	72	1.660	12965.635	23876.823	10911.188	0.457	8.956	13.400	0.785	62.400
1	Control	72	1.770	16134.391	25982.542	9848.152	0.379	9.240	12.600	0.761	64.300
2	Control	72	1.670	16356.231	26872.467	10516.236	0.391	10.789	12.700	0.766	66.300
3	Control	72	1.860	16580.635	27318.711	10738.076	0.393	10.608	12.800	0.771	62.200
4	Control	72	1.670	13774.938	24454.027	10679.089	0.437	10.299	13.000	0.750	63.000
5	Control	72	1.810	15840.742	26735.259	10894.518	0.407	10.247	13.300	0.798	62.900
1	Fe	120	1.600	19125.280	39481.595	20356.315	0.516	16.478	7.830	0.503	60.500
2	Fe	120	1.620	19123.300	39750.927	20627.627	0.519	20.326	8.260	0.539	60.000
1	Control	120	2.070	28590.699	45895.250	17304.551	0.377	29.378	9.180	0.571	61.600
2	Control	120	1.860	26570.713	44916.943	18346.230	0.408	20.055	9.140	0.552	61.500
1	Fe	168	1.740	34161.562	64179.022	30017.460	0.468	14.689	1.290	0.125	55.500
2	Fe	168	1.720	32261.683	61568.261	29306.578	0.476	15.556	2.320	0.181	55.400
6	Fe	168	1.730	25954.965	47954.558	21999.593	0.459	12.157	3.960	0.278	56.300
7	Fe	168	1.790	26911.196	48596.239	21685.044	0.446	13.171	3.400	0.231	57.800
8	Fe	168	1.720	28131.648	51238.455	23106.807	0.451	13.334	3.820	0.268	57.600
1	Control	168	2.390	48325.727	72187.453	23861.726	0.331	26.017	5.290	0.330	56.600
2	Control	168	2.220	49401.486	74194.279	24792.793	0.334	24.012	5.160	0.334	56.200
6	Control	168	2.380	40927.522	57221.187	16293.665	0.285	18.483	7.720	0.462	55.800
7	Control	168	2.370	46306.319	64776.667	18470.348	0.285	18.917	7.570	0.464	54.800
8	Control	168	2.290	34035.742	52823.785	18788.043	0.356	19.567	6.540	0.424	57.100

C.2 PRISM Short-Term Initial Conditions

Table C.5: PRISM Short-Term Initial Conditions 1.

Experiment	DOY	Time (GMT)	Lat °N	Lon °W	F_v/F_m	Chl	DIN	Phosphate	Silicate
1	6	22:10	-72.182	200.983	0.292	1.050	28.467	1.737	51.700
2	7	18:50	-73.379	194.891	0.368	0.383	29.400	1.860	54.800
3	8	16:14	-75.003	189.993	0.373	1.012	26.600	1.620	75.100
4	8	18:28	-75.003	189.993	0.262	11.920	22.267	1.377	72.133
5	10	04:40	-76.352	184.799	0.257	9.524	19.000	1.120	69.700
6	13	14:45	-76.667	171.289	0.185	13.250	10.967	0.466	37.667
7	14	01:00	-76.666	174.204	0.226	1.178	24.500	1.413	67.367
8	15	05:25	-76.730	170.475	0.246	16.777	8.380	0.392	37.500
9	17	12:30	-76.666	174.250	0.253	1.303	25.500	1.260	71.900
10	18	11:16	-76.680	170.333	0.257	26.234	9.580	0.504	40.800
11	20	17:20	-76.716	179.255	0.305	2.160	21.400	1.340	69.000
12	21	20:39	-76.985	179.251	0.255	5.547	19.500	1.120	66.400
13	24	03:18	-77.433	181.196	0.243	6.685	15.400	1.010	68.900
14	25	00:11	-77.748	177.815	0.288	7.382	18.600	1.180	74.200
15	25	14:30	-77.607	178.802	0.315	5.020	19.300	1.210	73.800
16	26	10:43	-76.716	179.247	0.326	1.458	22.800	1.450	71.600
17	28	10:07	-74.000	178.999	0.247	0.381	26.200	1.650	67.700
18	30	04:28	-74.601	177.497	0.234	4.775	24.300	1.510	72.400
19	31	04:00	-76.208	174.970	0.202	1.768	22.533	1.360	62.267
20	31	11:48	-76.667	171.136	0.250	6.633	17.500	0.957	48.800
21	31	19:59	-76.639	169.353	0.374	5.549	14.100	0.796	43.400
22	32	09:51	-76.767	169.009	0.179	7.563	14.200	0.803	49.000
23	33	01:38	-76.175	168.237	0.467	4.672	22.400	1.380	63.000
24	33	06:19	-76.267	169.001	0.341	4.414	14.000	0.732	41.500
25	33	20:08	-77.167	168.999	0.257	6.040	12.900	0.674	41.000
26	34	09:26	-77.167	169.997	0.252	3.007	20.600	1.150	76.600
27	35	03:55	-76.841	169.296	0.213	2.078	21.200	1.210	76.400
28	35	14:02	-76.752	166.762	0.258	6.840	15.100	0.832	47.900
29	36	00:01	-76.750	164.251	0.317	4.504	11.900	0.647	43.200

TABLE C.6: PRISM Short-Term Experiment Summary.

Experiment	$\Delta(F_v/F_m)_{24\ h}$	Std. err	$\Delta(F_v/F_m)_{48\ h}$	Std. err
1	0.020	0.004	0.033	0.004
2	0.028	0.024	-0.010	0.017
3	0.021	0.010	0.016	0.001
4	0.040	0.006	0.095	0.003
5	0.003	0.001	0.033	0.003
6	0.173	0.005	0.230	0.009
7	0.041	0.020	0.019	0.004
8	0.120	0.003	0.170	0.003
9	0.080	0.010	0.001	0.005
10	0.010	0.003	0.009	0.003
11	0.013	0.005	0.022	0.003
12	0.003	0.002	0.000	0.004
13	0.015	0.010	0.055	0.004
14	-0.030	0.018	0.005	0.005
15	0.004	0.004	0.040	0.026
16	-0.006	0.004	0.010	0.009
17	0.029	0.017	0.115	0.032
18	-0.013	0.001	0.053	0.006
19	0.010	0.010	0.134	0.005
20	-0.019	0.003	-0.006	0.004
21	0.041	0.002	0.014	0.008
22	0.009	0.002	0.036	0.002
23	-0.002	0.003	0.031	0.004
24	0.007	0.002	0.041	0.013
25	0.005	0.005	0.018	0.006
26	0.018	0.001	0.044	0.006
27	0.022	0.003	0.071	0.004
28	-0.001	0.001	0.003	0.001
29	0.001	0.001	0.033	0.007

Appendix D

PRISM Protein Data

Table D.1: PRISM RbcL:PsbA Ratio Summary.

Station	CTD	Lat (°S)	Long (°W)	RbcL:PsbA (mol mol^{-1})	Std. err
2	3	-73.379	194.891	20.145	1.240
3	4	-75.003	189.993	37.683	10.958
10	11	-76.730	170.475	41.378	10.069
24	25	-76.666	174.250	8.020	1.276
29	30	-76.680	170.333	17.891	3.175
38	39	-76.716	179.255	9.479	1.817
48	50	-76.985	179.251	6.372	0.535
56	58	-77.433	181.196	12.022	2.041
62	64	-77.748	177.815	7.706	1.312
65	67	-77.607	178.802	270.828	14.823
74	76	-76.716	179.247	70.257	0.110
79	81	-74.000	178.999	7.470	0.834
92	94	-74.601	177.497	10.428	1.445
94	96	-76.667	171.136	12.528	0.785
95	97	-76.639	169.353	10.137	0.590
96	98	-76.767	169.009	33.015	5.311
101	103	-76.175	168.237	41.406	9.942
102	104	-76.267	169.001	9.355	2.076
108	110	-77.167	168.999	43.432	3.434
113	115	-76.841	169.296	47.411	8.455
114	116	-76.752	166.762	22.167	4.056
116	118	-76.750	164.251	124.806	22.006

Table D.2: PRISM PsbA Concentrations Summary.

Station	CTD	Lat (°S)	Long (°W)	PsbA:TP (fmol μg^{-1})	Std. err	PsbA:Chl (mmol mol^{-1})	Std. err	Chl:PsbA (mol mol^{-1})	Std. err
2	3	-73.379	194.891	8.507	3.008	13.769	0.810	73.158	4.503
3	4	-75.003	189.993	4.691	0.050	9.150	3.130	135.207	39.316
10	11	-76.730	170.475	1.131	0.080	0.594	0.122	1869.853	454.998
24	25	-76.666	174.250	1.923	0.325	2.436	0.334	429.171	68.257
29	30	-76.680	170.333	3.339	0.561	0.479	0.083	2220.920	394.160
38	39	-76.716	179.255	0.577	0.112	1.276	0.275	852.977	163.483
48	50	-76.985	179.251	5.960	0.918	1.778	0.161	571.153	47.982
56	58	-77.433	181.196	3.000	0.234	2.020	0.359	526.427	89.377
62	64	-77.748	177.815	2.074	0.093	1.588	0.240	663.710	112.990
65	67	-77.607	178.802	0.806	0.286	0.879	0.319	1919.680	1081.683
74	76	-76.716	179.247	3.734	0.740	0.910	0.001	1099.372	1.728
79	81	-74.000	178.999	0.864	0.184	3.419	0.376	299.799	33.480
92	94	-74.601	177.497	1.414	0.270	0.811	0.260	1593.610	590.127
94	96	-76.667	171.136	2.588	0.120	1.109	0.073	909.201	56.943
95	97	-76.639	169.353	2.882	0.465	2.371	0.134	424.497	24.708
96	98	-76.767	169.009	6.317	1.093	1.249	0.177	839.023	134.982
101	103	-76.175	168.237	1.554	0.120	1.190	0.231	926.822	222.542
102	104	-76.267	169.001	1.376	0.057	2.242	0.291	463.461	66.952
108	110	-77.167	168.999	4.912	0.259	1.593	0.117	635.162	50.223
113	115	-76.841	169.296	1.779	0.177	1.598	0.258	663.506	118.332
114	116	-76.752	166.762	2.837	0.503	2.489	0.421	427.916	78.307
116	118	-76.750	164.251	0.419	0.126	0.331	0.068	3252.079	573.410

Table D.3: PRISM RbcLConcentrations Summary.

Station	CTD	Lat (°S)	Long (°W)	RbcL:TP (fmol μg^{-1})	Std. err	RbcL:Chl (mmol mol^{-1})	Std. err	Chl:RbcL (mol mol^{-1})	Std. err
2	3	-73.379	194.891	214.703	107.528	275.361	83.574	4.899	2.099
3	4	-75.003	189.993	152.293	17.359	278.704	72.014	4.020	0.840
10	11	-76.730	170.475	40.670	7.128	22.129	6.464	58.186	22.603
24	25	-76.666	174.250	48.944	0.169	62.901	2.677	15.954	0.654
29	30	-76.680	170.333	63.599	16.002	9.198	2.436	125.451	32.705
38	39	-76.716	179.255	10.350	4.658	19.121	2.040	53.562	5.955
48	50	-76.985	179.251	120.793	32.915	34.336	2.099	29.341	1.777
56	58	-77.433	181.196	85.474	16.423	54.657	5.041	18.603	1.668
62	64	-77.748	177.815	98.445	10.085	73.065	3.829	13.758	0.688
65	67	-77.607	178.802	57.304	4.245	61.801	8.000	47.451	2.317
74	76	-76.716	179.247	111.165	10.085	27.669	3.673	13.758	0.688
79	81	-74.000	178.999	26.297	1.964	113.930	25.044	9.939	2.668
92	94	-74.601	177.497	260.485	66.052	131.467	14.749	7.788	0.810
94	96	-76.667	171.136	61.370	7.184	25.966	1.232	38.694	1.925
95	97	-76.639	169.353	30.049	2.983	25.595	3.963	40.775	5.511
96	98	-76.767	169.009	122.947	8.936	24.490	2.051	41.427	3.557
101	103	-76.175	168.237	24.592	2.174	18.131	1.816	56.224	5.363
102	104	-76.267	169.001	35.767	3.626	58.657	9.957	18.318	3.742
108	110	-77.167	168.999	101.169	0.982	32.946	2.844	30.792	2.551
113	115	-76.841	169.296	37.213	2.634	33.256	4.459	31.142	4.033
114	116	-76.752	166.762	52.924	3.966	46.261	1.811	21.685	0.880
116	118	-76.750	164.251	5.247	1.025	4.555	1.366	265.754	80.719

Appendix E

Paper Submissions

E.1 First Author Submissions

E.1.1 IsiA Paper Submission to Journal of Phycology

Ryan-Keogh, T. J., Macey, A. I., Cockshutt, A. M., Moore, C. M. and Bibby, T. S., (2012), "The cyanobacterial chlorophyll-binding-protein IsiA acts to increase the *in vivo* effective cross-section of photosystem I under iron limitation", *Journal of Phycology*, Volume 48, Issue 1, Pages 145-154, doi: 10.1111/j.1529-8817.2011.01092.x.

Submitted: 8th March 2011.
Accepted: 5th June 2011.
Published: 12th December 2011

J. Phycol. **48,** 145–154 (2012)

DOI: 10.1111/j.1529-8817.2011.01092.x

THE CYANOBACTERIAL CHLOROPHYLL-BINDING-PROTEIN IsiA ACTS TO INCREASE THE IN VIVO EFFECTIVE ABSORPTION CROSS-SECTION OF PSI UNDER IRON LIMITATION[1]

Thomas J. Ryan-Keogh,[2] *Anna I. Macey*

School of Ocean and Earth Science, University of Southampton, National Oceanography Centre, Southampton, European Way, Southampton, SO14 3ZH, UK

Amanda M. Cockshutt

Department of Chemistry and Biochemistry, Mount Allison University, Sackville, NB E4L 1G7, Canada

C. Mark Moore and Thomas S. Bibby

School of Ocean and Earth Science, University of Southampton, National Oceanography Centre, Southampton, European Way, Southampton, SO14 3ZH, UK

Iron availability limits primary production in >30% of the world's oceans; hence phytoplankton have developed acclimation strategies. In particular, cyanobacteria express IsiA (iron-stress-induced) under iron stress, which can become the most abundant chl-binding protein in the cell. Within iron-limited oceanic regions with significant cyanobacterial biomass, IsiA may represent a significant fraction of the total chl. We spectroscopically measured the effective cross-section of the photosynthetic reaction center PSI (σ_{PSI}) in vivo and biochemically quantified the absolute abundance of PSI, PSII, and IsiA in the model cyanobacterium *Synechocystis* sp. PCC 6803. We demonstrate that accumulation of IsiA results in a ~60% increase in σ_{PSI}, in agreement with the theoretical increase in cross-section based on the structure of the biochemically isolated IsiA-PSI supercomplex from cyanobacteria. Deriving a chl budget, we suggest that IsiA plays a primary role as a light-harvesting antenna for PSI. On progressive iron-stress in culture, IsiA continues to accumulate without a concomitant increase in σ_{PSI}, suggesting that there may be a secondary role for IsiA. In natural populations, the potential physiological significance of the uncoupled pool of IsiA remains to be established. However, the functional role as a PSI antenna suggests that a large fraction of IsiA-bound chl is directly involved in photosynthetic electron transport.

Key index words: **chlorophyll-binding protein; cyanobacteria; iron limitation; IsiA; PSI**

Abbreviation: **σ_{PSI}, the effective absorption cross-section of PSI**

[1]Received 8 March 2011. Accepted 05 June 2011.
[2]Author for correspondence: e-mail t.ryan-keogh@noc.soton.ac.uk.

Chl in phytoplankton cells is primarily associated with the highly conserved photosynthetic reaction centers PSI and PSII, which catalyze oxygenic photosynthesis, or with peripheral, species-specific, light-harvesting protein complexes that enable niche adaptation to different light and nutrient environments (Ting et al. 2002, Chen and Bibby 2005, Varsano et al. 2006). It has been proposed, however, that the chl-binding protein IsiA, expressed in some cyanobacteria under iron stress (Burnap et al. 1993), is not directly involved in photosynthesis (Cadoret et al. 2004, Sarcina and Mullineaux 2004, Behrenfeld et al. 2006, Singh and Sherman 2007). Under iron limitation, IsiA can be the most abundant chl-binding protein in cyanobacteria cells (Burnap et al. 1993). IsiA-associated pigment may therefore significantly contribute to total chl in oceanic regions such as the Equatorial Pacific, where cyanobacteria comprise a substantial fraction of the total phytoplankton community, and the availability of the trace metal iron (Fe) has been shown to limit primary production (Martin et al. 1994, Behrenfeld et al. 1996, 2006, Behrenfeld and Kolber 1999). A recent whole-community genomic study has revealed that the cyanobacterial *isiA* gene is present specifically in this region, suggesting that it has a functional role that confers a selective advantage in situ (Bibby et al. 2009).

The IsiA protein is thought to bind 12 chl molecules in six transmembrane helices arranged in three sets of two dimers (Bricker and Frankel 2002). Its sequence and structural motif are homologous to the core antenna proteins of PSII (CP43 and CP47) (Pakrasi et al. 1985, Burnap et al. 1993) and to the light-harvesting antenna proteins (Pcbs) of the marine cyanobacterium *Prochlorococcus* (La Roche et al. 1996, Bibby et al. 2003). Both Pcbs and IsiA, however, lack the large hydrophilic loop that

joins the luminal ends of helices V and VI (Burnap et al. 1993). *Prochlorococcus* can have multiple *pcb* genes, each of which has a specific function: for example, as specific light-harvesting antenna for PSII, or PSI (expressed constitutively), or as a light-harvesting antenna system for PSI expressed under iron limitation (Garczarek et al. 2000, Bibby et al. 2001d, 2003). This six-trans-membrane chl-binding motif is therefore thought to be a core building block of photosynthesis that has been retained in some cyanobacteria because it offers a photosynthetic strategy, advantageous under iron limitation (Green 2003, Chen and Bibby 2005).

In addition to expressing IsiA under iron stress, cyanobacterial cells undergo chlorosis (loss of total chl per cell) (Guikema and Sherman 1983, Boyer et al. 1987, Strauss 1994, Erdner et al. 1999, Moseley et al. 2002), reduce the abundance of photosynthetic reaction centers (PSI and PSII) (Öquist 1974, Strauss 1994, Boekema et al. 2001, Küpper et al. 2008), and reduce their phycobilisome content (soluble light-harvesting systems that require iron-binding enzymes for synthesis) (Guikema and Sherman 1983). The biochemical isolation of an IsiA-PSI supercomplex from iron-limited cyanobacterial cells, in which 18 IsiA monomer proteins are functionally coupled to a PSI trimer (IsiA:PSI ratio 6:1) (Bibby et al. 2001a,b,c, Boekema et al. 2001), was thought to explain the role of this protein, namely to increase the functional antenna size of a restricted cellular quota of PSI reaction centers by ~70% under iron limitation, thus compensating for a reduction in PSI per cell (Andrizhiyevskaya et al. 2002, Melkozernov et al. 2003, Küpper et al. 2008). However, an increase in the cross-section of PSI (σ_{PSI}) has not been established in vivo (Ivanov et al. 2006). Instead, evidence from culture studies suggests that IsiA may have an alternative role in photoprotection or as a chl store for the cell (Guikema and Sherman 1983, Park et al. 1999, Sandström et al. 2001, 2002, Singh and Sherman 2007) and is therefore not directly involved in harvesting light for primary production (Behrenfeld et al. 2006).

The ratio of variable to maximal fluorescence (F_v/F_m) has frequently been used to establish and map phytoplankton iron stress in the field (Boyd and Abraham 2001, Behrenfeld et al. 2006, Bibby et al. 2008). However, the mechanistic basis of this response remains unclear (Suggett et al. 2009). The observed reduction in F_v/F_m within natural populations in low-iron regions (Behrenfeld et al. 2006, Nielsdóttir et al. 2009) and within cultures under iron-starvation conditions, although not necessarily steady-state iron limitation (Price 2005), probably reflects accumulation of nonphotochemically active chl. Consequently, rather than the original suggestion that lowered F_v/F_m reflects accumulation of damaged PSII reaction centers (Falkowski and Kolber 1995), it has been suggested that accumulation of uncoupled chl-binding IsiA protein, or proteins with similar iron-regulated control in eukaryotes (although a role of these other than as light-harvesting antenna also remains to be established, Varsano et al. 2006), may be primarily responsible for the observed reduction in F_v/F_m under iron stress (Behrenfeld et al. 2006). Establishing the role of IsiA and the potential for excess accumulation of this protein is thus crucial for understanding the physiological basis of active fluorescence data and potentially for interpreting large-scale satellite-based measurements of production (Behrenfeld et al. 2006, 2009). In addition, the iron-stress response of cyanobacteria may be representative of similar responses in photosynthetic eukaryotes (Varsano et al. 2006).

In this study, we measured the absolute abundance of the chl-binding proteins PSII, PSI, and IsiA, and the in vivo σ_{PSI} in cultures of the model cyanobacterium *Synechocystis* sp. PCC 6803 under conditions of increasing iron stress. We subsequently calculated a chl budget for the iron-limited cyanobacterial cell, and demonstrate that the primary function of IsiA in vivo is as a PSI antenna.

MATERIALS AND METHODS

Growth conditions. *Synechocystis* sp. PCC 6803 (Bricker et al. 1998) was grown photoheterotrophically in mineral medium in BG-11 (Williams 1988) supplemented with glucose at 30°C and with illumination of 10 μmol photons $\cdot$ $m^{-2} \cdot s^{-1}$ on a 12:12 light:dark (L:D) cycle. Iron-stressed cultures were obtained by inoculating into BG-11 medium without added iron. All cultures were grown under batch conditions for a period of 96 h, with inoculation of new experimental cultures carried out from cells grown under iron-replete conditions. Cells were harvested every day during the midpoint of the light cycle over the course of 96 h, with samples collected for physiological and molecular analysis. Within each experiment, analyses were performed on triplicate independent cultures. We further present results from a series of three independent experiments.

Samples for chl analysis were filtered onto Whatman GF/F filters (Whatman, GE Healthcare, Chalfont St. Giles, Buckinghamshire, UK) and extracted into 90% acetone for 24 h in the dark at 5°C before analysis using a Turner Designs 10-AU fluorometer (Turner Designs, Sunnyvale, CA, USA) (Welschmeyer 1994). Cell enumeration was performed using a Becton Dickinson Facsort™ flow cytometer (Becton Dickinson Biosciences, Oxford, UK) with a reference bead stock used as an internal standard.

Biophysical measurements. The apparent PSII photosynthetic efficiency (F_v/F_m) was assessed from chl fluorescence measurements performed using a Chelsea Scientific Instruments Fasttracka™ Mk II Fast Repetition Rate fluorometer (FRRf) integrated with a FastAct™ Laboratory system (Chelsea Technologies Group Ltd., West Molesey, Surrey, UK). All samples were dark acclimated for 30 min and measurements were corrected for the blank effect (Cullen and Davis 2003). Absorbance spectroscopy was undertaken using a Varian Cary 50 Scan™ UV-Visible spectrophotometer (Agilent Technologies UK Ltd., Wokingham, Berkshire, UK), on samples that had been sonicated on a freeze-thaw cycle using a Sonics and Material VibraCell™ (Sonics and Materials Inc., Newtown, CT, USA) to extract the thylakoid membranes. Scans were performed on a medium resolution from 600 to 800 nm on triplicate cultures from both iron-stressed and iron-replete treatments over the course of 96 h.

Redox kinetics of P700, the PSI primary donor, were measured by following absorption changes at 830 nm relative to 870 nm using a Walz Dual-PAM 100^{TM} (Heinz Walz GmbH, Effeltrich, Germany). A custom protocol was developed to quantitatively estimate σ_{PSI} by measuring the oxidation of P700 in response to 3 ms duration 635 nm LED light pulses at intensities from 5 to a saturating 20 mmol photons $\cdot$ m^{-2} $\cdot$ s^{-1}. Harvested whole cells were gently concentrated to increase signal to noise ratios and allow resolution of kinetic measurements of P700 oxidation at 7.5 μs time resolution over 50 ms timescales. Accurate estimates of absolute σ_{PSI} on cultures dense enough for ΔA_{830} measurements require correction for absorption of the actinic light within the culture (Zipfel and Owens 1991). Indeed, even relative changes in σ_{PSI} between cultures would be susceptible to artifacts resulting from the need to make such measurements in optically dense situations. Culture absorption was thus measured at the wavelength of the saturating pulse using a Varian Cary 50 Scan^{TM} UV-Visible spectrophotometer. Raw ΔA_{830} measurements were analyzed using custom software in a MATLAB^{TM} (Mathworks, Cambridge, UK) computing environment following Zipfel and Owens (1991). Briefly, the effective photochemical rate constant for P700 oxidation (K_{eff}) (ms^{-1}) measured under monochromatic saturating light (E[635]) (photons $\cdot$ m^{-2} $\cdot$ s^{-1}) will be related to the total absorption of the sample at that wavelength (A[635]) (m^{-1}) and the functional absorption cross-section (Zipfel and Owens 1991):

$$K_{\text{eff}} = \sigma_{\text{PSI}} E \frac{(1 - e^{-A})}{A} \quad (1)$$

Values for K_{eff} were derived from nonlinear least squares fitting of ΔA_{830} saturation kinetics as a function of time (t) to:

$$\Delta A_{830} = \Delta A_{830\max}(1 - e^{K_{\text{eff}} t}) \quad (2)$$

where $\Delta A_{830\ max}$ is the maximum absorption change measured in a given sample under saturating light. Correction for re-reduction of P700^{+} during the saturation flash (Zipfel and Owens 1991) was not performed, as kinetic measurements indicated that the effective reduction rate constant was an order of magnitude lower than K_{eff} (see below).

Formation of the IsiA-PSI supercomplex is expected to be capable of increasing σ_{PSI} by ~70% (Bibby et al. 2001b). For further comparison with measured values of σ_{PSI}, absolute theoretical cross-sections for an isolated PSI (trimer) and the IsiA-PSI supercomplex (Bibby et al. 2001b) were calculated using the in vivo absorption of a single chl molecule (Bidigare et al. 1990, Johnsen et al. 1994), and assuming 100 chl molecules in a single PSI protein complex (Jordan et al. 2001) and that every IsiA protein binds at least 12 chl molecules (Ferreira et al. 2004, Murray et al. 2006).

Protein immmunodetection and quantification. Protein samples were extracted using a liquid nitrogen freeze-thaw cycle combined with sonication to rupture the cell membrane. Protein concentrations were determined using a Lowry protein assay (Lowry et al. 1951, Peterson 1979). Quantitative Western blotting was performed using the Tricine-SDS-PAGE method as described in Schägger (2006). The SDS-PAGE and membrane transfer were run using an Invitrogen Life Technologies PowerEase 500^{TM} (Invitrogen, Paisely, UK) (see Results). Custom Agrisera^{TM} (Agrisera AB, Vännäs, Sweden) antibodies and protein standards were used for protein immunodetection according to the manufacturer's instructions (Brown et al. 2008). The membranes were imaged using a BioRad VersaDoc^{TM} (Bio-Rad Laboratories Ltd., Hemel Hempstead, Hertfordshire, UK) imaging system, and the images were processed using QuantityOne^{TM} software to quantify protein samples and standards. Quantification was performed within the unsaturated part of the calibration curve.

RESULTS

Physiological response. Iron-stress was induced by growing *Synechocystis* cells in BG-11 media lacking iron. When compared with control *Synechocystis* cultures (BG-11 containing iron), a marked difference in total chl concentration and cell density (Fig. 1a) and a marked decline in F_v/F_m (the photosynthetic

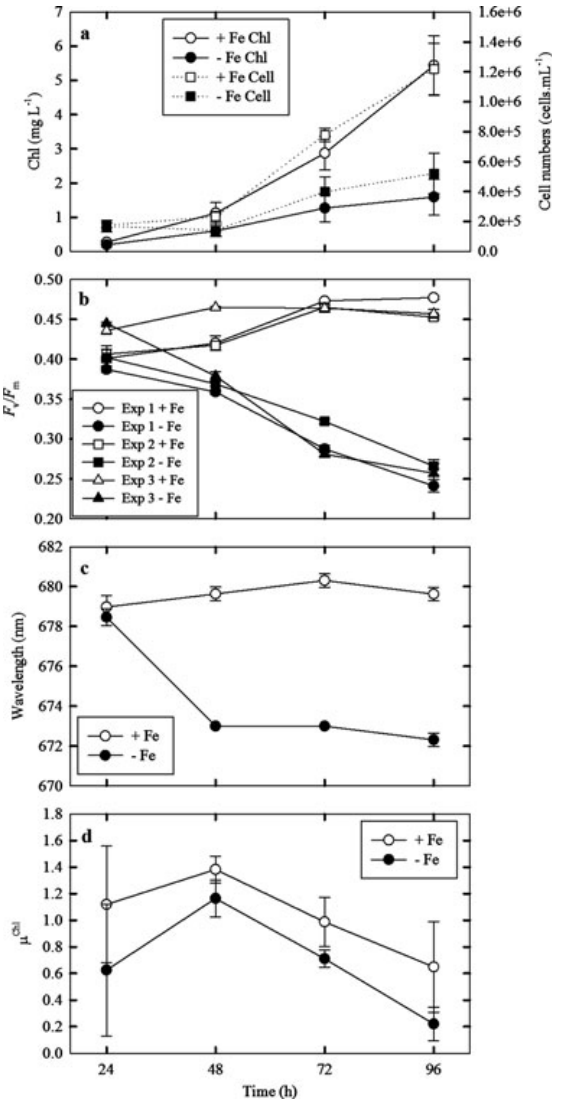

FIG. 1. Physiological measurements of *Synechocystis* PCC 6803 under iron-replete (+Fe) and iron-deplete conditions (−Fe). (a) Average chl concentrations (mg $\cdot$ L^{-1}) and average cell numbers (cells $\cdot$ mL^{-1}) enumerated using flow cytometry from three independent experiments. (b) Individual average F_v/F_m from the three independent experiments. (c) Wavelength shift of maximum absorption value between 670 and 685 nm measured at room temperature. (d) Growth rates (μ^{chl}) calculated from chl concentrations. Displayed are results averaged from triplicates from three independent experiments with ±standard errors (in a, c, d).

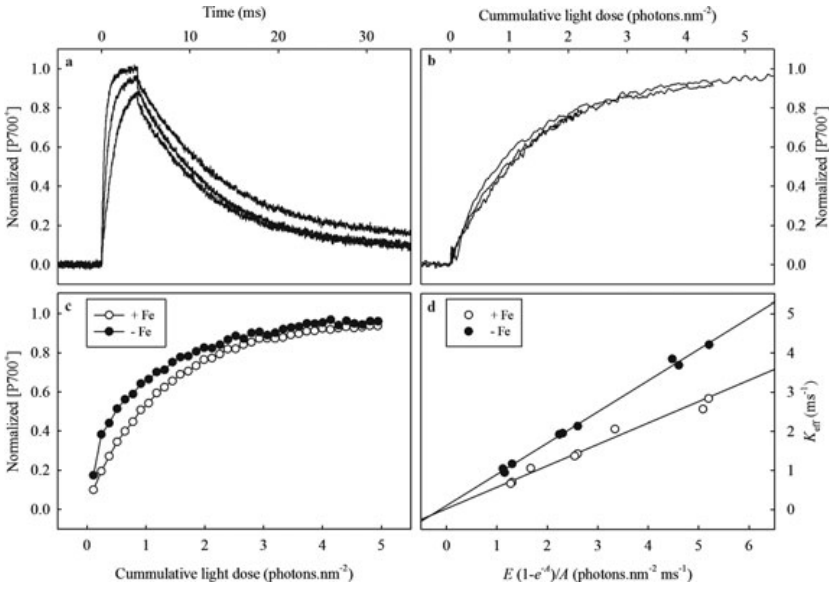

FIG. 2. Measurements of ΔA_{830} kinetics over a range of different light intensities on the same sample (a). (b) The rate of ΔA_{830} saturation normalized to cumulative photon dose. (c) Example measurements of ΔA_{830} normalized to cumulative photon dose of iron-replete and iron-deplete cultures. (d) K_{eff} (ms^{-1}) as a function of mean light intensity within the measurement cuvette for an iron-replete and iron-deplete culture measured at multiple excitation intensities and cell densities.

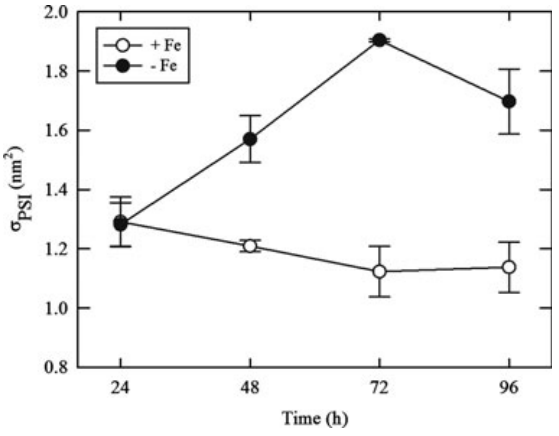

FIG. 3. The in vivo effective absorption cross-section of PSI (σ_{PSI}) measured on *Synechocystis* PCC 6803 under iron-replete (+Fe) and iron-deplete (−Fe) conditions. Displayed are results averaged from triplicates from three independent experiments with ±standard errors.

energy conversion efficiency) (Fig. 1b) became apparent 48 h after inoculation into low-iron media, indicating the point when the photophysiology switches to the iron-limited phenotype. This change was accompanied by a blue-shift of ~8 nm in the red-absorption peak of chl (indicative of expression of the *isiA* gene and accumulation of the IsiA protein) (Fig. 1c) and a decline in growth rate to ~84% of iron-replete cultures (Fig. 1d). Prolonged growth in iron-deplete media (>48 h) resulted in a continued reduction in F_v/F_m to 0.26, with significant differences from 48 h onward (*t*-test, $P < 0.05$) and further declines in growth rates to ~34% of iron-replete cultures, which had a μ^{max} of 1.38 ± 0.1. Alongside measurements of F_v/F_m, we calculated the absolute changes in F_o and F_m normalized to chl (data not shown). F_o and F_m remained relatively constant within iron-replete cultures, but increased from 48 h onward in the iron-deplete culture.

Measurements of ΔA_{830} during high-intensity light pulses displayed first-order saturation kinetics (Fig. 2a), with K_{eff} ranging from ~0.7 to 5 ms^{-1} (Fig. 2d). In contrast, first-order rate constants estimated from post-light-pulse ΔA_{830} relaxation kinetics ranged from 0.07 to 0.1 ms^{-1} (Fig. 2a). The rate of ΔA_{830} saturation normalized to cumulative photon dose at different saturation pulse intensities confirmed measurement of a photochemical absorption cross-section (Fig. 2b), and further confirmed the relative insensitivity of saturation kinetics to $P700^+$ re-reduction. When corrected for sample absorption, K_{eff} thus conformed to the expected linear function of excitation intensity (Fig. 2d), with a slope that will be equal to σ_{PSI} (eq. 1).

Clear differences in saturation kinetics were observed between iron-replete and iron-deplete cultures (Fig. 2, c and d). Measured values of σ_{PSI} indicated a significant shift between the two cultures from 48 h onward (Fig. 3), with the iron-replete culture remaining relatively constant at ~1.2 ±

0.1 nm^2, higher than, but still in reasonable agreement with, the theoretical cross-section for a PSI complex receiving absorption from only 100 chl molecules (Jordan et al. 2001, Ferreira et al. 2004). In contrast, σ_{PSI} increased from 48 h onward in the iron-starved culture to a maximum value of 1.90 ± 0.01 nm^2 on 72 h, ~60% larger than the iron-replete value at the same time point. Differences between treatments were significant from 48 h onward (*t*-test, $P < 0.05$).

Protein abundance. The absolute concentrations of the key photosynthetic proteins PSI, PSII, and IsiA, representing the vast majority of the chl-binding complexes in the cyanobacterial cell, were measured by quantitative Western blotting (Fig. 4) (Brown et al. 2008). In agreement with physiological measurements (Fig. 1c), protein abundances normalized to total protein concentration, indicated that the IsiA protein was only detectable from 48 h onward (Fig. 5a), increasing to a maximum of 0.53 ± 0.15 pmol IsiA · μg^{-1} total protein by 96 h. PSI decreased throughout to final value of 0.028 ± 0.012 pmol PSI · μg^{-1} total protein. PSII decreased between 48 and 72 h, remaining relatively constant until 96 h with a value of 0.035 ± 0.018 pmol PSII · μg^{-1} total protein.

When normalized to total cellular chl, IsiA:chl increased from 0.017 ± 0.002 to a maximum of 0.094 ± 0.041 mol · mol^{-1} on 96 h (Fig. 5b). This increase in IsiA:chl occurs alongside a decrease in PSI:chl while PSII:chl remained relatively constant, with final values of 0.0035 ± 0.0012 mol · mol^{-1} and 0.0015 ± 0.0006 mol · mol^{-1}, respectively (Fig. 5b). These measured values of protein abundance relative to total cellular chl were in good agreement with theoretical values (not shown) (Brown et al. 2008). These changes led to marked shifts in relative protein ratios, with the IsiA:PSI ratio increasing past the predicted ratio of 6:1 for an IsiA-PSI supercomplex after 48 h growth to a maximum of 27:1 at the end of the experiment, while PSII:PSI increased slightly from 0.4:1 to a final value of 0.8:1, in agreement with previous findings (Küpper et al. 2008).

The relative contribution of each protein complex (PSI, PSII, and IsiA) to the total cellular chl content was calculated using the protein ratios combined with numbers of chl molecules per complex (100, 36, and 12 per PSI, PSII, and IsiA, respectively) taken from structural studies that used the CP43 protein of PSII as a homolog for IsiA (Ferreira et al. 2004, Murray et al. 2006). On the basis of relative protein abundance and predicted chl budget, we further inferred how much of the IsiA protein could be structurally coupled to PSI based upon a theoretical IsiA:PSI ratio of 6:1 for the IsiA-PSI supercomplex combined with the observed ~60% increase in the functional PSI cross-section (from 72 h under Fe limitation), which suggested conversion of >80% of the total PSI pool to this state (Fig. 6a).

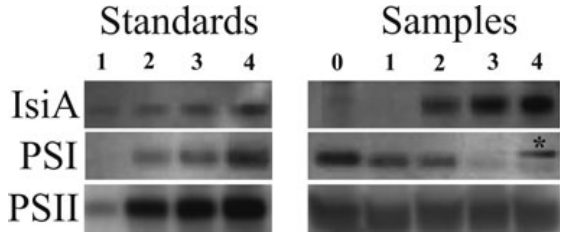

FIG. 4. Example of quantitative Western-blot detection of the chl-binding proteins (IsiA, PSI, and PSII). The left panel shows specific peptide standards at increasing concentrations (1–4). The right panel shows detection of specific peptide targets from total protein extracted from *Synechocystis* PCC 6803. The ''*'' indicates a band present under severe iron limitation that cross-reacts with PSI-specific global antibody not considered in quantification of this target.

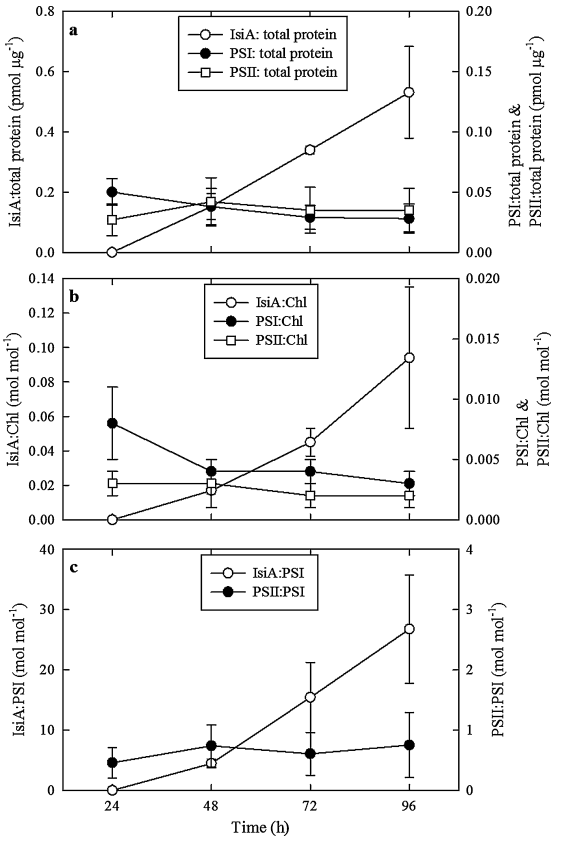

FIG. 5. Results from the protein quantification experiment. (a) Protein abundances determined by immunodetection on an iron-deplete culture. Measurements are normalized to total protein concentration in pmol · μg^{-1}. (b) Protein abundances normalized to chl in mol · mol^{-1}. (c) Protein ratios of an iron-deplete culture calculated from protein abundances normalized to chl, ratios in mol · mol^{-1}. Displayed are results averaged from three independent experiments with ±standard errors.

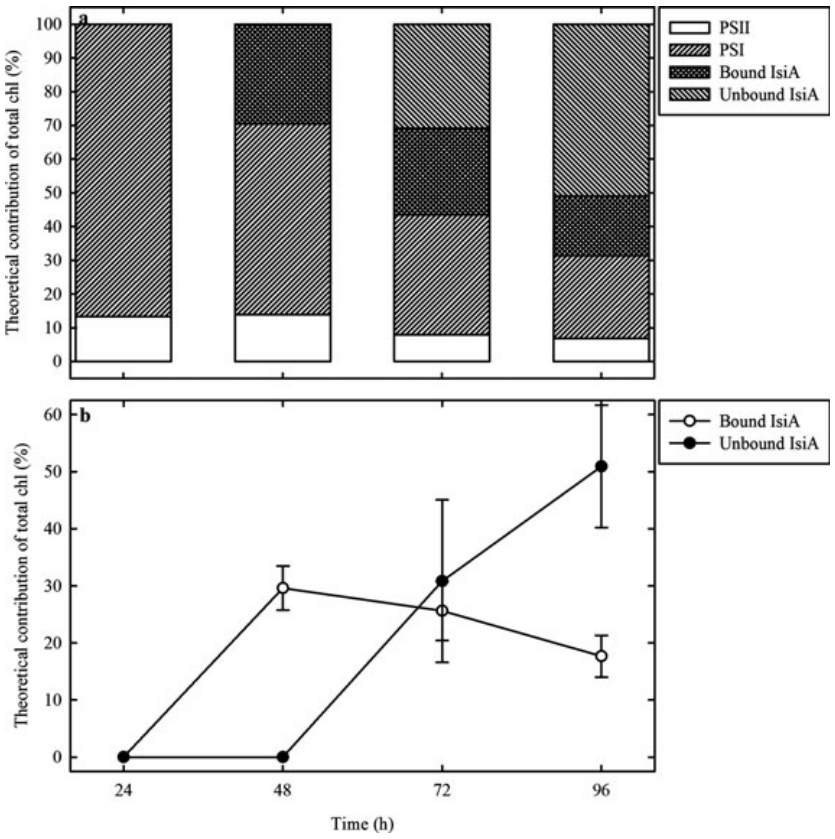

FIG. 6. The contribution to total chl content (%) by PSI, PSII, and IsiA proteins in an iron-deplete culture (a) and the contribution to total chl content (%) of bound and unbound IsiA plotted against time (b). Displayed are results averaged from three independent experiments with ±standard errors.

Using these calculations, it is clear that the IsiA protein is a substantial fraction of the total cellular chl content from 48 h onward. However, unbound IsiA was only inferred to represent a substantial fraction of total chl on 72 and 96 h. The potential contribution of bound and unbound IsiA thus shows differing trends (Fig. 6b). In particular, bound IsiA, as indicated by increased σ_{PSI}, becomes significant at the onset of iron stress. In contrast, the proportion of unbound IsiA only becomes significant after prolonged growth under iron stress.

DISCUSSION

In this paper, we describe the photosynthetic physiology of the cyanobacterium *Synechocystis* PCC 6803 grown under conditions of increasing iron stress at both biophysical and molecular levels. Biophysical measurements confirmed the development of increased iron-stress physiology over time. When compared with Fe-replete cultures, iron-depleted *Synechocystis* PCC 6803 showed a blue shift in the red chl absorption peak (Fig. 1c), indicative of accumulation of the iron-stress-induced protein IsiA (Burnap et al. 1993), and reductions in F_v/F_m (the photosynthetic energy conversion efficiency) (Fig. 1b) and growth rate (Fig. 1d). These are well-characterized responses of iron limitation and reflect an acclimation to growth under iron-limited conditions; the resulting different photosynthetic strategy enables photosynthesis to continue with a lower demand for iron (Behrenfeld et al. 1996, Bibby et al. 2001a).

Alongside clear evidence of iron stress, we provide the first demonstration of an increase of ~60% in σ_{PSI} in vivo (Fig. 3). This increase is consistent with the notion that the IsiA protein forms an antenna ring around PSI trimers, forming the IsiA-PSI supercomplex that has been biochemically isolated and shown to be energetically coupled (Melkozernov et al. 2003, Andrizhiyevskaya et al. 2004). Formation of this IsiA-PSI supercomplex has previously been proposed to represent a strategy to minimize the number of iron-containing PSI reaction centers required under iron-stress conditions (Bibby et al. 2001b,c, Küpper et al. 2008). The

increased effective cross-section was temporally correlated with both the ~8 nm blue shift in the red peak of the chl absorption and a reduction in F_v/F_m (Fig. 1, b and c).

In parallel with this physiological measurement, we have quantified the abundance of the photosynthetic reactions centers PSII and PSI and the iron-stress chl-binding protein IsiA, together representing the major pools of chl in the cell. Coincident with the initial increase in σ_{PSI}, the IsiA:PSI ratio increased from undetectable levels (no IsiA present) past the 6:1 ratio after 48 h (Fig. 5c). This is the ratio of PSI reaction centers to IsiA antenna proteins revealed in the 10 Å structure of the IsiA-PSI supercomplex (Bibby et al. 2003). At this point in progressive iron-stress development (48 h), the culture shows many signs of an iron-limited photophysiology, including a shift in the red-adsorption peak of chl (indicative of the accumulation of IsiA), and reductions in phycobilisomes (not shown), F_v/F_m and growth rate. At least 80% of the chl associated with expressed IsiA appears to be associated with PSI (Fig. 6a) if we are to account for the measured increase in σ_{PSI} (Fig. 3).

Under more severe iron stress (>48 h into iron limitation), while no further increase in σ_{PSI} or blue-shift in the red-absorption peak of chl is observed, IsiA continues to accumulate in the cell and F_v/F_m becomes severely reduced, alongside further reductions in growth rate. Cellular IsiA concentrations and IsiA:PSI ratios continued to increase to a maximum of 27:1 without a parallel increase in σ_{PSI}. The increase in IsiA:PSI ratios beyond 6:1 thus appears to represent the accumulation of IsiA that was functionally uncoupled from PSI in vivo. This pool of IsiA is therefore likely to be inactive in photosynthesis and may have an alternative role in the cell, such as a chl store or in photoprotection. It has been shown that IsiA can form a double ring around PSI (Chauhan et al. 2011). Theoretically, a double ring would have a cross-section of >2 nm^2 at 635 nm based upon an approximated 6-IsiA inner ring and an 8-IsiA outer ring. This value is higher than the maximal observed values of σ_{PSI} measured in this study (Fig. 3). The lack of a further increase in σ_{PSI} beyond day 48–72 suggests that the proportion of double ring complexes remains small in vivo.

Our estimated levels of uncoupled IsiA under progressive iron-stress conditions provide further evidence that this protein may not act solely as a peripheral antenna for PSI. A number of alternative roles have previously been suggested, including protecting PSII from excess light (Park et al. 1999) or acting as an alternate antenna for PSII (Pakrasi et al. 1985). The most likely alternative role would be as a chl storage protein (Sarcina and Mullineaux 2004, Singh and Sherman 2007); with ~50% of the total chl content in unbound IsiA, there is at least the possibility that this pool could act to rapidly increase photosynthesis under conditions of iron resupply (Behrenfeld et al. 2006). It has also been shown that an IsiA ring can form without a PSI trimer (Aspinwall et al. 2004), although whether such structures act as chl storage proteins or as a mechanism for protecting PSII via nonphotochemical quenching (Horton et al. 1996, Cadoret et al. 2004) also remains to be fully determined (Wilson et al. 2007, 2008). Irrespective of the functional role, increased levels of uncoupled IsiA observed under high iron-stress conditions should act to lower F_v/F_m by increasing F_o, as confirmed by the biophysical measurements.

The potential accumulation of significant amounts of unbound, and hence photochemically inactive, IsiA within natural iron-stressed phytoplankton populations where cyanobacteria dominate would have major implications for the interpretation of both in situ and remotely sensed data (Behrenfeld et al. 2006, 2009). As discussed above, unbound IsiA will likely have a high and nonvariable fluorescence yield, which will depress F_v/F_m as a result of increased F_o (Behrenfeld et al. 2006), thereby invalidating the strict interpretation of F_v/F_m as a measure of the photochemical quantum efficiency of PSII (Suggett et al. 2009). In addition, highly fluorescent unbound chl might contribute to the inferred high quantum yields of chl fluorescence in low-iron oceanic regions (Behrenfeld et al. 2009). The recent description of a eukaryotic chl-binding protein expressed under iron-stress conditions, Tidi (thylakoid iron-deficiency-induced) (Varsano et al. 2003, 2006), suggests that eukaryotic phytoplankton in oceanic regions could also potentially have a depressed F_v/F_m due to accumulation of nonphotosynthetically active chl. However, analogous to the IsiA-PSI supercomplex, Tidi has also only been shown to be an antenna system for PSI to date (Varsano et al. 2003, 2006). It is clear that a more detailed understanding of the role of iron-stress-induced chl-binding proteins in a range of marine phytoplankton may be required to interpret satellite-derived production estimates based on chl levels in large oceanic regions (Behrenfeld et al. 2006).

Establishing the contribution of unbound IsiA in natural populations will require an increased understanding of the levels of iron stress experienced by natural populations and how these relate to culture conditions. The batch culture experiments employed here and elsewhere (Bibby et al. 2001b,c, Yeremenko et al. 2004, Ivanov et al. 2006, Wang et al. 2010) will drive *Synechocystis* PCC 6803 into increasing levels of iron stress/starvation. Under these conditions, it appears that the primary role of IsiA is as a functioning PSI antenna (Fig. 3). However, subsequent excess accumulation may result from continued IsiA expression combined with down-regulation of the photosynthetic complexes (Fig. 5, a–c). Within natural populations, iron-limited

growth is more likely to approach a steady-state balance between iron uptake and resupply by regeneration owing to tight coupling between growth and loss terms (Cullen 1991, Morel et al. 1991). The relative contributions of bound and unbound IsiA to total chl (Fig. 6, a and b) suggests that unbound IsiA only increases under more severe cases of iron stress. Although we clearly cannot directly extrapolate from our laboratory measurements on a monoculture of a model organism, grown photoheterotrophically, to natural populations, we can propose that the time required under iron-starvation to accumulate large cellular pools of unbound IsiA may have limited ecological relevance. Although in situ growth rates of autotrophic prokaryotes clearly vary greatly in iron-limited systems (Mann and Chisholm 2000), given the high mortality rates reported (Landry et al. 1997), organisms with very low iron-limited growth rates would probably be outcompeted by other species.

Given the apparent role of IsiA as a functioning PSI antenna in combination with evidence for subsequent expression of uncoupled IsiA only under longer term iron-stress conditions, it may thus be premature to ascribe large-scale biophysical/biogeochemical patterns to the in situ expression of this protein and potential eukaryotic proteins with similar function (Behrenfeld et al. 2006, 2009). The role of chl-binding proteins, such as Tidi, which apparently acts as a functioning PSI antenna in eukaryotic algae, also needs to be studied further in culture and their presence verified in iron-limited oceanic regions (Varsano et al. 2006). In addition to model culture work to determine the functional role and identify the environmental conditions under which bound and unbound IsiA dominate, it is clearly necessary to obtain absolute quantification of IsiA and functionally similar proteins from iron-limited regions before it will be possible to determine whether a significant fraction of in situ chl is dominated by unbound pigment-protein complexes having no direct role in photosynthesis.

We thank S. R. Richier for help in running the protein samples and analysis of data. We also thank D. A. Campbell and S. E. Tulk for their work with the IsiA protein standard and method development. This work was supported by the Natural Environment Research Council (UK) through grants NF/F019254/1 and NE/G009155/1 to T. S. B. and C. M. M. and a studentship to T. R. K.

Andrizhiyevskaya, E. G., Frolov, D., van Grondelle, R. & Dekker, J. P. 2004. Energy transfer and trapping in the photosystem I complex of *Synechococcus* PCC 7942 and in its supercomplex with IsiA. *Biochim. Biophys. Acta* 1656:104–13.

Andrizhiyevskaya, E. G., Schwabe, T. M. E., Germana, M., D'Haene, S., Kruip, J., van Grondelle, R. & Dekker, J. P. 2002. Spectoscopic properties of PSI-IsiA supercomplexes from the cyanobacterium *Synechococcus* PCC 7942. *Biochim. Biophys. Acta* 1556:265–72.

Aspinwall, C. L., Duncan, J., Bibby, T. S., Mullineaux, C. W. & Barber, J. 2004. The trimeric organisation of photosystem I is not necessary for the iron-stress induced CP43' protein to functionally associate with this reaction centre. *FEBS Lett.* 574:126–30.

Behrenfeld, M. J., Bale, A. J., Kolber, Z. S., Aiken, J. & Falkowski, P. G. 1996. Confirmation of iron limitation of phytoplankton photosynthesis in the equatorial Pacific Ocean. *Nature* 383:508–11.

Behrenfeld, M. J. & Kolber, Z. S. 1999. Widespread iron limitation phytoplankton in the South Pacific Ocean. *Science* 283:840–3.

Behrenfeld, M. J., Westberry, T. K., Boss, E. S., O'Malley, R. T., Siegel, D. A., Wiggert, J. D., Franz, B. A., et al. 2009. Satellite-detected fluorescence reveals global physiology of ocean phytoplankton. *Biogeosciences* 6:779–94.

Behrenfeld, M. J., Worthington, K., Sherrell, R. M., Chavez, F. P., Strutton, P., McPhaden, M. & Shea, D. M. 2006. Controls on tropical Pacific Ocean productivity revealed through nutrient stress diagnostics. *Nature* 442:1025–8.

Bibby, T. S., Gorbunov, M. Y., Wyman, K. W. & Falkowski, P. G. 2008. Photosynthetic community responses to upwelling in mesoscale eddies in the subtropical North Atlantic and Pacific Oceans. *Deep-Sea Res. Part II Top. Stud. Oceanogr.* 55:1310–20.

Bibby, T. S., Mary, I., Nield, J., Partensky, F. & Barber, J. 2003. Low-light-adapted *Prochlorococcus* species possess specific antennae for each photosystem. *Nature* 424:1051–54.

Bibby, T. S., Nield, J. & Barber, J. 2001a. Antenna ring around trimeric photosystem I in oxyphotobacteria. *Photosynth. Res.* 69:71.

Bibby, T. S., Nield, J. & Barber, J. 2001b. Iron deficiency induces the formation of an antenna ring around trimeric photosystem I in cyanobacteria. *Nature* 412:743–5.

Bibby, T. S., Nield, J. & Barber, J. 2001c. Three-dimensional model and characterization of the iron stress-induced CP43'-photosystem I supercomplex isolated from the cyanobacterium *Synechocystis* PCC 6803. *J. Biol. Chem.* 276:43246–52.

Bibby, T. S., Nield, J., Partensky, F. & Barber, J. 2001d. Oxyphotobacteria – antenna ring around photosystem I. *Nature* 413:590.

Bibby, T. S., Zhang, Y. & Chen, M. 2009. Biogeography of photosynthetic light-harvesting genes in marine phytoplankton. *PLoS ONE* 4:e4601.

Bidigare, R. R., Ondrusek, M. E., Morrow, J. H. & Kiefer, D. A. 1990. In vivo absorption properties of algal pigments. *In* Spinrad, R. W. [Ed.] *Ocean Optics X.* Spie - Int Soc Optical Engineering, Bellingham, pp. 290–302.

Boekema, E. J., Hifney, A., Yakushevska, A. E., Piotrowski, M., Keegstra, W., Berry, S., Michel, K. P., Pistorius, E. K. & Kruip, J. 2001. A giant chlorophyll-protein complex induced by iron deficiency in cyanobacteria. *Nature* 412:745–8.

Boyd, P. W. & Abraham, E. R. 2001. Iron-mediated changes in phytoplankton photosynthetic competence during SOIREE. *Deep-Sea Res. Part II Top. Stud. Oceanogr.* 48:2529–50.

Boyer, G. L., Gillam, A. H. & Trick, C. G. 1987. Iron chelation and uptake. *In* Fay, P. & Van Baalen, C. [Eds] *The Cyanobacteria.* Elsevier, New York, pp. 415–36.

Bricker, T. M. & Frankel, L. K. 2002. The structure and function of CP47 and CP43 in photosystem II. *Photosynth. Res.* 72:131–46.

Bricker, T. M., Morvant, J., Marsi, N., Sutton, H. M. & Frankel, L. K. 1998. Isolation of a highly active photosystem II preparation from *Synechocystis* 6803 using a histidine-tagged mutant of CP47. *Biochim. Biophys. Acta* 1409:50–7.

Brown, C. M., MacKinnon, J. D., Cockshutt, A. M., Villareal, T. A. & Campbell, D. A. 2008. Flux capacities and acclimation costs in *Trichodesmium* from the Gulf of Mexico. *Mar. Biol.* 154:413–22.

Burnap, R. L., Troyan, T. & Sherman, L. A. 1993. The highly abundant chlorophyll-protein complex of iron-deficient *Synechococcus* sp. PCC 7942 (CP43') is encoded by the isiA gene. *Plant Physiol.* 103:893–902.

Cadoret, J.-C., Demoulière, R., Lavaud, J., van Gorkom, H. J., Houmard, J. & Etienne, A.-L. 2004. Dissipation of excess energy triggered by blue light in cyanobacteria with CP43' (*isiA*). *Biochim. Biophys. Acta* 1659:100–4.

Chauhan, D., Folea, I. M., Jolley, C. C., Kouřil, R., Lubner, C. E., Lin, S., Kolber, D., Wolfe-Simon, F., Golbeck, J. H., Boekema, E. J. & Fromme, P. 2011. A novel photosynthetic strategy for

adaptation to low-iron aquatic environments. *Biochemistry* 50:686–92.

Chen, M. & Bibby, T. S. 2005. Photosynthetic apparatus of antenna-reaction centres supercomplexes in oxyphotobacteria: insight through significance of Pcb/IsiA proteins. *Photosynth. Res.* 86:165–73.

Cullen, J. J. 1991. Hypotheses to explain high-nutrient conditions in the open sea. *Limnol. Oceanogr.* 36:1578–99.

Cullen, J. J. & Davis, R. F. 2003. The blank can make a big difference in oceanographic measurements. *Limnol. Oceanogr. Bull.* 12:29–35.

Erdner, D. L., Price, N. M., Doucette, G. J., Peleato, M. L. & Anderson, D. M. 1999. Characterization of ferredoxin and flavodoxin as markers of iron limitation in marine phytoplankton. *Mar. Ecol. Prog. Ser.* 184:43–53.

Falkowski, P. G. & Kolber, Z. 1995. Variations in chlorophyll fluorescence yields in phytoplankton in the world oceans. *Aust. J. Plant Physiol.* 22:341–55.

Ferreira, K. N., Iverson, T. M., Maghlaoui, K., Barber, J. & Iwata, S. 2004. Architecture of the photosynthetic oxygen-evolving centre. *Science* 303:1831–3.

Garczarek, L., Hess, W. R., Holtzendorff, J., Van der Staay, G. W. M. & Partensky, F. 2000. Multiplication of antenna genes as a major adaptation to low light in a marine prokaryote. *Proc. Natl. Acad. Sci. U. S. A.* 97:4098–101.

Green, B. R. 2003. The evolution of light harvesting antennas. *In* Green, B. R. [Ed.] *Light-Harvesting Antennas in Photosynthesis.* Kluwer Academic Publishers, Dordrecht, the Netherlands, pp. 129–68.

Guikema, J. A. & Sherman, L. A. 1983. Organization and functionof chlorophyll in membranes of cyanobacterium during iron starvation. *Plant Physiol.* 73:250–6.

Horton, P., Ruban, A. V. & Walters, R. G. 1996. Regulation of light harvesting in green plants. *Annu. Rev. Plant Physiol. Plant Mol. Biol.* 47:655–84.

Ivanov, A. G., Krol, M., Sveshnikov, D., Selstam, E., Sandström, S., Koochek, M., Park, Y.-I., Vasil'ev, S., Bruce, D., Öquist, G. & Huner, N. P. A. 2006. Iron deficiency in cyanobacteria causes monomerization of photosystem I trimers and reduces the capacity for state transitions and the effective absorption cross section of photosystem I in vivo. *Plant Physiol.* 141:1436–45.

Johnsen, G., Nelson, N. B., Jovine, R. V. M. & Prézelin, B. B. 1994. Chromoprotein-and pigment-dependent modelling of spectral light absorption in tow dinoflagellates, *Prorocentrum minimum* and *Heterocapsa pygmaea. Mar. Ecol. Prog. Ser.* 114:245–58.

Jordan, P., Fromme, P., Witt, H. T., Klukas, O., Saenger, W. & Krauss, N. 2001. Three-dimensional structure of cyanobacterial photosystem I at 2.5 angstrom resolution. *Nature* 411:909–17.

Küpper, H., Šetlík, I., Seibert, S., Prášil, O., Šetlikova, E., Strittmatter, M., Levitan, O., Lohscheider, J., Adamska, I. & Berman-Frank, I. 2008. Iron limitation in the marine cyanobacterium *Trichodesmium* reveals new insights into regulation of photosynthesis and nitrogen fixation. *New Phytol.* 179:784–98.

La Roche, J., Van der Staay, G. W. M., Partensky, F., Ducret, A., Aebersold, R., Li, R., Golden, S. S., Hiller, R. G., Wrench, P. M., Larkum, A. W. D. & Green, B. R. 1996. Independent evolution of the prochlorophyte and green plant chlorophyll a/b light-harvesting proteins. *Proc. Natl. Acad. Sci. U. S. A.* 93:15244–8.

Landry, M. R., Barber, R. T., Bidigare, R. R., Chai, F., Coale, K. H., Dam, H. G., Lewis, M. R., et al. 1997. Iron and grazing constraints on primary production in the central equatorial Pacific: an EqPac synthesis. *Limnol. Oceanogr.* 42:405–18.

Lowry, O. H., Rosebrough, N. J., Farr, A. L. & Randall, R. J. 1951. Protein measurement with the Folin phenol reagent. *J. Biol. Chem.* 193:265–75.

Mann, E. L. & Chisholm, S. W. 2000. Iron limits the cell division rate of *Prochlorococcus* in the eastern equatorial Pacific. *Limnol. Oceanogr.* 45:1067–76.

Martin, J. H., Coale, K. H., Johnson, K. S., Fitzwater, S. E., Gordon, R. M., Tanner, S. J., Hunter, C. N., et al. 1994. Testing the iron hypothesis in ecosystems of the Equatorial Pacific Ocean. *Nature* 371:123–9.

Melkozernov, A. N., Bibby, T. S., Lin, S., Barber, J. & Blankenship, R. E. 2003. Time-resolved absorption and emission show that the CP43' antenna ring of iron-stressed *Synechocystis* sp. PCC6803 is efficiently coupled to the photosystem I reaction center core. *Biochemistry* 42:3893–903.

Morel, F. M. M., Hudson, R. J. M. & Price, N. M. 1991. Limitation of productivity by trace metals in the sea. *Limnol. Oceanogr.* 36:1742–55.

Moseley, J. L., Allinger, T., Herzog, S., Hoerth, P., Wehinger, E., Merchant, S. & Hippler, M. 2002. Adaptation to Fe-deficiency requires remodelling of the photosynthetic apparatus. *EMBO J.* 21:6709–20.

Murray, J. W., Duncan, J. & Barber, J. 2006. CP43-like chlorophyll binding proteins: structural and evolutionary implications. *Trends Plant Sci.* 11:152–8.

Nielsdóttir, M. C., Moore, C. M., Sanders, R., Hinz, D. J. & Achterberg, E. P. 2009. Iron limitation of the postbloom phytoplankton communities in the Iceland Basin. *Glob. Biogeochem. Cycles* 23:1–13.

Öquist, G. 1974. Light-induced changes in pigment composition of photosynthetic lamellae and cell-free extracts from the blue-green alga *Anacystis nidulans. Physiol. Plant.* 30:45–8.

Pakrasi, H. B., Riethman, H. C. & Sherman, L. A. 1985. Organization of pigment proteins in the photosystem II complex of the cyanobacterium *Anacystis ridulans* R2. *Proc. Natl. Acad. Sci. U. S. A.* 82:6903–7.

Park, Y. I., Sandström, S., Gustafsson, P. & Öquist, G. 1999. Expression of the *isiA* gene is essential for the survival of the cyanobacterium *Synechococcus* sp. PCC 7942 by protecting photosystem II from excess light under iron limitation. *Mol. Microbiol.* 32:123–9.

Peterson, G. L. 1979. Review of the Folin phenol protein quantification method of Lowry, Rosebrough, Farr, and Randall. *Anal. Biochem.* 100:201–20.

Price, N. M. 2005. The elemental stoichiometry and composition of an iron-limited diatom. *Limnol. Oceanogr.* 50:1149–58.

Sandström, S., Ivanov, A. G., Park, Y. I., Öquist, G. & Gustafsson, P. 2002. Iron stress responses in the cyanobacterium *Synechococcus* sp. PCC7942. *Physiol. Plant.* 116:255–63.

Sandström, S., Park, Y. I., Öquist, G. & Gustafsson, P. 2001. CP43', the *isiA* gene product, functions as an excitation energy dissipator in the cyanobacterium *Synechococcus* sp. PCC 7942. *Photochem. Photobiol.* 74:431–7.

Sarcina, M. & Mullineaux, C. W. 2004. Mobility of the IsiA chlorophyll-binding protein in cyanobacterial thylakoid membranes. *J. Biol. Chem.* 279:36514–8.

Schägger, H. 2006. Tricine-SDS-PAGE. *Nat. Protocols* 1:16–22.

Singh, A. K. & Sherman, L. A. 2007. Reflections on the function of IsiA, a cyanobacterial stress-inducible, chl-binding protein. *Photosynth. Res.* 93:17–25.

Strauss, N. A. 1994. Iron deprivation: physiology and gene regulation. *In* Bryant, D. A. [Ed.] *The Molecular Biology of Cyanobacteria.* Kluwer Academic Publisher, Dordrecht, the Netherlands, pp. 731–50.

Suggett, D. J., Moore, C. M., Hickman, A. E. & Geider, R. J. 2009. Interpretation of fast repetition rate (FRR) fluorescence: signatures of phytoplankton community structure versus physiological state. *Mar. Ecol. Prog. Ser.* 376:1–19.

Ting, C. S., Rocap, G., King, J. & Chisholm, S. W. 2002. Cyanobacterial photosynthesis in the oceans: the origins and significance of divergent light-harvesting strategies. *Trends Microbiol.* 10:134–42.

Varsano, T., Kaftan, D. & Pick, U. 2003. Effects of iron deficiency on thylakoid membrane structure and composition in the alga *Dunaliella salina. J. Plant Nutr.* 26:2197–210.

Varsano, T., Wolf, S. G. & Pick, U. 2006. A chlorophyll *a/b*-binding protein homolog that is induced by iron deficiency is associated with enlarged photosystem I units in the eukaryotic alga *Dunaliella salina. J. Biol. Chem.* 281:10305–15.

Wang, Q., Hall, C. L., Al-Adami, M. Z. & He, Q. 2010. IsiA is required for the formation of photosystem I supercomplexes

and for efficient state transition in *Synechocystis* PCC 6803. *PLoS ONE* 5:e10432.

Welschmeyer, N. A. 1994. Fluorometric analysis of chlorophyll-a in the presence of chlorophyll-b and pheopigments. *Limnol. Oceanogr.* 39:1985–92.

Williams, J. G. K. 1988. Construction of specific mutations in photosystem II photosynthetic reaction center by genetic engineering methods in *Synechocystis* 6803. *Methods Enzymol.* 167:766–78.

Wilson, A., Boulay, C. & Kirilovsky, D. 2008. Light induced energy dissipation in iron-starved cyanobacteria. *Photosynth. Energy Sun* 24:1607–10.

Wilson, A., Boulay, C., Wilde, A., Kerfield, C. A. & Kirilovsky, D. 2007. Light-induced energy dissipation in iron starved cyanobacteria: roles of OCP and IsiA proteins. *Plant Cell* 19:656–72.

Yeremenko, N., Kouřil, R., Ihalainen, J. A., D'Haene, S., van Oosterwijk, N., Andrizhiyevskaya, E. G., Keegstra, W., et al. 2004. Supramolecular organization and dual function of the IsiA chlorophyll-binding protein in cyanobacteria. *Biochemistry* 43:10308–13.

Zipfel, W. & Owens, T. G. 1991. Calculation of absolute photosystem I absorption cross-sections from P700 photo-oxidation kinetics. *Photosynth. Res.* 29:23–35.

E.1.2 HLNA Submission to Limnology & Oceanography

Ryan-Keogh, T. J., Macey, A. I., Nielsdóttir, M. C., Lucas, M. I., Steigenberger, S. S., Stinchcombe, M. C., Achterberg, E. P., Bibby, T. S. and Moore, C. M., (2013), "Spatial and temporal development of phytoplankton iron stress in relation to bloom dynamics in the high latitude North Atlantic Ocean", *Limnology and Oceanography* ,Volume 58, Issue 2, Pages 533-545, dpi:10.4319/lo.2013.58.2.0533

Submitted: 26th June 2012

Accepted: 5th November 2012

Published: 4th February 2013

Limnol. Oceanogr., 58(2), 2013, 533–545

doi:10.4319/lo.2013.58.2.0533

Spatial and temporal development of phytoplankton iron stress in relation to bloom dynamics in the high-latitude North Atlantic Ocean

Thomas J. Ryan-Keogh,[a,*] Anna I. Macey,[a] Maria C. Nielsdóttir,[a] Michael I. Lucas,[b] Sebastian S. Steigenberger,[a] Mark C. Stinchcombe,[c] Eric P. Achterberg,[a] Thomas S. Bibby,[a] and C. Mark Moore [a]

[a] Ocean and Earth Science, National Oceanography Centre Southampton, University of Southampton, Waterfront Campus, Southampton, United Kingdom
[b] Marine Research Institute, University of Cape Town, Rondebosch, South Africa
[c] National Oceanography Centre, Southampton, Southampton, United Kingdom

Abstract

The high-latitude North Atlantic (HLNA) is characterized by a marked seasonal phytoplankton bloom, which removes the majority of surface macronutrients. However, incomplete nitrate depletion is frequently observed during summer in the region, potentially reflecting the seasonal development of an iron (Fe) limited phytoplankton community. In order to investigate the seasonal development and spatial extent of iron stress in the HLNA, nutrient addition experiments were performed during the spring (May) and late summer (July and August) of 2010. Grow-out experiments (48–120 h) confirmed the potential for iron limitation in the region. Short-term (24 h) incubations further enabled high spatial coverage and mapping of phytoplankton physiological responses to iron addition. The difference in the apparent maximal photochemical yield of photosystem II (PSII) ($F_v : F_m$) between nutrient (iron) amended and control treatments ($\Delta(F_v : F_m)$) was used as a measure of the relative degree of iron stress. The combined observations indicated variability in the seasonal cycle of iron stress between different regions of the Irminger and Iceland Basins of the HLNA, related to the timing of the annual bloom cycle in contrasting biogeochemical provinces. Phytoplankton iron stress developed during the transition from the prebloom to peak bloom conditions in the HLNA and was more severe for larger cells. Subsequently, iron stress was reduced in regions where macronutrients were depleted following the bloom. Iron availability plays a significant role in the biogeochemistry of the HLNA, potentially lowering the efficiency of one of the strongest biological carbon pumps in the ocean.

The high-latitude ($>\sim 50^{\circ}$N) North Atlantic (HLNA) is characterized by a pronounced spring phytoplankton bloom, representing one of the largest annual productivity cycles in the oceans (Siegel et al. 2002). The associated annual drawdown of macronutrients (e.g., > 10 μmol L^{-1} nitrate) (Sanders et al. 2005) and export production indicate that the biological carbon pump (Volk and Hoffert 1985) of the HLNA is one of the strongest of any large open oceanic region (Laws et al. 2000). Although the annual bloom cycle removes a large proportion of the macronutrients available at the end of winter, further indicating a highly efficient biological carbon pump, residual concentrations of both nitrate and phosphate (e.g., > 1 μmol L^{-1} nitrate) are frequently observed during summer in the region (Sanders et al. 2005; Nielsdóttir et al. 2009).

The large seasonal removal of macronutrients resulting from the North Atlantic spring bloom contrasts strongly with the other high-latitude systems of the subpolar North Pacific and Southern Ocean, which are both characterized by year round high-nitrate, low-chlorophyll (HNLC) conditions, at least partly as a consequence of low iron availability (Boyd et al. 2007). Consequently, despite some early evidence to the contrary (Martin et al. 1993), iron had not been considered to be a potentially limiting micronutrient in the HLNA. However, it was recently demonstrated that summer phytoplankton communities in the Iceland Basin are prone to iron limitation (Nielsdóttir et al. 2009). Consequently, as suggested for the Southern Ocean (Boyd 2002), the dominant bottom-up influences on phytoplankton growth may transition from irradiance during winter to iron during summer in the HLNA. From the perspective of limits on biomass formation (Cullen 1991), such observations are consistent with the relative input ratios of iron and nitrate being lower than phytoplankton requirements at higher latitudes in the North Atlantic (Measures et al. 2008; Nielsdóttir et al. 2009), partly due to low atmospheric iron supply (Jickells et al. 2005; Moore et al. 2006), at least in regions removed from potentially significant local sources (Prospero et al. 2012).

Top-down factors may also influence accumulation of phytoplankton biomass and nutrient drawdown (Walsh 1976; Banse 2002). In addition to a proposed role of predator–prey dynamics during bloom initiation (Behrenfeld 2010), zooplankton grazing (Walsh 1976), which may be particularly high for small phytoplankton groups, likely plays a major role in the subsequent progression and termination of the bloom (Banse 2002). Silicate limitation of large diatoms, which may otherwise have been able to escape grazing control (Cullen 1991), has also been hypothesized to contribute to incomplete nutrient drawdown in the HLNA (Henson et al. 2006). Rather than

* Corresponding author: T.Ryan-Keogh@noc.soton.ac.uk

acting alone, within the classical HNLC regions these mechanisms likely interact with iron stress in maintaining residual macronutrients (Cullen 1991; Price et al. 1994).

Beyond the available evidence for a limited region of the Iceland Basin during summer (Nielsdóttir et al. 2009), the seasonal and spatial extent of any potential iron stress in the HLNA remains poorly resolved. Consequently, the effect of iron availability on the large-scale biogeochemistry of the region is currently difficult to assess. In this study, changes in phytoplankton standing stocks and photophysiology were assessed in both 48–120 h grow-out experiments and high spatial resolution short-term (24 h) incubations in order to investigate the response of natural populations to the relief of potential nutrient stress.

The apparent maximal photochemical yield of photosystem II (PSII) as measured using variable chlorophyll fluorescence ($F_v : F_m$) is particularly sensitive to iron stress, and hence variability in this parameter can provide a powerful diagnostic for investigating iron stress in the field (Kolber et al. 1994; Boyd and Abraham 2001; Behrenfeld et al. 2006). The value of $F_v : F_m$ is frequently observed to be suppressed within HNLC systems and, more significantly, increases rapidly following iron resupply to iron-stressed field populations both in situ (Kolber et al. 1994; Boyd and Abraham 2001) and in bottle incubations (Greene et al. 1994; Moore et al. 2007; Nielsdóttir et al. 2009). Measurement of such rapid photophysiological changes following deliberate experimental manipulations avoids potential problems in the interpretation of, for example, the absolute value of $F_v : F_m$ in situ, where any physiological signal will be superposed over taxonomic variability (Suggett et al. 2009). In addition, because physiological changes will precede resultant changes in biomass accumulation, restricting experimental time when monitoring sensitive changes to the photosynthetic apparatus minimizes the influence of bottle effects on biomass accumulation and the potential confounding influence of shifts in community structure on physiological measurements (Geider and La Roche 1994; Greene et al. 1994).

The current study thus aimed to establish the seasonal cycle of iron stress across both the Iceland and Irminger Basins of the HLNA. By combining in vitro incubation experiments with remote sensing data and in situ measurements of phytoplankton physiology, macronutrients, and chlorophyll, we mapped the development of physiological iron stress. Moreover, contrasting responses to iron addition observed in different biogeographical regions allowed us to describe the seasonal progression of iron stress within the HLNA and assess the potential for both iron limitation of phytoplankton growth and macronutrient removal.

Methods

Data were obtained during two cruises of the RRS *Discovery* to the HLNA, a spring cruise (D350) from 28 April to 10 May 2010 (Day of Year (DOY) 118–130) and a summer cruise (D354) from 04 July to 10 August 2010 (DOY 185–222). During the spring cruise eight short-term (24 h) and two long-term (> 24 h) incubation experiments were performed. A further 17 short-term and 7 long-term incubation experiments were undertaken during the summer cruise. Trace metal clean water for the incubation experiments was pumped from a trace metal clean fish towed at a depth of ~ 4 m, while the ship was steaming at no less than 5 knots, into a dedicated clean chemistry container using a polytetrafluoroethylene diaphragm pump (Almatec 15).

Incubation experiments were performed using similar methods to those employed previously in the HNLC Southern Ocean and Iceland basin (Moore et al. 2007; Nielsdóttir et al. 2009). Water for the experiments was collected and transferred unscreened into acid-washed 1 liter polycarbonate bottles (Nalgene) for the 24 h incubation experiments and 4.5 liter polycarbonate bottles for the long-term incubation experiments. All water was collected during the hours of darkness. Incubation bottles were filled in a random order with the triplicate samples for initial measurements collected at the beginning, middle, and end of the filling process. In addition to an unamended control, within the 24 h incubation experiments, different treatments were amended with 0.2 nmol L^{-1} $FeCl_3$, 2.0 nmol L^{-1} $FeCl_3$, 1.0 μmol L^{-1} NO_3^-, or 2.0 nmol L^{-1} $FeCl_3$ and 1.0 μmol L^{-1} NO_3^- (hereafter, + 0.2 Fe, + 2.0 Fe, + 1.0 N and + FeN); all experimental conditions were conducted as biological duplicates or triplicates.

Long-term experiments were run for 48–120 h and consisted of two treatments, a control and 2.0 nmol L^{-1} Fe addition only (hereafter, + Fe), or four treatments, a control, 2.0 nmol L^{-1} Fe, 1.0 μmol L^{-1} NO_3^- and 2.0 nmol L^{-1} Fe + 1.0 μmol L^{-1} NO_3^- (hereafter, + Fe, + N, and + FeN). All bottle tops were sealed with film (Parafilm™), and bottles were double bagged with clear plastic bags to minimize contamination risks on deck. On-deck incubations were performed using "blue lagoon" filters (LEE Filters) to provide light levels corresponding to 35% of above surface irradiance. Running surface seawater was used to control the temperature in the incubators.

Samples for analysis of chlorophyll and macronutrients were collected from both the experiments and from the ship's nontoxic underway seawater supply, which has an intake depth of ~ 5 m. Samples for chlorophyll analysis (250 mL) were filtered onto GF/F or 5 μm polycarbonate filters (Whatman) and then extracted into 90% acetone for 24 h in the dark at 5°C before analysis with a fluorometer (TD70; Turner Designs) (Welschmeyer 1994). Macronutrient samples were drawn into 40 mL diluvials and immediately refrigerated at 4°C until analysis, which typically commenced within 12 h of sampling. A subset of macronutrient samples was filtered and frozen for post-cruise analysis. Concentrations of the macronutrients nitrate plus nitrite (hereafter dissolved inorganic nitrogen [DIN]), phosphate, and silicate were determined using a Skalar San Plus autoanalyzer as described previously (Sanders and Jickells 2000). Concentrations of dissolved iron for samples collected using the trace metal clean fish were determined by isotope dilution inductively coupled plasma mass spectrometry as described by Milne et al. (2010). Analysis was performed on an Element II instrument (ThermoFisher Scientific, Bremen, Germany)

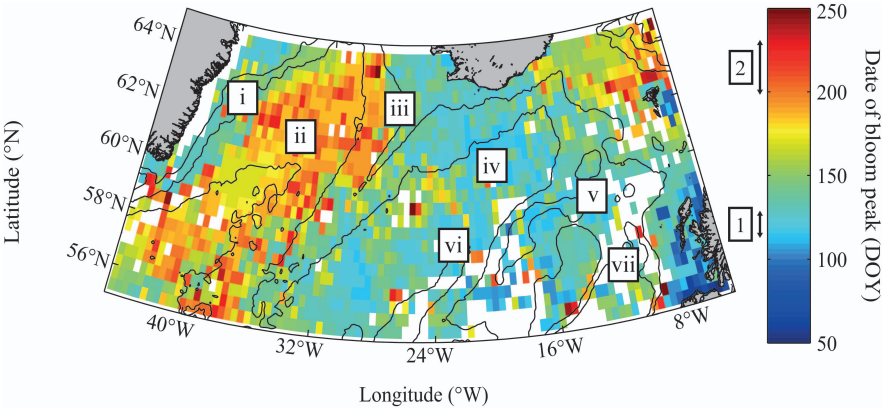

Fig. 1. Date of bloom peak for the HLNA calculated using MODIS data. Black contours correspond to bathymetry in 1000 m isobaths. Indicated on colorbar are approximate timings of both cruises, where 1 = D350 (spring) and 2 = D354 (summer). Geographic regions of the HLNA include i = Western Irminger Basin, ii = Central Irminger Basin, iii = Reykjanes Ridge, iv = Iceland Basin, v = Rockhall Bank, vi = Hatton Bank, and vii = Rockhall Trough.

following an offline preconcentration and matrix removal step via solid phase extraction on a column filled with the chelating resin Wako carboxymethylated pentaethylenehexamine (CM-PEHA). Accuracy of the method was verified by analysing 'sampling and analysis of iron reference (SAFE)' samples.

Chlorophyll fluorescence measurements for discrete water samples were performed using a Chelsea Scientific Instruments Fasttracka™ Mk II Fast Repetition Rate fluorometer (FRRf) integrated with a FastAct™ Laboratory system. Subsampling of incubations for chlorophyll, macronutrient concentrations, and FRRf occurred between 00:00 and 03:00 local time. All samples were dark acclimated for 30 min, and FRRf measurements were corrected for the blank effect using carefully prepared 0.2 μm filtrates for all experiments and time points (Cullen and Davis 2003). Blanks were typically around 1% and always $<$ 10% of the maximal fluorescence signal. Size-fractionated FRRf measurements were performed by gentle filtration through a 5 μm polycarbonate filter, with the $<$ 5 μm fraction measured directly on the filtrate and the $>$ 5 μm fraction measured following gentle resuspension of retained cells in 0.2 μm filtered seawater. Fluorescence was also recorded underway using a Chelsea Scientific Instruments Fasttracka™ Mk I FRRf. Protocols for FRRf measurements and data processing were similar to those detailed elsewhere (Moore et al. 2007).

Satellite ocean color data were used to place in situ and experimental data within the context of the annual spring bloom cycle. Moderate Resolution Imaging Spectroradiometer (MODIS) 8 day composites were first used to generate a 40 day running mean 0.42 degree, 8 day resolution time series of surface chlorophyll for 2010. The date of the bloom peak was then pragmatically identified at each location as the first time at which the rate of change of the net chlorophyll growth rate dropped below 8×10^{-4} d^{-2}, provided the bloom had already reached $>$ 0.7 μg Chl L^{-1}. Visual inspection of the satellite chlorophyll time series and comparison with in situ data (*see* below) confirmed that this criterion was a reasonable predictor of the early stage of the bloom peak in the region.

Results

Satellite data were used to derive the timing of the spring bloom in both the Iceland and Irminger Basins of the HLNA during 2010 (Fig. 1). The criterion chosen to identify the date of the peak indicated a later bloom in the Central Irminger Basin than elsewhere in the region (Fig. 1). This difference in bloom timing during 2010 was confirmed by in situ measurements of chlorophyll and macronutrients. In situ chlorophyll concentrations peaked during the spring cruise in the Iceland Basin (Fig. 2a) and the summer cruise in the Central Irminger Basin (Fig. 2b). Overall, the transition from spring to summer in the Iceland Basin corresponded to a decrease in average in situ chlorophyll concentrations from $\sim$ 2 to $\sim$ 1.5 μg L^{-1}, compared with an increase from $\sim$ 1.0 to $\sim$ 2.5 μg L^{-1} in the Central Irminger Basin. Alongside these changes in chlorophyll concentration, there were marked decreases in the in situ DIN (Fig. 2c,d) and silicate (Fig. 2e,f) concentrations from spring to summer, with the Iceland Basin having lower concentrations than the Irminger Basin for both seasons. In particular, summer DIN concentrations in the central Iceland Basin were $<$ 1 μmol L^{-1} (Fig. 2d), with silicate $<$ 0.3 μmol L^{-1} (Fig. 2f). Initial dissolved ($<$ 0.4 μm) iron concentrations at experimental locations were frequently lower in summer, with concentrations measured at more than half the summer stations (range $<$ 0.01–0.28 nmol L^{-1}) being below the minimum values encountered during spring (range 0.07–0.28 nmol L^{-1}).

Sea surface values of in situ $F_v : F_m$, measured during the period of darkness (local midnight $\pm$ 4 h) also displayed marked changes in both basins across the seasons, with generally higher values in spring. Superposed onto this seasonal signal, in situ values of $F_v : F_m$ were higher in the

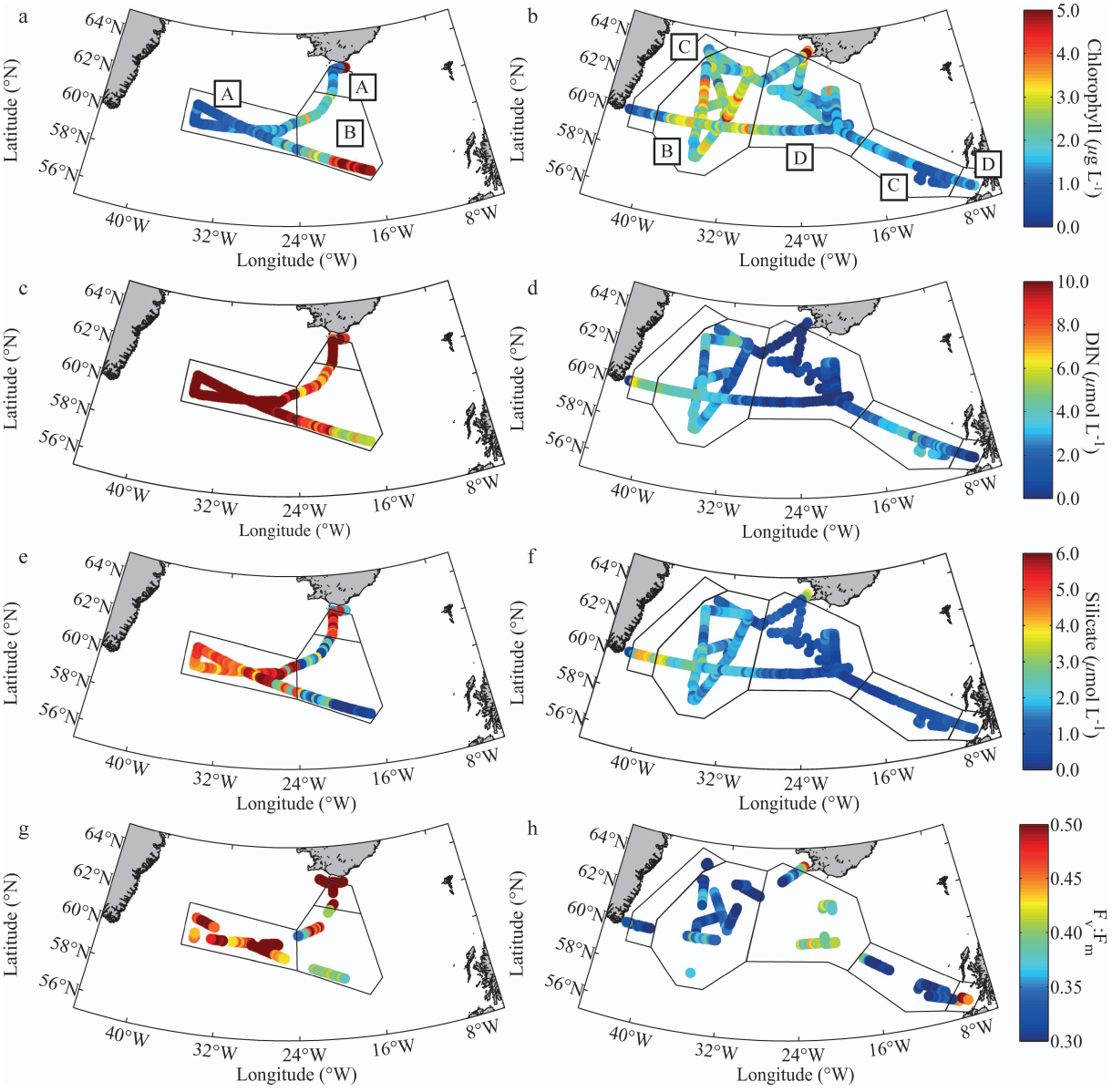

Fig. 2. (a,b) Sea surface chlorophyll concentrations (μg L^{-1}), (c,d) dissolved inorganic nitrogen (DIN) concentrations (μmol L^{-1}), (e,f) silicate concentrations (μmol L^{-1}), and (g,h) nighttime $F_v : F_m$ value during the (a,c,e,g) spring and (b,d,f,h) summer cruises. Solid black lines delineate regions on the basis of in situ sea surface variables and bloom timing during both cruises. (a,b) Regions are labeled according to conditions that correspond to (A) prebloom, (B) bloom, (C) postbloom, high DIN, and (D) postbloom, low DIN.

Irminger Basin than the Iceland Basin in spring (Fig. 2g) but lower in the Irminger Basin and Rockall region than the Iceland Basin in summer (Fig. 2h). By combining these in situ sea surface variables with the bloom timings, different regions of the HLNA could be defined and ascribed to the different bloom stages and conditions during both cruises. Satellite-derived bloom timing was first used to separate the temporal progression of bloom into broad prebloom, bloom, and postbloom periods. Regions and periods sampled under postbloom conditions were then further differentiated on the basis of observed residual macronutrient (DIN) concentrations. Consequently, we identify four broad conditions encountered in different regions over different periods during the two cruises, namely, prebloom (labeled A in Fig. 2), bloom (labeled B), postbloom high DIN (labeled C), and postbloom low

Table 1. Locations for long-term experiments conducted during D350 (spring) and D354 (summer) alongside values of initial and 24 h $F_v:F_m$, and net growth rates estimated from chlorophyll accumulation and nitrate drawdown over the first 72 h (except as noted below). Shown are averages ± standard errors ($n = 2$ or 3).

Cruise	Exp.	Lat. (°N)	Long. (°W)	$F_v:F_{m\ Initial}$	$F_v:F_{m\ Control}$, 24 h	$F_v:F_{m\ Fe}$, 24 h	$\mu^{Chl}_{Control}$ (d^{-1}), 0–72 h	μ^{Chl}_{Fe} (d^{-1}), 0–72 h	$\Delta NO_{3Control}^{-}$ ($\mu mol\ L^{-1}\ d^{-1}$), 0–72 h	ΔNO_{3Fe}^{-} ($\mu mol\ L^{-1}\ d^{-1}$), 0–72 h
D350	1	60.97	−34.86	0.38±0.02	0.57±0.01	0.58±0.00	0.10±0.02	0.12±0.01	0.18±0.03	0.20±0.03
D350	2	59.99	−29.20	0.48±0.01	0.49±0.01	0.50±0.00	0.11±0.03	0.09±0.00	1.47±0.04	1.52±0.03
D354	1	59.99	−19.91	0.19±0.04	*	*	0.22±0.02†	0.20±0.02†	0.35±0.00†	0.35±0.00†
D354	2	60.00	−20.47	0.36±0.00	0.37±0.01	0.39±0.01	−0.10±0.01†	−0.12±0.01†	0.14±0.00†	0.14±0.00†
D354	3	60.00	−34.38	0.32±0.01	0.26±0.04	0.33±0.01	−0.12±0.14	0.14±0.04	0.13±0.14	0.52±0.19
D354	4	63.03	−35.29	0.29±0.01	0.30±0.01	0.39±0.01	−0.04±0.02	0.25±0.01	0.19±0.04	0.57±0.05
D354	5	58.16	−35.03	0.34±0.00	0.33±0.01	0.39±0.00	0.02±0.01	0.24±0.01	0.18±0.00	0.52±0.02
D354	6	63.84	−34.74	0.29±0.00	0.31±0.00	0.40±0.00	0.04±0.00	0.28±0.01	0.81±0.05	0.76±0.23
D354	7	61.37	−21.16	0.37±0.01	0.36±0.01	0.41±0.01	0.03±0.01	0.15±0.02	0.19±0.01	0.21±0.00

* Measurement not performed.
† In D354 experiments 1 and 2, growth rates and nitrate drawdown were calculated over the first 48 h.

DIN (labeled D). These regions, defined on the basis of in situ observations and satellite-derived bloom timings, subsequently provided context for the analysis of the experimental observations.

Long-term (> 24 h) incubation experiments—Data from 48–120 h experiments indicated variable responses to iron addition to the extant phytoplankton communities (*see* Table 1). During spring, no evidence for iron stress was observed for an experiment initiated over the Reykjanes Ridge (experiment D350.2) (Fig. 3a), with no significant differences in $F_v:F_m$ (analysis of variance [ANOVA], $p > 0.05$) or chlorophyll concentration (Fig. 3b) (ANOVA, $p > 0.05$) observed between the iron addition and control bottles at any time point. During the same season an experiment set up in the Central Irminger Basin (experiment D350.1) provided some evidence that the in situ phytoplankton community had the potential to become iron stressed, with relative decreases in $F_v:F_m$ in the control treatment (Fig. 3c) and increased chlorophyll concentration (Fig. 3d) seen within the iron-addition treatment compared with the control treatment after 120 h of incubation. Enhanced nutrient drawdown (data not shown) after 120 h was also evident within the iron-addition treatment, with nitrate drawdown, calculated as the difference between the initial concentration and the final concentration (ΔNO_3^- ($\mu mol\ L^{-1}\ d^{-1}$)) being significantly higher (ANOVA, $p < 0.05$) at 0.26 ± 0.01 ($\mu mol\ L^{-1}\ d^{-1}$) in the iron-addition treatment compared with 0.21 ± 0.01 ($\mu mol\ L^{-1}\ d^{-1}$) for the control treatment.

During the summer, iron addition had a more pronounced influence on phytoplankton community responses, particularly in the Irminger Basin. Rapid increases in $F_v:F_m$ were frequently observed within 24 h of iron amendment, as illustrated by a representative experiment from the Western Irminger Basin (experiment D354.6) (Fig. 3e). These rapid physiological changes were subsequently followed by increased nutrient drawdown and biomass accumulation, as inferred from bulk chlorophyll concentrations (Fig. 3f; Table 1). Net growth rates estimated from increases in chlorophyll and nutrient drawdown following iron addition were frequently higher than that in controls, particularly in the Central and Western Irminger Basin (Table 1).

In contrast, within the Iceland Basin during the summer cruise, where surface nitrate concentrations were frequently undetectable (< 0.03 $\mu mol\ L^{-1}$) (Fig. 2d), no chlorophyll increases were observed on addition of nitrate alone, while the greatest increases in chlorophyll were typically observed only following the combined addition of both iron and nitrate. For example, during experiment D354.7 (Fig. 3h), net chlorophyll based growth rates within the combined (+ FeN) treatment were ~ 80% and 40% higher than observed in controls or iron alone additions, respectively. However, iron addition resulted in the same increase in $F_v:F_m$ as the combined treatment (+ FeN), while $F_v:F_m$ for the nitrate treatment was indistinguishable from the control (Fig. 3g). Consequently, although iron addition alone promoted a rapid photophysiological response (Fig. 3g), significantly higher chlorophyll accumulation within the

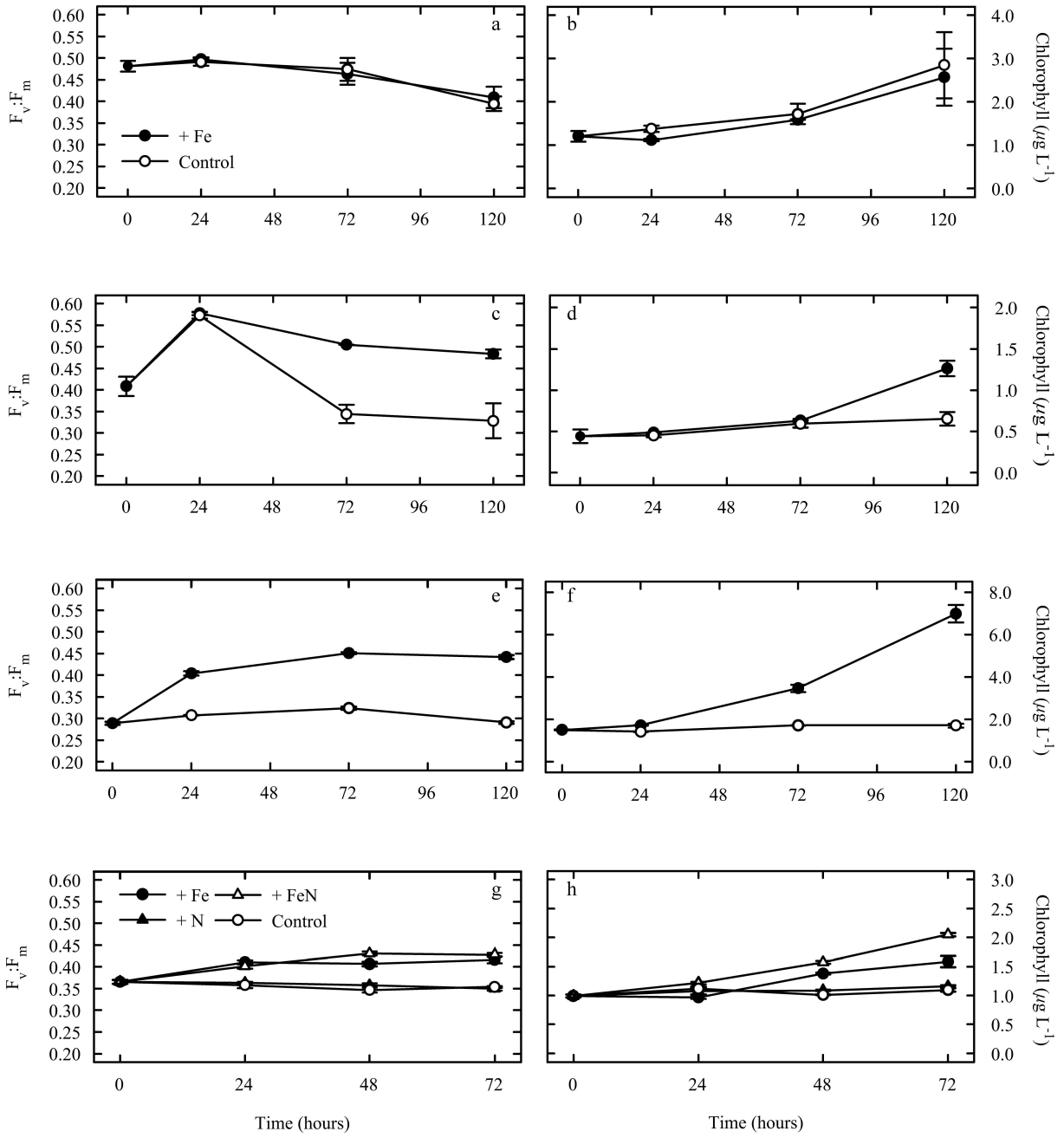

Fig. 3. $F_v:F_m$ and chlorophyll responses (μg L^{-1}) from representative long-term (> 24 h) experiments initiated over (a,b) the Reykjanes ridge (spring) (experiment D350.2), (c,d) the Irminger basin (spring) (experiment D350.1), (e,f) the Irminger basin (summer) (experiment D354.6), and (g,h) the Iceland basin (summer) (experiment D354.7). Shown are averages with ± standard errors, (n = 3 for all time points of the Iceland basin experiment, whereas n = 3, 2, 2, and 5 for time points 0, 24, 72, and 120 h, respectively, in the other experiments).

+ FeN (Fig. 3h) was suggestive of a system approximating a state of iron and nitrate colimitation (Arrigo 2005; Saito et al. 2008).

Short-term (24 h) incubation experiments—The 25 short-term 24 h incubation experiments conducted over both cruises further revealed variability between basins and seasons. Significant (ANOVA, $p < 0.05$) rapid changes in photophysiology ($F_v : F_m$) were often observed in these experiments, despite the lack of significant changes in other variables such as chlorophyll or nutrient concentration over the short 24 h time scale. In order to contrast relative changes in PSII photophysiology between the large numbers of experiments, we calculated the difference in $F_v : F_m$ between control and treatment bottles ($\Delta(F_v : F_m)$). $\Delta(F_v : F_m)$ was calculated for all the different nutrient addition treatments performed during both cruises over the two seasons (Fig. 4). For simplicity, calculated values of $\Delta(F_v : F_m)$ are hereafter subscripted "+ 1.0 N," "+ FeN," "+ 0.2 Fe," or "+ 2 Fe" corresponding to the 1 μmol L^{-1} nitrate, 1 μmol L^{-1} nitrate and 2.0 nmol L^{-1} Fe, 0.2 nmol L^{-1} and 2.0 nmol L^{-1} iron additions, respectively.

Values of $\Delta(F_v : F_m)_{+1.0\ N}$ were frequently indistinguishable from zero (Fig. 4) or slightly negative, due to a small drop in $F_v : F_m$ following N addition in some experiments, as previously observed in some other systems (Behrenfeld et al. 2006). In contrast, $\Delta(F_v : F_m)$ was frequently positive following iron addition (Figs. 4, 5), with the values calculated for the two iron alone treatments (+ 0.2 Fe and + 2.0 Fe) being highly correlated ($r^2 = 0.960$, $n = 23$, $p < 0.001$) and hence displaying consistent spatial patterns (Fig. 5). Moreover, within those natural populations displaying significant responses (ANOVA, $p < 0.05$), the addition of 2.0 nmol L^{-1} iron consistently resulted in a larger change in $F_v : F_m$ (on average 40% higher) than the addition of 0.2 nmol L^{-1} iron (Figs. 4b, 5). Consequently the observed variability of $\Delta(F_v : F_m)$ following iron addition ($\Delta(F_v : F_m)_{+0.2\ Fe\ or\ +2.0\ Fe}$) indicated spatially and temporally coherent physiological responses that scaled with increasing iron enrichment (Fig. 5). We thus interpret $\Delta(F_v : F_m)_{+0.2\ Fe\ or\ +2.0\ Fe}$ as a relative measure of the degree of iron stress, providing a means to compare and contrast the interbasin and intrabasin and seasonal variability.

Values of $\Delta(F_v : F_m)_{+0.2\ Fe\ or\ +2.0\ Fe}$ were lowest under the prebloom conditions (labeled A in Fig. 2), suggesting a lack of physiological iron stress for these populations (Figs. 4a; 5a,b), consistent with the lack of a treatment response in longer term grow-out experiments performed under the same conditions (Fig. 3a). Low $\Delta(F_v : F_m)$ was also observed following iron addition within the postbloom low DIN conditions (labeled D in Fig. 2) encountered in the Iceland Basin (Fig. 5c,d), where the + FeN treatment also tended to have a higher $\Delta(F_v : F_m)$ than that for iron alone (data not shown) and where longer term experiments indicated the potential for colimitation of chlorophyll accumulation by iron and nitrate (Fig. 3h). Higher values of $\Delta(F_v : F_m)_{+0.2\ Fe\ or\ +2.0\ Fe}$ were observed during the bloom conditions (labeled B in Fig. 2) encountered in the Iceland Basin during the spring cruise (Fig. 5a,b) and the Central Irminger Basin during the summer cruise (labeled B in Fig. 2) (Fig. 5c,d), while the highest values were observed under postbloom high DIN conditions (labeled C in Fig. 2), as encountered in the Western Irminger Basin and Rockall region during the summer cruise (Fig. 5c,d). These regions corresponded to the clearest influence of iron addition on chlorophyll accumulation and nitrate drawdown in longer term experiments (Fig. 3f, Table 1).

To provide a more quantitative comparison of short-term ($\leq$24 h) physiological responses to nutrient amendment with longer-term biomass responses inferred from bulk chlorophyll accumulation, we compared the value of $\Delta(F_v : F_m)_{+2.0\ Fe}$ observed after 24 h in the long-term experiments (Table 1) with differences in chlorophyll derived net growth rates over 72 h between iron amended and control treatments (Fig. 6). Values of $\Delta(F_v : F_m)_{+2.0\ Fe}$ and $\Delta\mu^{Chl}$ were highly correlated ($R^2 = 0.87$, $p < 0.05$, $n = 8$) (Fig. 6), indicating that the observed short-term physiological responses were predictive of subsequent biomass responses in experiments.

Size-fractionated photosynthetic physiology—Size-fractionated $F_v : F_m$ measurements performed on the initial samples from incubation experiments, revealed a consistent pattern throughout both basins, with the < 5 μm size fraction having a higher in situ $F_v : F_m$ than the > 5 μm size fraction. Overall, $F_v : F_m$ values for the < 5 μm and > 5 μm fractions were, respectively, $\sim$ 10% higher and $\sim$ 25% lower than those of the bulk community. Although both size classes physiologically responded to the addition of Fe (Fig. 7), the response of the > 5 μm size fraction was generally larger (Fig. 7a). For example, in a longer timescale experiment (experiment D354.6) performed in the Western Irminger Basin, the value of $F_v : F_m$ for the > 5 μm fraction had nearly increased to that of the iron-amended < 5 μm fraction after 120 h (Fig. 7a). The addition of iron also resulted in a net chlorophyll derived growth rate for the > 5 μm fraction (over 120 h) that was double that of the < 5 μm size fraction (0.45 ± 0.01 $\mu^{Chl>5}$ (d^{-1}) compared with 0.22 ± 0.01 $\mu^{Chl<5}$ (d^{-1})) (Fig. 7b). However, within the Iceland Basin, although $F_v : F_m$ was also lower for the > 5 μm size fraction than the < 5 μm size fraction (Fig. 7c), the increase was less pronounced and $F_v : F_{m>5\mu m}$ did not increase to a value equivalent to that of the initial or control < 5 μm size fraction. The chlorophyll concentration in the < 5 μm size fraction also remained higher than that for the > 5 μm size fraction in this experiment (Fig. 7d).

Discussion

The annual cycle of phytoplankton growth in the HLNA results in significant seasonality in surface macronutrient concentrations. During winter, photosynthesis is likely limited by low mean irradiance, with net phytoplankton growth occurring rapidly following the onset of stratification (Sverdrup 1953), although alternative controlling factors have been suggested for bloom initiation (Behrenfeld 2010). Subsequently, in contrast to the majority of high-latitude open ocean systems, where large seasonal macronutrient drawdown appears to be restricted by the

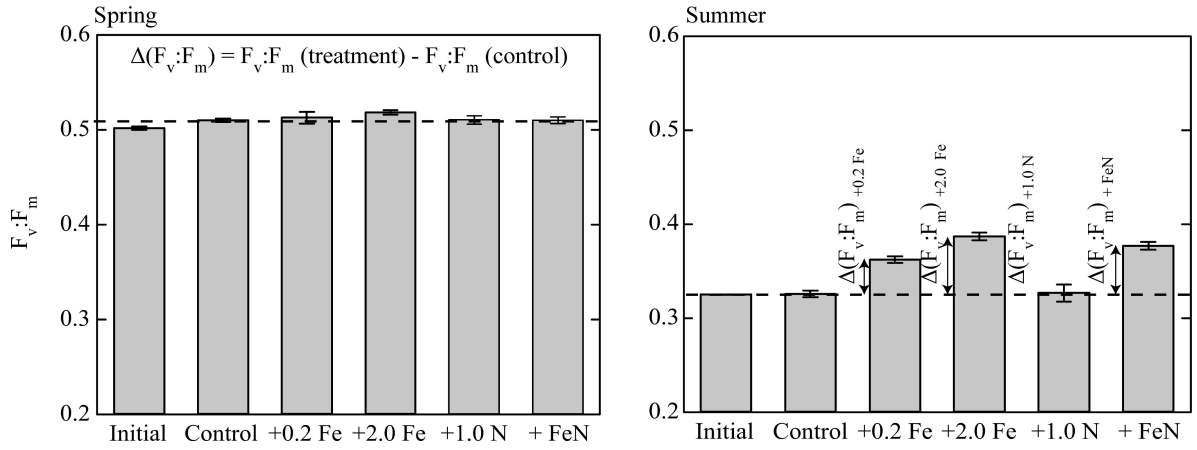

Fig. 4. Representative data from two short-term experiments set up during D350 (spring) and D354 (summer). $\Delta(F_v:F_m)$ is calculated as the difference between the $F_v:F_m$ of the nutrient amended treatment and the control treatment at the 24 h time point. Four different values were calculated, $\Delta(F_v:F_m)_{+0.2\ Fe}$, $\Delta(F_v:F_m)_{+2.0\ Fe}$, $\Delta(F_v:F_m)_{+1.0\ N}$, and $\Delta(F_v:F_m)_{+FeN}$. Dashed line represents level of control treatment. Shown are averages with ± standard errors, where $n = 3$ for all treatments.

availability of iron (Martin and Fitzwater 1988; De Baar et al. 1990; Boyd et al. 2007), macronutrient drawdown over the growing season in the HLNA can be substantial. However, despite the magnitude of the bloom, residual DIN concentrations have frequently been observed in the HLNA at the end of the growing season (Sanders et al. 2005; Nielsdóttir et al. 2009), suggesting that some factor is constraining the complete use of this nutrient resource (Cullen 1991; Greene et al. 1994). Although a lack of bioavailable iron is one possibility (Nielsdóttir et al. 2009), zooplankton grazing (Walsh 1976) or silicate limitation (Henson et al. 2006) could also play a role.

Satellite-derived estimates of bloom timing (Fig. 1) enabled us to place the observed spatial and temporal variability of in situ variables and experimental indices of iron stress within the annual bloom cycle (Fig. 8). In situ observations of chlorophyll and nutrients confirmed the temporal progression of a classical "spring bloom," with macronutrient drawdown accompanying the peak accumulation of phytoplankton biomass, as inferred by bulk

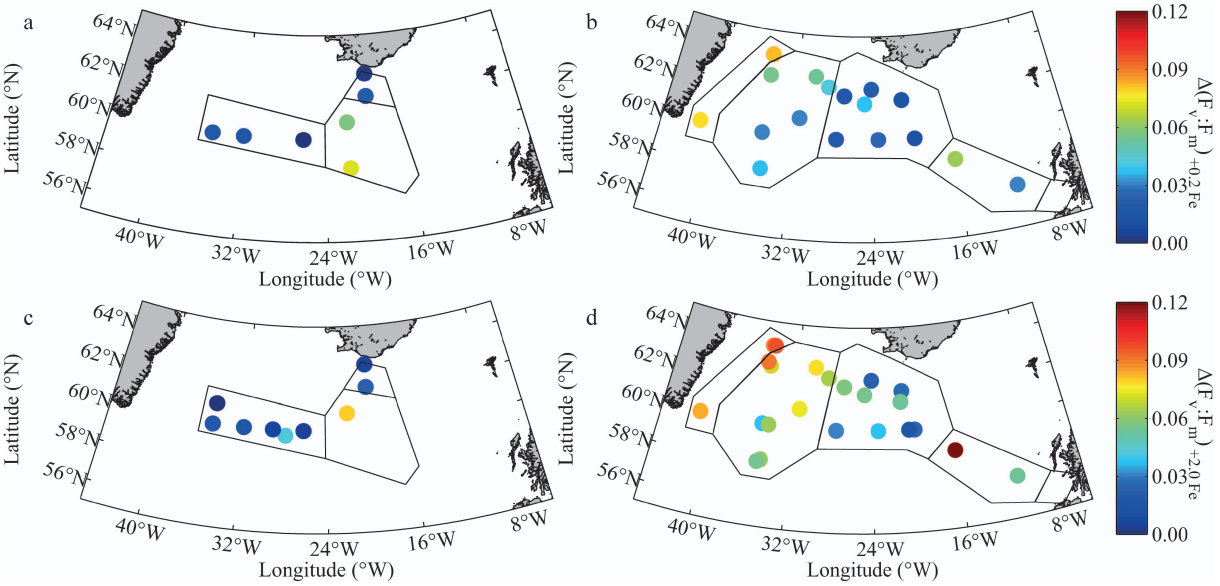

Fig. 5. Experimental values of $\Delta(F_v:F_m)$ calculated after 24 hr for (a,b) the 0.2 nmol L^{-1} iron (+ 0.2 Fe) and (c,d) the 2.0 nmol L^{-1} iron (+ 2.0 Fe) addition treatments during (a,c) the spring and (b,d) summer cruises. Regions are as indicated in Figure 1.

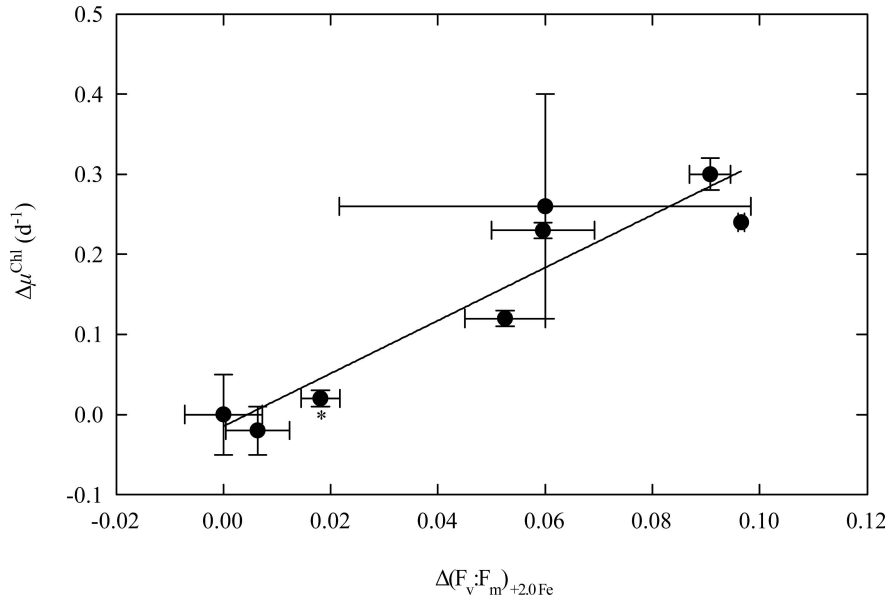

Fig. 6. $\Delta(F_v:F_m)_{+2.0\ Fe}$ plotted against the difference in chlorophyll derived net growth rates over 72 h ($\Delta\mu^{Chl}$ (d^{-1})) for all long-term experiments, where $\Delta\mu^{Chl}$ (d^{-1}) is μ^{Chl} (d^{-1}) for the + Fe treatment minus μ^{Chl} (d^{-1}) from the control treatment. *Growth rate calculated over 48 h only because of shortened experimental duration. Shown are averages with ± standard errors (where $n = 2$ or 3 for $\Delta(F_v:F_m)_{+2.0\ Fe}$ and $n = 3$ or 5 for $\Delta\mu^{Chl}$).

chlorophyll (Fig. 8). Clear spatial differences in bloom timing and progression were observed within the HLNA during 2010. The Iceland basin, Western Irminger Basin, and Rockall region bloomed earlier in the spring (Figs. 1, 2a). However, while there was near complete nutrient drawdown in the Iceland Basin by summer (Fig. 2d), there was incomplete nutrient drawdown (residual nitrate > 1 μmol L^{-1}) in the Western Irminger Basin and Rockall region. In contrast, the Central Irminger Basin bloomed later in the growing season (Figs. 1, 2b) with incomplete nutrient drawdown where the bloom was still underway (Fig. 2d). The almost complete nutrient drawdown observed in the Iceland Basin in the present study is anomalous for this region, with values (< 1 μmol L^{-1} DIN) being lower than typically recorded for the summer period (Sanders et al. 2005; Nielsdóttir et al. 2009), possibly indicative of an additional source of iron to this basin in 2010.

Grow-out bioassay incubation experiments (Fig. 3) demonstrated the development of iron limitation of the in situ phytoplankton population in the Central and Western Irminger Basin from spring to summer but showed evidence of an iron and nitrate colimited system in the Iceland Basin by summer (Table 1; Fig. 3). Size-fractionated analysis of the phytoplankton community in situ and during bioassay experiments suggested that the larger size fraction (> 5 μm) was experiencing greater iron stress and consequently responded more strongly to iron addition (Fig. 7). Such observations are consistent with the similar responses found during an in situ iron release in HNLC systems (Kolber et al. 1994) and suggest that smaller cells might be less susceptible to iron stress when availability is low (Cullen 1991; Price et al. 1994). Community-level characteristics of iron stress development within the HLNA spring bloom thus appear consistent with the hypothesis that iron limitation develops principally through broadly increasing levels of stress for larger cell sizes (Hudson and Morel 1990; Sunda and Huntsman 1997; De Baar et al. 2005). Subsequent iron limitation of macronutrient drawdown may then represent a combined effect of grazer control of the small-celled populations, with restrictions on the growth rates of the larger, less heavily grazed cells, resulting from low iron availability (Cullen 1991; Price et al. 1994; Sunda and Huntsman 1997).

Short duration iron-addition experiments conducted over the growing season enabled us to map the spatial and temporal extent of iron stress throughout the HLNA using the derived variable $\Delta(F_v:F_m)_{+0.2\ Fe\ or\ +2.0\ Fe}$ (Figs. 4, 5). Moreover, the value of $\Delta(F_v:F_m)_{+2.0\ Fe}$ was well correlated with observed differences in net growth rates inferred from chlorophyll accumulation following iron addition in the longer term grow-out experiments (Fig. 6). Such an empirical relationship between $\Delta(F_v:F_m)_{+2.0\ Fe}$ and $\Delta\mu^{Chl}$ should not be taken to infer any universal relationship between the absolute value of $F_v:F_m$ and phytoplankton growth rates (Parkhill et al. 2001; Price 2005; Kruskopf and Flynn 2006). For example, high values of $F_v:F_m$ have been observed under steady-state iron or nitrogen limitation in culture (Parkhill et al. 2001; Price 2005) and nitrogen (iron) (co-)limitation both in laboratory studies (Schrader et al. 2011) and in situ (Behrenfeld et al. 2006). However, the observed correlation between two independent measures of the relative level of iron stress within the studied natural communities (Fig. 6)

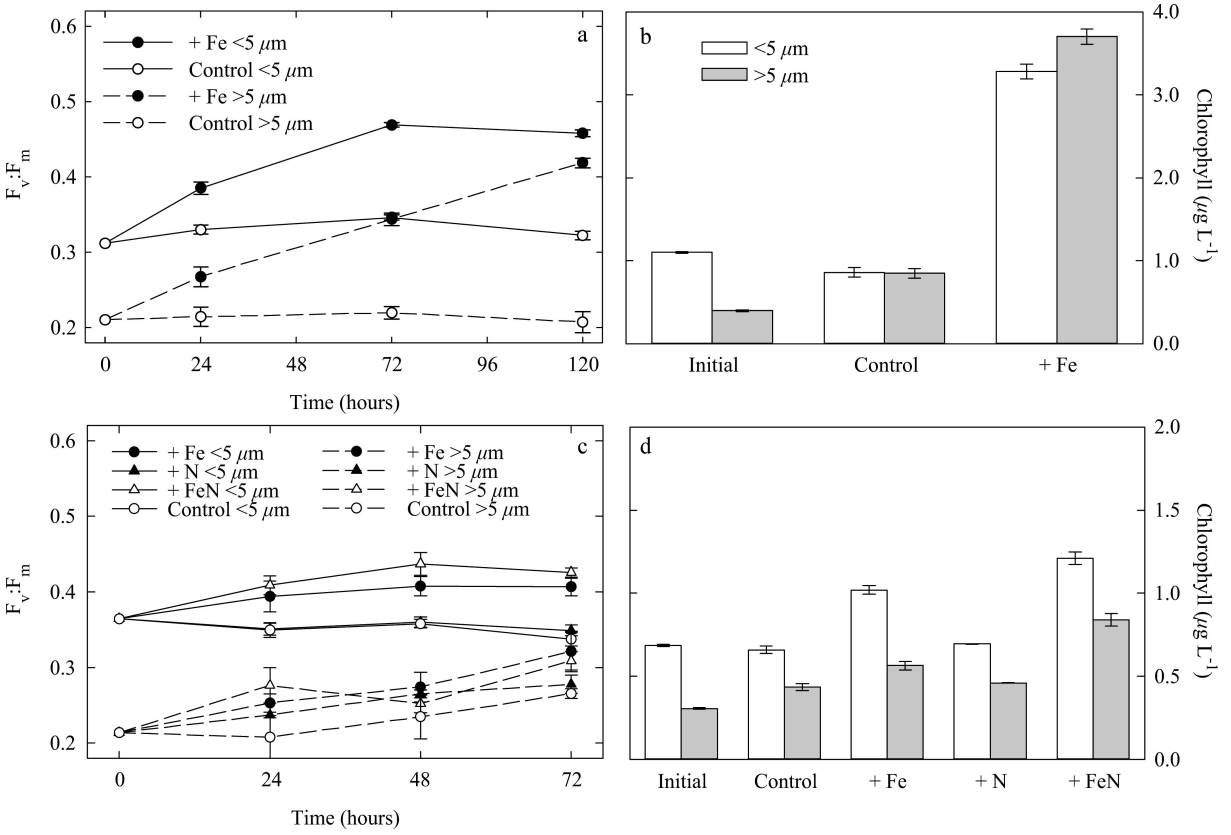

Fig. 7. (a,c) Size-fractionated $F_v:F_m$ and (b,d) chlorophyll responses from long-term (> 24 h) experiments set up in (a,b) the Irminger basin (experiment D354.6) and (c,d) the Iceland basin (experiment D354.7) during the summer. Shown are averages with ± standard errors (n = 3 for all time points of D354.7, and n = 3, 2, 2, and 5 for 0, 24, 72, and 120 h time points in D354.6).

provided empirical evidence that physiological iron stress, as indicated by the short-term response of a biomass-independent measure of phytoplankton physiology ($F_v:F_m$), was likely accompanied by a significant repression of phytoplankton community growth rates.

Placing our experimental results within the seasonal cycle resolved using satellite-derived bloom timing alongside the in situ chlorophyll and DIN concentrations (Fig. 8), the four broad stages representing (A) prebloom, (B) bloom, (C) postbloom high DIN, and (D) postbloom low DIN conditions (as defined in Fig. 2) could be related to differing levels of iron stress (Fig. 8). Low levels of iron stress, which were inferred from measurements of $\Delta(F_v:F_m)$ (Fig. 8b) and $\Delta\mu^{Chl}$ (Fig. 8c), were observed under prebloom conditions (e.g., spring in the Central Irminger Basin), when chlorophyll was low (Fig. 8a), DIN was high (Fig. 8b), and in situ $F_v:F_m$ was high (Fig. 2g). Low levels of iron stress were also observed under postbloom conditions (summer in Iceland Basin) when chlorophyll was low, DIN was depleted, and in situ $F_v:F_m$ was intermediate (Fig. 2h), with long-term grow-out experiments indicating a condition approximating Fe and N colimitation in this system (Fig. 3g,h). Between these two conditions, higher levels of iron stress coincided with the peak of the bloom (Fig. 8a), while the highest levels were observed under postbloom high DIN conditions (Fig. 8b), coincident with the lowest in situ values of $F_v:F_m$ (Fig. 2h). In 2010 such conditions prevailed during summer in the Western side of the Irminger Basin and the Rockall region (Fig. 2d).

Resource availability and loss terms are both crucial determinants of net community growth and hence ultimately biomass accumulation and/or (macro-) nutrient removal (Banse 1991; Banse 2002). Although significant levels of iron stress developed within the HLNA during the peak of the phytoplankton bloom, nitrate removal appeared to continue beyond this stage in some regions (Fig. 8b), indicating that the community retained a capacity for net growth (Fig. 8c). Consequently, although physiological iron stress appears to develop at some stage in the bloom cycle throughout the HLNA (Figs. 5, 8) and is likely linked to restriction of net community growth rates (Fig. 6), with $\mu^{Chl,\ net}$ up to 0.3 d^{-1} higher following the addition of iron (Table 1 and Fig. 8c), the development of iron stress may not necessarily correspond to an ultimate

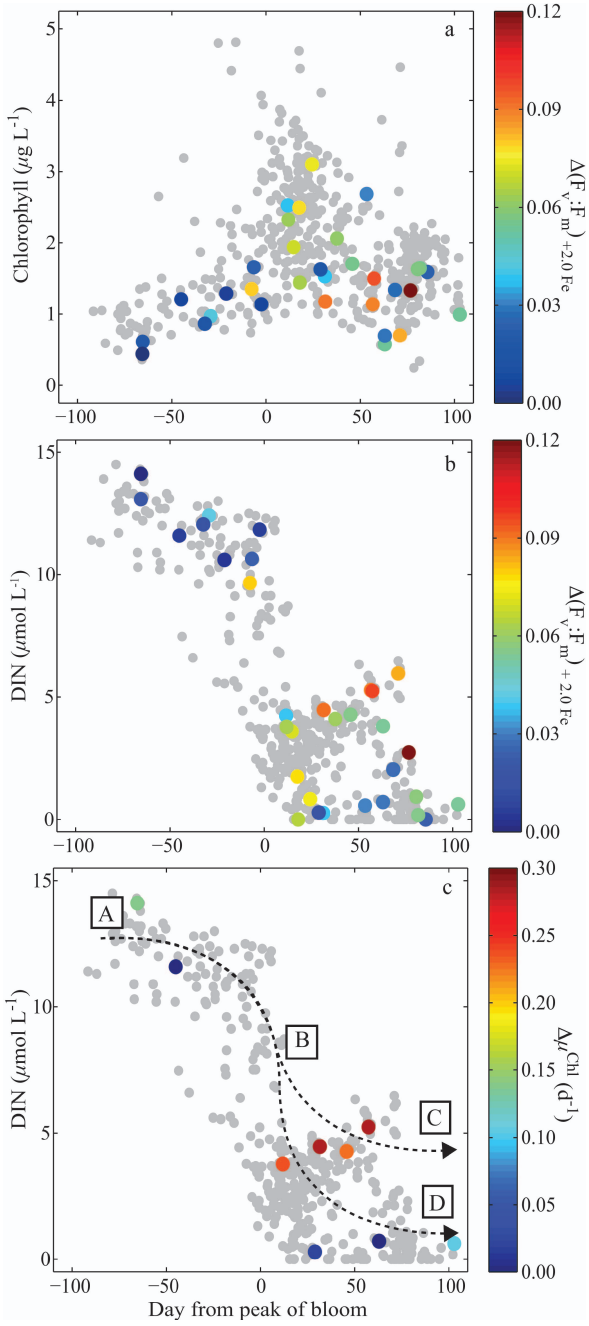

Fig. 8. (a) In situ chlorophyll data (μg L^{-1}) and relative degree of Fe stress ($\Delta(F_v:F_m)_{+2.0\ Fe}$), (b) in situ DIN ($\mu$mol L^{-1}) data and $\Delta(F_v:F_m)_{+2.0\ Fe}$, and (c) in situ DIN and difference in net chlorophyll growth rate following Fe addition ($\Delta\mu^{Chl}$ (d^{-1})) relative to time of peak of bloom. (c) superposed conceptualized model of bloom dynamics, demonstrating two different post-bloom scenarios (low DIN and high DIN) associated with different degrees of Fe stress and iron limited growth rates. Bloom timing as indicated in Fig. 1, with regions associated with different conditions defined as in Fig. 2.

restriction on overall biomass and nutrient drawdown, i.e., Liebig-type limitation (Cullen 1991), in all cases. Indeed, continued net community phytoplankton growth and nutrient drawdown beyond the point where some degree of iron stress develops only requires that any suppression of growth still leaves the gross rate higher than the combined loss terms, including, e.g., grazing (Walsh 1976), sinking (Walsby and Reynolds 1980), and viral lysis (Bratbak et al. 1993).

Although loss rates within long-term grow-out experiments will likely differ from in situ values (Banse 1991), mortality might be expected to be reasonably consistent between controls and nutrient amended treatments, at least over short timescales. Recognizing the additional caveats involved in inferring net phytoplankton growth rates from chlorophyll accumulation due to increases in cellular chlorophyll following relief of iron stress (Geider and La Roche 1994; Moore et al. 2007), the calculated values of $\Delta\mu^{Chl}$ (Fig. 6; Table 1) potentially provide an upper bound on the level of iron limitation of phytoplankton growth rates (Fig. 8c). Maximal phytoplankton growth rates at the in situ temperatures (6–14°C) would likely lie in the range from 1 to 2 d^{-1} (Eppley 1972). However, loss terms will be significant in situ (Banse 2002), and maximal net community growth rates within the bloom are typically < 0.1 d^{-1} (Behrenfeld 2010). Consequently, we suggest that levels of growth rate iron limitation approaching 0.3 d^{-1}, as were suggested by our long-term experiments (Figs. 3, 6; Table 1), would not only be sufficient to significantly influence bloom dynamics, but could also potentially act to terminate the bloom before complete macronutrient removal under some circumstances (Figs. 2d, 8). Such a scenario is entirely consistent with the apparent level of physiological iron stress (Figs. 3, 7) and hence potential growth rate limitation (Fig. 6), being highest under those postbloom conditions where macronutrients remain elevated (Fig. 8).

Our observations of near complete nitrate drawdown in the Iceland Basin (Fig. 2d), in marked contrast to previous observations (Nielsdóttir et al. 2009), alongside incomplete removal of nitrate in the Western Irminger Basin and Rockall regions in the same growing season (Fig. 2d), provide some indication of how finely poised the HLNA system may be between having sufficient or insufficient iron to drive complete macronutrient drawdown. We speculate that both variability in the overall supply ratios of iron and macronutrients (Nielsdóttir et al. 2009) and shifts in community composition between large cells experiencing greater iron stress and smaller cells experiencing lower iron stress (Fig. 7) may interact with group-specific variability in grazing mortality and other loss terms (Cullen 1991; Price et al. 1994) to dictate whether complete surface macronutrient removal occurs over the annual cycle.

We thus propose the following conceptual model for the influence of iron availability on the bloom dynamics of the HLNA (Fig. 8c). Low chlorophyll (Fig. 2a), high DIN (Fig. 2c), high $F_v:F_m$ (Fig. 2g), and a low $\Delta(F_v:F_m)_{+0.2\ Fe\ and\ +2.0\ Fe}$ (Fig. 5a,b) characterize the winter or prebloom condition (labeled A in Figs. 2 and 8), likely representing a nutrient replete, and possibly light-limited, system. As light limitation (Sverdrup 1953) and/or grazing

pressure (Behrenfeld 2010) is reduced, a bloom is initiated. Macronutrients are then consumed as the bloom develops (Fig. 8b, labeled B Fig. 2); however, restricted iron (bio-) availability in the HLNA results in the development of iron stress during the bloom. Ecosystem dynamics (Cullen 1991; Price et al. 1994; Banse 2002) interacting with group-specific susceptibility to iron stress (Fig. 7) may then combine with variable iron supply either interannually, interbasin, or intrabasin (Fig. 5) to dictate whether the macronutrients (e.g., DIN) are completely removed (Figs. 2d; 8b,c). Consequently, the postbloom condition either tends towards complete nitrate removal (labeled D in Fig. 2) and a N-limited or Fe- and N-colimited system (Fig. 3g,h), as observed in the Iceland Basin during 2010, or incomplete nitrate removal (labeled C in Fig. 2) and a Fe-limited system, as observed in the same basin in 2007 (Nielsdóttir et al. 2009) and in the Western Irminger Basin and Rockall region in 2010 (Fig. 3e,f).

The current study represents the first extensive spatial and temporal mapping of the degree of iron stress in a large oceanic region using rapid experimentally induced changes in photophysiology ($\Delta(F_v : F_m)$) placed in the context of the seasonal cycle. The results suggest that the development of iron stress in the HLNA is closely linked to the accumulation of phytoplankton biomass and hence presumably increasing iron requirements, alongside the tendency for cumulative whole community uptake to reduce iron availability. Consequently, in this system, the seasonal progression of the bloom appears to be a crucial control on the development of iron stress, which then plays a significant role in dictating overall macronutrient drawdown. Observed regional contrasts in the degree of iron stress were hence at least partially dictated by variability in the temporal development of the bloom. The North Atlantic clearly differs from the other high-latitude oceanic regions, where a lack of iron contributes to restricted major macronutrient removal, resulting in the HNLC condition. However, even in the highly productive HLNA system, iron availability appears to influence the overall extent of macronutrient removal and hence ultimately both the local strength and efficiency of the biological carbon pump.

Acknowledgments

We thank the captain and crew of the RRS *Discovery* during research cruises D350 and D354, alongside all the scientists involved in both cruises. Particular thanks to Stephanie Henson for initial help with the satellite data. Comments from two anonymous reviews are gratefully acknowledged. This work was supported by the Natural Environment Research Council (UK) through grant NE/E005489/1 to EPA and CMM and a studentship to T.R.K.

References

Arrigo, K. R. 2005. Marine microorganisms and global nutrient cycles. Nature **437:** 349–355, doi:10.1038/nature04159

Banse, K. 1991. Rates of phytoplankton cell devision in the field and in iron enrichment experiments. Limnol. Oceanogr. **36:** 1886–1898, doi:10.4319/lo.1991.36.8.1886

———. 2002. Steemann Nielsen and the zooplankton. Hydrobiologia **480:** 15–28, doi:10.1023/A:1021220714899

Behrenfeld, M. J. 2010. Abandoning Sverdrup's critical depth hypothesis on phytoplankton blooms. Ecology **91:** 977–989, doi:10.1890/09-1207.1

———, K. Worthington, R. M. Sherrell, F. P. Chavez, P. Strutton, M. Mcphaden, and D. M. Shea. 2006. Controls on tropical Pacific Ocean productivity revealed through nutrient stress diagnostics. Nature **442:** 1025–1028, doi:10.1038/nature05083

Boyd, P. W. 2002. Environmental factors controlling phytoplankton processes in the Southern Ocean. J. Phycol. **38:** 844–861, doi:10.1046/j.1529-8817.2002.t01-1-01203.x

———, and E. R. Abraham. 2001. Iron-mediated changes in phytoplankton photosynthetic competence during SOIREE. Deep-Sea Res. II **48:** 2529–2550, doi:10.1016/S0967-0645(01)00007-8

———, and others. 2007. Mesoscale iron enrichment experiments 1993–2005: Synthesis and future directions. Science **315:** 612–617, doi:10.1126/science.1131669

Bratbak, G., J. K. Egge, and M. Heldal. 1993. Viral mortality of the marine alga *Emiliania Huxleyi* (Haptophyceae) and termination of algal blooms. Mar. Ecol. Prog. Ser. **93:** 39–48, doi:10.3354/meps093039

Cullen, J. J. 1991. Hypotheses to explain high-nutrient conditions in the open sea. Limnol. Oceanogr. **36:** 1578–1599, doi:10.4319/lo.1991.36.8.1578

———, and R. F. Davis. 2003. The blank can make a big difference in oceanographic measurements. Limnol. Oceanogr. Bull. **12:** 29–35.

De Baar, H. J. W., A. G. J. Buma, R. F. Nolting, G. C. Cadee, G. Jacques, and P. J. Treguer. 1990. On iron limitation of the Southern Ocean: Experimental observations in the Weddell and Scotia Seas. Mar. Ecol. Prog. Ser. **65:** 105–122, doi:10.3354/meps065105

———, and others. 2005. Synthesis of iron fertilization experiments: From the iron age in the age of enlightenment. J. Geophys. Res. C Oceans **110:** C09S16, doi:10.1029/2004JC002601

Eppley, R. W. 1972. Temperature and phytoplankton growth in the sea. Fish. Bull. **70:** 1063–1085.

Geider, R. J., and J. La Roche. 1994. The role of iron in phytoplankton photosynthesis, and the potential for iron-limitation of primary productivity in the sea. Photosynth. Res. **39:** 275–301, doi:10.1007/BF00014588

Greene, R. M., Z. S. Kolber, D. G. Swift, N. W. Tindale, and P. G. Falkowski. 1994. Physiological limitation of phytoplankton photosynthesis in the eastern equatorial Pacific determined from variability in the quantum yield of fluorescence. Limnol. Oceanogr. **39:** 1061–1074, doi:10.4319/lo.1994.39.5.1061

Henson, S. A., R. Sanders, C. Holeton, and J. T. Allen. 2006. Timing of nutrient depletion, diatom dominance and a lower-boundary estimate of export production for Irminger Basin, North Atlantic. Mar. Ecol. Prog. Ser. **313:** 73–84, doi:10.3354/meps313073

Hudson, R. J. M., and F. M. M. Morel. 1990. Iron transport in marine-phytoplankton—kinetics of cellular and medium coordination reactions. Limnol. Oceanogr. **35:** 1002–1020, doi:10.4319/lo.1990.35.5.1002

Jickells, T. D., and others. 2005. Global iron connection between desert dust, ocean biogeochemistry, and climate. Science **308:** 67–71, doi:10.1126/science.1105959

Kolber, Z. S., R. T. Barber, K. H. Coale, S. E. Fitzwater, R. M. Greene, K. S. Johnson, S. Lindley, and P. G. Falkowski. 1994. Iron limitation of phytoplankton photosynthesis in the Equatorial Pacific-Ocean. Nature **371:** 145–149, doi:10.1038/371145a0

Kruskopf, M., and K. J. Flynn. 2006. Chlorophyll content and fluorescence responses cannot be used to gauge reliably phytoplankton biomass, nutrient status or growth rate. New Phytol. **169:** 525–536, doi:10.1111/j.1469-8137.2005.01601.x

Laws, E. A., P. G. Falkowski, W. O. Smith Jr., H. Ducklow, and J. J. Mccarthy. 2000. Temperature effects on export production in the open ocean. Global Biogeochem. Cycles **14:** 1231–1246, doi:10.1029/1999GB001229

Martin, J. H., and S. E. Fitzwater. 1988. Iron deficiency limits phytoplankton growth in the northeast Pacific subarctic. Nature **331:** 341–343, doi:10.1038/331341a0

———, ———, R. M. Gordon, C. N. Hunter, and S. J. Tanner. 1993. Iron, primary production and carbon nitrogen flux studies during the JGOFS North Atlantic bloom experiment. Deep-Sea Res. II **40:** 115–134, doi:10.1016/0967-0645(93)90009-C

Measures, C. I., W. M. Landing, M. T. Brown, and C. S. Buck. 2008. High-resolution Al and Fe data from the Atlantic Ocean CLIVAR-CO(2) repeat hydrography A16N transect: Extensive linkages between atmospheric dust and upper ocean geochemistry. Global Biogeochem. Cycles **22:** GB1005, doi:10.1029/2007GB003042

Milne, A., W. Landing, M. Bizimis, and P. Morton. 2010. Determination of Mn, Fe, Co, Ni, Cu, Zn, Cd and Pb in seawater using high resolution magnetic sector inductively coupled mass spectrometry (HR-ICP-MS). Anal. Chim. Acta **665:** 200–207, doi:10.1016/j.aca.2010.03.027

Moore, C. M., M. M. Mills, A. Milne, R. Langlois, E. P. Achterberg, K. Lochte, R. J. Geider, and J. La Roche. 2006. Iron limits primary productivity during spring bloom development in the central North Atlantic. Global Change Biol. **12:** 626–634, doi:10.1111/j.1365-2486.2006.01122.x

———, S. Seeyave, A. E. Hickman, J. T. Allen, M. I. Lucas, H. Planquette, R. T. Pollard, and A. J. Poulton. 2007. Iron-light interactions during the CROZet natural iron bloom and EXport experiment (CROZEX) I: Phytoplankton growth and photophysiology. Deep-Sea Res. II **54:** 2045–2065, doi:10.1016/j.dsr2.2007.06.011

Nielsdóttir, M. C., C. M. Moore, R. Sanders, D. J. Hinz, and E. P. Achterberg. 2009. Iron limitation of the postbloom phytoplankton communities in the Iceland Basin. Global Biogeochem. Cycles **23:** 1–13, doi:10.1029/2008GB003410

Parkhill, J., G. Maillet, and J. J. Cullen. 2001. Fluorescence-based maximal quantum yield for PSII as a diagnostic of nutrient stress. J. Phycol. **37:** 517–529, doi:10.1046/j.1529-8817.2001.037004517.x

Price, N. M. 2005. The elemental stoichiometry and composition of an iron-limited diatom. Limnol. Oceanogr. **50:** 1149–1158, doi:10.4319/lo.2005.50.4.1159

———, B. A. Ahner, and F. M. M. Morel. 1994. The Equatorial Pacific-Ocean—grazer-controlled phytoplankton populations in an iron-limited ecosystem. Limnol. Oceanogr. **39:** 520–534, doi:10.4319/lo.1994.39.3.0520

Prospero, J. M., J. E. Bullard, and R. Hodgkins. 2012. High-latitude dust over the North Atlantic: Inputs from Icelandic proglacial dust storms. Science **335:** 1078–1082, doi:10.1126/science.1217447

Saito, M. A., T. J. Goepfert, and J. T. Ritt. 2008. Some thoughts on the concept of colimitation: Three definitions and the importance of bioavailability. Limnol. Oceanogr. **53:** 276–290, doi:10.4319/lo.2008.53.1.0276

Sanders, R., S. Brown, S. A. Henson, and M. I. Lucas. 2005. New production in the Irminger basin during 2002. J. Mar. Syst. **55:** 291–310, doi:10.1016/j.jmarsys.2004.09.002

———, and T. Jickells. 2000. Total organic nutrients in Drake Passage. Deep-Sea Res. I **47:** 997–1014, doi:10.1016/S0967-0637(99)00079-5

Schrader, P. S., A. J. Milligan, and M. J. Behrenfeld. 2011. Surplus photosynthetic antenna complexes underlie diagnostics of iron limitation in a cyanobacterium. PLoS ONE **6:** e18753, doi:10.1371/journal.pone.0018753

Siegel, D. A., S. C. Doney, and J. A. Yoder. 2002. The North Atlantic spring phytoplankton bloom and Sverdrup's critical depth hypothesis. Science **296:** 730–733, doi:10.1126/science.1069174

Suggett, D. J., C. M. Moore, A. E. Hickman, and R. J. Geider. 2009. Interpretation of fast repetition rate (FRR) fluorescence: Signatures of phytoplankton community structure versus physiological state. Mar. Ecol. Prog. Ser. **376:** 1–19, doi:10.3354/meps07830

Sunda, W. G., and S. A. Huntsman. 1997. Interrelated influence of iron, light and cell size on marine phytoplankton growth. Nature **390:** 389–392, doi:10.1038/37093

Sverdrup, H. U. 1953. On conditions for the vernal blooming of phytoplankton. J. Cons. Int. Explor. Mer **18:** 287–295.

Volk, T., and M. I. Hoffert. 1985. Ocean carbon pumps: Analysis of relative strengths and efficiencies in ocean-driven atmospheric CO_2, p. 99–110. *In* E. T. Sundquist and W. S. Broecker [eds.], The carbon cycle and atmospheric CO_2: Natural varations Archean to Present. AGU.

Walsby, A. E., and C. S. Reynolds. 1980. Sinking and floating, p. 371–412. *In* I. Morris [ed.], The physiological ecology of phytoplankton. Studies in Ecology. Blackwell.

Walsh, J. J. 1976. Herbivory as a factor in patterns of nutrient utilization in the sea. Limnol. Oceanogr. **21:** 1–13, doi:10.4319/lo.1976.21.1.0001

Welschmeyer, N. A. 1994. Fluorometric analysis of chlorophyll-*a* in the presence of chlorophyll-b and pheopigments. Limnol. Oceanogr. **39:** 1985–1992, doi:10.4319/lo.1994.39.8.1985

Associate editor: Robert R. Bidigare

Received: 26 June 2012
Accepted: 05 November 2012
Amended: 20 November 2012

E.2 Co-Author Submissions

E.2.1 Volcanic Ash Submission to Nature Geosciences

Achterberg, E. P., Moore, C. M., Henson, S. A., Steigenberger, S., Stohl, A., Eckhardt, S., Cassidy, M., Hembury, D., Klar, J., Lucas, M. I., Macey, A. I., Marsay, C. M., Ryan-Keogh, T. J., (2012), "Natural iron fertilisation by the Eyjafjallajokull volcanic eruption", *Geophysical Research Letters*, Volume 40, Pages 1-6, doi:10.1002/grl.50221.

Submitted: 4th May 2012

Accepted: 3rd February 2013

Published: 14th March 2013

References

May 2013. URL `www.iup.uni-bremen.de`.

E. P. Achterberg, C. M. Moore, S. A. Henson, S. S. Steigenberger, A. Stohl, S. Eckhardt, L. C. Avendano, M. Cassidy, D. Hembury, J. K. Klar, M. I. Lucas, A. I. Macey, C. M. Marsay, and T. J. Ryan-Keogh. Natural iron fertilization by the eyjafjallajökull volcanic eruption. *Geophysical Research Letters*, 40:1–6, 2013.

A. E. Allen, J. LaRoche, U. Maheswari, M. Lommer, N. Schauer, P. J. Lopez, G. Finazzi, A. R. Fernie, and C. Bowler. Whole-cell response of the pennate diatom phaeodactylum tricornutum to iron starvation. *Proceedings of the National Academy of Sciences of the United States of America*, 105(30):10438–10443, 2008.

S. A. Amin, D. H. Green, M. C. Hart, F. C. Kupper, W. G. Sunda, and C. J. Carrano. Photolysis of iron-siderophore chelates promotes bacterial-algal mutualism. *Proceedings of the National Academy of Sciences of the United States of America*, 106(40): 17071–17076, 2009.

A. D. Anbar and A. H. Knoll. Proterozoic ocean chemistry and evolution: A bioinorganic bridge? *Science*, 297(5584):1137–1142, 2002.

E. Andrizhiyevskaya, T. Schwabe, M. Germana, S. D'Haene, J. Kruip, R. van Grondelle, and J. Dekker. Spectoscopic properties of psi-isia supercomplexes from the cyanobacterium synechococcus pcc 7942. *Biochimica et Biophysica Acta*, 1556(2-3):265–272, 2002.

E. Andrizhiyevskaya, D. Frolov, R. van Grondelle, and J. Dekker. Energy transfer and trapping in the photosystem i complex of synechococcus pcc 7942 and in its supercomplex with isia. *Biochimica et Biophysica Acta*, 1656:104–113, 2004.

M. V. Angel and M. J. R. Fasham. *Eddies and Biological Processes*, pages 492–524. Springer-Verlag, New York, 1983.

T. Anning, G. Harris, and R. J. Geider. Thermal acclimation in the marine diatom chaetoceros calcitrans (bacillariophyceae). *European Journal of Phycology*, 36(3):233–241, 2001.

E. V. Armbrust, J. A. Berges, C. Bowler, B. R. Green, D. Martinez, N. H. Putnam, S. G. Zhou, A. E. Allen, K. E. Apt, M. Bechner, M. A. Brzezinski, B. K. Chaal, A. Chiovitti, A. K. Davis, M. S. Demarest, J. C. Detter, T. Glavina, D. Goodstein, M. Z. Hadi, U. Hellsten, M. Hildebrand, B. D. Jenkins, J. Jurka, V. V. Kapitonov, N. Kroger, W. W. Y. Lau, T. W. Lane, F. W. Larimer, J. C. Lippmeier, S. Lucas, M. Medina, A. Montsant, M. Obornik, M. S. Parker, B. Palenik, G. J. Pazour, P. M. Richardson, T. A. Rynearson, M. A. Saito, D. C. Schwartz, K. Thamatrakoln, K. Valentin, A. Vardi, F. P. Wilkerson, and D. S. Rokhsar. The genome of the diatom thalassiosira pseudonana: Ecology, evolution, and metabolism. *Science*, 306(5693):79–86, 2004.

E. Aro, I. Virgin, and B. Andersson. Photoinhibition of photosystem ii. inactivation, protein damage and turnover. *Biochimica et Biophysica Acta*, 1143:113–134, 1993.

K. Arrigo. Marine microorganisms and global nutrient cycles. *Nature*, 437(7057):349–355, 2005.

K. R. Arrigo and G. L. van Dijken. Phytoplankton dynamics within 37 antarctic coastal polynya systems. *Journal of Geophysical Research-Oceans*, 108(C8), 2003. 3271.

K. R. Arrigo and G. L. van Dijken. Annual changes in sea-ice, chlorophyll a, and primary production in the ross sea, antarctica. *Deep-Sea Research Part Ii-Topical Studies in Oceanography*, 51(1-3):117–138, 2004.

K. R. Arrigo, D. Worthen, A. Schnell, and M. P. Lizotte. Primary production in southern ocean waters. *Journal of Geophysical Research-Oceans*, 103(C8):15587–15600, 1998.

K. R. Arrigo, D. H. Robinson, D. L. Worthen, R. B. Dunbar, G. R. DiTullio, M. VanWoert, and M. P. Lizotte. Phytoplankton community structure and the drawdown of nutrients and co2 in the southern ocean. *Science*, 283(5400):365–367, 1999.

K. R. Arrigo, G. R. DiTullio, R. B. Dunbar, D. H. Robinson, M. VanWoert, D. L. Worthen, and M. P. Lizotte. Phytoplankton taxonomic variability in nutrient utilization and primary production in the ross sea. *Journal of Geophysical Research-Oceans*, 105(C4):8827–8845, 2000.

K. R. Arrigo, G. van Dijken, and M. Long. Coastal southern ocean: A strong anthropogenic co2 sink. *Geophysical Research Letters*, 35(21), 2008. L21602.

C. Aspinwall, J. Duncan, T. S. Bibby, C. Mullineaux, and J. Barber. The trimeric organisation of photosystem i is not necessary for the iron-stress induced cp43' protein to functionally associate with this reaction centre. *Febs Letters*, 574:126–130, 2004.

S. Bailey, A. Melis, K. R. M. Mackey, P. Cardol, G. Finazzi, G. van Dijken, G. M. Berg, K. Arrigo, J. Shrager, and A. Grossman. Alternative photosynthetic electron flow to oxygen in marine synechococcus. *Biochimica et Biophysica Acta*, 1777(3):269–276, 2008.

K. Banse. Rates of phytoplankton cell devision in the field and in iron enrichment experiments. *Limnology and Oceanography*, 36(8):1886–1898, 1991.

K. Banse. Zooplankton: Pivotal role in the control of ocean production. *ICES Journal of Marine Science*, 52(3-4):265–277, 1995.

K. Banse. Sreemann nielsen and the zooplankton. *Hydrobiologia*, 480(1-3):15–28, 2002.

K. Barbeau, J. W. Moffett, D. A. Caron, P. L. Croot, and D. L. Erdner. Role of protozoan grazing in relieving iron limitation of phytoplankton. *Nature*, 380(6569): 61–64, 1996.

M. J. Behrenfeld. Abandoning sverdrup's critical depth hypothesis on phytoplankton blooms. *Ecology*, 91(4):977–989, 2010.

M. J. Behrenfeld and P. G. Falkowski. Photosynthetic rates derived from satellite-based chlorophyll concentration. *Limnology and Oceanography*, 42(1):1–20, 1997. Journal Article.

M. J. Behrenfeld and Z. S. Kolber. Widespread iron limitation phytoplankton in the south pacific ocean. *Science*, 283(5403):840–843, 1999. Journal Article.

M. J. Behrenfeld and A. J. Milligan. Photophysiological expressions of iron stress in phytoplankton. *Annual Review of Marine Science*, 5(1):null, 2013.

M. J. Behrenfeld, A. Bale, Z. Kolber, J. Aiken, and P. G. Falkowski. Confirmation of iron limitation of phytoplankton photosynthesis in the equatorial pacific ocean. *Nature*, 383:508–511, 1996.

M. J. Behrenfeld, O. Prášil, M. Babin, and F. Bruyant. In search of a physiological basis for covariations in light-limited and light-saturated photosynthesis. *Journal of Phycology*, 40:4–25, 2004.

M. J. Behrenfeld, E. Boss, D. A. Siegel, and D. M. Shea. Carbon-based ocean productivity and phytoplankton physiology from space. *Global Biogeochemical Cycles*, 19(1): [np], 2005. Journal Article.

M. J. Behrenfeld, K. Worthington, R. M. Sherrell, F. P. Chavez, P. Strutton, M. McPhaden, and D. M. Shea. Controls on tropical pacific ocean productivity revealed through nutrient stress diagnostics. *Nature*, 442(7106):1025–1028, 2006.

M. J. Behrenfeld, K. H. Halsey, and A. J. Milligan. Evolved physiological responses of phytoplankton to their integrated growth environment. *Philosophical Transactions of the Royal Society B-Biological Sciences*, 363(1504):2687–2703, 2008.

M. J. Behrenfeld, T. K. Westberry, E. S. Boss, R. T. O'Malley, D. A. Siegel, J. D. Wiggert, B. A. Franz, C. R. McClain, G. C. Feldman, S. C. Doney, J. K. Moore, G. Dall'Olmo, A. J. Milligan, I. Lima, and N. Mahowald. Satellite-detected fluorescence reveals global physiology of ocean phytoplankton. *Biogeosciences*, 6(5):779–794, 2009. Journal Article.

M. L. Bender and C. Gagner. Dissolved copper, nickel, and cadmium in sargasso sea. *Journal of Marine Research*, 34(3):327–339, 1976.

M. L. Bender, G. P. Klinkhammer, and D. W. Spencer. Manganese in seawater and marine manganese balance. *Deep-Sea Research*, 24(9):799–812, 1977.

J. Benesova, K. Nickova, N. Ferimazova, and D. Stys. Morphological and physiological differences in synechococcus elongatus during continuous cultivation at high iron, low iron, and iron deficient medium. *Photosynthetica*, 38(2):233–241, 2000.

R. Berera, I. van Stokkum, S. D'Haene, J. Kennis, R. van Grondelle, and J. Dekker. A mechanism of energy dissipation in cyanobacteria. *Biophysical Journal*, 96:2261–2267, 2009.

E. M. Bertrand, M. A. Saito, J. M. Rose, C. R. Riesselman, M. C. Lohan, A. E. Noble, A. Lee Peter, and G. R. DiTullio. Vitamin b12 and iron co-limitation of phytoplankton growth in the ross sea. *Limnology and Oceanography*, 52(3):1078–1093, 2007.

T. S. Bibby, J. Nield, and J. Barber. Antenna ring around trimeric photosystem i in oxyphotobacteria. *Photosynthesis Research*, 69(1-3):71, 2001a. 12th International Congress on Photosynthesis August 18-23, 2001 Brisbane, Australia.

T. S. Bibby, J. Nield, and J. Barber. Iron deficiency induces the formation of an antenna ring around trimeric photosystem i in cyanobacteria. *Nature*, 412(6848):743–745, 2001b.

T. S. Bibby, J. Nield, and J. Barber. Three-dimensional model and characterization of the iron stress-induced cp43 '-photosystem i supercomplex isolated from the cyanobacterium synechocystis pcc 6803. *Journal of Biological Chemistry*, 276(46):43246–43252, 2001c.

T. S. Bibby, J. Nield, F. Partensky, and J. Barber. Oxyphotobacteria - antenna ring around photosystem i. *Nature*, 413(6856):590–590, 2001d.

T. S. Bibby, I. Mary, J. Nield, F. Partensky, and J. Barber. Low-light-adapted prochlorococcus species possess specific antennae for each photosystem. *Nature*, 424(6952): 1051–1054, 2003.

T. S. Bibby, Y. Zhang, and M. Chen. Biogeography of photosynthetic light-harvesting genes in marine phytoplankton. *PLoS ONE*, 4(2):e4601, 2009.

R. R. Bidigare, M. E. Ondrusek, J. H. Morrow, and D. A. Kiefer. *Invivo Absorption Properties of Algal Pigments*, volume 1302 of *Proceedings of the Society of Photo-Optical Instrumentation Engineers (Spie)*, pages 290–302. Spie - Int Soc Optical Engineering, Bellingham, 1990. Proceedings Paper CONF ON OCEAN OPTICS 10 APR 16-18, 1990 ORLANDO, FL SOC PHOTO OPT INSTRUMENTAT ENGINEERS.

F. F. Blackman. Optima and limiting factors. *Annals of Botany*, 19:281–295, 1905.

S. Blain, B. Queguiner, L. Armand, S. Belviso, B. Bombled, L. Bopp, A. Bowie, C. Brunet, C. Brussaard, F. Carlotti, U. Christaki, A. Corbiere, I. Durand, F. Ebersbach, J. L. Fuda, N. Garcia, L. Gerringa, B. Griffiths, C. Guigue, C. Guillerm, S. Jacquet, C. Jeandel, P. Laan, D. Lefevre, C. Lo Monaco, A. Malits, J. Mosseri, I. Obernosterer, Y. H. Park, M. Picheral, P. Pondaven, T. Remenyi, V. Sandroni, G. Sarthou, N. Savoye, L. Scouarnec, M. Souhaut, D. Thuiller, K. Timmermans, T. Trull, J. Uitz, P. van Beek, M. Veldhuis, D. Vincent, E. Viollier, L. Vong, and T. Wagener. Effect of natural iron fertilization on carbon sequestration in the southern ocean. *Nature*, 446(7139):1070–74, 2007.

S. Blain, B. Queguiner, and T. Trull. The natural iron fertilization experiment keops (kerguelen ocean and plateau compared study): An overview. *Deep-Sea Research Part Ii-Topical Studies in Oceanography*, 55(5-7):559–565, 2008.

E. Boekema, A. Hifney, A. Yakushevska, M. Piotrowski, W. Keegstra, S. Berry, K. P. Michel, E. K. Pistorius, and J. Kruip. A giant chlorophyll-protein complex induced by iron deficiency in cyanobacteria. *Nature*, 412:745–748, 2001.

V. A. Boichenko and F. F. Litvin. Effective cross-sections for 2 photochemical-reactions of the photosynthesis and the discrete nature of the photosynthetic unit size variations in green-algae. *Doklady Akademii Nauk SSSR*, 286(3):733–737, 1986.

H. R. Bolhàr-Nordenkampf and G. Öquist. *Chlorophyll fluorescence as a tool in photosynthesis research*, pages 193–206. Chapman and Hall, London, 1993.

A. R. Bowie, M. T. Maldonado, R. D. Frew, P. L. Croot, E. P. Achterberg, R. F. C. Mantoura, P. J. Worsfold, C. S. Law, and P. W. Boyd. The fate of added iron during a mesoscale fertilisation experiment in the southern ocean. *Deep-Sea Research II*, 48 (11-12):2703–2743, 2001.

A. R. Bowie, D. Lannuzel, T. A. Remenyi, T. Wagener, P. J. Lam, P. W. Boyd, C. Guieu, A. T. Townsend, and T. W. Trull. Biogeochemical iron budgets of the southern ocean south of australia:decoupling of iron and nutrient cycles in the subantarctic zone by the summertime supply. *Global Biogeochemical Cycles*, 23:GB4034, 2009.

P. W. Boyd. Environmental factors controlling phytoplankton processes in the southern ocean. *Journal of Phycology*, 38:844–861, 2002.

P. W. Boyd and E. R. Abraham. Iron-mediated changes in phytoplankton photosynthetic competence during soiree. *Deep-Sea Research II*, 48:2529–2550, 2001.

P. W. Boyd and S. C. Doney. Modelling regional responses by marine pelagic ecosystems to global climate change. *Geophysical Research Letters*, 29(16):1806 10.1029/2001GL014130, 2002.

P. W. Boyd and M. J. Ellwood. The biogeochemical cycle of iron in the ocean. *Nature Geoscience*, 3:675–682, 2010.

P. W. Boyd, C. S. Law, D. A. Hutchins, E. R. Abraham, P. L. Croot, M. Ellwood, R. D. Frew, M. Hadfield, J. Hall, S. Handy, C. Hare, J. Higgins, P. Hill, K. A. Hunter, K. LeBlanc, M. T. Maldonado, R. M. McKay, C. Mioni, M. Oliver, S. Pickmere, M. Pinkerton, K. Safi, S. Sander, S. A. Sanudo-Wilhelmy, M. Smith, R. Strzepek, A. Tovar-Sanchez, and S. W. Wilhelm. Fecycle: Attempting an iron biogeochemical budget from a mesoscale sf6 tracer experiment in unperturbed low iron waters. *Global Biogeochemical Cycles*, 19(4), 2005.

P. W. Boyd, T. Jickells, C. S. Law, S. Blain, E. A. Boyle, K. O. Buesseler, K. H. Coale, J. J. Cullen, H. J. W. de Baar, M. Follows, M. Harvey, C. Lancelot, M. Levasseur, N. P. J. Owens, R. Pollard, R. B. Rivkin, J. Sarmiento, V. Schoemann, V. Smetacek, S. Takeda, A. Tsuda, S. Turner, and A. J. Watson. Mesoscale iron enrichment experiments 1993-2005: Synthesis and future directions. *Science*, 315(5812):612–617, 2007.

P. W. Boyd, S. C. Doney, R. Strzepek, J. Dusenberry, K. Lindsay, and I. Fung. Climate-mediated changes to mixed-layer properties in the southern ocean: assessing the phytoplankton response. *Biogeosciences*, 5(3):847–864, 2008.

P. W. Boyd, K. R. Arrigo, R. Strzepek, and G. L. van Dijken. Mapping phytoplankton iron utilization: Insights into southern ocean supply mechanisms. *Journal of Geophysical Research-Oceans*, 117, 2012. C06009.

M. Boye, C. M. G. van den Berg, J. T. M. de Jong, H. Leach, P. Croot, and H. J. W. de Baar. Organic complexation of iron in the southern ocean. *Deep-Sea Research Part I-Oceanographic Research Papers*, 48(6):1477–1497, 2001.

G. Boyer, A. Gillam, and C. G. Trick. *Iron chelation and uptake*, pages 415–436. Elsevier, New York, 1987.

E. Boyle and J. M. Edmond. Copper in surface waters south of new-zealand. *Nature*, 253(5487):107–109, 1975.

L. E. Brand. Minimum iron requirements of marine phytoplankton and the implications for the biogeochemical control of new production. *Limnology and Oceanography*, 36 (8):1756–1771, 1991. 1991. American Society of Limnology and Oceanography Symp.: What Controls Phytoplankton Production in Nutrient-Rich Areas of the Open Sea?, San Marcos, CA (USA), 22-24 Feb 1991 Journal Article; Conference.

L. E. Brand, W. G. Sunda, and R. R. L. Guillard. Limitation of marine phytoplankton reproduction rates by zinc, manganese and iron. *Limnology and Oceanography*, 28(6): 1182–1198, 1983.

G. Bratbak, J. K. Egge, and M. Heldal. Viral mortality of the marine alga emiliania huxleyi (haptophyceae) and termination of algal blooms. *Marine Ecology-Progress Series*, 93(1-2):39–48, 1993.

T. M. Bricker and L. K. Frankel. The structure and function of cp47 and cp43 in photosystem ii. *Photosynthesis Research*, 72:131–146, 2002.

T. M. Bricker, J. Morvant, N. Marsi, H. M. Sutton, and L. K. Frankel. Isolation of a highly active photosystem ii preparation from synechocystis 6803 using a histidine-tagged mutant of cp47. *Biochimica et Biophysica Acta*, 1409:50–57, 1998.

V. Brovkin, A. Ganopolski, D. Archer, and S. Rahmstorf. Lowering of glacial atmospheric co2 in response to changes in oceanic circulation and marine biogeochemistry. *Paleoceanography*, 22(4), 2007. PA4202.

C. M. Brown, J. D. MacKinnon, A. M. Cockshutt, T. A. Villareal, and D. A. Campbell. Flux capacities and acclimation costs in trichodesmium from the gulf of mexico. *Marine Biology*, 154:413–422, 2008.

J. S. Bunt and E. J. F. Wood. Microbiology of antarctic sea-ice. microalgae and antarctic sea-ice. *Nature*, 199((4900)):1254–1255, 1963.

R. Burnap, T. Troyan, and L. A. Sherman. The highly abundant chlorophyll-protein complex of iron-deficient synechococcus sp. pcc 7942 (cp43') is encoded by the isia gene. *Plant Physiology*, 103:893–902, 1993.

N. J. Butterfield. A vauchera-like fossil from the neoproterozoic of spitsbergen. *Geological Society of America Abstract Program*, 34:169, 2002.

R. H. Byrne, L. R. Kump, and K. J. Cantrell. The influence of temperature and ph on trace metal speciation in sea water. *Marine Chemistry*, 25:163–181, 1988.

J.-C. Cadoret, R. Demoulière, J. Lavaud, H. van Gorkom, J. Houmard, and A.-L. Etienne. Dissipation of excess energy triggered by blue light in cyanobacteria with cp43' (isia). *Biochimica et Biophysica Acta*, 1659:100–104, 2004.

K. Caldeira and M. E. Wickett. Oceanography: Anthropogenic carbon and ocean ph. *Nature*, 425:365, 2003.

D. Campbell, V. Hurry, A. K. Clarke, P. Gustafsson, and G. Oquist. Chlorophyll fluorescence analysis of cyanobacterial photosynthesis and acclimation. *Microbiology and Molecular Biology Reviews*, 62:667–683, 1998.

P. Cardol, B. Bailleul, F. Rappaport, E. Derelle, D. Béal, C. Breyton, S. Bailey, F. Wollman, A. Grossman, H. Moreau, and G. Finazzi. An original adaptation of photosynthesis in the marine geen alga ostreococcus. *PNAS*, 105(22):7881–7886, 2008.

D. A. Caron, M. R. Dennett, D. J. Lonsdale, D. M. Moran, and L. Shalapyonok. Microzooplankton herbivory in the ross sea, antarctica. *Deep-Sea Research Part Ii-Topical Studies in Oceanography*, 47(15-16):3249–3272, 2000.

D. Chauhan, I. M. Folea, C. C. Jolley, R. Kouřil, C. E. Lubner, S. Lin, D. Kolber, F. Wolfe-Simon, J. H. Golbeck, E. J. Boekema, and P. Fromme. A novel photosynthetic strategy for adaptation to low-iron aquatic environments. *Biochemistry*, 50: 686–692, 2011.

M. Chen and T. S. Bibby. Photosynthetic apparatus of antenna-reaction centres supercomplexes in oxyphotobacteria: insight through significance of pcb/isia proteins. *Photosynthesis Research*, 86:165–173, 2005.

S. M. Chiswell. Annual cycles and spring blooms in phytoplankton: Don't abandon sverdrup completely. *Marine Ecology Progress Series*, 443:39–50, 2011.

K. H. Coale, X. J. Wang, S. J. Tanner, and K. S. Johnson. Phytoplankton growth and biological response to iron and zinc addition in the ross sea and antarctic circumpolar current along 170 degrees w. *Deep-Sea Research Part Ii-Topical Studies in Oceanography*, 50(3-4):635–653, 2003. PII S0967-0645(02)00588-X.

K. H. Coale, R. M. Gordon, and X. Wang. The distribution and behaviour of dissolved and particulate iron and zinc in the ross sea and antarctic circumpolar current along 170 °w. *Deep-Sea Research I*, 52:295–318, 2005.

W. P. Cochlan, D. A. Bronk, and K. H. Coale. Trace metals and nitrogenous nutrition of antarctic phytoplankton: experimental observations in the ross sea. *Deep-Sea Research Part Ii-Topical Studies in Oceanography*, 49(16):3365–3390, 2002. PII S0967-0645(02)00088-7 Southern Ocean Joint Global Ocean Flux Symposium (SO-JGOFS) JUL 08-12, 2000 BREST, FRANCE.

J. C. Comiso, C. R. McClain, C. W. Sullivan, J. P. Ryan, and C. L. Leonard. Coastal zone color scanner pigment concentrations in the southern-ocean and relationships to geophysical surface-features. *Journal of Geophysical Research-Oceans*, 98(C2):2419–2451, 1993.

J. J. Cullen. Hypotheses to explain high-nutrient conditions in the open sea. *Limnology and Oceanography*, 36(8):1578–1599, 1991. SYMP ON WHAT CONTROLS PHYTOPLANKTON PRODUCTION IN NUTRIENT-RICH AREAS OF THE OPEN SEA FEB 22-24, 1991 SAN MARCOS, CA.

J. J. Cullen and R. F. Davis. The blank can make a big difference in oceanographic measurements. *Limnology and Oceanography - Bulletin*, 12(2):29–35, 2003.

M. Davey and R. J. Geider. Impact of iron limitation on the photosynthetic apparatus of the diatom chaetoceros muelleri (bacillariophyceae). *Journal of Phycology*, 37(6): 987–1000, 2001.

H. J. W. de Baar. von liebig's law of the minimum and plankton ecology (1899-1991). *Progress in Oceanography*, 33:347–386, 1994.

H. J. W. de Baar, A. Buma, R. Nolting, G. Cadee, G. Jacques, and P. Treguer. On iron limitation of the southern ocean: Experimental observations in the weddell and scotia seas. *Marine Ecology Progress Series*, 65:105–122, 1990.

H. J. W. de Baar, J. T. M. de Jong, D. C. E. Bakker, B. M. Loscher, C. Veth, U. Bathmann, and V. Smetacek. Importance of iron for plankton blooms and carbon-dioxide drawdown in the southern-ocean. *Nature*, 373(6513):412–415, 1995.

H. J. W. de Baar, P. W. Boyd, K. H. Coale, M. R. Landry, A. Tsuda, P. Assmy, D. C. E. Bakker, Y. Bozec, R. T. Barber, M. A. Brezinski, K. O. Buesseler, M. Boyé, P. L. Croot, F. Gervais, M. Y. Gorbunov, P. J. Harrison, W. T. Hiscock, P. Laan, C. Lancelot, C. S. Law, M. Levasseur, A. Marchetti, F. J. Millero, J. Nishioka, Y. Nojiri, T. van Oijen, U. Riebesell, M. J. A. Rijkenberg, H. Saito, S. Takeda, K. R. Timmermans, M. J. W. Veldhuis, A. M. Waite, and C. S. Wong. Synthesis of iron fertilization experiments. *Journal of Geophysical Research. C. Oceans*, 110:C09S16, 2005.

C. F. Delwiche. Tracing the thread of plastid diversity through the tapestry of life. *American Naturalist*, 154:S164–S177, 1999. S.

D. DeMaster, R. Pope, J. Smoak, C. Nittrouer, and G. Pierson. The cycling and accumulation of organic matter and biogenic silica in high latitude environments: The ross sea. *Oceanography*, 5:146–153, 1992.

T. E. Desquilbet, J. C. Duval, B. Robert, J. Houmard, and J. C. Thomas. In the unicellular red alga rhodella violacea iron deficiency induces an accumulation of uncoupled lhc. *Plant and Cell Physiology*, 44(11):1141–1151, 2003.

M. S. Dinniman, J. M. Klinck, and W. O. Smith. Cross-shelf exchange in a model of the ross sea circulation and biogeochemistry. *Deep-Sea Research Part Ii-Topical Studies in Oceanography*, 50(22-26):3103–3120, 2003.

G. R. DiTullio and W. O. Smith. Spatial patterns in phytoplankton biomass and pigment distributions in the ross sea. *Journal of Geophysical Research-Oceans*, 101(C8):18467–18477, 1996.

R. A. Duce and N. W. Tindale. Atmospheric transport of iron and its deposition in the ocean. *Limnology and Oceanography*, 36(8):1715–1726, February 1991.

H. W. Ducklow and R. P. Harris. Introduction to the jgofs north-atlantic bloom experiment. *Deep-Sea Research II*, 40(1-2):1–8, 1993.

D. G. Durnford, J. A. Deane, S. Tan, G. I. McFadden, E. Gantt, and B. R. Green. A phylogenetic assessment of the eukaryotic light-harvesting antenna proteins, with implications for plastid evolution. *Journal of Molecular Evolution*, 48:59–68, 1999.

V. A. Elrod, W. M. Berelson, K. H. Coale, and K. S. Johnson. The flux of iron from continental shelf sediments: a missing source for global budgets. *Geophysical Research Letters*, 31(12):4 pp., 2004.

S. Z. Elsayed, D. C. Biggs, and O. Holmhansen. Phytoplankton standing crop, primary productivity, and near-surface nitrogenous nutrient fields in the ross sea, antarctica. *Deep-Sea Research Part a-Oceanographic Research Papers*, 30(8):871–886, 1983.

R. W. Eppley. Temperature and phytoplankton growth in the sea. *Fishery Bulletin*, 70 (4):1063–1085, 1972.

R. W. Eppley and B. J. Peterson. Particulate organic matter flux and planktonic new production in the deep ocean. *Nature*, 282:677–680, 1979.

D. L. Erdner, N. M. Price, G. J. Doucette, M. L. Peleato, and D. M. Anderson. Characterization of ferredoxin and flavodoxin as markers of iron limitation in marine phytoplankton. *Marine Ecology Progress Series*, 184:43–53, 1999. 1999. Journal Article.

P. G. Falkowski. Evolution of the nitrogen cycle and its influence on the biological sequestration of co_2 in the ocean. *Nature*, 387:272–275, 1997.

P. G. Falkowski and Z. Kolber. Variations in chlorophyll fluorescence yields in phytoplankton in the world oceans. *Australian Journal of Plant Physiology*, 22(2):341–355, 1995. Robertson Symposium on Chlorophyll Fluorescence - Origins, Measurements, Interpretations and Applications MAY 27-29, 1994 CANBERRA, AUSTRALIA.

P. G. Falkowski and J. La Roche. Acclimation to spectra irradiance in algae. *Journal of Phycology*, 27:8–14, 1991.

P. G. Falkowski and T. G. Owens. Light-shade adaptation - two strategies in marine phytoplankton. *Plant Physiology*, 66:592–595, 1980.

P. G. Falkowski and J. A. Raven. *Aquatic Photosynthesis*. Blackwell Science, Oxford, 1997.

P. G. Falkowski and J. A. Raven. *Aquatic Photosynthesis*. Princeton University Press, second edition, 2007.

P. G. Falkowski, D. Ziemann, Z. Kolber, and P. K. Bienfang. Role of eddy pumping in enhancing primary production in the ocean. *Nature*, 352(6330):55–58, 1991.

P. G. Falkowski, R. T. Barber, and V. Smetacek. Biogeochemical controls and feedbacks on ocean primary production. *Science*, 281(5374):200–206, 1998.

P. G. Falkowski, M. E. Katz, A. H. Knoll, A. Quigg, J. A. Raven, O. Schofield, and F. J. R. Taylor. The evolution of modern eukaryotic phytoplankton. *Science*, 305: 354–360, 2004.

K. Fennel, M. Follows, and P. G. Falkowski. The co-evolution of the nitrogen, carbon and oxygen cycles in the proterozoic ocean. *American Journal of Science*, 305(6-8): 526–545, 2005. SI.

F. Ferreira and N. A. Straus. Iron deprivation in cyanobacteria. *Journal of Applied Phycology*, 6:199–210, 1994.

K. N. Ferreira, T. M. Iverson, K. Maghlaoui, J. Barber, and S. Iwata. Architecture of the photosynthetic oxygen-evolving centre. *Science*, 303:1831–1833, 2004.

C. B. Field, M. J. Behrenfeld, J. T. Randerson, and P. Falkowski. Primary production of the biosphere: Integrating terrestrial and oceanic components. *Science*, 281(5374): 237–240, 1998.

J. R. Fishwick, J. Aiken, R. Barlow, H. Sessions, S. Bernard, and J. Ras. Functional relationships and bio-optical properties derived from phytoplankton pigments, optical and photosynthetic parameters; a case study of the benguela ecosystem. *Journal of the Marine Biological Association of the United Kingdom*, 86:1267–1280, 2006.

S. E. Fitzwater, K. S. Johnson, R. M. Gordon, K. H. Coale, and W. O. Smith. Trace metal concentrations in the ross sea and their relationship with nutrients and phytoplankton growth. *Deep-Sea Research Part Ii-Topical Studies in Oceanography*, 47 (15-16):3159–3179, 2000.

B. W. Frost. The role of grazing in nutrient-rich areas of the open sea. *Limnology and Oceanography*, 36(8):1616–1630, 1991.

D. M. Gaiero, J. L. Probst, P. J. Depetris, S. M. Bidart, and L. Leleyter. Iron and other transition metals in patagonian riverborne and windborne materials: Geochemical control and transport to the southern south atlantic ocean. *Geochimica Et Cosmochimica Acta*, 67(19):3603–3623, 2003.

N. S. Garcia, P. N. Sedwick, and G. R. DiTullio. Influence of irradiance and iron on the growth of colonial phaeocystis antarctica: implications for seasonal bloom dynamics in the ross sea, antarctica. *Aquatic Microbial Ecology*, 57(2):203–220, 2009.

E. Garcia-Mendoza and M. F. Colombo-Pallotta. The giant kelp macrocystis pyrifera presents a different nonphotochemical quenching control than higher plants. *New Phytologist*, 173(3):526–536, 2007.

L. Garczarek, W. R. Hess, J. Holtzendorff, G. W. M. Van der Staay, and F. Partensky. Multiplication of antenna genes as a major adaptation to low light in a marine prokaryote. *Proceedings of the National Academy of Sciences USA*, 97:4098–4101, 2000.

R. J. Geider and J. La Roche. The role of iron in phytoplankton photosynthesis, and the potential for iron-limitation of primary productivity in the sea. *Photosynthesis Research*, 39(3):275–301, 1994.

R. J. Geider, R. M. Greene, Z. S. Kolber, H. L. MacIntyre, and P. G. Falkowski. Fluorescent assessment of the maximum quantum efficiency in the western north atlantic. *Deep-Sea Research Part I Oceanographic Research Papers*, 40:1205–1224, 1993a.

R. J. Geider, J. La Roche, R. M. Greene, and M. Olaizola. Response of the photosynthetic apparatus of phaeodactylum tricornutum (baccilariophyceae) to nitrate, phosphate or iron starvation. *Journal of Phycology*, 29:755–766, 1993b.

U. Geiss, J. Vinnemeier, A. Kunert, I. Lindner, B. Gemmer, M. Lorenz, M. Hagemann, and A. Schoor. Detection of the isia gene across cyanobacterial strains: Potential for probing iron deficiency. *Applied and Environmental Microbiology*, 67(11):5247–4253, 2001.

t. n. German. *Organic World One Billion Years Ago*. Nauka, Leningrad, 1990.

M. Ghassemian and N. A. Straus. Fur regulates the expression of iron-stress genes in the cyanobacterium synechococcus sp. strain pcc 7942. *Microbiology*, 142(pt 6): 1469–1476, 1996. 1996. Journal Article.

S. L. C. Giering, S. Steigenberger, E. P. Achterberg, R. Sanders, and D. J. Mayor. Elevated iron to nitrogen recycling by mesozooplankton in the northeast atlantic ocean. *Geophysical Research Letters*, 39, 2012. L12608.

A. Goffart, G. Catalano, and J. H. Hecq. Factors controlling the distribution of diatoms and phaeocystis in the ross sea. *Journal of Marine Systems*, 27(1-3):161–175, 2000. 30th International Liege Colloquium on Ocean Hydrodynamics MAY 04-08, 1998 LIEGE, BELGIUM.

H. H. Gran. On the conditions for the production of plankton in the sea. *Rapp. Proc. Verb. Reun. Cons. Int. Explor. Mer*, 75:37–46, 1931.

H. H. Gran. Studies on the biology and chemistry of the gulf of maine. ii. distribution of phytoplankton in august 1932. *Biological Bulletin (Woods Hole)*, 64:159–182, 1933.

J. Granger and N. M. Price. The importance of siderophores in iron nutrition of heterotrophic marine bacteria. *Limnology and Oceanography*, 44(3):541–555, 1999.

B. R. Green. *The evolution of light harvesting antennas*, pages 129–168. Kluwer Academic Publishers, Netherlands, 2003.

B. R. Green and D. G. Durnford. The chlorophyll-carotenoid proteins of oxygenic photosynthesis. *Annual Review of Plant Physiology and Plant Molecular Biology*, 47: 685–714, 1996.

N. L. Greenbaum and D. Mauzerall. Measurement of the optical cross section of photosystem-i in chlorella. *Photochemistry and Photobiology*, 43(SUPPL):101S–101S, 1986. 14TH ANNUAL MEETING OF THE AMERICAN SOCIETY FOR PHOTOBIOLOGY, LOS ANGELES, CALIF., USA, JUNE 22-26, 1986. PHOTOCHEM PHOTOBIOL.

N. L. Greenbaum, A. C. Ley, and D. C. Mauzerall. Use of a light-induced respiratory transient to measure the optical-cross-section of photosystem-i in chlorella. *Plant Physiology*, 84(3):879–882, 1987.

R. M. Greene, R. J. Geider, and P. G. Falkowski. Effect of iron limitation on photosynthesis in a marine diatom. *Limnology and Oceanography*, 36:1772–1782, 1991.

R. M. Greene, R. J. Geider, Z. Kolber, and P. G. Falkowski. Iron-induced changes in light harvesting and photochemical energy-conversion processes in eukaryotic marine-algae. *Plant Physiology*, 100(2):565–575, 1992.

R. M. Greene, Z. S. Kolber, D. G. Swift, N. W. Tindale, and P. G. Falkowski. Physiological limitation of phytoplankton photosynthesis in the eastern equatorial pacific determined from variability in the quantum yield of fluorescence. *Limnology and Oceanography*, 39(5):1061–1074, 1994.

M. T. Gudmundsson, T. Thordarson, A. Hoskuldsson, G. Larsen, H. Bjornsson, F. J. Prata, B. Oddsson, E. Magnusson, T. Hognadottir, G. N. Petersen, C. L. Hayward, J. A. Stevenson, and I. Jonsdottir. Ash generation and distribution from the april-may 2010 eruption of eyjafjallajokull, iceland. *Scientific Reports*, 2, 2012. 572.

J. A. Guikema and L. A. Sherman. Organization and functionof chlorophyll in membranes of cyanobacterium during iron starvation. *Plant Physiology*, 73:250–256, 1983.

B. Hales and T. Takahashi. High-resolution biogeochemical investigation of the ross sea, antarctica, during the aesops (u. s. jgofs) program. *Global Biogeochemical Cycles*, 18 (3), 2004. GB3006.

K. H. Halsey, A. J. Milligan, and M. J. Behrenfeld. Physiological optimization underlies growth rate-independent chlorophyll-specific gross and net primary production. *Photosynthesis Research*, 103:125–137, 2010.

T. J. Hart. On the phytoplankton of the southwest atlantic and the bellingshausen sea. *Discovery Reports*, 8:1–268, 1934.

H. W. Harvey. The supply of iron to diatoms. *Journal of the Marine Biological Association of the United Kingdom*, 22:205–219, 1938.

H. W. Harvey. *The chemistry and fertility of sea waters*. Cambridge University Press, Cambridge, 1966.

M. Havaux, G. Guedeney, M. Hagemann, N. Yeremenko, H. C. P. Matthijs, and R. Jeanjean. The chlorophyll-binding protein isia is inducible by high light and protects the

cyanobacterium synechocystis pcc6803 from photooxidative stress. *Febs Letters*, 579 (11):2289–2293, 2005. Journal Article.

M. G. Haygood, P. D. Holt, and A. Butler. Aerobactin production by a planktonic marine vibrio sp. *Limnology and Oceanography*, 38(5):1091–1097, 1993.

N. I. Hendey. The plankton dynamics of the southern seas. *Discovery Reports*, 16: 151–364, 1937.

S. Henson, R. Sanders, C. Holeton, and J. T. Allen. Timing of nutrient depletion, diatom dominance and a lower-boundary estimate of export production for irminger basin, north atlantic. *Marine Ecology Progress Series*, 313:73–84, 2006.

S. A. Henson, R. Sanders, J. T. Allen, I. S. Robinson, and L. Brown. Seasonal constraints on the estimation of new production from space using temperature-nitrate relationships. *Geophysical Research Letters*, 30(17), 2003. 1912.

R. G. Herrmann. Biogenesis and evolution of photosynthetic (thylakoid) membranes. *Bioscience Reports*, 19:355–365, 1999.

W. R. Hess, G. Rocap, C. S. Ting, F. Larimer, S. Stilwagen, J. Lamerdin, and S. W. Chisholm. The photosynthetic apparatus of prochlorococcus: Insights through comparative genomics. *Photosynthesis Research*, 70(1):53–71, 2001.

E. E. Hoffman and J. M. Klinck. *Hydrography and circulation of the Antarctic continental shelf: 150°E eastward to the Greenwich Meridian*, volume 11 of *The Sea, The Global Coastal Ocean, Regional Studies and Synthesis*, pages 997–1042. Harvard University Press, Harvard, 1998.

S. Honjo, S. J. Manganini, R. A. Krishfield, and R. Francois. Particulate organic carbon fluxes to the ocean interior and factors controlling the biological pump: A synthesis of global sediment trap programs since 1983. *Progress in Oceanography*, 76(3):217–285, 2008.

P. Horton, A. V. Ruban, and R. G. Walters. Regulation of light harvesting in green plants. *Annual Review of Plant Physiology and Plant Molecular Biology*, 47:655–684, 1996.

R. J. M. Hudson and F. M. M. Morel. Iron transport in marine-phytoplankton - kinetics of cellular and medium coordination reactions. *Limnology and Oceanography*, 35(5): 1002–1020, 1990.

D. A. Hutchins and K. W. Bruland. Grazer-mediated regeneration and assimilation of fe, zn and mn from planktonic prey. *Marine Ecology-Progress Series*, 110(2-3):259–269, 1994.

D. A. Hutchins and K. W. Bruland. Iron-limited diatom growth and si:n uptake ratios in a coastal upwelling region. *Nature*, 393:561–564, 1998.

J. Ihalainen, S. D'Haene, N. Yeremenko, H. van Roon, A. A. Arteni, E. Boekema, R. van Grondelle, H. C. P. Matthijs, and J. Dekker. Aggregates of the chlorophyll-binding protein isia (cp43') dissipate energy in cyanobacteria. *Biochemistry*, 44:10846–10853, 2005.

Y. Isozaki. Permo-triassic boundary superanoxia and stratified superocean: Records from lost deep sea. *Science*, 276(5310):235–238, 1997.

A. G. Ivanov, Y. I. Park, E. Miskiewicz, J. A. Raven, N. P. A. Huner, and G. Öquist. Iron stress restricts photosynthetic intersystem electron transport in synechococcus sp, pcc 7942. *Febs Letters*, 485(2-3):173–177, 2000.

A. G. Ivanov, M. Krol, D. Sveshnikov, E. Selstam, S. Sandström, M. Koochek, Y.-I. Park, S. Vasil'ev, D. Bruce, G. Öquist, and N. P. A. Huner. Iron deficiency in cyanobacteria causes monomerization of photosystem i trimers and reduces the capacity for state transitions and the effective absorption cross section of photosystem i in vivo. *Plant Physiology*, 141(4):1436–1445, 2006. Journal Article.

S. S. Jacobs, A. F. Amos, and Bruchhau.Pm. Ross-sea oceanography and antarctic bottom water formation. *Deep-Sea Research*, 17(6):935–, 1970.

R. Jeanjean, E. Zuther, N. Yeremenko, M. Havaux, H. C. P. Matthijs, and M. Hagemann. A photosystem 1 psafj-null mutant of the cyanobacterium synechocystis pcc 6803 expresses the isiab operon under iron replete conditions. *Febs Letters*, 549(1-3):52–56, 2003. Journal Article.

T. Jickells, Z. An, K. Andersen, A. R. Baker, G. Bergametti, N. Brooks, J. Cao, P. W. Boyd, R. A. Duce, C. N. Hunter, H. Kawahata, N. Kubilay, J. La Roche, P. S.

Liss, N. Mahowald, J. Prospero, A. Ridgwell, I. Tegen, and R. Torres. Global iron connection between desert dust, ocean biogeochemistry, and climate. *Science*, 308: 67–71, 2005.

G. Johnsen, N. B. Nelson, R. V. M. Jovine, and B. B. Prézelin. Chromoprotein-and pigment-dependent modelling of spectral light absorption in tow dinoflagellates, prorocentrum minimum and heterocapsa pygmaea. *Marine Ecology Progress Series*, 114: 245–258, 1994.

K. S. Johnson. Iron supply and demand in the upper ocean: Is extraterrestrial dust a significant source of bioavailable iron? *Global Biogeochemical Cycles*, 15(1):61–63, 2001.

K. S. Johnson, F. P. Chavez, and G. E. Friederich. Continental-shelf sediment as a primary source of iron for coastal phytoplankton. *Nature*, 398(6729):697–700, 1999.

K. S. Johnson, V. A. Elrod, S. E. Fitzwater, J. Plant, E. Boyle, B. Bergquist, K. W. Bruland, A. M. Aguilar-Islas, K. Buck, M. C. Lohan, G. J. Smith, B. M. Sohst, K. H. Coale, M. Gordon, S. Tanner, C. I. Measures, J. Moffett, K. A. Barbeau, A. King, A. R. Bowie, Z. Chase, J. J. Cullen, P. Laan, W. Landing, J. Mendez, A. Milne, H. Obata, T. Doi, L. Ossiander, G. Sarthou, P. N. Sedwick, S. Van den Berg, L. Laglera-Baquer, J.-F. Wu, and Y. Cai. Developing standards for dissolved iron in seawater. *Eos, Transactions American Geophysical Union*, 88(11):131–132, 2007.

W. K. Johnson, L. A. Miller, N. E. Sutherland, and C. S. Wong. Iron transport by mesoscale haida eddies in the gulf of alaska. *Deep-Sea Research Part Ii-Topical Studies in Oceanography*, 52(7-8):933–953, 2005.

P. Jordan, P. Fromme, H. T. Witt, O. Klukas, W. Saenger, and N. Krauss. Three-dimensional structure of cyanobacterial photosystem i at 2.5 angstrom resolution. *Nature*, 411(6840):909–917, 2001.

W. Junge. Atp synthase and other motor proteins. *Proceedings of the National Academy of Sciences of the United States of America*, 96:4735–4737, 1999.

D. Karl, R. Leteller, L. Tupas, J. Dore, J. Christian, and D. Hebel. The role of nitrogen fixation in biogeochemical cycling in the subtropical north pacific ocean. *Nature*, 388: 533–538, 1997.

D. L. Kirchman. Oceanography - microbial ferrous wheel. *Nature*, 383(6598):303–304, 1996.

M. Klunder, P. Laan, R. Middag, H. J. W. De Baar, and J. V. Ooijen. Dissolved iron the southern ocean (atlantic sector). *Deep Sea Research Part II: Topical Studies in Oceanography*, 58(25-26):2678–2694, 2011.

G. A. Knauer and J. H. Martin. Seasonal-variations of cadmium, copper, manganese, lead, and zinc in water and phytoplankton in monterey bay, california. *Limnology and Oceanography*, 18(4):597–604, 1973.

A. H. Knoll, R. K. Bambach, D. E. Canfield, and J. P. Grotzinger. Comparative earth history and late permian mass extinction. *Science*, 273(5274):452–457, 1996.

K. E. Kohfeld, C. Le Quere, S. P. Harrison, and R. F. Anderson. Role of marine biology in glacial-interglacial co2 cycles. *Science*, 308(5718):74–78, 2005.

Z. Kolber, J. Zehr, and P. Falkowski. Effects of growth irradiance and nitrogen limitation on photosynthetic energy-conversion in photosystem-ii. *Plant Physiology*, 88(3):923–929, 1988.

Z. S. Kolber, K. D. Wyman, and P. G. Falkowski. Natural variability in photosynthetic energy conversion efficiency: a field study in the gulf of maine. *Limnology and Oceanography*, 35:72–79, 1990.

Z. S. Kolber, R. T. Barber, K. H. Coale, S. E. Fitzwater, R. M. Greene, K. S. Johnson, S. Lindley, and P. G. Falkowski. Iron limitation of phytoplankton photosynthesis in the equatorial pacific-ocean. *Nature*, 371(6493):145–149, 1994.

Z. S. Kolber, O. Prášil, and P. G. Falkowski. Measurements of variable chlorophyll fluorescence using fast repetition rate techniques: defining methodology and experimental protocols. *Biochimica et Biophysica Acta*, 1367:88–106, 1998.

M. Kruskopf and K. J. Flynn. Chlorophyll content and fluorescence responses cannot be used to gauge reliably phytoplankton biomass, nutrient status or growth rate. *New Phytologist*, 169:525–536, 2006.

N. Kumar, R. F. Anderson, R. A. Mortlock, P. N. Froelich, P. Kubik, B. Dittrichhannen, and M. Suter. Increased biological productivity and export production in the glacial southern-ocean. *Nature*, 378(6558):675–680, 1995.

A. Kunert, J. Vinnemeier, N. Erdmann, and M. Hagemann. Repression by fur is not the main mechanism controlling the iron-inducible isiab operon in the cyanobacterium synechocystis sp. pcc 6803. *FEMS Microbiology Letters*, 227(2):255–262, 2003. Journal Article.

H. Küpper, I. Šetlík, S. Seibert, O. Prášil, E. Šetlikova, M. Strittmatter, O. Levitan, J. Lohscheider, I. Adamska, and I. Berman-Frank. Iron limitation in the marine cyanobacterium trichodesmium reveals new insights into regulation of photosynthesis and nitrogen fixation. *New Phytologist*, 179:784–798, 2008.

J. La Roche, H. Murray, M. Orellana, and J. Newton. Flavodoxin expression as an indicator of iron limitation in marine diatoms. *Journal of Phycology*, 31:520–530, 1995.

J. La Roche, P. W. Boyd, R. M. L. McKay, and R. J. Geider. Flavodoxin as an in situ marker for iron stress in phytoplankton. *Nature*, 382(6594):802–805, 1996a. 1996. Journal Article.

J. La Roche, G. W. M. Van der Staay, F. Partensky, A. Ducret, R. Aebersold, R. Li, S. S. Golden, R. G. Hiller, B. R. Green, and et al. Independent evolution of the prochlorophyte and green plant chlorophyll a/b light-harvesting proteins. *PNAS*, 93 (23):15244–15248, 1996b. Journal Article.

M. R. Landry, R. T. Barber, R. R. Bidigare, F. Chai, K. H. Coale, H. G. Dam, M. R. Lewis, S. T. Lindley, J. J. McCarthy, M. R. Roman, D. K. Stoecker, P. G. Verity, and J. R. White. Iron and grazing constraints on primary production in the central equatorial pacific: An eqpac synthesis. *Limnology and Oceanography*, 42(3):405–418, 1997.

S. Laney. Assessing the error in photosynthetic properties determined by fast repetition rate fluorometry. *Limnology and Oceanography*, 48(6):2234–2242, 2003.

D. Lannuzel, V. Schoemann, J. de Jong, L. Chou, B. Delille, S. Becquevort, and J. L. Tison. Iron study during a time series in the western weddell pack ice. *Marine Chemistry*, 108(1-2):85–95, 2008.

D. E. Laudenbach and N. A. Strauss. Characterization of a cyanobacterial iron stress-induced gene similar to psbc. *Journal of Bacteriology*, 170:5018–5026, 1988.

E. A. Laws, P. G. Falkowski, W. O. Smith Jr., H. Ducklow, and J. J. McCarthy. Temperature effects on export production in the open ocean. *Global Biogeochemical Cycles*, 14(4):1231–1246, 2000.

B.-G. Lee and N. S. Fisher. Release rates of trace elements and protein from decomposing planktonic debris. 1. phytoplankton debris. *Journal of Plankton Research*, 51:391–421, 1993.

W. K. W. Li and I. Morris. Temperature adaptation in phaeodactylum tricornutum bohlin: photosynthetic rate compensation and capacity. *Journal of Experimental Marine Biology and Ecology*, 58:135–150, 1982.

S. Lin, C. J. Gobler, and E. J. Carpenter. Cytological and biochemical responses of dunaliella tertiolecta (volvocales, chlorophyta) to iron stress. *Phycologia*, 40(5):403–410, 2001.

A. Longhurst, S. Sathyendranath, T. Platt, and C. Caverhill. An estimate of global primary production in the ocean from satellite radiometer data. *Journal of Plankton Research*, 17(6):1245–1271, 1995.

O. H. Lowry, N. J. Rosebrough, A. L. Farr, and R. J. Randall. Protein measurement with the folin phenol reagent. *Journal of Biological Chemistry*, 193:265–275, 1951.

C. Luo, N. Mahowald, T. Bond, P. Y. Chuang, P. Artaxo, R. Siefert, Y. Chen, and J. Schauer. Combustion iron distribution and deposition. *Global Biogeochemical Cycles*, 22(1), 2008.

D. J. Mackey, J. E. O'Sullivan, and R. J. Watson. Iron in the western pacific: A riverine or hydrothermal source for iron in the equatorial undercurrent. *Deep-Sea Research*, 40:877–893, 2002.

K. R. M. Mackey, A. Paytan, A. Grossman, and S. Bailey. A photosynthetic strategy for coping in a high-light, low-nutrient environment. *Limnology and Oceanography*, 53(3):900–913, 2008.

D. S. Mackie, P. W. Boyd, G. H. McTainsh, N. W. Tindale, T. K. Westberry, and K. A. Hunter. Biogeochemistry of iron in australian dust: From eolian uplift to marine uptake. *Geochemistry, Geophysics, Geosystems*, 9:Q03Q08, 2008.

N. Mahowald and C. Luo. A less dusty future? *Geophysical Research Letters*, 30(17): 1903 doi:10.1029/2003GL917880, 2003.

M. T. Maldonado and N. M. Price. Reduction and transport of organically bound iron by thalassiosira oceanica (bacillariophyceae). *Journal of Phycology*, 37(2):298–309, 2001.

M. T. Maldonado, P. W. Boyd, P. J. Harrison, and N. M. Price. Co-limitation of phytoplankton growth by light and fe during winter in the ne subarctic pacific ocean. *Deep-Sea Research II*, 46:2475–2485, 1999.

E. L. Mann and S. W. Chisholm. Iron limits the cell division rate of prochlorococcus in the eastern equatorial pacific. *Limnology and Oceanography*, 45(5):1067–1076, 2000.

R. Maranger, D. F. Bird, and N. M. Price. Iron acquisition by photosynthetic marine phytoplankton from ingested bacteria. *Nature*, 396(6708):248–251, 1998.

A. Marchetti, M. S. Parker, L. P. Moccia, E. O. Lin, A. L. Arrieta, F. Ribalet, M. E. P. Murphy, M. T. Maldonado, and E. V. Armbrust. Ferritin is used for iron storage in bloom-forming marine pennate diatoms. *Nature*, 457(7228):467–470, 2009.

A. Marchetti, D. M. Schruth, C. A. Durkin, M. S. Parker, R. B. Kodner, C. T. Berthiaume, R. Morales, A. E. Allen, and E. V. Armbrust. Comparative metatransciptomics identifies molecular bases for the physiological responses of phytoplankton to varying iron availability. *Proceedings of the National Academy of Sciences of the United States of America*, 109(6):E317–E325, 2012.

I. Marinov, A. Gnanadesikan, J. R. Toggweiler, and J. L. Sarmiento. The southern ocean biogeochemical divide. *Nature*, 441:964–967, 2006.

J. H. Martin and S. E. Fitzwater. Iron deficiency limits phytoplankton growth in the northeast pacific subarctic. *Nature*, 331:341–343, 1988.

J. H. Martin, R. M. Gordon, S. E. Fitzwater, and W. W. Broenkow. Vertex: phytoplankton iron studies in the gulf of alaska. *Deep-Sea Research*, 36:649–680, 1989.

J. H. Martin, R. M. Gordon, and S. E. Fitzwater. Iron in antarctic waters. *Nature*, 345 (6271):156–158, 1990. 1990. Journal Article.

J. H. Martin, R. M. Gordon, and S. E. Fitzwater. The case for iron. *Limnology and Oceanography*, 36(8):1793–1802, 1991.

J. H. Martin, S. E. Fitzwater, R. M. Gordon, C. N. Hunter, and S. J. Tanner. Iron, primary production and carbon nitrogen flux studies during the jgofs north atlantic bloom experiment. *Deep-Sea Research II*, 40(1-2):115–134, 1993.

J. H. Martin, K. H. Coale, K. S. Johnson, S. E. Fitzwater, R. M. Gordon, S. J. Tanner, C. N. Hunter, V. A. Elrod, J. L. Nowicki, T. L. Coley, R. T. Barber, S. Lindley, A. J. Watson, K. Van Scoy, and C. S. Law. Testing the iron hypothesis in ecosystems of the equatorial pacific ocean. *Nature*, 371(6493):123–129, 1994. 1994. Journal Article.

J. M. Maucher and G. R. DiTullio. *Flavodoxin as a diagnostic indicator of chronic iron limitation in the Ross Sea and New Zealand sector of the Southern Ocean*, volume 78, pages 35–52. American Geophysical Union, 2003.

D. J. McGillicuddy, L. A. Anderson, S. C. Doney, and M. E. Maltrud. Eddy-driven sources and sinks of nutrients in the upper ocean: Results from a 0.1 degrees resolution model of the north atlantic. *Global Biogeochemical Cycles*, 17(2), 2003. 1035.

R. M. L. McKay, J. La Roche, A. F. Yakunin, D. G. Durnford, and R. J. Geider. Accumulation of ferredoxin and flavodoxin in a marine diatom in response to fe. *Journal of Phycology*, 35:510–519, 1999.

C. I. Measures, J. Yuan, and J. A. Resing. Determination of iron in seawater by flow injection analysis using in-line preconcentration and spectrophotometric detection. *Marine Chemistry*, 50:3–12, 1995.

C. I. Measures, W. M. Landing, M. T. Brown, and C. S. Buck. High-resolution al and fe data from the atlantic ocean clivar-co(2) repeat hydrography a16n transect: Extensive linkages between atmospheric dust and upper ocean geochemistry. *Global Biogeochemical Cycles*, 22(1):GB1005, 2008. GB1005.

A. Melis. Kinetic-analysis of p-700 photoconversion - effect of secondary-electron donation and plastocyanin inhibition. *Archives of Biochemistry and Biophysics*, 217(2): 536–545, 1982.

A. Melis and J. M. Anderson. Structural and functional-organization of the photosystems in spinach-chloroplasts - antenna size, relative electron-transport capacity, and chlorophyll composition. *Biochimica et Biophysica Acta*, 724(3):473–484, 1983.

A. N. Melkozernov, T. S. Bibby, S. Lin, J. Barber, and R. E. Blankenship. Time-resolved absorption and emission show that the cp43′ antenna ring of iron-stressed synechocystis sp. pcc6803 is efficiently coupled to the photosystem i reaction center core. *Biochemistry*, 42(13):3893–3903, 2003. Journal Article.

D. W. Menzel and J. H. Ryther. Nutrients limiting the production of phytoplankton in the sargasso sea with special reference to iron. *Deep-Sea Research*, 7:276–281, 1961.

K. P. Michel and E. K. Pistorius. Adaptation of the photosynthetic electron transport chain in cyanobacteria to iron deficiency: The function of idia and isia. *Physiologia Plantarum*, 120:36–50, 2004.

F. J. Millero, R. Woosley, B. Ditrolio, and J. Waters. Effect of ocean acidification on the speciation of metals in seawater. *Oceanography*, 22(4):72–85, 2009.

A. J. Milligan. *The influence of iron availability on nitrogen assimilation in the marine diatom Thalassiosira weissflogii*. PhD thesis, Department of Botany, 1998.

A. Milne, W. Landing, M. Bizimis, and P. Morton. Determination of mn, fe, co, ni, cu, zn, cd and pb in seawater using high resolution magnetic sector inductively coupled mass spectrometry (hr-icp-ms). *Analytica Chimica Acta*, 665(2):200–207, 2010.

C. E. Mioni, L. Poorvin, and S. W. Wilhelm. Virus and siderophore-mediated transfer of available fe between heterotrophic bacteria: characterization using an fe-specific bioreporter. *Aquatic Microbial Ecology*, 41(3):233–245, 2005.

T. Mock, P. Manoj, V. Iverson, C. Berthiaume, M. Robison, K. Holterman, C. Durkin, S. BonDurant, K. Richmond, M. Rodesch, T. Kallas, E. Huttlin, F. Cerrina, M. Sussman, and E. Armbrust. Whole-genome expression profiling of the marine diatom thalassiosira pseudonana identifies genes involved in silicon bioprocesses. *PNAS*, 105 (5):1579–1584, 2008.

C. M. Moore, M. I. Lucas, R. Sanders, and R. Davidson. Basin-scale variability of phytoplankton bio-optical characteristics in relation to bloom state and community structure in the northeast atlantic. *Deep-Sea Research I*, 52:401–419, 2005.

C. M. Moore, M. M. Mills, A. Milne, R. Langlois, E. Achterberg, K. Lochte, R. J. Geider, and J. La Roche. Iron limits primary productivity during spring bloom development in the central north atlantic. *Global Change Biology*, 12:626–634, 2006a.

C. M. Moore, D. J. Suggett, A. E. Hickman, Y.-N. Kim, J. F. Tweddle, J. Sharples, R. J. Geider, and P. M. Holligan. Phytoplankton photoacclimation and photoadaptation in response to environmental gradients in a shelf sea. *Limnology and Oceanography*, 51 (2):936–949, 2006b.

C. M. Moore, S. Seeyave, A. E. Hickman, J. T. Allen, M. I. Lucas, H. Planquette, R. T. Pollard, and A. J. Poulton. Iron-light interactions during the crozet natural iron bloom and export experiment (crozex) i: Phytoplankton growth and photophysiology. *Deep-Sea Research II*, 54(18-20):2045–2065, 2007.

C. M. Moore, M. M. Mills, R. Langlois, A. Milne, E. Achterberg, J. La Roche, and R. J. Geider. Relative influence of nitrogen and phosphorus availability on phytoplankton physiology and productivity in the oligotrophic sub-tropical north atlantic ocean. *Limnology and Oceanography*, 53(1):291–305, 2008.

J. K. Moore and O. Braucher. Sedimentary and mineral dust sources of dissolved iron to the world ocean. *Biogeosciences*, 5(3):631–656, 2008.

J. K. Moore, S. C. Doney, D. M. Glover, and I. Y. Fung. Iron cycling and nutrient-limitation patterns in surface waters of the world ocean. *Deep-Sea Research I*, 49 (463-507), 2001.

F. Morales, N. Moise, R. Quilez, A. Abadia, J. Abadia, and I. Moya. Iron deficiency interrupts energy transfer from a disconnected part of the antenna to the rest of photosystem ii. *Photosynthesis Research*, 70(2):207–220, 2001.

F. M. M. Morel, R. J. M. Hudson, and N. M. Price. Limitation of productivity by trace metals in the sea. *Limnology and Oceanography*, 36(8):1742–1755, 1991.

J. L. Moseley, T. Allinger, S. Herzog, P. Hoerth, E. Wehinger, S. Merchant, and M. Hippler. Adaptation to fe-deficiency requires remodelling of the photosynthetic apparatus. *The EMBO Journal*, 21(24):6709–6720, 2002.

J. W. Murray, J. Duncan, and J. Barber. Cp43-like chlorophyll binding proteins: structural and evolutionary implications. *TRENDS in Plant Science*, 11(3):152–158, 2006.

N. Nelson and A. Ben-Shem. The complex architecture of oxygenic photosynthesis. *Nature Reviews - Molecular Cell Biology*, 5:1–12, 2004.

M. Nielsdóttir, C. Moore, R. Sanders, D. Hinz, and E. Achterberg. Iron limitation of the postbloom phytoplankton communities in the iceland basin. *Global Biogeochemical Cycles*, 23:1–13, 2009.

M. C. Nielsdóttir, T. S. Bibby, C. M. Moore, D. J. Hinz, R. Sanders, M. Whitehouse, R. Korb, and E. P. Achterberg. Seasonal and spatial dynamics of iron availability in the scotia sea. *Marine Chemistry*, 130:62–72, 2012.

J. Nishioka, T. Ono, H. Saito, T. Nakatsuka, S. Takeda, T. Yoshimura, K. Suzuki, K. Kuma, S. Nakabayashi, D. Tsumune, H. Mitsudera, W. K. Johnson, and A. Tsuda. Iron supply to the western subarctic pacific: Importance of iron export from the sea of okhotsk. *Journal of Geophysical Research-Oceans*, 112, 2007.

R. J. Olson, H. M. Sosik, A. M. Chekalyuk, and A. Shalapyonok. Effects of iron enrichment on phytoplankton in the southern ocean during late summer: active fluoerscence and floy cytometric analyses. *Deep-Sea Research II*, 47:3181–3200, 2000.

G. Öquist. Light-induced changes in pigment composition of photosynthetic lamellae and cell-free extracts from the blue-green alga anacystis nidulans. *Physiologia Plantarum*, 30(1):45–48, 1974.

A. Oschlies. Can eddies make ocean deserts bloom? *Global Biogeochemical Cycles*, 16 (4), 2002. 1106.

A. Oschlies and V. Garcon. Eddy-induced enhancement of primary production in a model of the north atlantic ocean. *Nature*, 394(6690):266–269, 1998.

H. B. Pakrasi, H. C. Riethman, and L. A. Sherman. Organization of pigment proteins in the photosystem ii complex of the cyanobacterium anacystis ridulans r2. *Proceedings of the National Academy of Sciences USA*, 82:6903–6907, 1985.

J. D. Palmer. The symbiotic birth and spread of plastids: How many times and whodunit? *Journal of Phycology*, 39(1):4–11, 2003.

Y. I. Park, S. Sandström, P. Gustafsson, and G. Öquist. Expression of the isia gene is essential for the survival of the cyanobacterium synechococcus sp. pcc 7942 by protecting photosystem ii from excess light under iron limitation. *Molecular Microbiology*, 32(1):123–129, 1999.

J. Parkhill, G. Maillet, and J. J. Cullen. Fluorescence-based maximal quantum yield for psii as a diagnostic of nutrient stress. *Journal of Phycology*, 37:517–529, 2001.

J. A. Peloquin and J. Smith, Walker O. Phytoplankton blooms in the ross sea, antarctica: Interannual variability in magnitude, temporal patterns, and composition. *Journal of Geophysical Research-Oceans*, 112(C8), 2007. C08013.

G. L. Peterson. Review of the folin phenol protein quantification method of lowry, rosebrough, farr, and randall. *Analytical Biochemistry*, 100:201–220, 1979.

D. Petroutsos, A. M. Terauchi, A. Busch, I. Hirschmann, S. S. Merchant, G. Finazzi, and M. Hippler. Pgrl1 participates in iron-induced remodeling of the photosynthetic apparatus and in energy metabolism in chlamydomonas reinhardtii. *Journal of Biological Chemistry*, 284(47):32770–32781, 2009.

R. Pollard, R. Sanders, M. I. Lucas, and P. J. Statham. The crozet natural iron bloom and export experiment. *Deep-Sea Research II*, 54(18-20):1905–1914, 2007.

O. Prasil, D. J. Suggett, J. J. Cullen, M. Babin, and Govindjee. Aquafluo 2007: chlorophyll fluorescence in aquatic sciences, an international conference held in nove hrady. *Photosynthesis Research*, 95(1):111–5, 2008.

B. B. Prézelin, E. E. Hofmann, C. Mengelt, and J. M. Klinck. The linkage between upper circumpolar deep water (ucdw) and phytoplankton assemblages on the west antarctic peninsula continental shelf. *Journal of Marine Research*, 58(2):165–202, 2000.

B. B. Prézelin, E. E. Hofmann, M. Moline, and J. M. Klinck. Physical forcing of phytoplankton community structure and primary production in continental shelf waters of the western antarctic peninsula. *Journal of Marine Research*, 62(3):419–460, 2004.

N. M. Price. The elemental stoichiometry and composition of an iron-limited diatom. *Limnology and Oceanography*, 50:1149–1158, 2005.

N. M. Price and F. M. M. Morel. *Biological cycling of iron in the sea*, volume 35 of *Metal Ions in Biological Systems*, chapter Iron transport and storage in microorganisms, plants, and animals, pages 1–36. Taylor Francis, Oxford, 1998.

N. M. Price, B. A. Ahner, and F. M. M. Morel. The equatorial pacific-ocean - grazer-controlled phytoplankton populations in an iron-limited ecosystem. *Limnology and Oceanography*, 39(3):520–534, 1994.

J. M. Prospero, J. E. Bullard, and R. Hodgkins. High-latitude dust over the north atlantic: inputs from icelandic proglacial dust storms. *Science*, 335(6072):1078–82, 2012.

A. Quigg, Z. Finkel, A. Irwin, Y. Rosenthal, T.-Y. Ho, J. Reinfelder, O. Schofield, F. Morel, and P. G. Falkowski. The evolutionary influence of elemental stoichiometry in marine phytoplankton. *Nature*, 425:291–294, 2003.

R. Raiswell and D. E. Canfield. The iron biogeochemical cycle past and present. *Geochemical Perspectives*, 1(1):1–217, 2012.

J. A. Raven. Predictions of mn and fe use efficiencies of phototrophic growth as a function of light availability for growth and c assimilation pathway. *New Phytologist*, 116:1–18, 1990.

T. E. Reddy, K. R. Arrigo, and D. M. Holland. The role of thermal and mechanical processes in the formation of the ross sea summer polynya. *Journal of Geophysical Research-Oceans*, 112(C7), 2007. C07027.

A. C. Redfield. *On the proportions of organic derivations in sea water and their relation to the composition of plankton*, pages 177–192. Liverpool University Press, Liverpool, 1934.

A. C. Redfield. The biological control of chemical factors in the environment. *American Science*, 46:205–221, 1958.

H. C. Riethman and L. A. Sherman. Purification and characterization of an iron stress-induced chlorophyll-protein from the cyanobacterium anacystis nidulans r2. *Biochimica et Biophysica Acta*, 935:141–151, 1988.

G. Rocap, F. W. Larimer, J. Lamerdin, S. Malfatti, P. Chain, N. A. Ahlgren, A. Arellano, M. Coleman, L. Hauser, W. R. Hess, Z. I. Johnson, M. Land, D. Lindell, A. F.

Post, W. Regala, M. Shah, S. L. Shaw, C. Steglich, M. B. Sullivan, C. S. Ting, A. Tolonen, E. A. Webb, E. R. Zinser, and S. W. Chisholm. Genome divergence in two prochlorococcus ecotypes reflects oceanic niche differentiation. *Nature*, 424(6952): 1042–1047, 2003.

T. J. Ryan-Keogh, A. I. Macey, A. M. Cockshutt, C. M. Moore, and T. S. Bibby. The cyanobacterial chlorophyll-binding-protein isia acts to increase the in vivo effective absorption cross-section of photosystem i under iron limitation. *Journal of Phycology*, 48(1):145–154, 2012.

T. J. Ryan-Keogh, A. I. Macey, M. Nielsdóttir, M. I. Lucas, S. S. Steigenberger, M. C. Stinchcombe, E. P. Achterberg, T. S. Bibby, and C. M. Moore. Spatial and temporal development of phytoplankton iron stress in relation to bloom dynamics in the high-latitude north atlantic ocean. *Limnology and Oceanography*, 58(2):533–545, 2013.

J. H. Ryther and R. R. L. Guillard. Enrichment experiments as a means of studying nutrients limiting to phytoplankton populations. *Deep-Sea Research*, 6:65–69, 1959.

J. H. Ryther and D. D. Kramer. Relative iron requirement of some coastal and offshore-plankton algae. *Ecology*, 42(2):444–446, 1960.

M. A. Saito, G. Rocap, and J. W. Moffett. Production of cobalt binding ligands in a synechococcus feature at the costa rica upwelling dome. *Limnology and Oceanography*, 50:279–290, 2005.

M. A. Saito, T. J. Goepfert, and J. T. Ritt. Some thoughts on the concept of colimitation: Three definitions and the importance of bioavailability. *Limnology and Oceanography*, 53(1):276–290, 2008.

R. N. Sambrotto, A. Matsuda, R. Vaillancourt, M. Brown, C. Langdon, S. S. Jacobs, and C. Measures. Summer plankton production and nutrient consumption patterns in the mertz glacier region of east antarctica. *Deep-Sea Research Part Ii-Topical Studies in Oceanography*, 50(8-9):1393–1414, 2003.

R. Sanders, S. Brown, S. A. Henson, and M. I. Lucas. New production in the irminger basin during 2002. *Journal of Marine Systems*, 55(3-4):291–310, 2005.

S. Sandström, Y. I. Park, G. Öquist, and P. Gustafsson. Cp43', the isia gene product, functions as an excitation energy dissipator in the cyanobacterium synechococcus sp. pcc 7942. *Photochemistry and Photobiology*, 74:431–437, 2001.

S. Sandström, A. G. Ivanov, Y. I. Park, G. Öquist, and P. Gustafsson. Iron stress responses in the cyanobacterium synechococcus sp. pcc7942. *Physiologia Plantarum*, 116:255–263, 2002.

M. Sarcina and C. Mullineaux. Mobility of the isia chlorophyll-binding protein in cyanobacterial thylakoid membranes. *The Journal of Biological Chemistry*, 279(35): 36514–36518, 2004.

J. Sarmiento, N. Gruber, M. Brzezinski, and J. Dunne. High-latitude controls of thermocline nutrients and low latitude biological productivity. *Nature*, 427:56–60, 2004.

J. L. Sarmiento, T. M. C. Hughes, R. J. Stouffer, and S. Manabe. Simulated response of the ocean carbon cycle to anthropogenic climate warming. *Nature*, 393(6682):245–249, 1998.

G. Sarthou, D. Vincent, U. Christaki, I. Obernosterer, K. R. Timmermans, and C. P. D. Brussaard. The fate of biogenic iron during a phytoplankton bloom induced by natural fertilisation: Impact of copepod grazing. *Deep-Sea Research Part Ii-Topical Studies in Oceanography*, 55(5-7):734–751, 2008.

G. H. Schatz, H. Brock, and A. R. Holtzwarth. A kinetic and energetic model for the primary processes in photosystem ii. *Biophysical Journal*, 54:397–405, 1988.

P. S. Schrader, A. J. Milligan, and M. J. Behrenfeld. Surplus photosynthetic antenna complexes underlie diagnostics of iron limitation in a cyanobacterium. *PLoS ONE*, 6 (4):e18753, 2011.

P. Sedwick, E. Sholkovitz, and T. Church. Impact of anthropogenic combustion emissions on the fractional solubility of aerosol iron: Evidence from the sargasso sea. *Geochemistry Geophysics Geosystems*, 8(10):Q10Q06 doi: 10.1029/2007/GC001586, 2007a.

P. N. Sedwick and G. R. DiTullio. Regulation of algal blooms in antarctic shelf waters by the release of iron from melting sea ice. *Geophysical Research Letters*, 24:2515–2518, 1997.

P. N. Sedwick, G. R. DiTullio, and D. J. Mackey. Iron and manganese in the ross sea, antarctica: seasonal iron limitation in antarctic shelf waters. *Journal of Geophysical Research*, 105:11321–11336, 2000.

P. N. Sedwick, N. S. Garcia, S. F. Riseman, C. M. Marsay, and G. R. DiTullio. Evidence for high iron requirements of colonial phaeocystis antarctica at low irradiance. *Biogeochemistry*, 83(1-3):83–97, 2007b. Meeting of the Scientific-Committee on Oceanic Research AUG 30-SEP 03, 2005 Univ Groningen, Haren, NETHERLANDS Dutch Royal Acad Sci; Rug-GUF; Univ Res Sch CEES.

P. N. Sedwick, C. M. Marsay, B. M. Sohst, A. M. Aguilar-Islas, M. C. Lohan, M. C. Long, K. R. Arrigo, R. B. Dunbar, M. A. Saito, J. Smith, W. O., and G. R. DiTullio. Early season depletion of dissolved iron in the ross sea polynya: implications for iron dynamics on the antarctic continental shelf. *Journal of Geophysical Research*, 116: C12019, 2011.

J. Seppala, T. Tamminen, and S. Kaitala. Experimental evaluation of nutrient limitation of phytoplankton communities in the gulf of riga. *Journal of Marine Systems*, 23:107–126, 1999.

D. M. Sherman and L. A. Sherman. Effect of iron deficiency and iron restoration on ultrastructure of anacystis nidulans. *Journal of Bacteriology*, 156:393–401, 1983.

T. Shi, Y. Sun, and P. G. Falkowski. Effects of iron limitation on the expression of metabolic genes in the marine cyanobacterium trichodesmium erythraeum ims101. *Environmental Microbiology*, 9(12):2945–2956, 2007.

D. A. Siegel, S. C. Doney, and J. A. Yoder. The north atlantic spring phytoplankton bloom and sverdrup's critical depth hypothesis. *Science*, 296(5568):730–733, 2002.

D. M. Sigman and E. A. Boyle. Glacial/interglacial variations in atmospheric carbon dioxide. *Nature*, 407(6806):859–869, 2000.

A. K. Singh and L. A. Sherman. Iron-independent dynamics of isia production during the transition to stationary phase in the cyanobacterium synechocystis sp. pcc 6803. *FEMS Microbiology Ecology*, 256:159–164, 2006.

A. K. Singh and L. A. Sherman. Reflections on the function of isia, a cyanobacterial stress-inducible, chl-binding protein. *Photosynthesis Research*, 93(1-3):17–25, 2007. Journal Article; Review.

C. Six, J.-C. Thomas, L. Garczarek, M. Ostrowski, A. Dufresne, N. Blot, D. J. Scanlan, and F. Partensky. Diversity and evolution of phycobilisomes in marine synechococcus spp.: a comparative genomics study. *Genome Biology*, 8(12), 2007. R259.

W. M. Smethie and S. S. Jacobs. Circulation and melting under the ross ice shelf: estimates from evolving cfc, salinity and temperature fields in the ross sea. *Deep-Sea Research Part I-Oceanographic Research Papers*, 52(6):959–978, 2005.

J. Smith, W. O. and D. M. Nelson. Phytoplankton bloom produced by receding ice edge in the ross sea: Spatial coherence with the density field. *Science*, 227:163–166, 1985.

J. Smith, Walker O., A. R. Shields, J. A. Peloquin, G. Catalano, S. Tozzi, M. S. Dinniman, and V. A. Asper. Interannual variations in nutrients, net community production, and biogeochemical cycles in the ross sea. *Deep-Sea Research Part Ii-Topical Studies in Oceanography*, 53(8-10):815–833, 2006.

K. L. Smith, B. H. Robison, J. J. Helly, R. S. Kaufmann, H. A. Ruhl, T. J. Shaw, B. S. Twining, and M. Vernet. Free-drifting icebergs: Hot spots of chemical and biological enrichment in the weddell sea. *Science*, 317(5837):478–482, 2007.

W. O. Smith and V. A. Asper. A balanced nitrogen budget of the surface layer of the southern ross sea, antarctica. *Geophysical Research Letters*, 27(17):2721–2724, 2000.

W. O. Smith and V. L. Asper. The influence of phytoplankton assemblage composition on biogeochemical characteristics and cycles in the southern ross sea, antarctica. *Deep-Sea Research Part I-Oceanographic Research Papers*, 48(1):137–161, 2001.

W. O. Smith and R. B. Dunbar. The relationship between new production and vertical flux on the ross sea continental shelf. *Journal of Marine Systems*, 17(1-4):445–457, 1998. International JGOFS Symposium on Carbon Fluxes and Dynamic Processes in the Southern Ocean - Present and Past AUG 28-31, 1995 BREST, FRANCE European Inst Marine Studies; Univ W Brittany.

W. O. Smith and L. I. Gordon. Hyperproductivity of the ross sea (antarctica) polynya during austral spring. *Geophysical Research Letters*, 24(3):233–236, 1997.

W. O. Smith, J. Marra, M. R. Hiscock, and R. T. Barber. The seasonal cycle of phytoplankton biomass and primary productivity in the ross sea, antarctica. *Deep-Sea Research Part Ii-Topical Studies in Oceanography*, 47(15-16):3119–3140, 2000.

W. O. Smith, M. R. Dennett, S. Mathot, and D. A. Caron. The temporal dynamics of the flagellated and colonial stages of phaeocystis antarctica in the ross sea. *Deep-Sea Research Part Ii-Topical Studies in Oceanography*, 50(3-4):605–617, 2003. PII S0967-0645(02)00586-6.

Y. Sohrin, S. Iwamoto, M. Matsui, H. Obata, E. Nakayama, K. Suzuki, N. Handa, and M. Ishii. The distribution of fe in the australian sector of the southern ocean. *Deep-Sea Research Part I-Oceanographic Research Papers*, 47(1):55–84, 2000.

N. A. Strauss. *Iron Deprivation: Physiology and Gene Regulation*, pages 731–750. Kluwer Academic Publisher, Dordrecht, 1994.

R. F. Strzepek, M. T. Maldonado, J. L. Higgins, J. Hall, K. Safi, S. W. Wilhelm, and P. W. Boyd. Spinning the "ferrous wheel": The importance of the microbial community in an iron budget during the fecycle experiment. *Global Biogeochemical Cycles*, 19(4), 2005.

R. F. Strzepek, K. A. Hunter, R. D. Frew, P. J. Harrison, and P. W. Boyd. Iron-light interactions differ in southern ocean phytoplankton. *Limnology and Oceanography*, 57 (4):1182–1200, 2012.

D. V. Subba Rao and P. A. Yeats. Effect of iron on phytoplankton production in the sargasso sea. *Journal of Experimental Marine Biology and Ecology*, 81:281–289, 1984.

D. Suggett, C. Moore, A. Hickman, and R. Geider. Interpretation of fast repetition rate (frr) fluorescence: signatures of phytoplankton community structure versus physiological state. *Marine Ecology Progress Series*, 376:1–19, 2009.

D. J. Suggett, H. L. MacIntyre, and R. J. Geider. Evaluation of biophysical and optical determinations of light absorption by photosystem ii in phytoplankton. *Limnology and Oceanography Methods*, 2:316–332, 2004.

D. J. Suggett, S. C. Maberly, and R. J. Geider. Gross photosynthesis and lake community metabolism during the spring phytoplankton bloom. *Limnology and Oceanography*, 51:2064–2076, 2006a.

D. J. Suggett, C. M. Moore, E. Marañon, C. Omachi, R. A. Varela, J. Aiken, and P. M. Holligan. Photosynthetic electron turnover in the tropical and subtropical atlantic ocean. *Deep-Sea Research Part II*, 53:1573–1592, 2006b.

D. J. Suggett, E. Le Floc'H, G. N. Harris, N. Leonardos, and R. J. Geider. Different strategies of photoacclimation by two strains of emiliana huxleyi (haptophyte). *Journal of Phycology*, 43:1209–1222, 2007.

W. G. Sunda. *Bioavailability and Bioaccumulation of Iron in the Sea*, pages 41–84. Wiley, Chichester, 2001.

W. G. Sunda and S. A. Huntsman. Interrelated influence of iron, light and cell size on marine phytoplankton growth. *Nature*, 390:389–392, 1997.

W. G. Sunda, D. Swift, and S. A. Huntsman. Iron growth requirements in oceanic and coastal phytoplankton. *Nature*, 351:55–57, 1991.

K. Suzuki, H. B. Liu, T. Saino, H. Obata, M. Takano, K. Okamura, Y. Sohrin, and Y. Fujishima. East-west gradients in the photosynthetic potential of phytoplankton and iron concentration in the subarctic pacific ocean during early summer. *Limnology and Oceanography*, 47(6):1581–1594, 2002.

M. Suzumura and E. D. Ingall. Distribution and dynamics of various forms of phosphorus in seawater: Insights from field observations in the pacific ocean and a laboratory experiment. *Deep-Sea Research I*, 51(8):1113–1130, 2004.

H. U. Sverdrup. On conditions for the vernal blooming of phytoplankton. *Journal du Conseil International pour l'Exploration de la Mer*, 18:287–295, 1953.

C. Sweeney, W. O. Smith, B. Hales, R. R. Bidigare, C. A. Carlson, L. A. Codispoti, L. I. Gordon, D. A. Hansell, F. J. Millero, M. O. Park, and T. Takahashi. Nutrient and carbon removal ratios and fluxes in the ross sea, antarctica. *Deep-Sea Research Part Ii-Topical Studies in Oceanography*, 47(15-16):3395–3421, 2000.

A. Tagliabue and K. R. Arrigo. Anomalously low zooplankton abundance in the ross sea: An alternative explanation. *Limnology and Oceanography*, 48(2):686–699, 2003.

A. Tagliabue, L. Bopp, and O. Aumont. Ocean biogeochemistry exhibits contrasting responses to a large scale reduction in dust deposition. *Biogeosciences*, 5(1):11–24, 2008.

S. Takeda. Influence of iron availability on nutrient comsumption ratio of diatoms in oceanic waters. *Nature*, 393:774–777, 1998.

A. Telfer, H. Bottin, J. Barber, and P. Mathis. The effect of magnesium and phosphorylation of light-harvesting chlorophyll a/b-protein on the yield of p-700-photooxidation in pea-chloroplasts. *Biochimica et Biophysica Acta*, 764(3):324–330, 1984.

K. R. Timmermans, L. J. A. Gerringa, H. J. W. de Baar, B. van der Wagt, M. J. W. Veldhuis, J. T. M. de Jong, P. L. Croot, and M. Boye. Growth rates of large and small southern ocean diatoms in relation to availability of iron in natural seawater. *Limnology and Oceanography*, 46(2):260–266, 2001.

K. R. Timmermans, B. van der Wagt, and H. J. W. de Baar. Growth rates, half-saturation constants, and silicate, nitrate, and phosphate depletion in relation to iron availability of four large, open-ocean diatoms from the southern ocean. *Limnology and Oceanography*, 49(6):2141–2151, 2004.

D. J. Tranter, R. R. Parker, and G. R. Cresswell. Are warm-core eddies unproductive. *Nature*, 284(5756):540–542, 1980.

D. R. Turner, M. Whitfield, and A. G. Dickson. The equilibrium speciation of dissolved components in freshwater and seawater at 25 °c at 1 atm. pressure. *Geochimica Cosmochimica Acta*, 45:855–882, 1981.

C. M. van Hilst and W. O. Smith. Photo synthesis/irradiance relationships in the ross sea, antarctica, and their control by phytoplankton assemblage composition and environmental factors. *Marine Ecology-Progress Series*, 226:1–12, 2002.

M. A. van Leeuwe and H. J. W. de Baar. Photoacclimation by the antarctic flagellate pryamimonas sp. (prasinophyceae) in response to iron limitation. *European Journal of Phycology*, 36:295–303, 2000.

T. Varsano, D. Kaftan, and U. Pick. Effects of iron deficiency on thylakoid membrane structure and composition in the alga dunaliella salina. *Journal of Plant Nutrition*, 26(10-11):2197–2210, 2003.

T. Varsano, S. G. Wolf, and U. Pick. A chlorophyll a/b-binding protein homolog that is induced by iron deficiency is associated with enlarged photosystem i units in the

eukaryotic alga dunaliella salina. *Journal of Biological Chemistry*, 281(15):10305–10315, 2006.

I. R. Vassiliev, O. Prášil, K. D. Wyman, Z. S. Kolber, A. K. Hanson, J. E. Prentice, and P. G. Falkowski. Inhibition of psii photochemistry by par and uv radiation in natural phytoplankton communities. *Photosynthesis Research*, 42:51–64, 1994.

I. R. Vassiliev, Z. Kolber, K. D. Wyman, D. Mauzerall, V. K. Shukla, and P. G. Falkowski. Effects of iron limitation on photosystem-ii composition and light utilization in dunaliella-tertiolecta. *Plant Physiology*, 109(3):963–972, 1995.

E. L. Venrick. Mesoscale patterns of chlorophyll-a in the central north pacific. *Deep-Sea Research Part a-Oceanographic Research Papers*, 37(6):1017–1031, 1990.

T. Volk and M. I. Hoffert. *Ocean carbon pumps: analysis of relative strengths and efficiencies in ocean-driven atmospheric CO2*, pages 99–110. AGU, Washington D.C., 1985.

J. Von Liebig. *Organic chemistry in its application to agriculture and physiology.* Taylor and Walton, London, 1840.

A. E. Walsby and C. S. Reynolds. *Sinking and Floating*, pages 371–412. Studies in Ecology. Blackwell, 1980. ED.

J. J. Walsh. Herbivory as a factor in patterns of nutrient utilization in the sea. *Limnology and Oceanography*, 21:1–13, 1976.

Q. Wang, C. L. Hall, M. Z. Al-Adami, and Q. He. Isia is required for the formation of photosysytem i supercomplexes and for efficient state transition in synechocystis pcc 6803. *PLoS ONE*, 5(5):e10432, 2010.

A. J. Watson and P. S. Liss. Marine biological controls on climate via the carbon and sulphur geochemical cycles. *Philosophical Transactions of the Royal Society of London Series B-Biological Sciences*, 353(1365):41–51, 1998.

N. A. Welschmeyer. Fluorometric analysis of chlorophyll-a in the presence of chlorophyll-b and pheopigments. *Limnology and Oceanography*, 39(8):1985–1992, 1994.

M. S. Wetz, B. Hales, Z. Chase, P. A. Wheeler, and M. M. Whitney. Riverine input of macronutrients, iron, and organic matter to the coastal ocean off oregon, usa, during the winter. *Limnology and Oceanography*, 51(5):2221–2231, 2006.

P. B. Wignall and R. J. Twitchett. Oceanic anoxia and the end permian mass extinction. *Science*, 272(5265):1155–1158, 1996.

J. G. K. Williams. Construction of specific mutations in photosystem ii photosynthetic reaction center by genetic engineering methods in synechocystis 6803. *Methods in Enzyomology*, 167:766–778, 1988.

R. G. Williams and M. J. Follows. *Physical transport of nutrients and the maintenance of biological production*, pages 19–51. Springer, 2003.

A. Wilson, G. Ajlani, J. M. Verbavatz, I. Vass, C. A. Kerfeld, and D. Kirilovsky. A soluble carotenoid protein involved in phycobilisome-related energy dissipation in cyanobacteria. *Plant Cell*, 18(4):992–1007, 2006.

A. Wilson, C. Boulay, A. Wilde, C. A. Kerfield, and D. Kirilovsky. Light-induced energy dissipation in iron starved cyanobacteria: Roles of ocp and isia proteins. *The Plant Cell*, 19:656–672, 2007.

A. Wilson, C. Boulay, and D. Kirilovsky. Light induced energy dissipation in iron-starved cyanobacteria. *Photosynthesis. Energy from The Sun*, 24:1607–1610, 2008.

J. Wu, W. G. Sunda, E. A. Boyle, and D. Karl. Phosphate depletion in the western north atlantic ocean. *Science*, 289:759–762, 2000.

N. Yeremenko, R. Kouřil, J. Ihalainen, S. D'Haene, N. van Oosterwijk, E. Andrizhiyevskaya, W. Keegstra, H. Dekker, M. Hagemann, E. Boekema, H. C. P. Matthijs, and J. Dekker. Supramolecular organization and dual function of the isia chlorophyll-binding protein in cyanobacteria. *Biochemistry*, 43:10308–10313, 2004.

N. Yousef, E. K. Pistorius, and K. P. Michel. Comparative analysis of idia and isia transcription under iron starvation and oxidative stress in synechococcus elongatus pcc 7942 wild-type and selected mutants. *Archives of Microbiology*, 180(6):471–483, 2003. Journal Article.

O. C. Zafiriou and M. B. True. Inter conversion of fe(iii) hydroxy complexes in sea water. *Marine Chemistry*, 8:281–288, 1980.

L. A. Zaslavskaia, J. C. Lippmeier, C. Shih, D. Ehrhardt, A. R. Grossman, and K. E. Apt. Trophic obligate conversion of an photoautotrophic organism through metabolic engineering. *Science*, 292(5524):2073–2075, 2001.

F. Zhang, G. M. Lee, and K. Jacobson. Protein lateral mobility as a reflection of membrane microstructure. *BioEssays*, 15(9):579–588, 1993.

W. Zipfel and T. G. Owens. Calculation of absolute photosystem i absorption cross-sections from p700 photo-oxidation kinetics. *Photosynthesis Research*, 29:23–35, 1991.

A. Zouni, H. T. Witt, J. Kern, P. Fromme, N. Krauss, W. Saenger, and P. Orth. Crystal structure of photosystem ii from synechococcus elongatus at 3.8 angstrom resolution. *Nature*, 409(6821):739–743, 2001. Journal Article.

M. V. Zubkov and P. H. Burkill. Syringe pumped high speed flow cytometry of oceanic phytoplankton. *Cytometry Part A*, 69A(9):1010–1019, 2006.